NASA CONTRACTOR REPORT

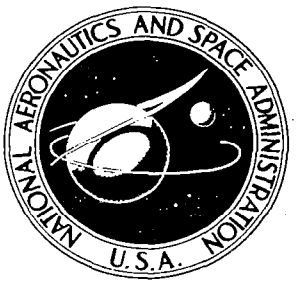

NASA CR-2

NASA CR-2762

CONTRIBUTIONS TO THE SIMULATION OF TURBULENCE

John A. Dutton, Bryan R. Kerman, and Erik L. Petersen

Prepared by
THE PENNSYLVANIA STATE UNIVERSITY
University Park, Penn. 16802
for George C. Marshall Space Flight Center

NATIONAL AERONAUTICS AND SPACE ADMINISTRATION • WASHINGTON, D. C. • DECEMBER 1976

TECHNICAL REPORT STANDARD TITLE PAGE

1. REPORT NO.	2. GOVERNMENT ACCESSION NO.	3. RECIPIENT'S CATALOG NO.
NASA CR-2762		

4. TITLE AND SUBTITLE	5. REPORT DATE
Contributions to the Simulation of Turbulence	December 1976
	6. PERFORMING ORGANIZATION CODE

7. AUTHOR(S)	8. PERFORMING ORGANIZATION REPORT #
John A. Dutton, Bryan R. Kerman, and Erik L. Petersen	M-191

9. PERFORMING ORGANIZATION NAME AND ADDRESS	10. WORK UNIT NO.
Department of Meteorology The Pennsylvania State University University Park, Pennsylvania 16802	11. CONTRACT OR GRANT NO. NAS8-21140

12. SPONSORING AGENCY NAME AND ADDRESS	13. TYPE OF REPORT & PERIOD COVERED
National Aeronautics and Space Administration Washington, D. C. 20546	Contractor
	14. SPONSORING AGENCY CODE

15. SUPPLEMENTARY NOTES

This report was prepared under the technical monitorship of the Aerospace Environment Division, Space Sciences Laboratory, NASA/Marshall Space Flight Center.

16. ABSTRACT

The simulation of atmospheric turbulence is of major importance in the solution of problems related to aeronautical and aerospace engineering. This report documents the results of research concerned with developing new techniques for simulating atmospheric turbulence time histories in the context of satisfying both second-order empirical turbulence statistics and certain higher-order statistics. The report consists of two sections. The first section is concerned with turbulence simulation involving nonlinear, non-Gaussian, kernel interaction models. The second section is concerned with simulation of atmospheric turbulence with proper orthogonal function representations. The report gives complete developments of the theory with examples.

17. KEY WORDS	18. DISTRIBUTION STATEMENT
Turbulence Simulation Aviation Safety Flight Simulation Control Systems Aviation Vehicle Dynamics	Cat. 47 47

19. SECURITY CLASSIF. (of this report)	20. SECURITY CLASSIF. (of this page)	21. NO. OF PAGES	22. PRICE
Unclassified	Unclassified	284	$8.75

* For sale by the National Technical Information Service, Springfield, Virginia 22161

FOREWORD

This research was conducted by The Pennsylvania State University for the National Aeronautics and Space Administration, George C. Marshall Space Flight Center, Huntsville, Alabama. Dr. George H. Fichtl of the Aerospace Environment Division, Space Sciences Laboratory, was the scientific monitor. Professor John A. Dutton, Department of Meteorology, The Pennsylvania State University, was the principal investigator. The support for this research was provided by Mr. John Enders of the Aviation Safety Technology Branch, Office of Aeronautics and Space Technology, NASA Headquarters.

The research reported herein was motivated by the need in the aviation community for advanced turbulence simulation schemes that provide simulated turbulence time histories for flight simulation applications which satisfy not only the known second-order statistics of the atmospheric turbulence as in the state-of-the-art turbulence simulation schemes now being used by the aviation community, but in addition include information concerning higher-order statistics as manifest by the non-Gaussian nature of atmospheric turbulence. In this context, it is believed that the work presented herein represents a major step forward in stochastic process theory as related to atmospheric turbulence simulation. However, it should be noted that the results of this report, when used alone, are only applicable to the case in which an aeronautical system is completely immersed in the gusts; i.e., absence of gust gradient effects. In this regard, additional work is under way to develop gust gradient simulation schemes whereby the gust velocity time histories generated by the technique reported herein and the gust gradients simulated by the techniques now under development are applied with a Taylor series expansion (truncated at the first-order term) of the gust velocity vector field about the vehicle center of gravity, so that the gust environment at any point on the vehicle can be generated during a flight simulation.

TABLE OF CONTENTS

TABLE OF CONTENTS (continued)

TABLE OF CONTENTS (continued)

LIST OF FIGURES

PART I

LIST OF FIGURES (continued)

LIST OF FIGURES (continued)

PART II

LIST OF FIGURES (continued)

LIST OF TABLES

PART I

PART II

SUMMARY

The method of simulating a turbulent time series by filtering a white noise series is consolidated and extended. The development of linear filters from empirical spectra is expanded for forms based on boundary layer similarity under stratification and for generalized spectral shapes. Some properties of the filters under various stratifications, heights and viscosities are examined. The method of linear simulation is extended to multi-component processes by the diagonalization of the spectral matrix, spectral factorization of the eigenvalues, followed by a rotation involving a special unitary transformation. Results indicate that the addition of a cross-response increases the total response.

The method of simulation by filtering is extended to several non-linear, non-Gaussian models. These models are based on ad hoc approximations of the kernel interactions. It is found that the method of separable kernels for a representation of velocity is inappropriate for simulating the characteristic inertial transfer of turbulent energy. However, the separable kernel representation of acceleration better approximates the energy transfer in the viscous subrange for sufficiently small Reynolds number.

An evaluation of the linear and non-linear models, with computations carried out in phase space, is included. Because the non-linear simulation method requires a more precisely Gaussian stimulating process than is commonly available, special generative techniques were developed and examined. Results indicate that non-linear simulations will require large arrays of very nearly white, Gaussian noise in applications.

1.0 INTRODUCTION

The increasing sophistication of design techniques in a variety of engineering and environmental applications requires the simulation of the statistical structure of wind gusts. As man-made structures have been made larger and more flexible, it has become imperative that the effects of the wind, both as a static and fluctuating force, be incorporated in structural and economic designs. In addition, in response to increasing concern for the quality of the environment, the need to understand the wind-driven diffusion mechanism distributing air-borne pollutants through the atmospheric environment has increased. Fortunately, there exists a wealth of information about the statistical structure of the wind, particularly near the ground. However, an important difficulty lies in incorporating such information into applications in a manner that is at once practical and realistic as it conveys important aspects of the meteorological dynamics of the problem.

1.1 Statement of the Problem

In this study, the method of incorporating the statistical structure of the turbulent wind field near the ground into applications is consolidated and expanded.

The linear spectral representation of turbulence has provided a useful interface between the meteorologist and the engineer. Consequently, its properties, successes and failures are well known. The interest of the meteorologist has been generally centered on providing

the best possible estimates about the structure of the wind field, both as it relates to the vertical distribution of the averaged wind and to the spectral distribution of the fluctuating wind.

Models to simulate turbulence which require the specification of the mean wind with height and thermal stratification vary in their sophistication and reliance on the principles of boundary layer similarity. As a result, the description of the vertical profile of wind has tended to be a potpourri of empirical relationships and approximations. Because the numerous parameters which characterize turbulence in the atmospheric boundary layer have often not been measured simultaneously, the applicability of some empirical results is unknown.

Accordingly, there is a need to consolidate aspects of the vertical structure of the wind, in order to have them consistent with known similarity properties of the flow, and to be able to incorporate further results as they become available.

Another crucial feature of simulation models of turbulence near the ground is the approximation used for the spectral distribution of the variance in the fluctuating components of the wind, particularly, in the range of scales of size equal to or less than the distance, z, from the ground. Simulation models which lead to modeled realizations of the turbulence have required the so-called Dryden spectral form, which for sufficiently small scales varies as k^{-2}, where k is the wave number. This spectral form has no basis in theory or observations and has been chosen only for its analytical properties. Other applications not requiring modeled realizations have been based on the von Kármán spectral form which tends to $k^{-5/3}$, for $kz \gg 1$, in accordance with

the well-known properties of the Kolmogorov inertial subrange. However, the von Kármán spectrum requires the specification of a length with which to characterize the bandwidth of the spectrum, but this length parameter bears no known dynamical relationship to the structural properties of the turbulence in the atmospheric boundary layer. As a result, the implied spectral dynamics of von Kármán's model cannot be determined by recourse to theoretical considerations of the boundary layer. The determination of such lengths must of necessity be made empirically. It remains to determine alternative spectral forms which are dynamically consistent with, say, the vertical profile of wind and dissipation determined by similarity arguments.

It is also well known that the concept of a linear representation of turbulence in terms of a Gaussian, white noise process is inconsistent with the observed non-Gaussian and non-linear structure of the turbulence. In particular, linear Gaussian models are inadequate for the simulation of the large gust structure. Therefore, an extension of the representation of turbulence is considered in this study which systematically incorporates some basic properties of the non-linear and non-Gaussian probabilistic structure of the turbulence. The mathematical formulation of this extension is most conveniently based on a functional series expansion in terms of the simple and convenient Gaussian, white noise process -- the same as is used in linear modeling.

The method of functional representation will be shown to lead naturally to a concept of a discrete gust form. As such, the method of the representation is superior to other discrete gust models where mathematically convenient, ad hoc forms are specified. Because here

the discrete gust form is a derived property of the process, a consistent formulation for the statistical structure of the turbulence in the boundary layer allows for a systematic analysis of this discrete gust form for various thermal stratifications and Reynolds number effects.

In summary, it is the purpose of this study to consolidate the simulation modeling of turbulence in the boundary layer in terms of boundary layer similarity principles and empirical results, and to extend the modeling for some aspects of the non-linear and non-Gaussian structure of the turbulence there. It is also the intention of this work to identify some properties of the discrete gust form structure of the modeled turbulence.

1.2 Importance of the Problem

The study of the structural effects of turbulence in the earth's boundary layer divides naturally into three main streams of research and development (1) the collection and assimilation of turbulence data; (2) the theoretical modeling of the statistical and dynamical nature of the turbulence; and (3) the development of methods by which to specify the response, structural or otherwise, to the turbulence. While a considerable effort has been made to measure, describe and model the flow field throughout the planetary boundary layer, the development of methods of application of this accumulated wealth of information has not been rapid.

The need for applied models of turbulence near the ground is ubiquitous. The need is perhaps most severe in the design and operation of aircraft and other aerospace vehicles. In aeronautical

operations, cross-winds and wind shear may on occasion present a hazard in the approach and landing stages of a flight. In addition to questions of structural integrity and passenger comfort, the principal concern of the designer is that the pilot may lose control as the aircraft is accelerated, or may aggravate the situation by initiating the wrong corrective procedure. The control problem is compounded for VSTOL aircraft and helicopters whose lift characteristics are more sensitive to the direction of air flow relative to the lifting surfaces. More recently, the need has developed to study the response of rockets to turbulence during launch because the wind fluctuations affect the stability and navigation of the vehicle.

The concern about wind effects is shared by many other engineers. Turbulent buffeting of surface structures, particularly of large flexible bridges and office towers, must be considered at the design stage. Further, the design of surface transportation systems and vehicles also requires a specification of the range of probabilities of significant wind events and a method of estimating the response or result. Of interest, particularly in large urban areas, is the effect of turbulence in the dispersion of pollutants in the atmosphere. Yet another important area requiring the modeling of the wind field is that of water wave formation and maintenance, in as much as the wave environment effects over-water transportation, recreation, and the dispersion of pollutants in or on the water.

1.3 General Characteristics of Simulation Models

Of course, not all requirements for simulating the statistical structure of the wind field can be met by developing a particular model.

For example, the methods used to simulate the dynamics of turbulence (Kraichnan, 1965; Herring, 1966; Deardorff, 1972a), while useful in testing the consequences of the approximations characterizing each model, are either not theoretically compatible with the inhomogeneous structure of turbulence in the atmospheric boundary layer or else are impractical to implement.

The method found most suitable by engineers for simulating turbulence is the so-called spectral filtering, or forcing, technique pioneered by Liepmann (1954). The spectral filtering model essentially characterizes the response of an aircraft or structure, or any process driven by turbulence, as a signal derived by filtering a sequence of pulses uncorrelated sequentially whose amplitudes are derived probabilistically from a Gaussian distribution. The desirable property of the latter process is the constant spectrum, which, from optics, is referred to as a white spectrum. Because of the wide variety of applications (Houbolt, 1973), the method remains a useful technique. Its success to a considerable degree is attributable to its simplicity.

The spectral filtering method, as the name implies, is based on the use of the spectrum of the atmospheric turbulence to characterize the flow field. The characterization of the spectrum over scales important to the application in turn requires specifying the spectral form as well as its variance and its bandwidth. Variations exist in the representation of the spectrum and its controlling variables (Teunissen, 1970), and are discussed in more detail later. The mathematical details of the method are also postponed for later consideration.

The simulated turbulence resulting from the linear filtering of a Gaussian process is itself Gaussian. However, turbulence is not a

Gaussian process (Dutton, 1970). In order to produce a non-Gaussian process which simulates turbulence from a white, Gaussian process requires non-linear filters. The introduction of non-linear filters to synthesize turbulence is a recent development (Reeves, 1969; Kurkowski, et al., 1971; Gerlach, et al., 1973). However, the non-linear models which have been developed suffer from a lack of consistency in terms of the observed, non-linear properties of boundary layer turbulence. Therefore, what is needed is a systematic methodology by which to introduce the observations of the non-linearity of atmospheric turbulence into the filtering method.

1.4 Structure of the Atmospheric Boundary Layer

For a steady, horizontally homogeneous mean flow in the boundary layer, sufficiently near the ground, the vertical variation of the turbulence fluxes is negligible (Blackadar and Tennekes, 1968); in particular

$$\tau(z)/\rho_o = - \overline{uw} = u_*^2 \qquad (1.4.1.)$$

and

$$H(z)/\rho_o \, c_p = \overline{w\theta} = - u_* \, T_* \qquad (1.4.2)$$

are independent of height. In (1.4.1) and (1.4.2), τ/ρ_o and $H(z)/\rho_o \, c_p$ are the specific momentum and heat fluxes respectively; ρ_o is the density of the air and c_p the specific heat at constant pressure.

Equations (1.4.1) and (1.4.2) also serve as definitions for the characteristic velocity, u_*, and temperature T_*. According to the hypothesis of Monin and Oboukhov (1954) the structure of the mean wind shear and temperature gradient (sufficiently near the ground so that inertial effects due to the earth's rotation are unimportant) can be derived on the basis of dimensional arguments. That is, the mean shear and temperature gradient are given by

$$\frac{\partial \bar{U}}{\partial z} = \frac{u_*}{\kappa z} \phi_m(z/L) \tag{1.4.3}$$

and

$$\frac{\partial \bar{\theta}}{\partial z} = \frac{T_*}{\kappa z} \phi_h(z/L) \tag{1.4.4}$$

where L, the Monin-Oboukhov length, is

$$L = \frac{u_*^2 T_o}{g \kappa T_*} \tag{1.4.5}$$

In (1.4.3) to (1.4.5), $\bar{U}$ is the mean wind speed, $\bar{\theta}$ the mean potential temperature, T_o the depth averaged boundary temperature, κ (a similarity parameter) is von Kármán's constant, and ϕ_m and ϕ_h are the similarity functions for the shear and the temperature gradient. It is convenient in what follows to define z/L by

$$\zeta = z/L \tag{1.4.6}$$

In fact, the Monin-Oboukhov hypothesis states that all statistics of the turbulence sufficiently near the ground, in diabatic situations, for ideal steady, horizontally homogeneous flows, become functions of ζ only, if velocities are scaled with u_*, temperatures by T_* and lengths by κz. Accordingly the moments M_i^n, of the probabilistic density function of the i^{th} turbulence velocity components are also functions of ζ,

$$\overline{u_i^n} = M_i^n(\zeta) \tag{1.4.7}$$

The spectral distribution, Φ_{ij}, of variance or covariance over the range of wave numbers, κ, for which there is any shear or buoyantly induced turbulence, becomes, under the appropriate scaling,

$$\frac{k\,\Phi_{ij}}{S_i S_j} = G_{ij}\,(f,\zeta) \tag{1.4.8}$$

In (1.4.8), S_i represents the appropriate scaling variable, u_* or T_*, and f, where

$$f = \kappa z\, k \tag{1.4.9}$$

represents a normalized wave number. The use of subscripts 1 through 3 assumes the standard meteorological usage (Lumley and Panofsky, 1964) and the subscript θ refers to temperature.

For scales, $f >> 1$, such that the turbulence becomes asymptotically independent of the details of the mechanisms generating the turbulence

(Tennekes and Lumley, 1972, Chapter 8), the spectra, G_{ii} are similar, in the sense of dimensional analysis, under the hypothesis of Kolmogorov (1941), so that

$$G_{ii}(f) = \alpha_i \, \phi_{ii}(\zeta) \, f^{-2/3} \tag{1.4.10}$$

Specifically, for a sufficiently large Reynolds number, defined by

$$\text{Rey} = \kappa z \, u_*/\nu \tag{1.4.11}$$

where ν is the kinematic viscosity,

$$\phi_{11} = \phi_{22} = \phi_{33} = \phi_\varepsilon^{2/3}(\zeta) \tag{1.4.12}$$

and

$$\phi_{\theta\theta} = \phi_\chi(\zeta) \, \phi_\varepsilon^{-1/3}(\zeta) \tag{1.4.13}$$

The functions ϕ_χ and ϕ_ε represent the similarity functions under Monin-Oboukhov scaling, for the dissipation rates of kinetic energy, ε, and temperature variance, χ, and are defined by

$$\phi_\varepsilon(\zeta) = \kappa z \varepsilon / u_*^3 \tag{1.4.14}$$

and

$$\phi_\chi(\zeta) = \kappa z \chi / u_* T_*^2 \tag{1.4.15}$$

A considerable effort has been made by many investigators to identify the similarity structure, both of the low order moments of turbulence near the ground, under diabatic conditions, and of the spectral and co-spectral forms. An excellent summary and review is provided by several authors in a monograph edited by Haugen (1973), and will not be duplicated here. A summary of empirical forms for ϕ_m, ϕ_h, ϕ_ε, ϕ_χ, and M_i^n, as functions of ζ, are given in Appendix A, as well as empirical spectra and co-spectra, G_{ij}, as functions of ζ and f.

In order to utilize the similarity relationships of Monin and Oboukhov, it is necessary to estimate the factors u_* and T_* by an independent method. For a steady, horizontally homogeneous boundary layer, Kazanski and Monin (1961) derived the resistance laws

$$\ln(G/fz_o) = B + \ln (G/u_*) + (\kappa^2 G^2/u_*^2 - A^2)^{1/2} \qquad (1.4.16)$$

and

$$\sin \alpha = - \frac{A}{\kappa} \frac{u_*}{G} \qquad (1.4.17)$$

In (1.4.16) and (1.4.17), G is the geostrophic wind modulus and f is the Coriolis parameter (= $2\Omega \sin \psi$ where Ω is the earth's angular velocity and ψ is latitude), α is the angle between the direction of the surface stress and the geostrophic velocity, and z_o is the surface roughness. The functions, A and B, are similarity functions, which for diabatic conditions are hypothesized to be universal in the stability parameter, μ given by

$$\mu = h/L \tag{1.4.18}$$

where h is the so-called Ekman height

$$h = \kappa u_*/f \tag{1.4.19}$$

characteristic of the depth of the boundary layer under neutral stratification. An analogous development by Zilitinkevich and Chalikov (1968) for the transfer of heat across a turbulent boundary layer is given by

$$\Delta\theta/T_* = P_o[\ln(u_*/f\ z_o) - C(\mu)] \tag{1.4.20}$$

where $\Delta\theta$ is defined as the potential temperature difference between the surface and the level where the flow is geostrophic, P_o is the turbulent Prandtl number ($\simeq 0.7$) under near-neutral conditions and C is a universal function of μ. From empirical formulations for $A(\mu)$, $B(\mu)$ and $C(\mu)$, (Kerman, 1974a), it is possible to construct algorithms for the momentum drag coefficient, u_*/G and the 'thermal drag' coefficient, $T_*/\Delta\theta$, as functions of the dimensionless parameters, Ro and S_g, given by

$$Ro = G/fz_o \tag{1.4.21}$$

and

$$S_g = g/T_o(\Delta\theta/Gf) \qquad (1.4.22)$$

Accordingly, u_* and T_* can be derived immediately given the external, controlling variables of the problem -- G, z_o, and $\Delta\theta$.

The combined similarity theories of Monin and Oboukhov and the resistance laws make it possible to estimate the turbulent statistics at a given height, z, in the constant flux layer, at a particular location and time, having estimated G, z_o and $\Delta\theta$.

It is emphasized here that since the basic meteorological dynamics, as conveyed by the similarity theories, are self-consistent with the empirical representations (such as those given in Appendix A), it is pointless to introduce additional variables through ad hoc models of the spectra. That is, in models such as von Kármán's (Teinissen, 1970, p. 40) the scaling lengths there are not linked dynamically to similarity theories. In fact, it is often observed that a form other than the von Kármán spectral form, may be appropriate for representing the large scale structure of the spectrum. For these reasons, only spectra based on direct observations are considered in the models developed here.

2.0 FORMULATION OF THE SIMULATION MODEL

In order to extend the methods of simulating turbulence to processes with rather general spectral and non-Gaussian characteristics, it is necessary to develop a suitable mathematical structure, explore some of its properties, and determine whether its application is practical. This chapter outlines a particular functional representation for turbulence that allows for a systematic development based on a Gaussian process. We also consider here the method of spectral factorization for calculating a filter for those cases in which a linear sub-process can be identified.

The concept of a functional representation (Wiener, 1958) of turbulence arises from a picture of a turbulent velocity field as the result of random impulses. The process of generating a response to a stimulus is equivalent to a black-box process. The triplet of input, black-box. and response are the characteristic elements of a mathematical identify called a system. It is the intent of this research to consolidate and extend present system representations which use random pulses to produce a response resembling turbulence.

2.1 Functional Representation of Turbulence

The mathematical formulation used here for analysis of a system is based on the original work of Volterra (1930). A functional transformation is defined as the operation which transforms a function to a number -- an operation such as a definite integral. In the application of functionals to systems, the black-box is modeled by the functional

transformation which maps the temporal function representing the evolved history of the input to the present (single) value of the output. If an input function, $\xi(t)$, as evolved up to time t, is represented as a point in a space of functions, then the functional transformation maps the input into a point in a new space of output functions, say, $y(t)$. As $\xi(t)$ varies with the parameter, t, then the transformation will map $\xi(t)$ to a varying output, $y(t)$. Volterra showed that a continuous functional (transformation) could be uniquely approximated by a polynomial series of functionals given by

$$y(t) = K^0 + \int_{-\infty}^{\infty} K^1(t;t_1)\, \xi(t_1)dt_1 + \int_{-\infty}^{\infty}\int_{-\infty}^{\infty} K^2(t;t_1,t_2)\, \xi(t_1)\, \xi(t_2)\, dt_1\, dt_2 + \int_{-\infty}^{\infty}\int_{-\infty}^{\infty}\int_{-\infty}^{\infty} K^3(t;t_1,t_2,t_3)\, \xi(t_1)\, \xi(t_2)\, \xi(t_3)\, dt_1\, dt_2\, dt_3 + \ldots \tag{2.1.1}$$

(All integrals hereafter will have a range $(-\infty, \infty)$ unless otherwise specified.) The functions, K^i, are referred to as the kernels of the representation. A physically realizable situation, in which the transformation of any signal can act only on the past of an input, requires that

$$K^i(t;t_1,t_2,\ldots t_i) = 0 \qquad (t_i > t) \tag{2.1.2}$$

For a horizonally homogeneous turbulent flow whose statistics are advected according to Taylor's hypothesis, the turbulent process is also temporally invariant, or stationary, so that

$$K^i(t;t_1,t_2,\ldots t_1) = K^i(t-t_1,t-t_2,\ldots,t-t_i) \qquad (2.1.3)$$

In addition to determining the transformation of the input to the output functions, the kernels also determine the statistics of the output from those of the input. A simple, linear, temporally invariant system is represented by

$$y(t) = \int K^1(t-\tau)\ \xi(\tau)\ d\tau \qquad (2.1.4)$$

For convenience, we take the input to have zero mean ($\bar{x} = 0$).

Formation of statistical averages of the input and output leads to

$$\overline{y(t)\ y(t+\tau)} = R_{yy}(\tau) = \iint K^1(\tau_1)\ \overline{R_{\xi\xi}(\tau+\tau_1+\tau_2)}\ d\tau_1\ d\tau_2 \qquad (2.1.5)$$

and

$$\overline{y(t)\ \xi(t+\tau)} = R_{y\xi}(\tau) = \int K^1(T_1)\ \overline{R_{\xi\xi}(\tau-T_1)}\ dT_1 \quad , \qquad (2.1.6)$$

In (2.1.5), the output variance, R_{yy}, is represented as a transformation of the input variance, $R_{\xi\xi}$. The utility of using a white-noise input process, defined by

$$R_{\xi\xi}(\tau) = \delta(\tau) \qquad (2.1.7)$$

(δ is the Dirac delta function) is shown by substituting (2.1.7) in (2.1.5) and (2.1.6) to form

$$R_{yy}(\tau) = \int K^1(\tau_1)\, K^1(\tau-\tau_1)\, d\tau_1 \tag{2.1.8}$$

$$R_{y\xi}(\tau) = K^1(\tau) \tag{2.1.9}$$

The kernel, K^1, is therefore derivable by cross-correlating the input and output, and the kernels for the functional transformation of the white noise process share variance properties with the output.

It is important to note that while the above technique of determining the kernel of a linear system is used in many fields of engineering, here the supposition that both the input pulse and output response are available for correlation is not valid. The input forcing mechanism, as represented by the functional transformation (2.1.1), is internal to the fluid and not measurable. This makes the problem of determining the kernels in practice more complicated than the usual situation where both input and output are available simultaneously.

The significance of (2.1.8) is better seen in a spectral representation. Consider a Fourier transform defined by

$$f(t) = \frac{1}{2\pi} \int \hat{f}(\omega) e^{-i\omega t}\, d\omega \tag{2.1.10}$$

applied to (2.1.4). The result is given by

$$\hat{y}(\omega) = \hat{K}^1(\omega)\, \hat{\xi}(\omega) \tag{2.1.11}$$

which for the white-noise property

$$|\hat{\xi}|^2 = 1 \tag{2.1.12}$$

becomes

$$|\hat{y}|^2 = |\hat{K}^1|^2 \tag{2.1.13}$$

Thus the spectrum of the kernel is equal to that of the output for a linear system. Equation (2.1.13) forms the basis for many of the applications of the linear simulation of turbulence. A major question remaining, then, is how to determine K^1, given that its spectrum is that of the turbulence. A recent computational development is explored in Section 2.4 to determine K^1 for a relatively general class of spectra.

An important consideration in developing a simulation model is the ease of application. Parente (1970) has outlined the method of treating interacting systems. In most applications of turbulence models, the simulated turbulence is used in turn to stimulate a system representing a structure or perhaps another geophysical process. By the algebra of functionals (Parente), the final response statistics are derivable from those of the turbulence without recourse to actually generating simulated realizations. Of course, such a consideration is basic to linear filtering, but it is useful to note that its application is also valid with non-linear simulations such as discussed in Chapter 5.0.

As shown by Barrett (1963), the functional expansion of (2.1.1) can be made more efficient by an orthogonalization of the basis, or

input process, $\xi(t)$. The question is what process to use for maximum efficiency. The philosophy of this study is that in cases where the turbulent process may be considered nearly Gaussian, the obvious basis to use to expand the flow field is one based on orthogonalization relative to the Gaussian process -- the Hermite polynomials. Some questions about the conditions under which such an expression is likely to be successful are discussed next.

2.2 Probabilistic Structure of Surface Turbulence

For many years (Batchelor, 1953) the one-point turbulent velocity probability density function (p.d.f.) was observed to be indistinguishable from a Gaussian distribution. Stewart (1951) was the first to establish the pronounced non-Gaussian structure of turbulence with decreasing scale. Further investigations of the moment distributions over scale (Frenkiel and Klebanoff, 1967) confirm the converse of Stewart's work -- that there is a quasi-Gaussian structure at scales commensurate with the energy containing sizes.

Arguments concerning Gaussian structure are not extendable to the joint p.d.f. of two velocities at neighboring points because of the non-linear effects (Batchelor, Chapter VIII) which led to an inertial transfer of energy across wavenumbers. Because non-linear interactions within the turbulence increase with decreasing scale up to the viscous limit, a resulting increase of non-Gaussian characteristics with decreasing scale is to be expected. The probability distribution of the dissipation rate

$$\varepsilon = 15\nu \left(\frac{\overline{\partial u}}{\partial x}\right)^2 \qquad (2.2.1)$$

for isotropic turbulence (or equivalently local accelerations) is a convenient measure of the non-linear (and non-Gaussian) structure over a wide wavenumber region of engineering concern. According to Kolmogorov (1962), Oboukhov (1962) and Grant et al. (1962), the equilibrium structure implied in Kolmogorov's original similarity result required a refinement to a more local, volume-averaged dissipation rate, $< \varepsilon >$. It has been suggested (Gurvich and Yaglom, 1967) that $< \varepsilon >$ has a log-normal distribution. This prediction has been disputed by Tennekes and Wyngaard (1972) and Gibson and Masiello (1971) on the basis of experimental data taken at a very large Reynolds number. At present, the only workable hypotheses on the probability structure appear to be empirical (Tennekes and Wyngaard, 1972; Frenkiel and Kelbanoff, 1967).

In summary, it is reasonable to attempt a simulation of the energy containing structure of surface layer turbulence in terms of a quasi-Gaussian process. The fact that the observed structure of the surface layer turbulent velocity field is nearly Gaussian (Appendix A), as expected by the preceding discussion, is encouraging for modeling purposes. However, from the discussions of the strongly non-linear spectral region, it is concluded that an expansion about a Gaussian process at scales much smaller than the energy generative region is limited.

2.3 Wiener-Hermite Functional Representation

The orthogonal functional Hermite polynomials based on input realizations, $\xi(t)$, drawn from a white, Gaussian, stationary process are (Barrett, 1963)

$$H_o(\xi) = 1 \tag{2.3.1}$$

$$H_1(t_1;\xi) = \xi(t_1) \tag{2.3.2}$$

$$H_2(t_1,t_2;\xi) = \xi(t_1)\,\xi(t_2) - \delta(t_1-t_2) \tag{2.3.3}$$

$$H_3(t_1,t_2,t_3;\xi) = \xi(t_1)\,\xi(t_2)\,\xi(t_3) - \xi(t_1)\,\delta(t_2-t_3) - \xi(t_2)\,\delta(t_3-t_1) - \xi(t_1)\,\delta(t_1-t_2) \tag{2.3.4}$$

The Wiener-Hermite (hereafter referred to W-H) representation of a velocity component, u(t), by a white, Gaussian, stationary process is given by

$$u(t) = \int K^1(t-t_1)\,H_1(t_1)\,dt_1 + \iint K^2(t-t_1,t-t_2)\,H_2(t_1,t_2)\,dt_1\,dt_2 + \iiint K^3(t-t_1,t-t_2,t-t_3)\,H_3(t_1,t_2,t_3)\,dt_1\,dt_2\,dt_3 + \ldots \tag{2.3.5}$$

where both input, $\xi(t)$, and output, u(t), are understood to have a mean of zero. An equivalent representation follows from a Fourier transformation (2.1.10) of (2.3.5)

$$\hat{u}(\omega) = \hat{K}^1(\omega)\,\hat{H}_1(\omega) + \int \hat{K}^2(\omega_1,\omega-\omega_1)\,\hat{H}_2(\omega_1,\omega-\omega_1)\,d\omega_1 + \ldots \tag{2.3.6}$$

The orthogonality conditions for the Hermite-polynomials given by

$$\overline{H_o(t_1;\xi)\ H_o(t_2;\xi)} = 1 \tag{2.3.7}$$

$$\overline{H_1(t_1;\xi)\ H_2(t_2;\xi)} = \delta(t_1-t_2) \tag{2.3.8}$$

$$\overline{H_2(t_1,t_2;\xi)\ H_2(t_3,t_4;\xi)} = \delta(t_1-t_3)\ \delta(t_2-t_4) + \delta(t_1-t_4)\ \delta(t_2-t_3) \tag{2.3.9}$$

or, their Fourier transformed equivalent,

$$\overline{\hat{H}_1(\omega_1)\ \hat{H}_1(\omega_2)} = \delta(\omega_1+\omega_2) \tag{2.3.10}$$

$$\overline{\hat{H}_2(\omega_1,\omega_2)\ \hat{H}_2(\omega_3,\omega_4)} = \delta(\omega_1+\omega_3)\ \delta(\omega_2+\omega_4) + \delta(\omega_1+\omega_4)\ \delta(\omega_2+\omega_3) \tag{2.3.11}$$

considerably reduce the complexity of computing the output statistics. For example, by utilizing the orthogonality conditions, the expression for the spectral density of the u-process, ϕ_u, defined by

$$\overline{\hat{u}(\omega_1)\ \hat{u}(\omega_2)} = \phi_u(\omega_1)\ \delta(\omega_1+\omega_2) \tag{2.3.12}$$

is given by

$$\phi_u(\omega) = |\hat{K}^1(\omega)|^2 + \frac{1}{\pi}\int |\hat{K}^2(\omega_1,\omega-\omega_1)|^2 \, d\omega_1 + \ldots \qquad (2.3.13)$$

Equation (2.3.13) expresses the decomposition of the spectrum of the process into a sequence of positive definite contributions. The positive definiteness of the W-H representation is a desirable feature of the method. Not every moment expansion scheme (Ogura, 1963; Deardorff, 1972b) can guarantee such a property, and in this respect these other methods contain basic inconsistencies. The implicit assumption made in using the W-H representation as a representation of nearly Gaussian process is that the contributions to the spectrum will tend to concentrate the variance in the low order terms of (2.3.13). Because the Hermite polynomials, and hence individual Hermite functionals of the expansion (2.3.5) and (2.3.6) are orthogonal, the truncation

$$K^i = 0 \qquad i \geq 2 \qquad (2.3.14)$$

is consistent with the well-known result for linear white, Gaussian forcing

$$\phi(\omega) = |\hat{K}^1(\omega)|^2 \qquad (2.3.15)$$

Successive moment expansions arising from (2.3.5) or (2.3.6) become progressively more complicated. For example, the skewness (or bi-spectrum) -- truncated to second order terms is given by

$$\overline{\hat{u}(\omega_1)\,\hat{u}(\omega_2)\,\hat{u}^*(\omega_1+\omega_2)} = 4\pi\,\hat{K}^1(\omega_1)\,\{\hat{K}^1(\omega_2)\,\hat{K}^{2^*}(\omega_1,\omega_2)$$

$$+\,\hat{K}^1(\omega_1)\,\hat{K}^{1^*}(\omega_1+\omega_2)\,\hat{K}^2(-\omega_1,\omega_1+\omega_2)$$

$$+\,\hat{K}^2(-\omega_1,\omega_1+\omega_2)\,\hat{K}^1(\omega_1)\,\hat{K}^{1^*}(\omega_1+\omega_2) \qquad (2.3.16)$$

$$+\,\frac{1}{\pi}\int[\hat{K}^2(\omega_1-p,p)\,\hat{K}^2(\omega_1+\omega_2-p,p-\omega_1)\,\hat{K}^{2^*}(p,\omega_1+\omega_2-p)$$

$$+\,\hat{K}^2(\omega_2-p,p)\,\hat{K}^2(\omega_1+\omega_2-p,p-\omega_2)\,\hat{K}^{2^*}(p,\omega_1+\omega_2-p)]\}dp\ +\ \ldots$$

Equation (2.3.16) indicates several other features of the W-H representation. In general, a description of turbulence with an infinity of moments is equivalent to a description with an infinity of kernels. Also higher moments representing the non-Gaussian structure are characterized by interactions between the K^i, or equivalently among a hierarchy of non-linearities. It is possible, at least in principle, to recover one set of statistics from another by solving the (infinite) set of coupled integral equations.

Some simplification is obviously needed. The truncation of the W-H expansion is yet another case in which the closure problem of turbulence must be faced. Attempts to determine the kernels dynamically (Meecham and Siegel, 1964) have been shown to be inappropriate (Orszag and Bissonnette, 1967). Attempts to produce the equivalent of a stimulation technique (George, 1959; Dutton, 1970) and correlate the input and output are not applicable. The method of Robinson (1967a,b) based on Wiener's original work as a method of determining the kernels of a linear (or

equivalent linear) system, by predictive decomposition is unwieldly and time consuming.

For a W-H representation of a nearly Gaussian process, where the non-linearities are weak, it is advantageous to represent higher order kernels in terms of lower order kernels (Chapter 5.0). The result is an expansion about linearity, and the determination of the kernels reduces to calculating just K^1. The next section outlines a method of solving for K^1 for a generalized class of spectra which is compact and computationally efficient.

2.4 Spectral Factorization

As a demonstration of the baaic features of spectral factorization, consider the first order linear system driven by white noise defined by the differential equation

$$\frac{dy(t)}{dt} + T^{-1} y(t) = \xi(t) \qquad (2.4.1)$$

where y(t) is the response to the white noise $\xi(t)$, and T characterizes the response time. For convenience, let us scale the problem so that T = 1. This equation is often employed (for example, Skelton, 1968) to describe aircraft response to turbulence. The solution of (2.4.1.) is given by

$$y(t) = \int_0^\infty e^{-t_1} \xi(t-t_1)\, dt_1 \qquad (2.4.2)$$

The kernel, K^1, is given by e^{-t}, for $t > 0$. The Fourier transform of (2.4.1) is

$$\hat{y}(i\omega-1) = \hat{\xi} \tag{2.4.3}$$

or, from (2.1.11)

$$\hat{K}^1(\omega) = (i\omega-1)^{-1} \tag{2.4.4}$$

The spectrum follows from (2.4.4) as

$$\begin{aligned} \phi_y(\omega) &= \overline{\hat{y}\,\hat{y}^*} = \hat{K}^1\,\hat{K}^{1*} \\ &= (i\omega+1)^{-1}\,(-i\omega+1)^{-1} \\ &= (\omega^2+1)^{-1} \end{aligned} \tag{2.4.5}$$

The spectral factorization problem is the inverse problem. Given the spectrum, ϕ_y, and the fact it was derived from a white, Gaussian stationary process, find $\hat{K}^1$ and K^1. In the above example the spectral factors, $1+i\omega$ and $i-i\omega$, are well-known and derivable analytically in several ways. In fact, applications with this spectrum (often referred to as a Dryden spectrum) have been made simply to utilize the known spectral factors and simple form of the kernel (even though it is known that the turbulence spectrum varies as $\omega^{-5/3}$. Such an assumption is useful because the analytical determination of the factors of other spectra, such as von Kármán's spectrum, is prohibitive.

However finding $\hat{K}^1$ from ϕ_y is not a unique process, as the problem is stated above. There are an infinity of functions, y(t), which one could study, either by observation or simulation which would have the property

$$\overline{\hat{y}\,\hat{y}^*} = \hat{K}^1\,\hat{K}^{1*} = \phi_y \tag{2.4.6}$$

which is the only defining property of $\hat{K}^1$ given. It is necessary therefore to distinguish $\hat{K}^1$ from any $\hat{y}$ which has the same spectrum.

As a demonstration of the defining characteristics of $\hat{K}^1$ and K^1 consider a simpler problem where the input is a single pulse,

$$\xi(t) = \delta(t) \tag{2.4.7}$$

From (2.4.2) the output response is

$$y(t) = K^1(t) \qquad (t > 0) \tag{2.4.8}$$

that is, the kernel function is the response for a single pulse. (Consequently, K^1 is referred to, in what follows, as a kernel or a response function.) The function, $K^1(t)$, of (2.4.8) is, from (2.4.2),

$$\begin{aligned} K^1(t) &= e^{-t} \qquad t \geq 0 \\ &= 0 \qquad\quad t < 0 \end{aligned} \tag{2.4.9}$$

so that for a pulse ($\delta(t)$) at $t = 0$, the response is instantaneously at its maximum after the impulse begins. This property is referred to as the minimum phase or delay characteristic, because the modeled physical system responds with the minimum possible delay to a change in the input. Physically, of course, a finite delay would be required before the system achieved its maximum response. It is noted that the modeled process (2.4.1) is free from frictional effects which intuitively we would expect to delay the initial response.

The spectral factorization process using the minimum delay criterion was also shown by Bode and Shannon (1950) to be equivalent to determining a function with a given modulus (spectrum) with zeroes confined to one half of the complex plane. The general factorization problem was solved by Kolmogorov and is discussed in detail by Doob (1953).

In what follows, the development is heuristic. Also, because the remaining development and computations will necessarily be in discrete, tabulated form, the formulation is given in an equivalent, discrete representation. That is, $\hat{K}$ (dropping the super-script 1 for convenience) is re-defined as

$$\hat{K}(\omega) = \sum_{t=0}^{\infty} k_t \, e^{i\omega t} \tag{2.4.10}$$

where k_i is the kernel tabulated over the index t and the summation limits reflect the condition that

$$k_i = 0 \qquad i < 0 \tag{2.4.11}$$

The phase characteristic, $H(\omega)$, of the Fourier transform of the kernel, is defined by

$$\hat{K}(\omega) = \phi^{1/2}(\omega)\, e^{i\Theta(\omega)} \tag{2.4.12}$$

Consider a Fourier transformation of the logarithm of $\hat{K}$, given by

$$\begin{aligned} \ln \hat{K} &= \sum_{t=0}^{\infty} L_t\, e^{i\omega t} \\ &= L_o + \sum_{t=1}^{\infty} L_t \cos \omega t + i \sum_{t=1}^{\infty} L_t \sin \omega t \end{aligned} \tag{2.4.13}$$

The one-sided nature of (2.4.13) results from the equivalence of the physical realizability condition on K (2.4.11) and the lack of poles in the lower half plane (complex) of frequency (Robinson, 1967a). The integration (2.4.13) is equivalent to evaluating singularities in the upper half plane only. The Fourier transform of $\ln \phi^{1/2}$ is given by

$$\ln \phi^{1/2} = \alpha_o + 2 \sum_{t=1}^{\infty} \alpha_t \cos \omega t \tag{2.4.14}$$

where the symmetric nature of the spectrum alters the range of summation. Accordingly, the coefficients, α, are derived from the inverse transform of $\ln \phi^{1/2}$,

$$\alpha_t = \frac{1}{2\pi} \int_{-\pi}^{\pi} \cos \omega t \ln \phi^{1/2}(\omega)\, d\omega \tag{2.4.15}$$

From (2.4.15), by forming logarithms of both sides, we have

$$\log \hat{K}(\omega) = L_o + \sum_{t=1}^{\infty} L_t \cos \omega t + i \sum_{t=1}^{\infty} L_t \sin \omega t$$

$$= \alpha_o + 2 \sum_{t=1}^{\infty} \alpha_t \cos \omega t + i\theta(\omega) \tag{2.4.16}$$

By equating coefficients in cos ωt and sin ωt we are led to

$$L_o = \alpha_o \tag{2.4.17}$$

$$L_t = 2\alpha_t \qquad \text{for } t > 0 \tag{2.4.18}$$

The phase $\theta(\omega)$ in (2.4.12) essentially selects a function $\hat{K}$ with no singularities in the lower half plane. The particular phase relationship is given by

$$\theta(\omega) = \sum_{t=1}^{\infty} L_t \sin \omega t$$

$$= 2 \sum_{t=1}^{\infty} \alpha_t \sin \omega t \tag{2.4.19}$$

Equation (2.4.19) is the essential result of this section. The analytical problem of spectral factorization is now complete because the phase characteristic that distinguishes the kernel from any other function with spectrum ϕ can be computed in terms of the spectrum itself. This result is clear if we substitute (2.4.15) into (2.4.19) to produce

$$\theta(\omega) = \frac{2}{\pi} \sum_{t=1}^{\infty} \sin \omega t \int_0^{\pi} \cos \omega_1 t \, \ln \phi^{1/2} (\omega_1) \, d\omega_1 \tag{2.4.20}$$

The class of spectra to which such an operation will apply depends on whether the spectrum obeys the Paley-Wiener condition

$$\int_{-\infty}^{\infty} \frac{\ln \phi(\omega)}{(1+\omega^2)} d\omega > -\infty \qquad (2.4.21)$$

This constraint is discussed in Appendix B as it relates to numerical approximations.

Katzenelson and Gould (1962, 1965) have described a method of extending the spectral factorization method to the evaluation of non-linear kernels of a functional representation. Their method involves the successive minimization of error between a sampled realization and the output from an n^{th} order representation in order to determine the optimum n+1 kernel. Several hypotheses implicit in their approach are not valid in the problem here. First, the assumption that there is a freedom to generate an output realization of turbulence at will, is not appropriate. Second, the higher order spectra (bispectra, ...) which are needed in Katzenelson and Gould's method are not yet available except in very tentative form (Elderkin et al., 1972). Also there is no guarantee that these higher order spectra will obey the factorable properties required by the technique.

We now move to the implementation of the mathematical development.

3.0 LINEAR REPRESENTATION OF UNI-COMPONENT TURBULENCE

In this chapter, linear models of a single component of turbulence that are consistent with surface layer similarity are considered and extended to generalized spectral forms using spectral factorization. Because the response functions or kernels are a relatively novel concept in describing the structure of atmospheric turbulence, it is interesting to study their form under varying meteorological conditions. Properties derived from the response function, including measures of the predictability and memory of the model turbulence also are examined. The discussion of this chapter will be limited to the vertical velocity component, partly for convenience and partly because of its importance in aeronautical response problems.

3.1 Model of the Vertical Velocity

The importance of the vertical velocity spectra, both in modeling the response of aircraft to turbulence and in studying the vertical flux of momentum and heat near the earth's surface, is indicated by the availability of empirical estimates of its spectral form. Busch and Panofsky (1968) have approximated the w spectra (normalized by u_*^2) by a form

$$f\, G_w(f) = \frac{A_w f}{1+B_w f^{5/3}} \qquad (3.1.1)$$

based on data drawn from several sites (f is defined in (1.4.9)). They note that at low wave numbers, $f < 1$, their empirical form is an improvement over that suggested by Pasquill and Butler (1964),

$$f\,G_w(f) = \frac{A_w f}{(1+B_w\,f)^{5/3}} \tag{3.1.2}$$

Confirmation of the Busch-Panofsky form is supplied by Kaimal et al. (1972) based on the Kansas data. However, the estimates for (A_w,B_w), for neutral stability, vary between the estimates of Kaimal (1.0,1.5) and Busch and Panofsky (1.5,2.7). The variation in these coefficients is indicative of the accuracy that can be expected in estimating characteristics associated with spectra, such as variance, length scale, dissipation, and response functions. All empirical spectra behave asymptotically as $f^{-5/3}$, which is characteristic of the Kolmogorov region ($1 \ll f \ll f_{KOL}$).

Another spectral form (Appendix A)

$$f\,G_w(f) = \frac{A_w\,\phi_\varepsilon^{2/3}\,f^{2/3}}{1+(B_w\,f)^{4/3}} \tag{3.1.3}$$

is convenient mathematically but does not have the usual front slope of +1 found by observations. The convenience of (3.1.3) lies in its form after a transformation of variables

$$f' \sim f^{2/3} \tag{3.1.4}$$

From the invariance of energy with a change of variables

$$f\,G_w = f'\,G'_w \tag{3.1.5}$$

we are led to

$$f' G' \sim \frac{f'}{1+(B_w' f')^2} \tag{3.1.6}$$

which is a form familiar in filtering problems (Section 2.4) and which has a well-defined kernel for a linear response to white noise given by

$$\begin{aligned} K^1(x') &= \exp - x'/B_w' \qquad x' > 0 \\ &= 0 \qquad\qquad\quad x' < 0 \end{aligned} \tag{3.1.7}$$

Because (3.1.4) is related to a transformation of the space variables

$$x' \sim x^{2/3} \tag{3.1.8}$$

the general form of the response function will be

$$K^1(x) = \gamma_w^{1/2} \exp -(x/B_w)^{2/3} H(x/B_w) \tag{3.1.9}$$

where the function H carries the effect of the linear Fourier transformation involved in factoring (3.1.6) to obtain (3.1.9). The coefficient γ_w can be shown to be

$$\begin{aligned} \gamma_w &= A_w \phi_\varepsilon^{2/3} B_w^{-2/3} \\ &= \frac{4}{3\pi} \overline{\tilde{w}^2} \end{aligned} \tag{3.1.10}$$

The response function of any empirical formulation for w spectra, to the extent that it approximates (3.1.3), can be expected to vary

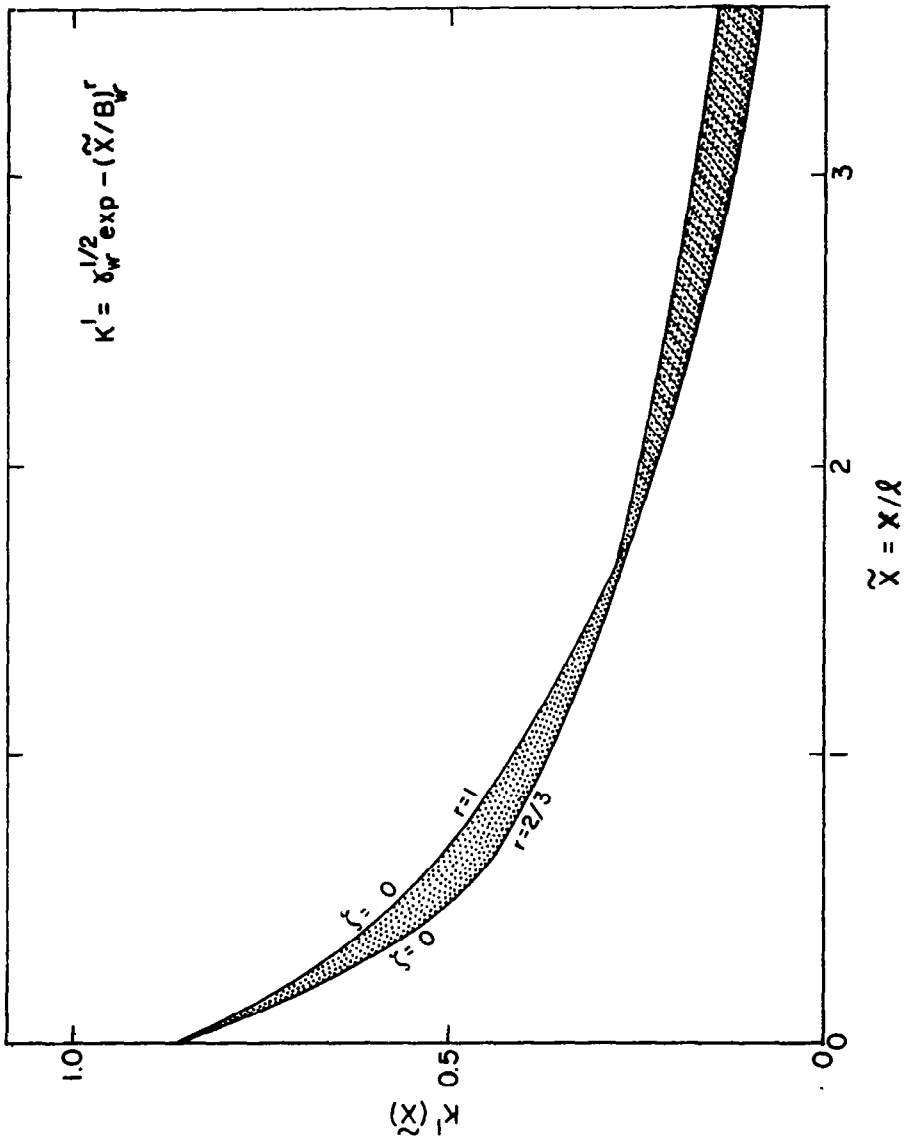

Figure 3.1. Comparison of response function (r = 1 and r = 2/3) for neutral stability.

according to (3.1.9). Therefore it is useful to examine the basic structure of response functions in (3.1.9) for H = 1.

3.1.1 Analytical Characteristics of Response Structure. The form of the approximate analytical kernel is shown in Figure 3.1, both as a function of scale distance and of stability, where the parameter ζ is defined in (1.4.6). The variation of $\gamma_w^{1/2}(\zeta)$ and $B_w(\zeta)$ is based on the empirical relationships of Appendix A and is given in Figure 3.2. The general feature of the solution for K^1 is a monotonic decrease of the response with distance (in the direction from which the turbulence is advected). For a given longitudinal separation x, as the height (and scale length, ℓ) increase, $\tilde{x} = x/\ell$ decreases. From Figure 3.1, a decrease in $\tilde{x}$ is equivalent to an increased response. The kernel for separations less than $\ell(\tilde{x} < 1)$ decrease faster than $\exp(-\tilde{x})$ but decreases less rapidly than the response of a simple linear oscillation system for $\tilde{x} > 1$. That is, the approximate analytical solution, $\exp(-\tilde{x}^{2/3})$, indicates a decrease in the response for small lags (relative to ℓ/u_*), or equivalently, indicates that the filter will give less weight to the more immediate past. On the other hand, the response for large lags will be greater than that for the common first order linear model.

The effects of stratification on the kernel, also given in Figure 3.1, are two-fold. First, the initial response ($\tilde{x} = 0$) varies with stability, and is a minimum in neutral conditions. Second, the rate of decay of response decreases with decreasing stability. The minimum initial response is a reflection of the minimum in $\overline{\tilde{w}^2}$ at $\zeta = 0$ (Figure A.3). The rate of decrease of K^1 is determined by B_w.

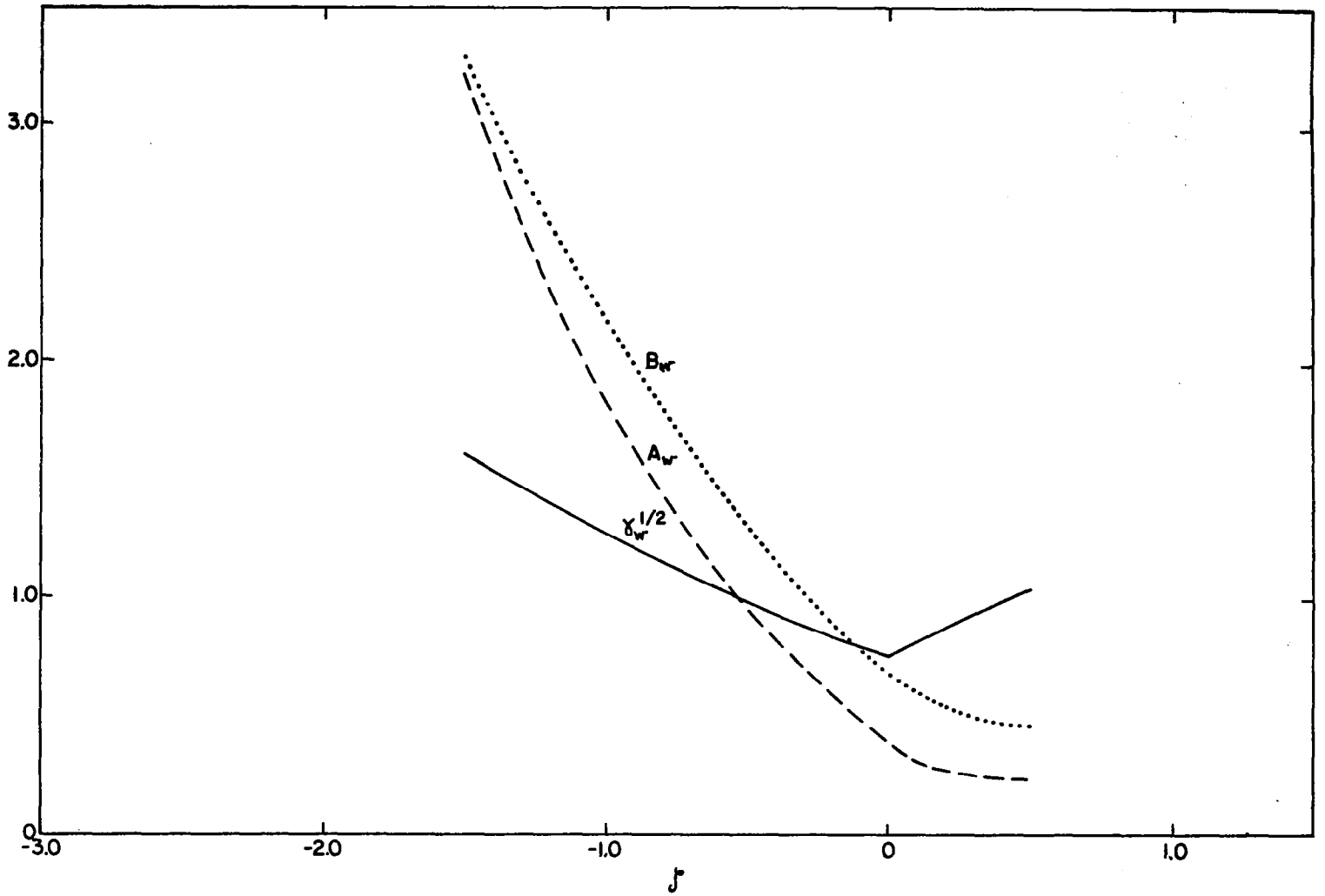

Figure 3.2. Variation with thermal stability of parameters of analytical approximation to linear response function.

For increasing instability (Figure 3.2), B_w increases as more energy is introduced at larger f (Lumley and Panofsky, Chapter 5). Therefore, from (3.1.9), the response at a given $\tilde{x}$ increases.

Another concept which can be demonstrated for the simple analytical approximation is the memory of the system. Intuitively, memory may be considered as the integrated effect of past stimuli. For convenience, it is desirable to compare the memory of the process representing turbulence with that of a simple linear first order process with the same variance. Memory is defined tentatively as

$$\begin{aligned} \text{Mem} &= \{\int_0^\infty K^1(y)\ dy\} \ / \ \{K^1(0) \int_o^\infty \exp(-y)dy\} \\ &= \frac{1}{K^1(0)} \int_0^\infty K^1(y)\ dy \end{aligned} \tag{3.1.12}$$

It is noted that this definition is only useful if $K^1(0) \neq 0$. For the kernel (3.1.9), Mem $\simeq$ 1.33, which indicates a net increase in memory of about 0.33 relative to a simple first order process. For a slightly different version of the memory concept, given by

$$\text{Mem}(\tilde{x}) = \frac{1}{K^1(0)} \int_0^{\tilde{x}} K^1(y)\ dy \tag{3.1.13}$$

the memory as a function of distance or time from a stimulus is itself a function of scale. From Figure 3.1, $\text{Mem}(\tilde{x}) < 1$, for $\tilde{x} > 1$. Therefore the increased total memory which is greater than unity ($\text{Mem}(\infty) = 1.33$), results from the large scale structure of K^1.

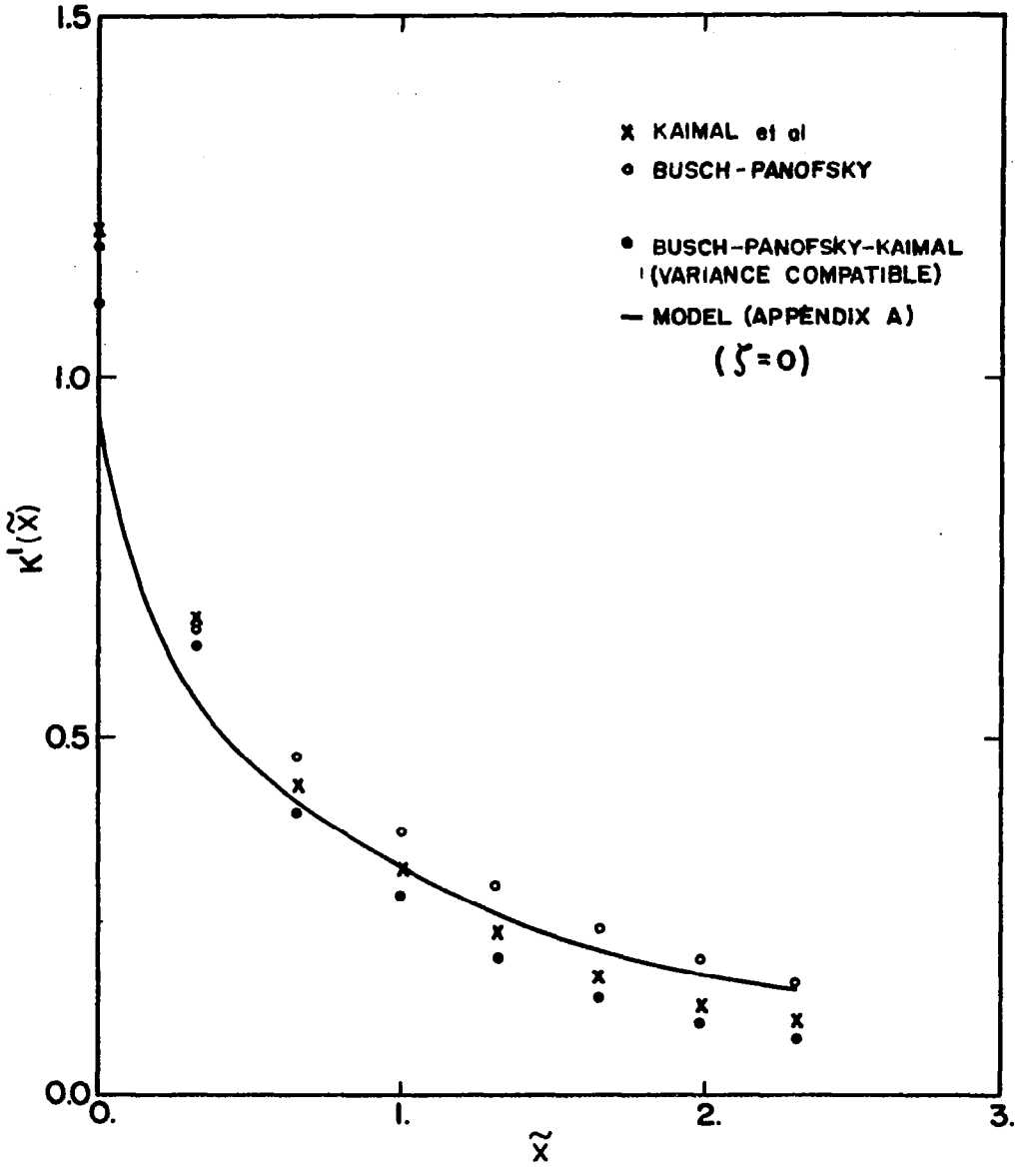

Figure 3.3. Response functions for various empirical spectra.

This completes the discussion of the general properties of the approximate analytical structure of K^1. It remains to contrast this intuitive and preliminary discussion later with more exact numerical solutions for a variety of empirical spectra.

3.1.2 Kernels for Different Empirical Spectra. The spectral factorization procedure was applied numerically to some of the empirical spectral representations of Busch and Panofsky, Kaimal et al., and Pasquill and Butler as well as the spectrum discussed in Appendix A and Section 3.1.1. The objective was to determine the range of response estimates which could be expected from variations in empirical representations of the w spectra. This variability provides a realistic estimate of accuracy against which to contrast other sources of variability, such as arise in the parameterization of the thermal stability.

The kernel K^1 obtained by factorization of some of the empirical spectra are given in Figure 3.3. Also shown are the results for K^1 arising from the common spectral form used by Busch and Panofsky and Kaimal et al., but with A_w and B_w altered for compatability with the variance and Kolmogorov range structure (Appendix A). The final kernel plotted in Figure 3.3, and termed "model", corresponds to the spectral form $f^{-1/3}(1+B_w f)^{4/3})^{-1}$, with coefficients chosen for compatability with the variance and inertial range structure.

The response function, as expected, is monotonic and similar to the basic $\exp(-\tilde{x}^{2/3})$ form of Section 3.1.1. It is noted that estimates of K^1 using the Busch-Panofsky formulation differ significantly with increasing scale from either of the formulations based on the Kansas

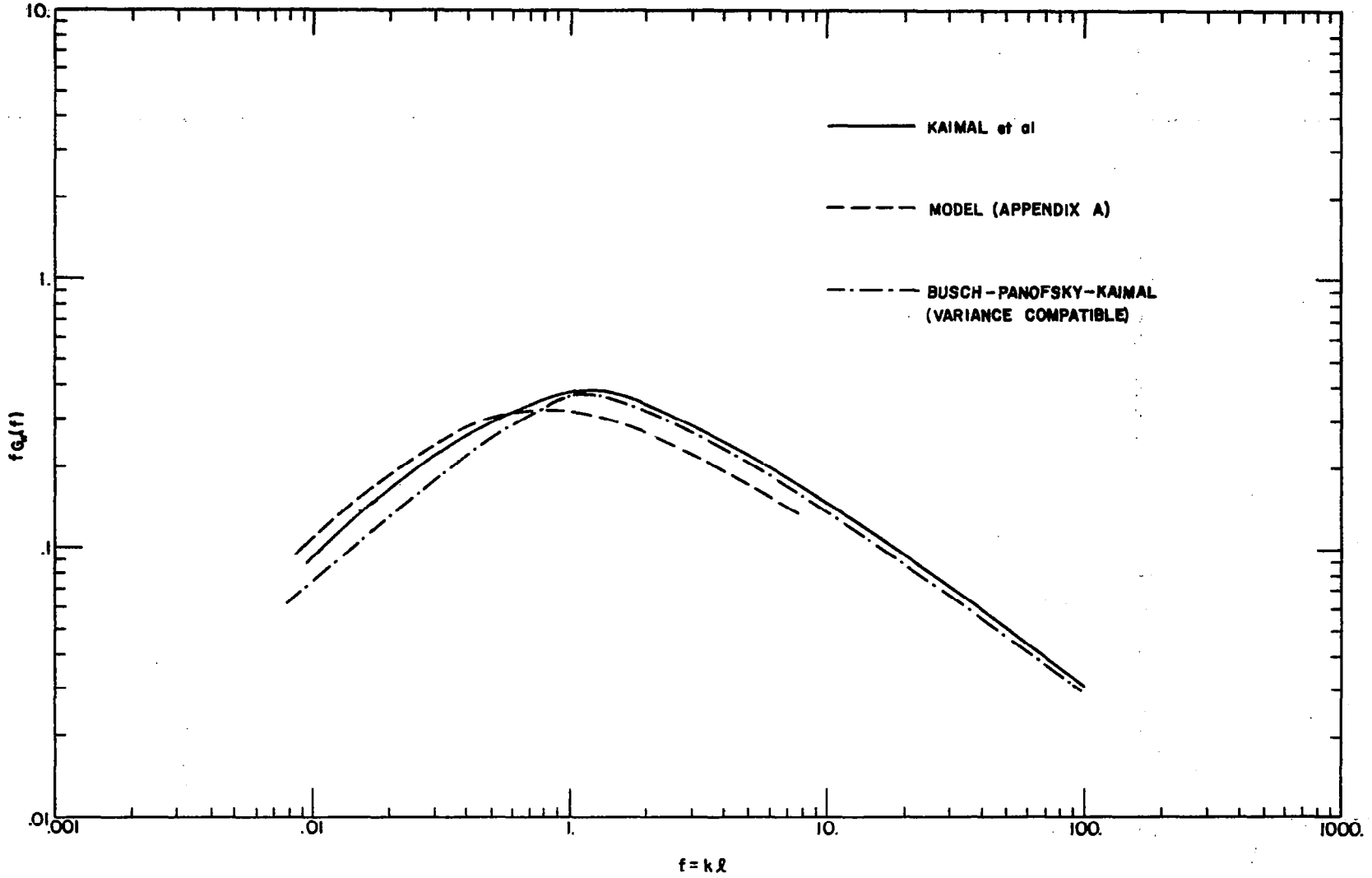

Figure 3.4. Comparison of various empirical spectra.

data. The response based on the Kansas data for $\tilde{x} > 1$ is not as large as the kernel derived from the Busch-Panofsky data. The variance compatible spectrum, based on the common mathematical form used by both Kaimal et al. and Busch and Panofsky, results in a response structure markedly different from the Busch-Panofsky form alone. It is concluded that the normalized variance characteristics of the data set drawn from the Kansas experiment and that used by Busch and Panofsky differ significantly.

The underlying reasons for this disparity are not clear, but may be attributed to some degree to the larger roughness characteristic of the Busch-Panofsky data set, or perhaps a difference in similarity involving the average structure of the large scale flows (Kerman, 1974b). Whatever the cause of the disparity in the form of K^1, the results indicate that a significant difference exists in the response representation at scales, $\tilde{x} > 1$, resulting from various experiments. From Figure 3.1, the estimated errors between the functional forms are about equivalent to an error of $\pm$ 0.25 in an estimate of ζ. The numerical estimate of the kernel corresponding to the model spectrum underestimates the small scale response and overestimates the large scale response. An examination of the different spectra factored to produce the response estimates (Figure 3.4) reveals the close relationship that exists between the relative distributions of variance of the spectra and the relative response structures. For spectra with additional variance at scales, $f < 1$, (for example, the analytical model spectrum) the result is an increased response at scales, $\tilde{x} > 1$, and vice versa.

The objective of this section was to compare and contrast filters arising from various empirical spectra. In summary, it is concluded that perceptible differences in the response structure occur according to the empirical representation of the spectra. These differences in turn are related to the relative spectral content between empirical formulation both for the large and small scale regions.

The response structure is next studied as a function of stratification.

3.1.3 Stratification Effects on Kernels. As discussed in Section 3.1.1, the function, K^1, could be described by two of its characteristics -- its initial response at $\tilde{x} = 0$, and its integral, or memory. The function $K^1(0)$ and its memory is displayed in Figure 3.5 as a function of ζ, for the particular model described in Appendix A. The calculations in the spectral factorization are performed with 128 points in the Fast Fourier Transform (FFT) algorithm. The response at $\tilde{x} = 0$ differs from that of Figure 3.2 because of the approximations made near f_{max} (Appendix B).

In Figure 3.5, the initial response increases with $|\zeta|$ and the memory increases monotonically with increasing instability. The response function implied in Figure 3.5 is equivalent to that shown in Figure 3.1. The response for a given $\tilde{x} > 0$ is less for stable stratification than for unstable stratification and a minimum for neutral stability. The structure of the response function, normalized by its initial value, also follows from qualitative consideration of the change in the spectra with stratification. While the variance, $\overline{\tilde{w}^2}$ (which in (3.1.12) determines the initial response) increases in

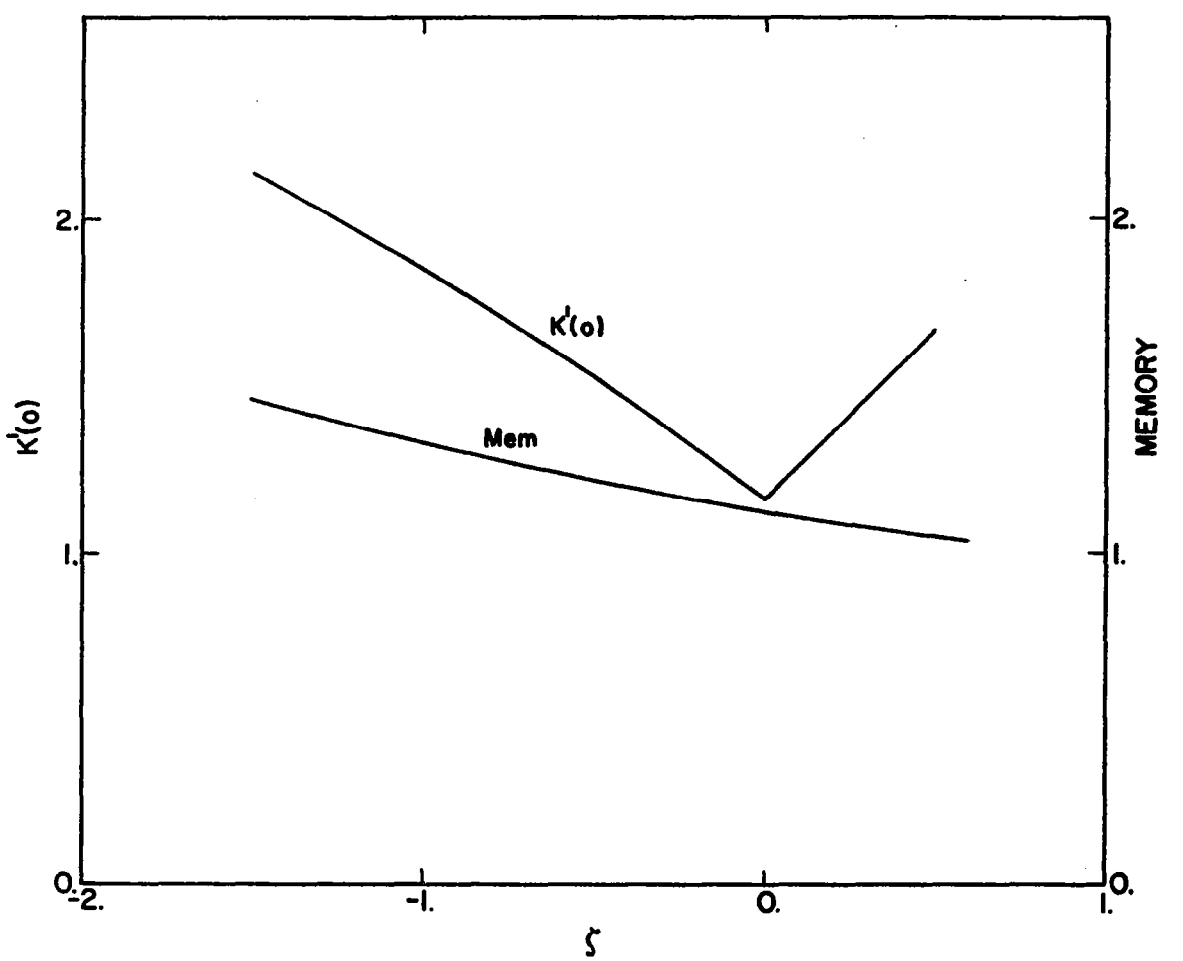

Figure 3.5. Initial response and memory for model spectrum.

both stratifications, the spectral bandwidth, B_w, (which determines the decay rate of response) increases monotonically with decreasing stability. Accordingly, the excitement of more large-scale energy results in an increased response at scales $\tilde{x} > 1$.

It follows from the scaling of the spectra that the response for an arbitrary stability, scaled by its initial response, is only a function of $\tilde{x}/B_w$. For a constant flux layer in which the Monin-Oboukhov length, L, is also constant with height, one may equate changes in $\zeta (= z/L)$ with changes in height. Therefore, for a given x, $\tilde{x}/B_w$ will decrease with height, both because $\tilde{x} (= x/\ell)$ decreases with height and because B_w^{-1} decreases with height (Figure 3.2). Therefore, the response will increase as a result of an increase in $\overline{\tilde{w}^2}$ with height and a decrease in $\tilde{x}/B_w$ with height. Under unstable conditions, B_w increases approximately linearly with height, as does $\gamma_w^{1/2}$, so that from (3.1.9), for a given x,

$$K^1(z) \sim z \exp(- z^{-4/3}) \tag{3.1.16}$$

Under stable conditions, B_w is approximately constant, while $\gamma_w^{1/2}$ again varies linearly with height, so that for a given x,

$$K^1(z) \sim z \exp(- z^{-2/3}) \tag{3.1.17}$$

For neutral conditions, both $\gamma_w^{1/2}$ and B_w are constants in height, and the response function has a form

$$K^1(z) \sim \exp(- z^{-2/3}) \tag{3.1.18}$$

For large enough z, assuming $\kappa z/\ell$ is still nearly unity, the response, for a given x, will vary linearly with height in stratified cases and approach a constant in neutral cases.

It is concluded that the response structure varies appreciably in various stratifications. The results for the initial response and memory, as a function of ζ, are intuitively consistent with qualitative discussions of the spectrum. It is now useful to consider another effect on the simulated turbulent process --- that of viscosity for low Reynolds number.

3.1.4 Viscosity Effects on Kernels. The empirical spectra discussed in the previous sections, were obtained in flows whose Reynolds number was sufficiently large that the viscous range was well removed from the energy-containing eddies. Accordingly, the models discussed there should probably be called 'inertial' but we will refer to them as inviscid for mnemonic and comparative purposes. It is useful to consider modifications of the Reynolds number (Re) criterion in order to study the response structure in the presence of viscosity. This problem is not germane to the usual application of filters which simulate the energy containing scales. Rather it is preparatory for later attempts (Chapter 5.0) to simulate the derivative structure of the small scale region ($f \sim f_{KOL}$).

The response functions may be considered as the velocity field that would be produced by a single impulse (Section 2.4)). For inviscid flows, the response to the stimulus is immediate, giving a discontinuity at the time of the impulse. In a viscous flow, the formation of such infinite curvatures is impossible, requiring that response functions rise smoothly to a maximum value.

The viscous adjustment to the three dimensional Kolmogorov spectrum of the inertial subrange is illustrated by the model spectrum (Pao, 1965)

$$E(k) = \alpha\varepsilon^{2/3} k^{-5/3} \exp\left[-\frac{3}{2}\alpha(k\eta^{-1})^{4/3}\right] \tag{3.1.19}$$

where η^{-1} is the Kolmogorov wave number, $(\varepsilon \nu^{-3})^{1/4}$. The corresponding one-dimensional spectrum for the isotropic region (Batchelor, 1953, p. 50) is

$$\phi_{33}(k_1) = \alpha_w^{2/3} k_1^{-5/3} J_w(\hat{k}_1) \tag{3.1.20}$$

where

$$J_w(\hat{k}_1) = \frac{55}{24}\int_0^1 (1+\xi^2)\xi^{2/3} \exp\left[-\frac{3}{2}\alpha(\hat{k}_1/\xi)^{4/3}\right]d\xi \tag{3.1.21}$$

and

$$\hat{k}_1 = k_1\eta \tag{3.1.22}$$

In (3.1.20)

$$\alpha_w = \frac{24}{55}\alpha \tag{3.1.23}$$

where α is the three-dimensional Kolmogorov constant ($\simeq 1.5$)). A model of the spectrum over the entire scale range from energy-containing to dissipative is therefore given by

$$f\, G_w(f) = \frac{A_w\, \phi_\varepsilon^{2/3}\, f^{2/3}}{1 + (B_w\, f)^{4/3}}\, J_w\, (f/f_{KOL}) \qquad (3.1.24)$$

where (Appendix A)

$$f_{KOL} = \phi_\varepsilon^{1/4}\, Re^{3/4} \qquad (3.1.25)$$

For a given ζ, and fixed ϕ_ε, the effective cut-off wave number, f_{KOL}, of (3.1.24) varies as $Re^{3/4}$.

The method of digital spectral factorization was applied to (3.1.24) for $\zeta = 0$, and several ranges of Re. The response for a given value of Re rises from an initial zero value, overshoots the inviscid case, reaches a maximum, K^1_{max}, at a distance $\tilde{x}_{max}$ from the origin, and then settles down to the inviscid solution. The variation of K^1_{max} and $\tilde{x}_{max}$ are given in Figure 3.6 as a function of the Reynolds number. Interpreting the figure, we can see that for a decrease in viscosity, the maximum response increases and the displacement of the location of the maximum response from the origin is reduced. For $Re = 10^3$, the resulting form of K^1 closely resembles the inviscid result, and the maximum response of this viscid case and initial response of the inviscid case are approximately equal. The location of the maximum response for $Re = 10^3$ occurs within a distance, 1/100, from the origin, or impulse point.

However, for low Reynolds numbers, say, $Re \leq 10^2$, the effective loss of variance due to the viscous spectral cut-off (by J_w) is not reflected in the coefficients A_w and B_w. Accordingly the computations displayed in Figure 3.6 for K^1_{max} are underestimates for the lower Reynolds number range.

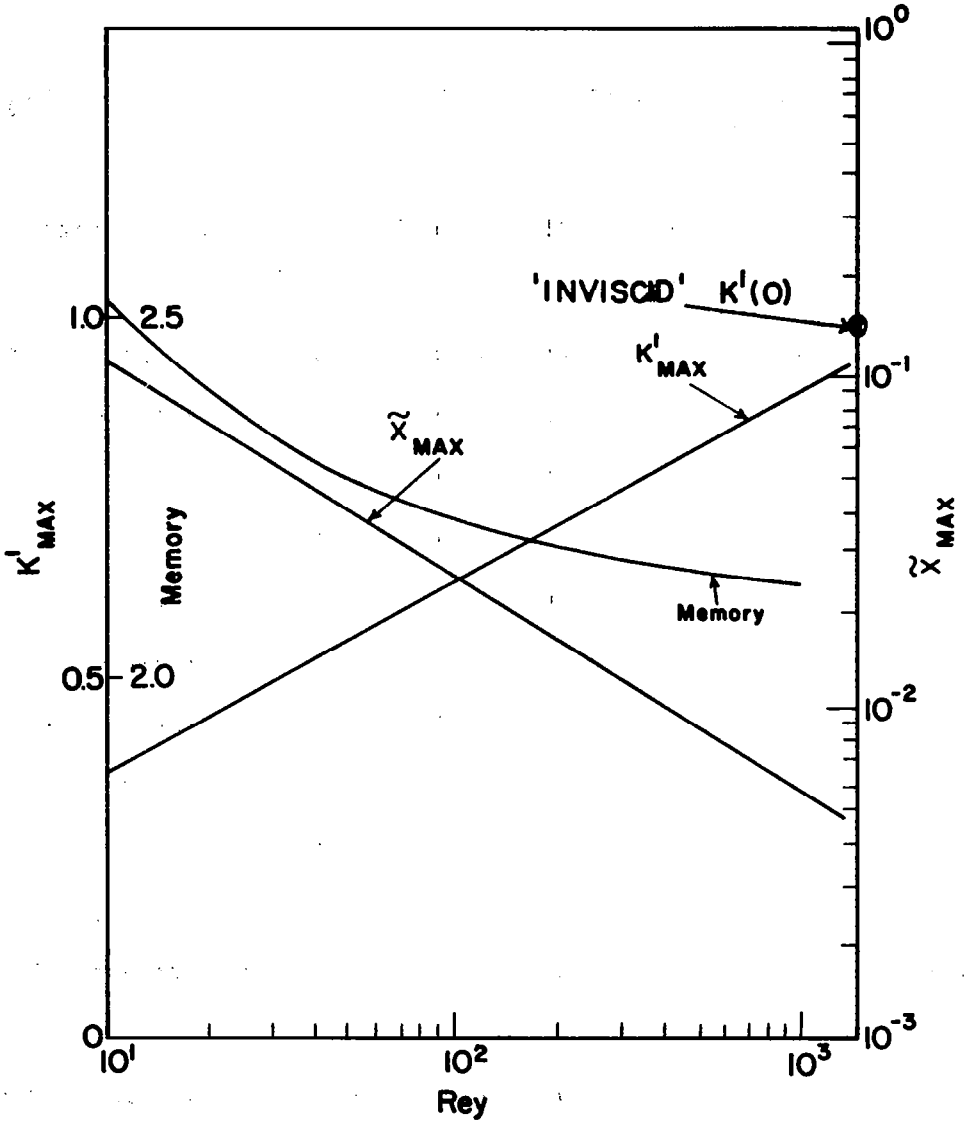

Figure 3.6. Magnitude and location of maximum response and memory for various Reynolds numbers.

Another feature of the viscous response structure (not shown here) is the convergence of each kernel, irrespective of Re, to the corresponding inviscid kernel, for sufficiently large $\tilde{x}$. The convergence occurs at progressively smaller $\tilde{x}$ with increasing values of Re. This result is in keeping with the intuitive notion that a decreased viscosity is felt at progressively smaller scales where large gradients are possible. Equivalently, as the range of unaffected scales extends to larger f, the response over a wider scale range becomes indistinguishable from the inviscid result.

The concept of memory (3.1.14) does not apply for a viscous model because $K^1(0) = 0$. Therefore, it is necessary to consider another ad hoc normalization, $\overline{\tilde{w}^2}^{1/2}$, rather than the equivalent response of the common first order linear model. The memory is redefined as

$$\text{Mem} = \int_0^\infty K^1(x)\, dx \;/\; \{\int_0^\infty [K^1(x)]^2\, dx\}^{1/2} \qquad (3.1.26)$$

Estimates of memory by (3.1.26) are given also in Figure 3.6. Variation of Re from 10^1 to 10^3 results in a 20 percent decrease in the memory. This result is compatible with the intuitive concept of decreased memory with increased turbulent scrambling as the viscosity is reduced. Another aspect of the memory structure of the simulated process is its predictability based on its past history. This aspect is examined next.

3.1.5 Predictive Structure of the Model. In the development of control systems it is advantageous to be able to predict the turbulent velocity field at some future time, on the basis of past observations. In order to be able to apply some properties of linear stochastic

processes to the linear, Gaussian model of the vertical velocity component, it is necessary to examine another property of response functions (Section 2.1). An inverse linear functional, K^{-1}, is defined by

$$\int K(t_1)\, K^{-1}\, (\tau - t_1)\, dt_1 = \delta(t) \tag{3.1.27}$$

A Fourier transformation of (3.35) produces an equivalent definition

$$\hat{K}(\omega)\, \hat{K}^{-1}(\omega) = 1 \tag{3.1.28}$$

Accordingly, the inverse linear functional is derivable from the kernel, K, by the method implied in (3.1.27) or (3.1.28). For a perfect system, without noise, the inverse functional generates a white, Gaussian process, ξ, from a shaped spectral process, w, in the manner

$$\xi(t) = \int K^{-1}(T)\, w(t-T)\, dT \tag{3.1.29}$$

Let us consider a prediction of w in terms of its filtered past. The filter is determined so as to minimize the least squares error between the prediction and verification (Robinson, 1967b). The linearly predicted value, $w_p(t+\alpha)$, at a time α in the future is given by

$$w_p(t+\alpha) = \int M(\tau;\alpha)\, w(t-\tau)\, d\tau \tag{3.1.30}$$

For a linear W-H representation of w (Robinson, 1967b), the prediction kernel, M, is given in terms of K and K^{-1} by the expression

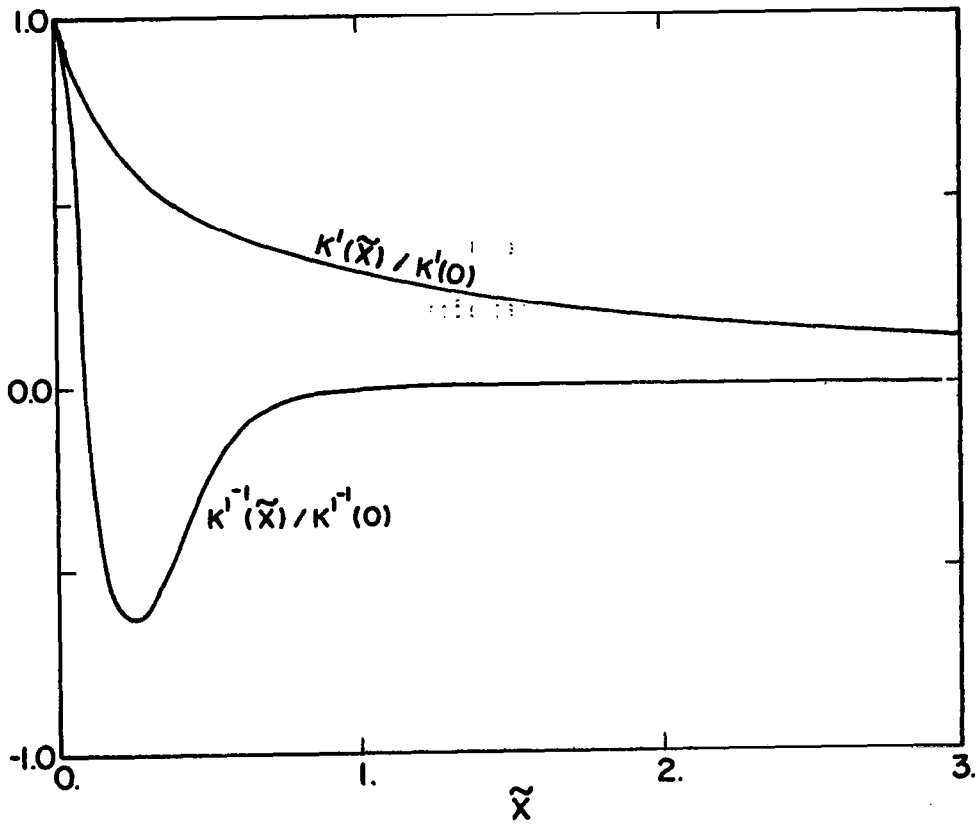

Figure 3.7. Comparison of response and inverse response functions.

$$M(\tau;\alpha) = \int K(p+\alpha)\ K^{-1}(\tau-p)\ dp \qquad (3.1.31)$$

From (3.1.27) or (3.1.28), equation (3.1.31) can be considered as a relationship between M and K.

The inverse filter K^{-1} computed from the kernel of the spectral model of Appendix A, under neutral, inviscid conditions, is given in Figure 3.7. The physical effect of K^{-1} is to filter a correlated time series to produce a white noise process. In Figure 3.7, this decoupling of the time series is accomplished by the alternate oscillating weights near $\tilde{x} = 0$ in what amounts to a shredding action. A measure of the effect of an inverse filter therefore lies in the difference $K^{-1}(0) - K^{-1}(\Delta\tilde{x})$, where $\Delta\tilde{x}$ is the resolution for the white noise process which will be generated. The larger the difference, the more the necessary shredding action to destroy the turbulent correlations. Accordingly, for situations with different spectral bandwidth in different thermal stabilities the oscillations in K^{-1} near $\tilde{x} = 0$ will increased for decreased stability.

The results for the prediction kernel, M, are given in Figure 3.8 for several values of $\alpha\Delta\tilde{x}$. The most distinctive feature of the structure of M is the very rapid decrease in predictive weighting for even $\tilde{x} < 0.25$. The implication is that the best estimate (in the least squares sense) of w at a distance $\alpha\Delta\tilde{x}$ ahead is given effectively as a multiple of its present value. The error of a prediction $\alpha\Delta\tilde{x}$ units ahead is given by

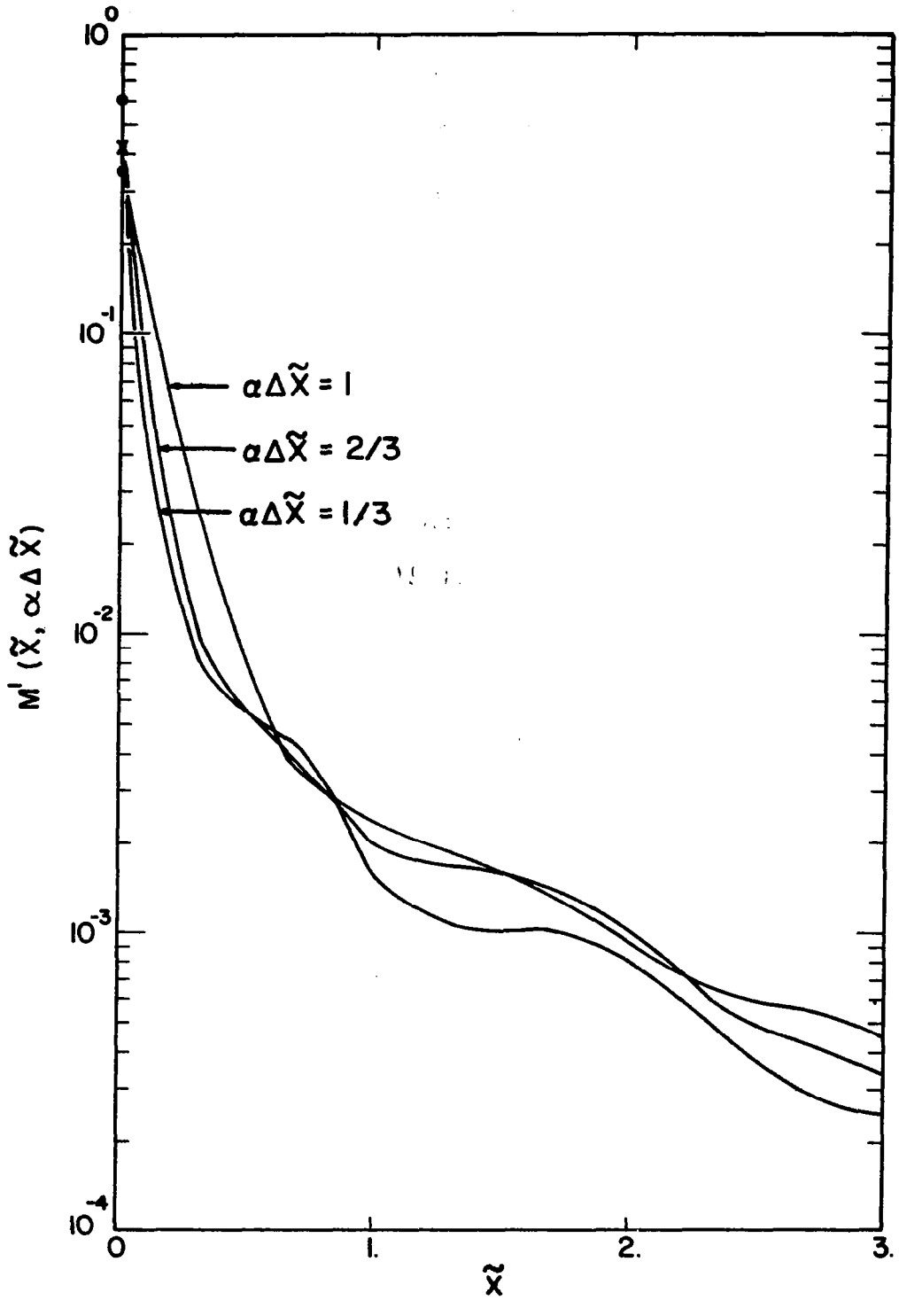

Figure 3.8. Prediction function for several prediction distances.

$$\Sigma^2(\alpha\Delta\tilde{x}) = |\tilde{w}(\tilde{x} + \alpha\Delta\tilde{x}) - \tilde{w}_p(\tilde{x} + \alpha\Delta\tilde{x}|^2$$

$$= 1 - \int M(r\Delta\tilde{x}, \alpha\Delta\tilde{x})\ \overline{\tilde{w}^2}((\alpha+r)\ \Delta\tilde{x})\ d(r\Delta\tilde{x}) \qquad (3.1.32)$$

Intuitively, the rate of growth of error Σ^2, with distance into the future, is a measure of the predictability of the turbulent process simulated by the linear representation.

The error of prediction of the model of Appendix A is given in Figure 3.9. The deterioration of the prediction at even short distances is apparent. For example, at $\alpha\Delta\tilde{x} = 0.5$, $\Sigma^2(0.5) \simeq 0.6$, or $\Sigma \simeq 0.8$. That is, at a distance of about $\ell/2$, the root mean square error in estimating the vertical velocity will be about 80 percent of $\overline{w^2}^{1/2}$. For comparison, a test was conducted of the common first order linear process, with comparable bandwidth. The results are shown also in Figure 3.9. A comparison of the mean square error Σ^2 of the turbulent spectral model ($f^{-5/3}$) and the common first order model (f^{-2}) indicates a modest improvement in predictability at scales comparable to ℓ. It is concluded on the basis of this comparison that modeled turbulence is the more predictable process. This result is also in agreement with the discussions in Section 3.1.1 of the memory of the simulated turbulence.

The basis of the previous discussions is the response function K^1 because from it can be derived the memory and predictability characteristics. An empirical formulation for K^1 is next summarized for convenience.

3.1.6 Empirical Formulae for Simulation Model. In Section 3.1.1, the filter for simulation purposes was represented in the form

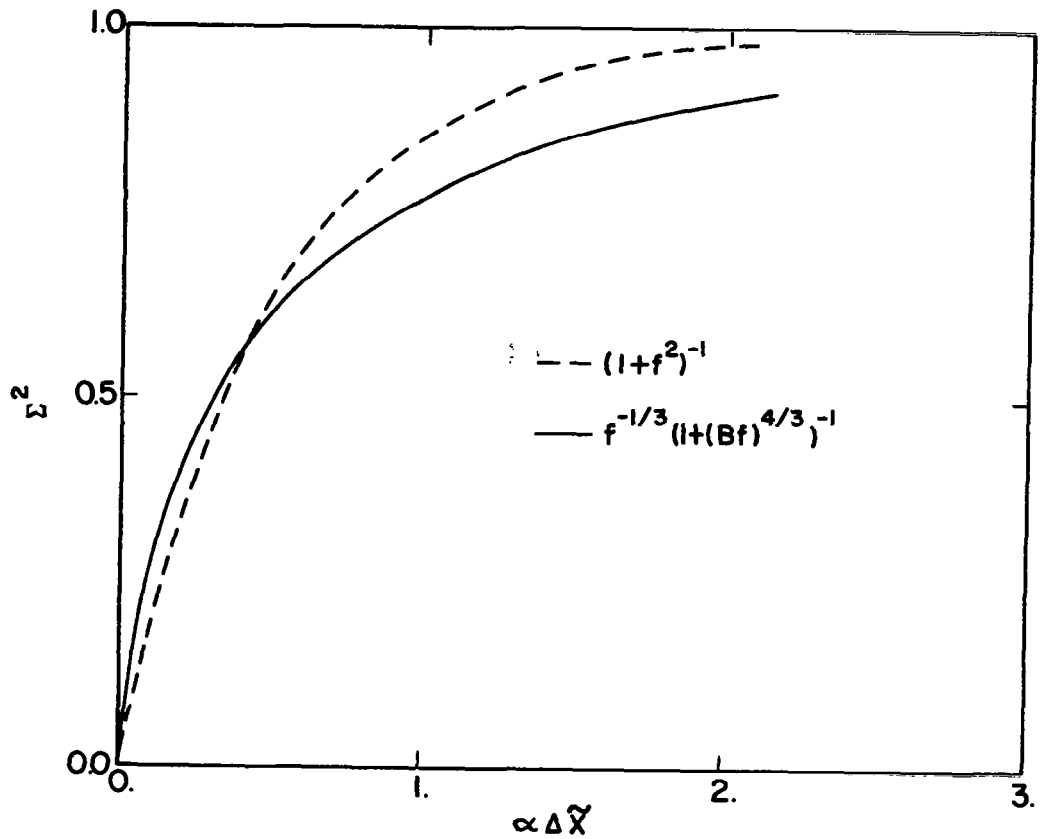

Figure 3.9. Comparison of mean square error of prediction for the model and Dryden form of spectrum.

$$K^1(\tilde{x}) = \gamma_w^{1/2} \exp-(\tilde{x}/B_w)^{2/3} H(\tilde{x}) \qquad (3.1.34)$$

For the purpose of application of the model, it is convenient to summarize the forms γ_w, B_w and H.

The factor $H(\tilde{x})$ was computed from numerical results for K^1 for various stabilities, ζ, using the following empirical formulae for γ_w and B_w

$$\gamma_w^{1/2} = 0.75 \ (1 + 0.75|\zeta|) \qquad (3.1.35)$$

$$B_w = 0.7 \qquad (1 + 0.75 \ \zeta + 3.0 \ \zeta^2) \qquad (3.1.36)$$

over the range $-1.5 < \zeta < 0.5$. The results from $H(\tilde{x})$ for the extremes of the stability range, are shown in Figure 3.10. Apparently, H is only a weak function of the bandwidth, B_w, of the spectrum used. Accordingly, stability effects are ignored in approximately H. The form chosen to represent H empirically is given by

$$H(\tilde{x}) = 0.5 \ (1 + \exp[- 2.5 \ \tilde{x}^{2/3}]) \qquad (3.1.37)$$

The specification (3.1.34) of the first order kernel of the linear, Gaussian vertical velocity model is now complete. The application of these formulae requires establishing estimates of u_* and T_* for a given height, roughness and geostrophic wind speed to denormalize the tabulated functions. An example using the resistance law formulations is given by Kerman (1974a).

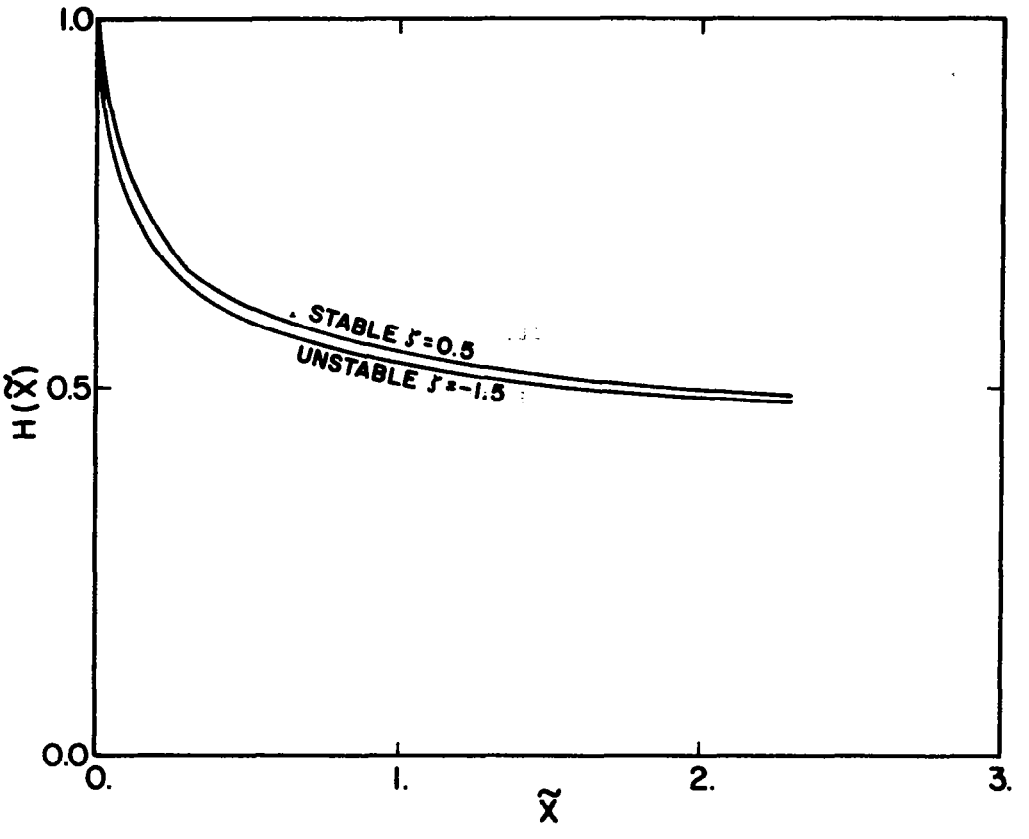

Figure 3.10. Correction to analytical approximation of response function to model spectrum.

3.2 Model of the Vertical Velocity Derivative

In some applications, such as the simulation of the diffusion of passive airborne contaminants or the testing of instrument systems to measure turbulence, it may be advantageous to have a simulation of the derivative of a velocity component. However, the derivative process has several distinctive properties which make simulation more difficult. First, the maximum spectral content of the derivative of a turbulent velocity component lies in the fine scale, viscous sub-range. Second, from observations, (for example, Tennekes and Wyngaard, 1972), it is known that the actual turbulent process of the derivative is distinctly non-Gaussian. In this section the properties of a Gaussian derivative process are studied. A somewhat more realistic non-Gaussian model is presented in Chapter 5.0.

Let the derivative of a linear process, w, be represented in terms of a white, Gaussian process, ξ, by

$$\frac{\partial w(t)}{\partial t} = \int_0^t D^1 (t-T)\ \xi(T)\ dT \qquad (3.2.1)$$

A relationship exists between this representation (3.2.1) and the representation of the velocity, given by

$$w(t) = \int_0^t K^1(t-T)\ \xi(T)\ dT \qquad (3.2.2)$$

which, by application of Leibnitz's rule, can be shown to be

$$D^1(t) = \frac{\partial}{\partial t} K^1(t) \qquad (3.2.3)$$

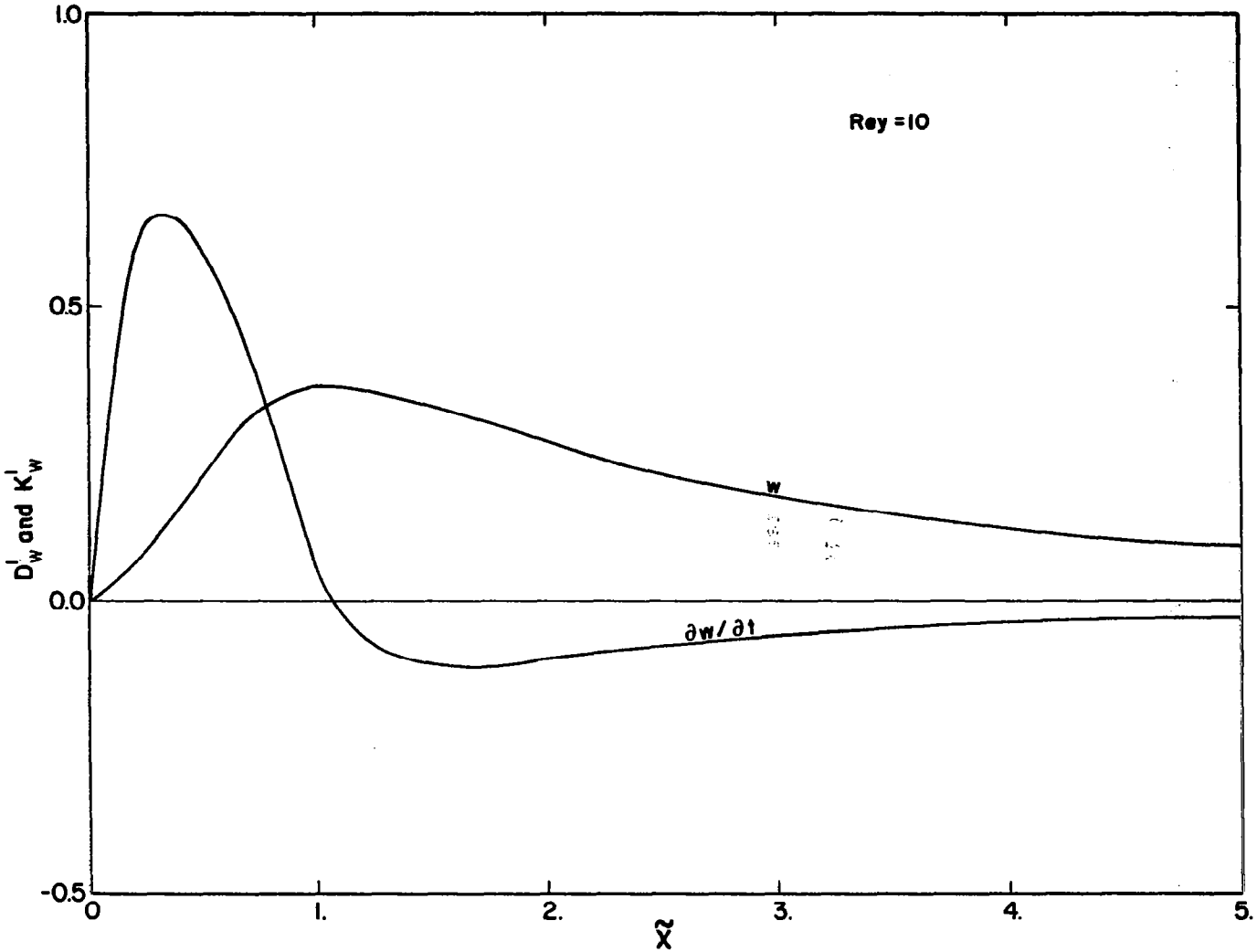

Figure 3.11. Comparison of response of vertical velocity and its derivative.

for $K^1(0) = 0$. Therefore, it is equivalent to compute D^1 directly by the spectral factorization arising from the representation (3.2.1) or by differentiation in (3.2.3). From the discussion for the spectrum near the viscous sub-range (Section 3.1.4) the spectrum for the derivative, is given by

$$G_{\partial w/\partial t}(f) = f^2 G_w(f) = \alpha_w \phi_\varepsilon^{2/3} f^{1/3} J_w(f/f_{KOL}) \qquad (3.2.4)$$

There is no need to include the parameterization of the low wave number range in the spectrum of $\partial w/\partial t$ because the spectral contributions to the derivative are neglible near $f = 1$. However, the effect of stability is retained in ϕ_ε and the viscous effects are parameterized in f_{KOL}, for a given stability.

The response function for $\partial w/\partial t$ for neutral stability and Re = 10, is given in Figure 3.11 as well as the corresponding kernel for the w process. The maximum response, D^1_{max}, in the derivative process occurs at the location of the maximum positive derivative in K^1. The correspondence of D^1 and K^1 through (3.2.3) is shown clearly. The extensive region of negative response in D^1 corresponds to the monotonically decreasing form of K^1 over the same range. The resulting estimate of the memory (3.1.26) of the derivative process is significantly smaller than the memory of the velocity process. This is supported by observations that realizations of the derivative of a stochastic process, are more disorganized than the velocity field. In Figure 3.12, the maximum response of the derivative process increases with increasing Reynolds number. The location, $\tilde{x}_{max}$, of the

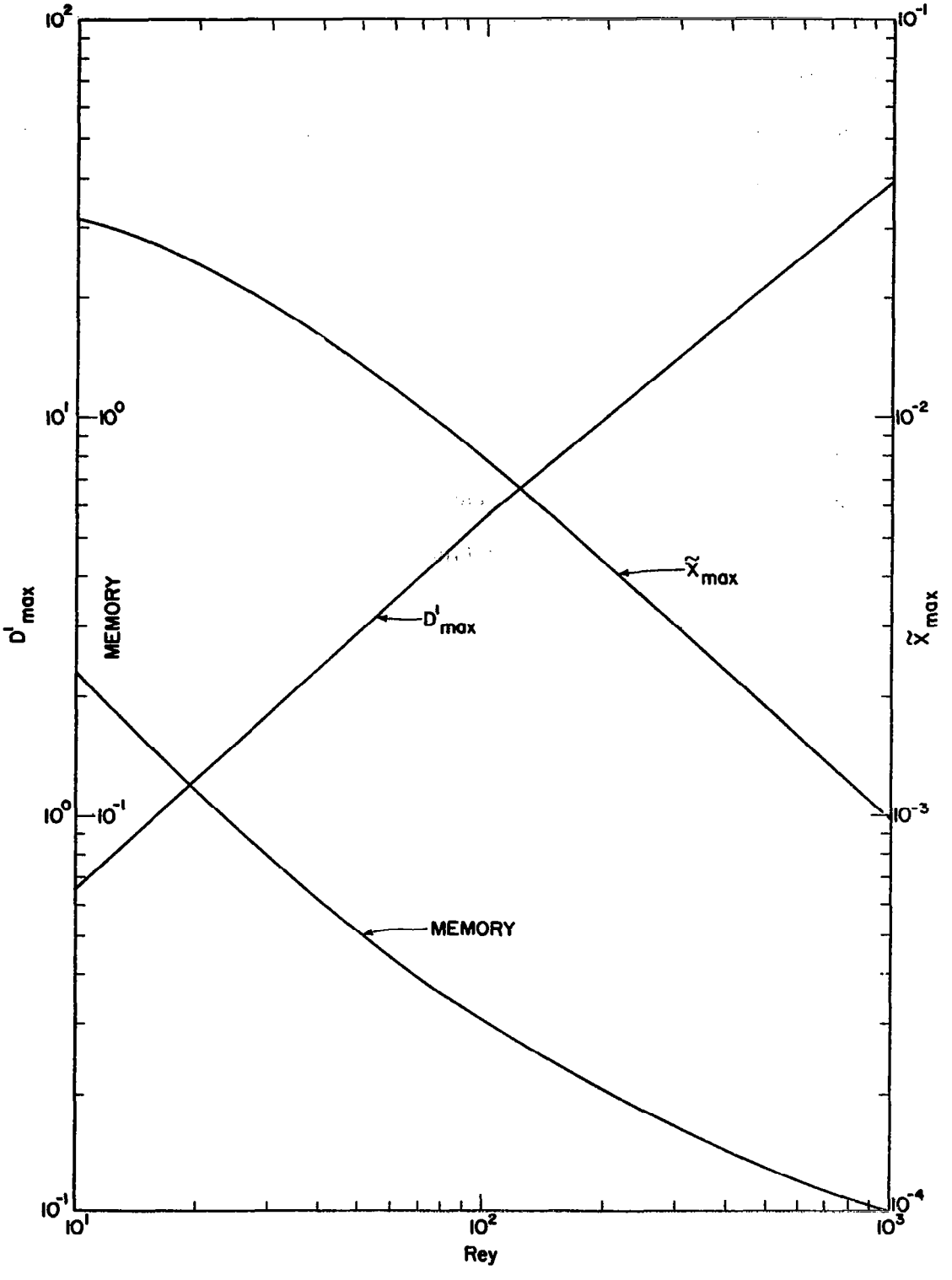

Figure 3.12. Magnitude and location of maximum response of derivative of vertical velocity and memory of process.

maximum response converges to the origin in the same manner as K^1_{max} approaches the inviscid limit for large Re in the velocity process. However the negative response also increases in width and magnitude with increasing Re so that the memory continues to decrease. Therefore, different time or space series of a realization of $\partial w/\partial t$ would display increasing disorder with increasing Re. Qualitatively, however, such realizations would not display the patchy nature often observed in real turbulent realizations (Stewart, 1969). An actual turbulent derivative signal would include more large negative excursions (rapid decelerations) than large positive excursions and have more large excursions of any sign than a purely linear Gaussian process. An analysis of these features is given in Chapter 5.0.

4.0 LINEAR REPRESENTATION OF MULTI-COMPONENT TURBULENCE

The development of the previous chapter assumed that a velocity or derivative component was uncorrelated with any other component. But requirements exist, or may be foreseen for simulating the longitudinal velocity, u, the vertical velocity, w, and the buoyancy, θ, components of a turbulent flow near the ground. For example, the requirement for a multi-component model of turbulence for VSTOL response problems has been outlined by several authors (Case, 1968; Skelton, 1968; Houboult, 1973).

The method which is used to calculate multi-component filters involves the reduction of the spectral matrix to an equivalent series of single component spectra, with subsequent spectral factorization. The reduction process is discussed next.

4.1 Model Development

Consider a multi-component, linear representation in terms of a white, Gaussian process for the longitudinal and vertical velocity components and buoyancy, in the direction of the mean wind speed

$$\tilde{u}_i(\tilde{x}) = \int K_{ij}(\tilde{x}') \; \xi_i(\tilde{x}-\tilde{x}') \; d\tilde{x}' \qquad (4.1.1)$$

For later consistency, it is convenient to define a velocity, u_b, from the buoyancy fluctuation

$$u_b = \{\frac{g}{T_o} \frac{Kz}{u_*}\} \; \theta \qquad (4.1.2)$$

so that $\tilde{u}_i$ is understood to be the array $(\tilde{u}, \tilde{w}, \tilde{u}_b)$. The kernel K_{ij} represents the response of the i^{th} output velocity component to the j^{th} white, Gaussian input component. It is not necessary to include the lateral velocity component, v, because it is uncorrelated with all other variables and can be simulated independently.

A Fourier transformation of (4.1.1), results in the expression

$$\hat{\tilde{u}}_i(f) = \hat{K}_{ij}(f)\, \hat{\tilde{\xi}}_j(f) \tag{4.1.3}$$

and the spectral matrix is given by

$$\begin{aligned} \phi_{mn}(f) &= \overline{\hat{\tilde{u}}_m \hat{\tilde{u}}_n^*} \\ &= \hat{K}_{mj}\, \hat{K}_{jn} \end{aligned} \tag{4.1.4}$$

Because the process, ϕ_{mn}, is Hermitian $(\hat{K}_{ij} = \hat{K}_{ji}^*)$, there exists an equivalent diagonal process such that

$$\Phi\, \phi\, \Phi^{\dagger} = \Omega \tag{4.1.5}$$

where Ω is diagonal. Φ is the eigenvector metrix of ϕ. (The symbol $\dagger$ represents the adjoint, or transposed complex conjugate of a matrix.) Because the diagonalization procedure is a linear operation, equation (4.1.5) applies at each scale independently. The diagonal elements of $\Omega(\omega)$ represent an uncorrelated process equivalent to a single-component spectrum. Therefore, we consider next the spectral factorization of

each eigenspectrum (or diagonal element of Ω). The result of the operation on uncorrelated diagonal elements is itself a diagonal matrix (of spectral factors), say, λ, where

$$\Omega = \lambda \lambda^{\dagger} \tag{4.1.6}$$

From (4.1.4) and (4.1.5)

$$\Omega = (\Phi \hat{K}) (\phi \hat{K})^{\dagger} \tag{4.1.7}$$

so that

$$\lambda\gamma = \Phi \hat{K} \tag{4.1.8}$$

where γ is an arbitrary unitary matrix. After essentially a trial and error analysis, it was found that the equivalence

$$\gamma = \Phi \tag{4.1.9}$$

preserved the minimum phase characteristics of $\hat{K}$. Consequently, from (4.1.8) and (4.1.9)

$$\lambda = \Phi \hat{K} \Phi^{\dagger} \tag{4.1.10}$$

or, the eigenvectors, Φ, diagonalize both ϕ and $\hat{K}$.

This completes the mathematical development of the multi-component model. In summary, the procedure is first to reduce a matrix of spectra

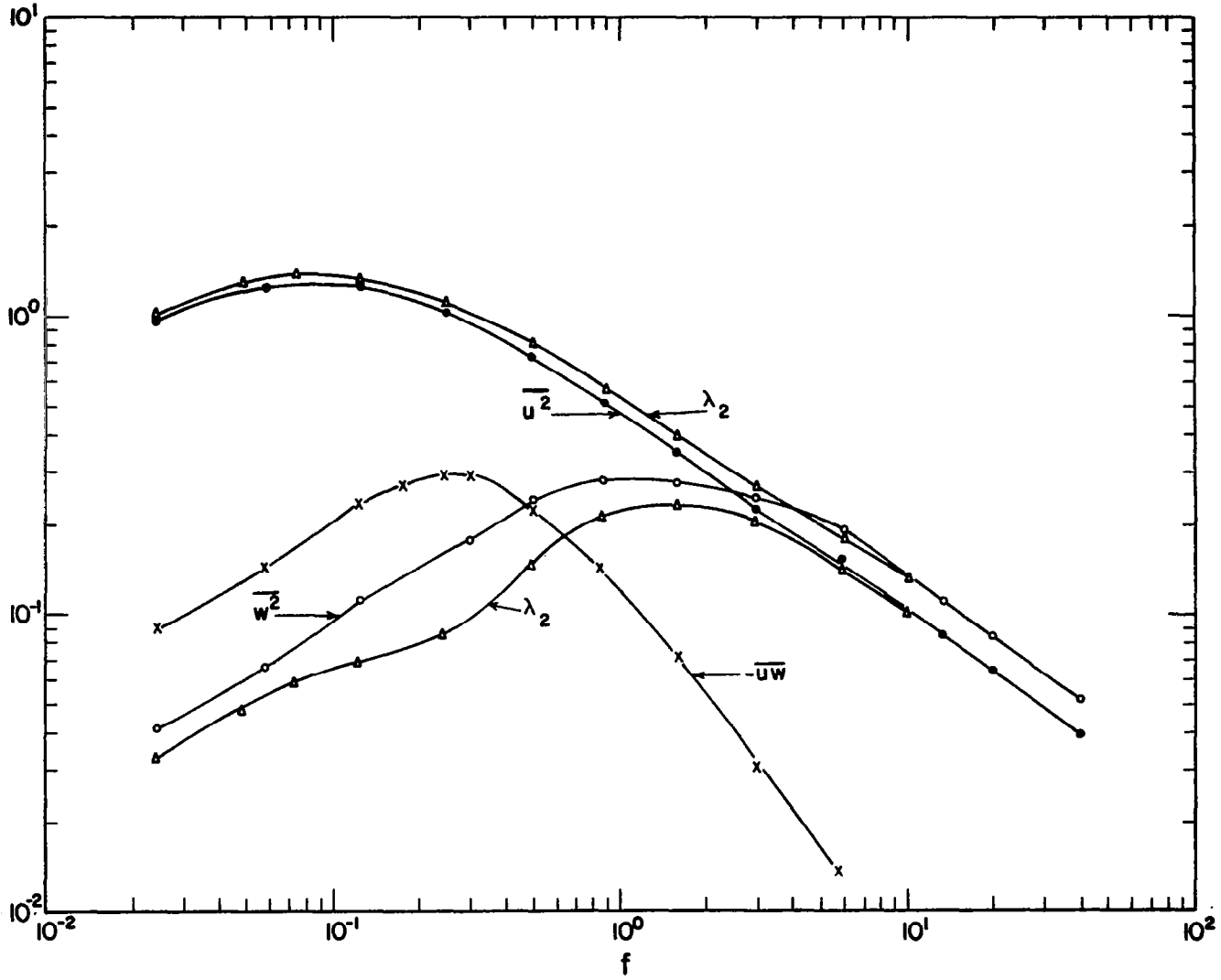

Figure 4.1. Spectra, co-spectrum and eigen-spectra of two component model.

on the other hand, underestimates the w spectrum in the large scale region but converges to the u spectrum in the inertial sub-range.

The response functions corresponding to the eigenspectrum (termed eigenresponse for convenience) are similar in form to the single component model. The multi-component functions derived from the eigenresponse functions by rotation using the eigenvectors (4.1.10) are displayed in Figure 4.2 The response, K^1_{11}, of u to the first Gaussian input is similar to the first order response function, K^1_u. The kernel K^1_{11} has a larger response at small scales ($\tilde{x} > 0.5$) than a single component model, but a smaller response at larger scales ($\tilde{x} > 0.5$). The effect of a downward momentum flux on the vertical component is to decrease the response for all scales. The response K^1_{13} ($= K^1_{31}$) is negligible for small scales and becomes approximately constant for $\tilde{x} > 0.5$ Although both the self-responses, K^1_{11} and K^1_{33}, are reduced by the presence of the stress, the total response for simultaneous, equal and opposite impulses in the input channels will be larger than if the u and w components were uncorrelated.

The predictability of the multi-component model was also studied. The mean-square error for the single components and the mean square error of w for a multi-component simulation are plotted in Figure 4.3 The errors of prediction are significantly different between the u and w components in single component models. The w component is inherently less predictable and the imposition of a cross-correlation makes only a minor change to Σ^2_w. Equivalently, the prediction functions M^1_{ij} are only slightly different than the single component estimates.

It is concluded that the response for $\tilde{x} \geq 0.1$ for a multi-component mode in neutral stratification may be increased by the presence of a

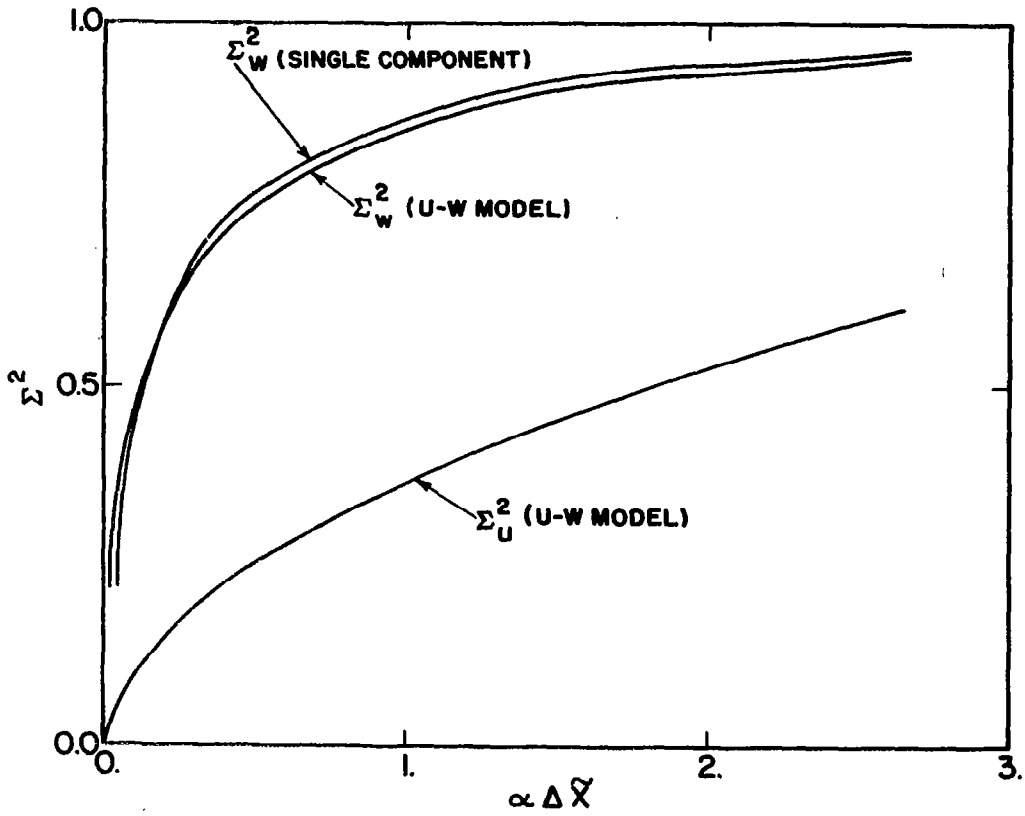

Figure 4.3. Comparison of mean square error of prediction between single and two component model.

downward momentum flux. However, predictions based on u and w simultaneously show only marginal improvement over single component models.

4.2.2 Model in Non-Neutral Stratification. The basic u-w model of Section 4.2.1 was enlarged to include u-θ and w-θ correlations. Co-spectra involving the lateral, v, component were neglected but the v spectrum was included. The structure of characteristics of the response, memory, and predictability for a multi-component model under various stratifications, ζ, are discussed next.

The distribution of initial response ($\tilde{x} = 0$) of the eigen-response functions for various stabilities (Figure 4.4) is similar to the single component response functions. The ranking and indexing of λ_i is by magnitude. The minimum response of the eigenstructure is the same as for the single component w model in neutral stratification. Whereas the initial responses of the first and second orders are identical, their memories (Figure 4.5) differ. Accordingly, the order 1 and 2 eigenfunctions represent two distinct processes but with the same initial response. The eigenmemories increase generally with increasing instability -- a property shared by single component models.

The transformation from the eigen-response to the multi-component response structure by the use of the eigenvectors results in the same qualitative picture as outlined for the eigen- and single-component structure. As before, initial responses are greater in non-neutral stratification with all variables, and the memories increasing with increasing instability. The initial response structure of the v component is identical to that of the w component because of their identical inertial sub-range structure.

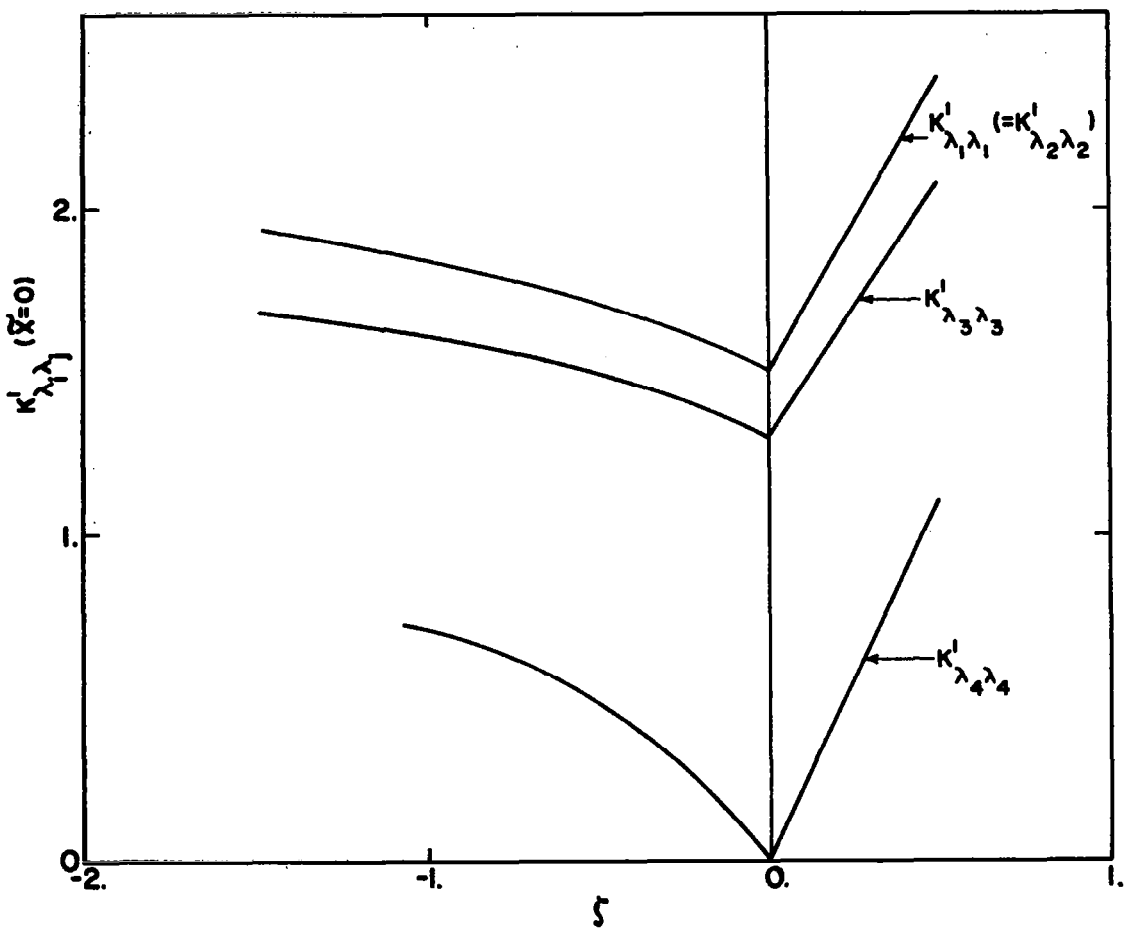

Figure 4.4. Initial eigen-response for four component model as a function of thermal stability.

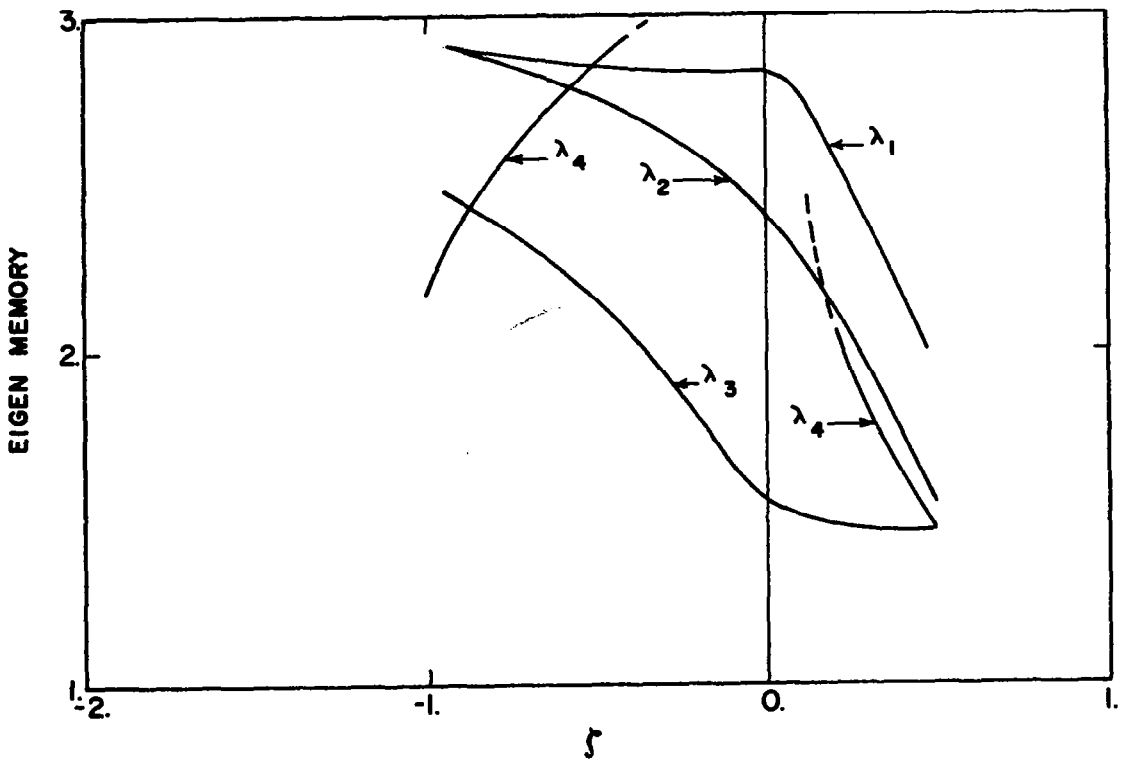

Figure 4.5. Eigen-memories for four component model as a function of thermal stability.

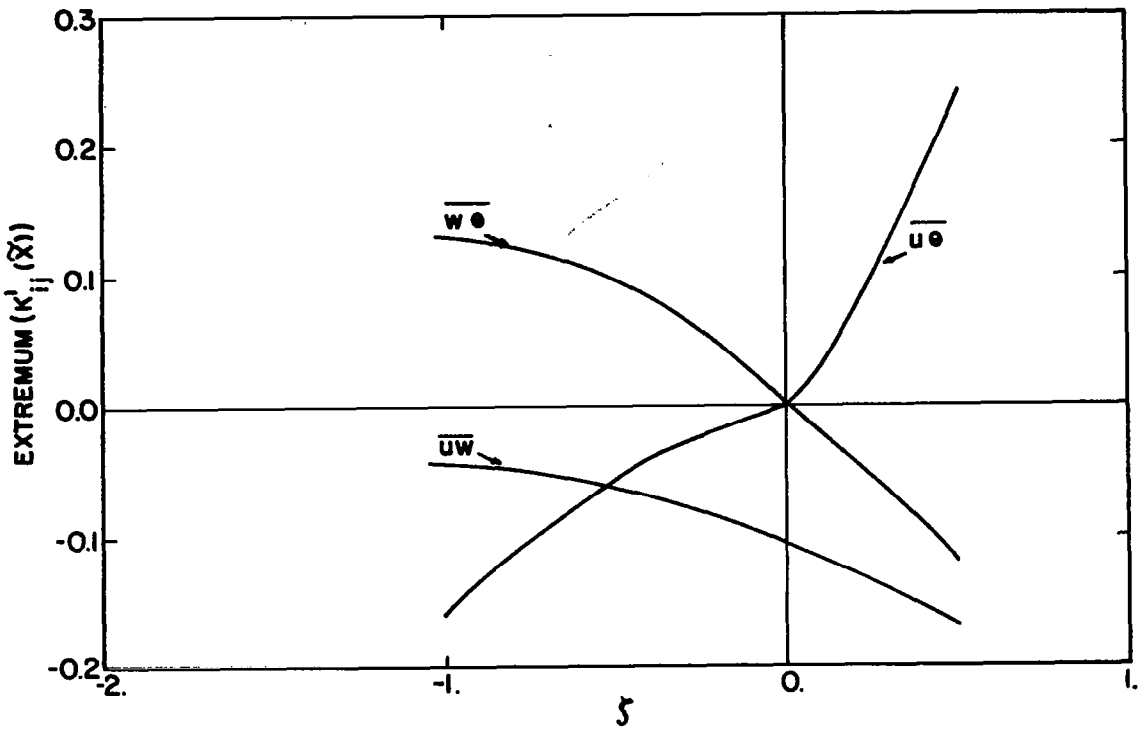

Figure 4.6. Extrema of response of stress and heat fluxes as a function of thermal stability.

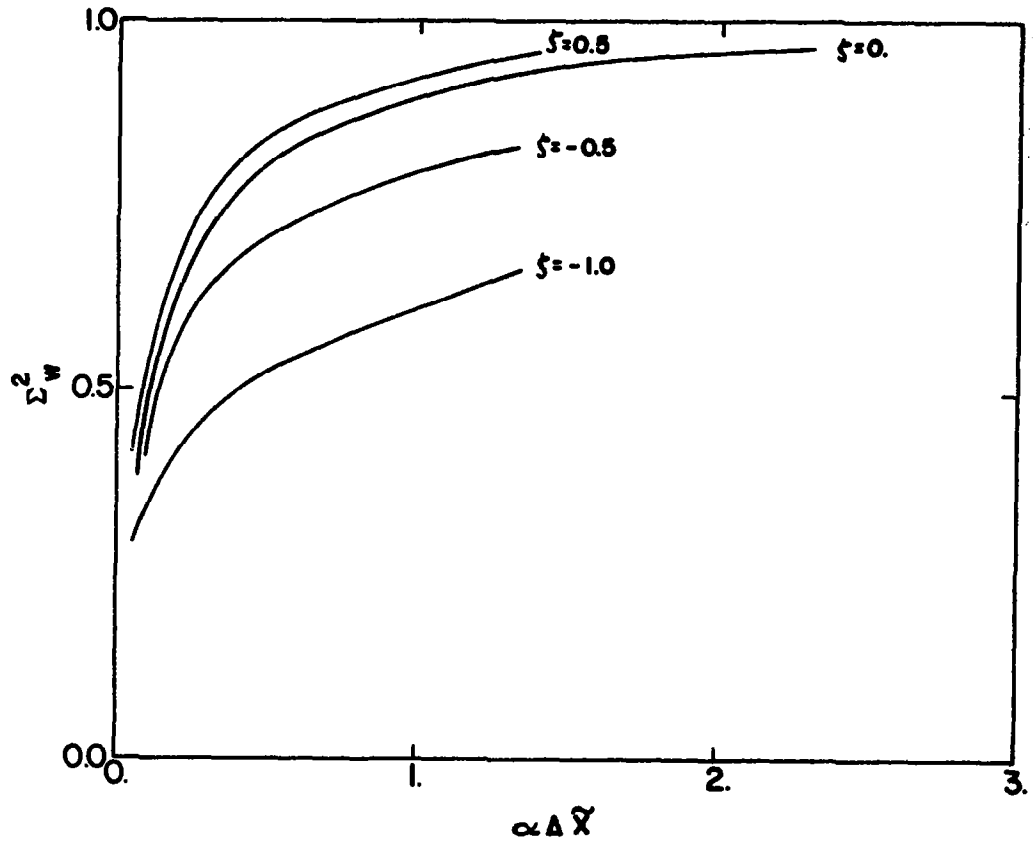

Figure 4.7. Mean square error of prediction of vertical velocity for various stabilities.

The cross-response $K^1_{ij}(i \neq j)$ is a measure of the coupling between the components, u_i and u_j. The major cross-response functions each have zero initial response, similar to the result of the previous section. Another feature of the absolute value of the cross-response functions is a maximum value obtained at a scale comparable to $\tilde{x} = 1$. These extreme values for K^1_{13}, $K^1_{1\theta}$ and $K^1_{3\theta}$ are plotted in Figure 4.6 as a function of stability. The response function, K_{13} represents the response of u_1 to ξ_3, or, of u_3 to ξ_1, and therefore the coupling between u and w. From Figure 4.6, the coupling between u and w decreases with increasing instability. This result is in accordance with the results of Wyngaard et al. (1971b) who deduced that the approach to free convection implies a loss of preferred longitudinal, or x, direction. Their argument was based on the negligible value of $\overline{\tilde{u}\,\theta}$ for $\xi > 1$. On the other hand, the absolute maximum values of the response functions, $K^1_{1\theta}$ and $K^1_{3\theta}$, as seen in Figure 4.6, increase away from neutral stability. This represents an increase in coupling in stratified flows, initially between w and the buoyancy, and subsequently between u and θ.

The effect of thermal stratification on the predictability of the multi-component flow was also studied. The mean square error of the w component as a function of the prediction distance $\alpha\Delta\tilde{x}$ and several values of stability is shown in Figure 4.7. The predictability of w in neutral cases was discussed in the previous section. The predictability of w increases with thermal instability and decreases with stable conditions. It is concluded that the predictability is increased or decreased by the increase or decrease of low frequency content of the flow under various stabilities.

This completes our discussion of linear, Gaussian models and we now move to a discussion of several non-linear and non-Gaussian models.

5.0 NON-LINEAR REPRESENTATION OF TURBULENCE

Observations of turbulence in the atmospheric boundary layer, as reviewed in Section 2.2 and Appendix A, have established that the velocity structure of the energy containing region of the spectrum is nearly Gaussian. This fact is exploited in this chapter to build a weakly non-linear model to simulate the low order moments and spectrum of surface layer turbulence. The development in terms of W-H functionals allows for systematically incorporating some characteristics of turbulence, such as its so-called patchiness. Previous simulations of the non-Gaussian structure have relied on ad hoc methods (Dutton, 1970; Reeves, 1969).

The extension of filtering methods to non-linear models is not without its difficulties, particularly with respect to the implications about the dynamics of turbulence. Models of turbulence in the energy containing region and of the derivative structure in the fine scale spectral region are developed and studied in this chapter. The derivative model is shown to simulate the transfer of energy towards the viscous subrange in a manner similar to a theoretical model of Pao (1965, 1968).

5.1 Velocity Model

In Section 2.3, the equivalence between the statistical structure of turbulence in the form of moments of the probability density function, and in the form of kernels of a functional representation was examined briefly. Let us pursue this equivalence somewhat further.

The W-H functional expansion of a (one-dimensional) representation of velocity is given by

$$u(x) = \int K^1(x_1)\, H_1(x - x_1)\, dx_1 + \iint K^2(x_1, x_2)$$

$$H_2(x - x_1, x - x_2)\, dx_1\, dx_2 + \iiint K^3(x_1, x_2, x_3) \qquad (5.1.1)$$

$$H_3(x - x_1, x - x_2, x - x_3)\, dx_1\, dx_2\, dx_3 + \ldots$$

A hierarchy of moments follows from (5.1.1) by forming successive products between $u(x)$ and $u(x + \Delta x)$ and averaging in x. The result is a set of simultaneous integral equations in the kernels, which, for $\Delta x = 0$, is given symbolically by

$$\bar{u} = 0$$

$$\overline{u^2} = \int \cdot \int K^1K^1 + 2 \int \cdot \int K^2K^2 + 6 \int \cdot \int K^3K^3 + \ldots \qquad (5.1.2)$$

$$\overline{u^3} = 3 \int \cdot \int K^1K^1K^2 + \int \cdot \int K^2K^2K^2$$

$$+ 3 \int \cdot \int K^2K^3K^3 + \ldots \qquad (5.1.3)$$

$$\overline{u^4} = \int \cdot \int K^1K^1K^1K^1 + 4 \int \cdot \int K^1K^1K^1K^3 + 6 \int \cdot \int K^1K^1K^2K^2$$

$$+ \int \cdot \int K^2K^2K^2K^2 + \int \cdot \int K^1K^1K^3K^3 \qquad (5.1.4)$$

$$+ 6 \int \cdot \int K^1K^2K^2K^3 + \ldots.$$

In the derivation of (5.1.2) - (5.1.4), the orthogaonality of the Hermite polynomials, H_i, with respect to the p.d.f., (Barrett, 1963) implied in the averaging, has reduced the many cross-products among the polynomials to simple integer coefficients which indicate the multiplicity of products of the Dirac δ-function. A corresponding reduction in the order of the integrations is also implied in the symbolism $\int \cdot \int K^i K^j$.

The hierarchy of moments is infinite both in the number of moments and the number of terms in each series. However, as observations only exist up to $\overline{u^4}$ (Appendix A) for the atmospheric boundary layer, the problem reduces to a finite sub-problem. Consequences of this method of closure will be examined in analyzing the results of the model.

The formulation of the resulting finite set of coupled integral equations (truncated at K^3) is given by (5.1.2) - (5.1.4). These equations are not easily amenable to solution without further simplication. A convenient method of approximation which overcomes many of the computational difficulties associated with the integral equation structure is an assumption that higher order kernels are multiples of the linear kernel, say

$$K^j(x_1 \ldots . x_j) = A_j \prod_{k=1}^{j} K^1(x_k) \qquad (5.1.5)$$

We shall refer to this approximation as the method of separable kernels. Equation (5.1.5) is analogous to the turbulent closure schemes in which higher order statistics are expressed in terms of lower order statistics. For example, in the classical closure scheme of most

boundary layer models, the stress is expressed in terms of the shear of the mean flow. Similar arguments are proposed in the quasi-normal models of Donaldson (1972) and Deardorff (1972b) for the vertical energy flux (a triple velocity product) in terms of the local energy (variance) structure.

Physically, the separability hypothesis (5.1.5), when applied, say, for K^2, implies that the conditional response at the present instant for an impulse at x_1, given a previous impulse at x_2, is given by the response at x_1 weighted by a multiple, A_2, of the response at x_2. However, the conditioning of the response at x_1 by a multiple of the response at a time, or separation x_2-x_1 distant, is physically unrealistic. Instead, the weighting of the impulse as x_1 would depend more likely on the integrated history of the response from x_2 up to x_1. Accordingly, a more physically consistent closure scheme for K^2 would be

$$K^2(x_1, x_2) = A_2 \, K^1(x_1) \int_{x_2}^{x_1} K^1(x) \, dx \qquad (5.1.6)$$

This representation will be discussed again in terms of a separable kernel model for the derivative. There, the concepts leading to (5.1.6) are shown to be somewhat easier to specify in a phase space representation. Just as the simple Newtonian stress-shear relationship is often questioned (Lumley, 1970) on the basis of local representations, the overwhelming practicality and reasonable experimental agreement demand it be retained in lieu of a workable alternative. As demonstrated next, the simplicity of local separability (5.1.5)

reduces an otherwise unmanageable problem to workable proportions. At the same time, it is possible by this method to achieve a reasonable simulation of the moment and spectral structure of the turbulence of the atmospheric boundary layer. The separability conditions

$$K^2 = A_2 K^1 K^1 \tag{5.1.7}$$

$$K^3 = A_3 K^1 K^1 K^1 \tag{5.1.8}$$

are substituted in the truncated moment expansions (5.1.2) to (5.1.4). The result is

$$\overline{u^2} = L^2 + 2A_2^2 L^4 + 6A_3^2 L^6 \tag{5.1.9}$$

$$\overline{u^3} = 6A_2 L^4 + 8A_2^3 L^6 + 36 A_2 A_3 L^6 + 108 A_2 A_3 L^8 \tag{5.1.10}$$

$$\overline{u^4} = 3L^6 + 24 A_3 L^6 + 60 A_2^3 L^6 + 60 A_2^4 L^8 \tag{5.1.11}$$

where

$$L^2 = \int [K^1(x)]^2 \, dx, \qquad L^4 = (L^2)^2, \ldots. \tag{5.1.12}$$

The utility of the assumption of local separability is now clear. The problem has been reduced from a problem in simultaneous integral equations to a problem in simultaneous algebraic equations. Further, the expansion is in terms of L^2, which from (5.1.9) can be seen to be

the linear contribution to the variance. Therefore, for a weakly non-linear functional representatin of a weakly non-Gaussian process, the moment expansions are perturbations about the linear, Gaussian process. Further, it is reasonable to describe such a representation as a quasi-linear model.

A similar expansion for the spectrum arises from the separability conditions,

$$\phi(f) = |\hat{K}^1(f)|^2 + 2A_2^2 \int |\hat{K}^1(f_1)|^2 \, |\hat{K}^1(f - f_1)|^2 \, df_1$$

$$+ 6A_3^2 \iint |\hat{K}^1(f_1)|^2 \, |\hat{K}^1(f_2)|^2$$

$$|\hat{K}^1(f - f_1 - f_2)|^2 \, df_1 \, df_2 \qquad (5.1.13)$$

The spectrum is then also expanded in the linear contribution to the spectrum, $|\hat{K}^1|^2$.

The distribution of the moments (variance, skewness and kurtosis) of velocity and buoyancy, as a function of thermal stability, ζ, are described in Appendix A. The data are drawn from the Kansas experiment. The solution for L^2, A_2 and A_3 from (5.1.9) to (5.1.11) will therefore also be a function of stability. For convenience, the model is restricted to a non-Gaussian extension for the vertical velocity component.

Equations (5.1.9) to (5.1.11) were solved by iteration. The results for the contributions to the variance, skewness and kurtosis for various thermal stabilities are given in Figures 5.1 to 5.3.

In Figure 5.1, the linear contribution, L^2, is the principal source of variance. The non-linear contributions ($2A_2^2 \, L^4$ and $6A_3^2 \, L^6$) increase

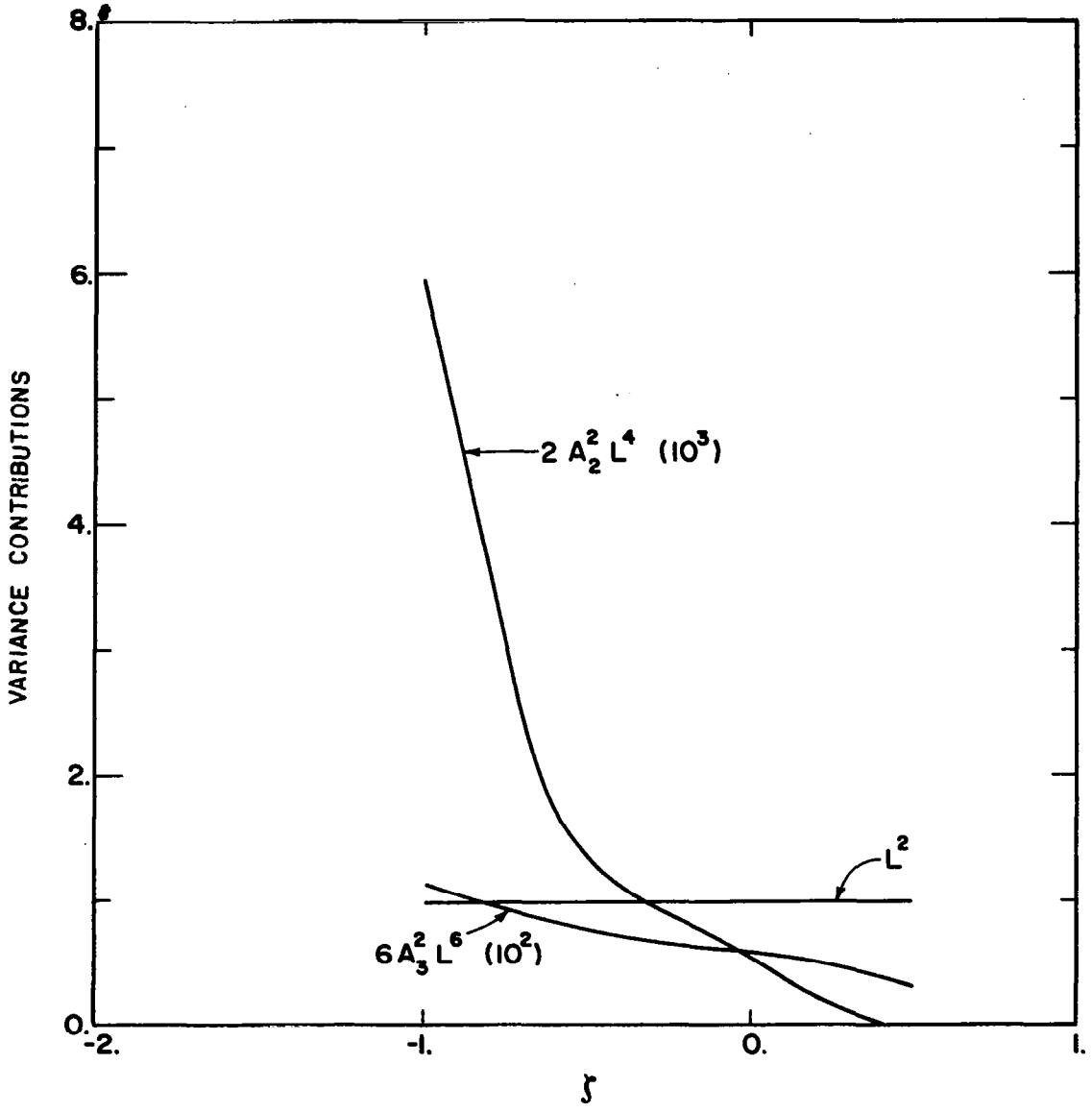

Figure 5.1. Partition of variance of vertical velocity for a cubic, separable model.

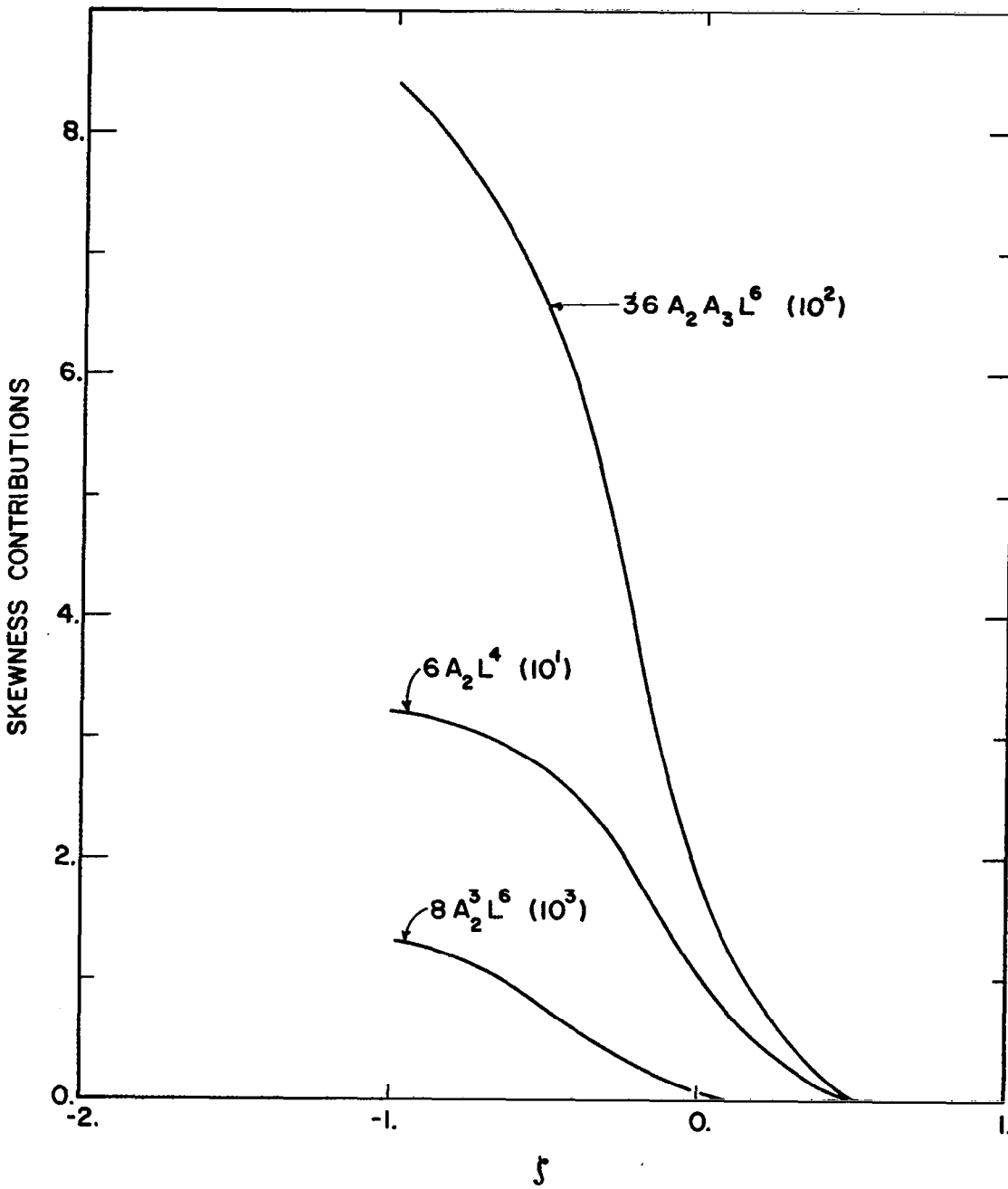

Figure 5.2. Partition of skewness of vertical velocity for a cubic, separable model.

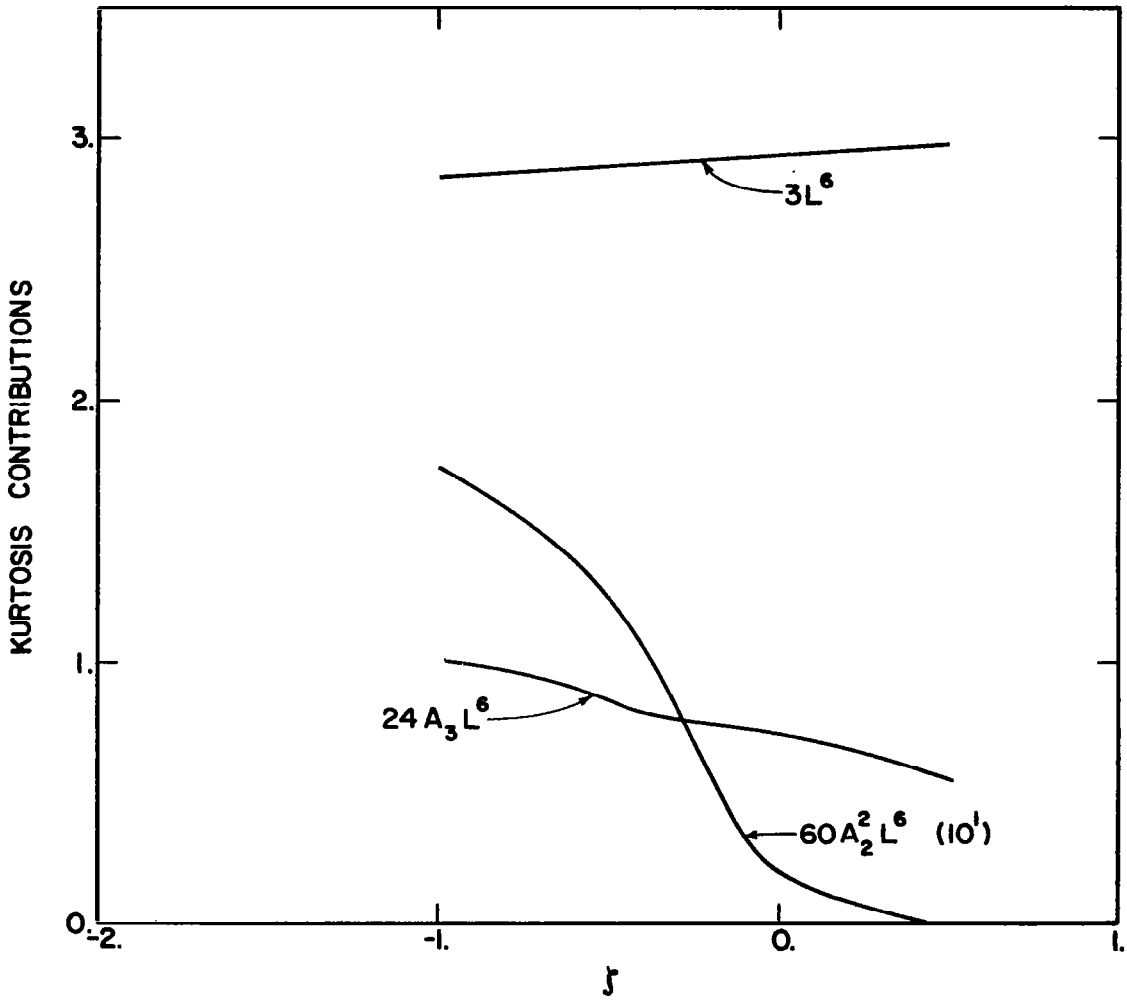

Figure 5.3. Partition of kurtosis of vertical velocity for a cubic, separable model.

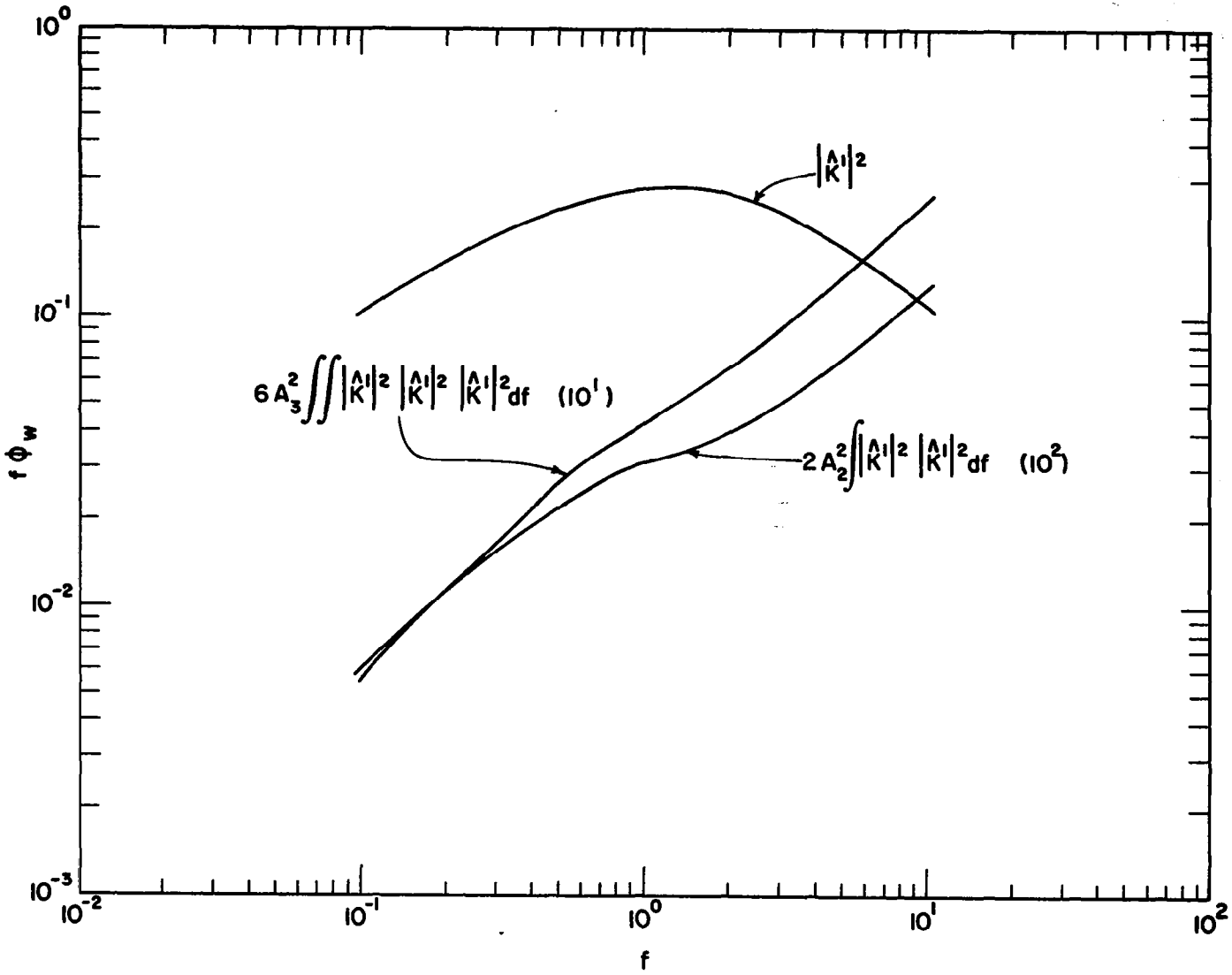

Figure 5.4. Partition of spectrum of vertical velocity for a cubic, separable model.

monotonically with decreasing thermal stability. The cubic contribution to the variance exceeds the quadratic portion. In Figure 5.2, for the partitioning of the skewness, the major contributor at all ζ is from the term $6A_2L^4$. The term $36A_2A_3L^6$ becomes only an appreciable fraction of the total skewness for $\zeta \simeq 1$. However, in the contributions to the kurtosis (Figure 5.3), the cubic term, $24A_3L^6$, dominates the quadratic term $60A_2^2L^6$.

In summary, the major contribution to the (non-zero) skewness involves a term linear in A_2, as shown in Figure 5.2, and the deviation of the kurtosis from a Gaussian representation is accounted for by a term quadratic in A_3, as shown in Figure 5.3. However, the major non-linear contribution to the variance (Figure 5.1) occurs from the third order effect in A_3 rather than a quadratic effect in A_2. Alternatively, the distribution of variance is not monotonic with the order of the kernel. This effect has been reported and examined by Crow and Canavan (1970).

The spectral partition of variance (5.1.13) resulting from an iterative solution using the values of L^2, A_2 and A_3 for neutral stability is presented in Figure 5.4. Both the quadratic and cubic contributions increase with decreasing scale. The increased effect of non-linearities with increasing f is qualitatively consistent with the results of Stewart (1951) and Frenkiel and Klebanoff (1967). From dynamical considerations, it is expected that non-linear effects are dominant in the inertial sub-range, say $f \sim 10$. However, the largest relative contribution to the variance (non-linear/linear) at $f = 10$ is only about 0.25. Although this ratio increases with stable stratification, its maximum value under any stratification is only 0.5.

Therefore, there are indications that the dynamical structure of the model is not represented properly. This point is examined further in a later discussion.

In Chapter 3.0, the concept of memory, for a linear system, was defined by

$$\text{Mem} = \int_0^\infty K^1(x)dx \Big/ \int_0^\infty \{[K^1(x)]^2 dx\}^{1/2} \quad . \tag{5.1.14}$$

An alternate concept for memory, based on (5.1.14) is the limiting response as $x \to \infty$ of the system to a step function at $x = 0$, that is,

$$\xi(x) = 1 \qquad (x > 0) \tag{5.1.15}$$

$$= 0 \qquad (x < 0) \tag{5.1.16}$$

The normalization by $\int [K^1(x)]^2 dx$ simply redefines the system as one having an output with unit variance. It is natural to extend this alternate concept of memory to a non-linear system. The resulting definition of memory is given by

$$\text{Mem} = \{\text{Mem}_1 + A_2(\text{Mem}_1)^2 + A_3(\text{Mem}_1)^3\}/\overline{u^2} \tag{5.1.17}$$

where

$$\text{Mem}_1 = \int_0^\infty K^1(x)dx \tag{5.1.18}$$

In (5.1.17)

$$\overline{u^2} = L^2 + 2A_2^2(L^2)^2 + 6A_3^2(L^2)^3 \qquad (5.1.19)$$

Equation (5.1.17) is consistent with previous decompositions because the total memory is itself expanded in terms of its corresponding linear contribution, Mem_1.

The decomposition of the memory for the non-linear representation of the w process, using the solution for L^2, A_2 and A_3, is presented in Figure 5.5. The linear memory contribution, Mem_1 (defined in (5.1.18)) is less than that for a totally linear representation. The loss of linear memory follows from Figure 5.4 for the spectral distribution of linear variance. Because the ratio of non-linear variance increases with f, the contribution to K^1 near $\tilde{x} = 0$ must be less for a non-linear model than a linear representation. Accordingly, the linear memory is reduced. The linear contribution, Mem_1, represents more of the total memory in stable stratification than in unstable stratifications. This trend is consistent with previous results for the increasing effect of the non-linear aspects of the functional representation for decreasing ζ. In Figure 5.5, the relative contributions of variance in the quadratic and cubic terms is also reflected in the relative contributions of the cubic and quadratic terms of the total memory.

The response function, K^1, of a non-linear representation departs most from the corresponding function of a linear representation $\tilde{x} = 0$. The non-linear memory changes are exaggerated by the squaring and cubing operations in (5.1.17). For initial responses greater than unity, (such as occur for $\zeta < 0$) the result is an increase in the contributions to

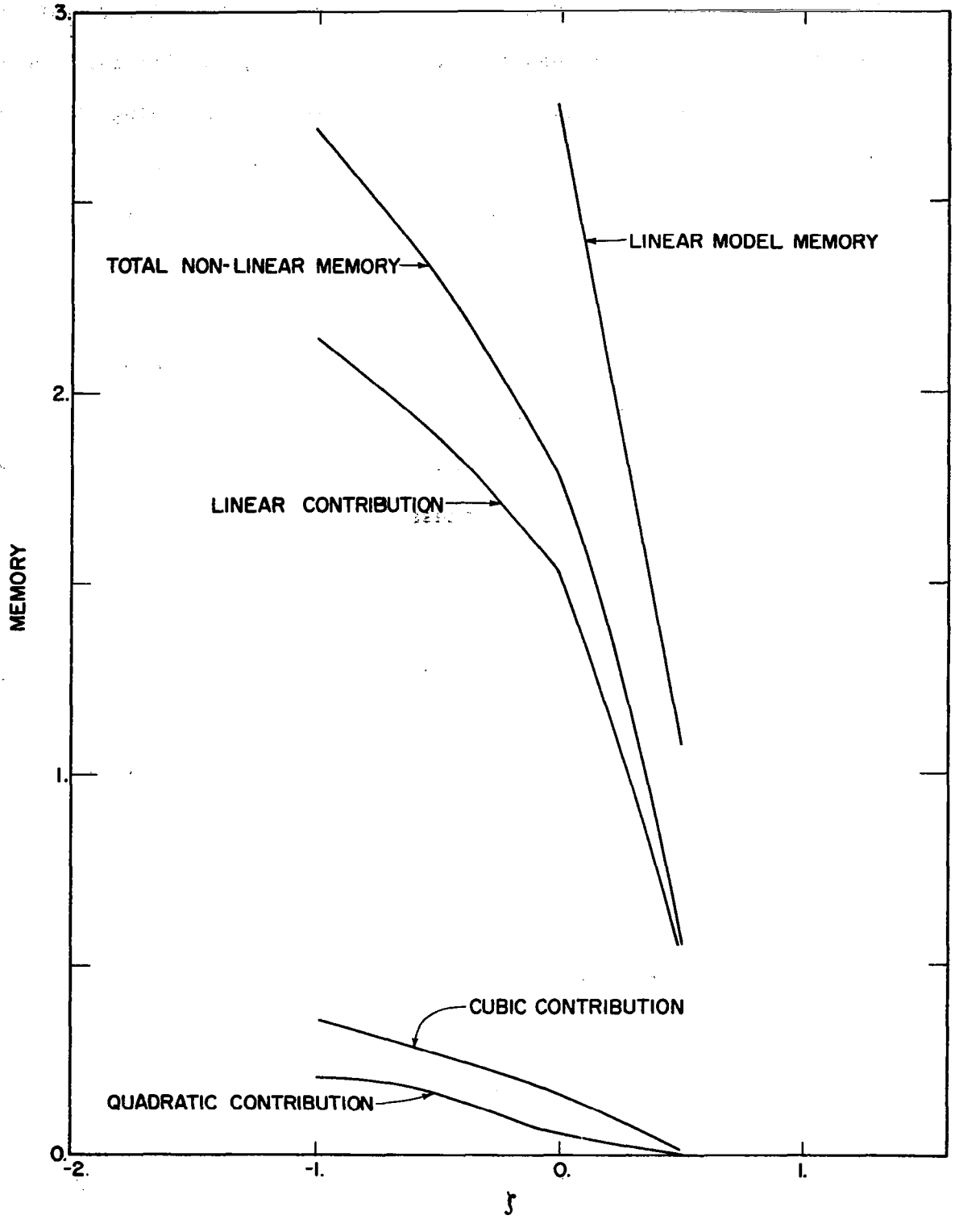

Figure 5.5. Partition of memory of vertical velocity for a cubic, separable model and a comparison with linear model.

the non-linear memory components at the expense of the linear component. Conversely, for initial responses less than unity, (as for the stably stratified region, $\zeta > 0$), the effect of squaring and cubing the linear memory contribution is to reduce the non-linear memory contributions relative to the linear part. Both of these conclusions are consistent with the relative distributions of memory in Figure 5.5.

An energy cascade by interactions among wave numbers is an important characteristic of turbulent flows with a large Reynolds number. Therefore, it is interesting to estimate the inertial transfer of energy arising from the non-linear term of the equation of motion ($u\partial u/\partial x$) for the simulated one-dimensional process. First, let us consider the Fourier transform of the inertial term. The result is

$$Tr(f) = -\frac{f}{2\pi} \text{Im} \{\hat{u}^*(f) \int \{\hat{u}(f_1)\hat{u}(f - f_1)\, df_1\} \qquad (5.1.20)$$

where Im{} represents the imaginary part of a complex argument. For the W-H expansion of $\hat{u}$, given by (2.3.6), the expected value of (5.1.20) becomes

$$\begin{aligned}\overline{Tr}(f) = -\frac{f}{\pi^3} \text{Im}\{&\hat{K}^1(-f) \int \hat{K}^1(-p)\, \hat{K}^2(f,p)\, dp \\ &- \frac{1}{2} \int \hat{K}^2(p, f-p)\, \hat{K}^1(-p)\, \hat{K}^1(p-f)\, dp \\ &+ \frac{1}{\pi} \int \hat{K}^2(p, f-p) \int \hat{K}^2(-p, r)\, \hat{K}^2(-r, p-f)\, dr\, dp \\ &+ \ldots\ldots \}\end{aligned} \qquad (5.1.21)$$

Further, the separability condition, (5.1.7) reduces (5.1.21) to

$$\overline{Tr}(f) = -\frac{f}{\pi^2}\,\mathrm{Im}\,\{A_2|\hat{K}^1(f)|^2\int|\hat{K}^1(p)|^2\,dp$$

$$-\frac{A_2}{2}\int|\hat{K}^1(p)|^2\cdot|\hat{K}^1(f-p)|^2\,dp \qquad (5.1.22)$$

$$+\frac{A_2^3}{\pi}\int\cdot|\hat{K}^1(p)|^2\,|\hat{K}^1(f-p)|^2\int|\hat{K}^1(r)|^2$$

$$dr\,dp + \ldots\}$$

An inspection of (5.1.22) reveals that the terms bracketed by {} are all real. Therefore, $\overline{Tr}$ is given as the imaginary part of a real number, and consequently

$$\overline{Tr}(f) = 0 \qquad (5.1.23)$$

Accordingly, there is no transfer of energy at all by the separable kernel model of velocity. In its present form, the quasi-linear model is dynamically inconsistent with known characteristics of turbulent flow.

In order to have a non-trivial transfer of energy, it is necessary to have an imaginary part to the terms bracketed by {} in the right hand side of (5.1.21). The fact that the separable kernel model has only a real part stems from the lack of phasing between the Fourier transforms of the kernels. The interactions between kernels have been shown by Crow and Canavan (1970) to be the equivalent mechanism for transfering energy as the interactions between velocity components at

different wave numbers. These authors also demonstrated that the W-H functional representation is handicapped by a need to include very many kernel interactions to simulate the interactions of $\hat{u}$ over wave number space. Therefore, the quasi-linear model for velocity shares the dynamical shortcomings of W-H functional representations that are significantly more sophisticated.

However, the redeeming feature of the separable kernel method is that it leads to a faithful reproduction of the low order statistical structure of observed data. We next examine a model for the derivative of the longitudinal velocity component which better represents the dynamics of energy transfer.

5.2 Derivative Model

In earlier discussions (Section 2.2), it was noted that the small scale ($f >> 1$) structure of the derivative of velocity in isotropic turbulence was distinctly non-Gaussian, and that the dynamical process at such scales was distinctly non-linear. The results for the non-linear velocity model of the previous section indicate that a simulation of the dynamics of turbulence with a truncated set of kernels, even for a weakly non-Gaussian situation, requires a more sophisticated closure scheme. We now demonstrate that the method of separable kernels applied to a model of the derivative of longitudinal velocity, for a modest range of Reynolds number, results in a plausible dynamical analogy.

Consider the W-H functional expansion of a derivative of the longitudinal velocity in the mean wind direction

$$\frac{\partial u}{\partial x} - d(x) = \int D^1 H_1 + \iint D^2 H_2 + \ldots \tag{5.2.1}$$

The relationship of the moments of (5.2.1) in relationship to the kernels, D^1, is similar to that given in (5.1.2) to (5.1.4). In the same abbreviated notation, the interrelationships are

$$\overline{d^2} = \int \cdot \int D^1 D^1 + 2 \int \cdot \int D^2 D^2 + 6 \int \cdot \int D^3 D^3 + \ldots \tag{5.2.2}$$

$$\overline{d^3} = 3 \int \cdot \int D^1 D^1 D^2 + \int \cdot \int D^2 D^2 D^2 + 3 \int \cdot \int D^2 D^3 D^3 + \ldots \tag{5.2.3}$$

$$\overline{d^4} = \int \cdot \int D^1 D^1 D^1 D^1 + 4 \int \cdot \int D^1 D^1 D^1 D^3 + 6 \int \cdot \int D^1 D^1 D^2 D^2 + \int \cdot \int D^2 D^2 D^2 D^2 + \int \cdot \int D^1 D^1 D^3 D^3 + 6 \int \cdot \int D^1 D^2 D^2 D^3 \tag{5.2.4}$$

where the orthogonality of the Hermite polynomials has determined the integer coefficients. Again, in analogy with the non-linear velocity model, it is convenient to assume that the kernels of the derivative process are separable,

$$D^1(x_1, \ldots x_i) = \Delta_i \prod_{j=1}^{i} D^1(x_j) \tag{5.2.5}$$

The coefficients Δ_i correspond to the coefficients A_i of the velocity

model. The result of substituting (5.2.5) in (5.2.2) to (5.2.4) is a set of algebraic equations

$$\overline{d^2} = \lambda^2 + 2\Delta_2^2 \lambda^4 + 6 \Delta_3^2 \lambda^6 + \ldots \tag{5.2.6}$$

$$\overline{d^3} = 6\Delta_2 \lambda^4 + 8\Delta_2^3 \lambda^6 + 36 \Delta_2 \Delta_3 \lambda^6 + 108 \Delta_2 \Delta_3 \lambda^8 + \ldots \tag{5.2.7}$$

$$\overline{d^4} = 3\lambda^6 + 24 \Delta_3 \lambda^6 + 60 \Delta_2^2 \lambda^6 + 60 \Delta_2^4 \lambda^8 + \ldots \tag{5.2.8}$$

where λ^2 is the linear contribution to the variance of the derivative given by

$$\lambda^2 = \int [D^1(x)]^2 \, dx \tag{5.2.9}$$

The structure of moments for the derivative, up to $\overline{d^4}$, are drawn from results reported by Wyngaard and Tennekes (1970). Their results for the skewness and kurtosis for the longitudinal velocity component form a convenient basis for a truncated representation similar to that given in Section 5.1. Based on the log-normal probability density function for a derivative process (Gurvich and Yaglom, 1967), and Kolmogorov's (1962) hypothesis concerning the probabilistic structure of the local dissipation, Wyngaard and Tennekes found from some empirical data that

$$\overline{d^3}/(\overline{d^2})^{3/2} = - c_1 R_T^{3/16} \tag{5.2.10}$$

$$\overline{d^4}/(\overline{d^2})^2 = c_2 \, R_T^{1/2} \tag{5.2.11}$$

where R_T is Reynolds number based on the Taylor microscale. Examination of Figures 5 and 6 of the paper of Wyngaard and Tennekes lead to the empirical estimates

$$c_1 = 0.16 \tag{5.2.12}$$

$$c_2 = 0.40 \tag{5.2.13}$$

Further, the Taylor microscale, λ_T, can be related to the generative scale length, ℓ, for turbulence in local balance between generation and dissipation (Tennekes and Lumley, 1972, p. 67)

$$\frac{\ell}{\lambda_T} \sim \left(\frac{Re}{15}\right)^{1/2} \tag{5.2.14}$$

and consequently

$$R_T = (15 \, Re)^{1/2} \tag{5.2.15}$$

In terms of the Reynolds number of the generative region, Re, the skewness and kurtosis of the derivative become

$$\overline{d^3}/(\overline{d^2})^{3/2} = - \, 0.21 \, Re^{3/32} \tag{5.2.16}$$

$$\overline{d^4}/(\overline{d^2})^2 = 0.79 \, Re^{1/4} \tag{5.2.17}$$

Wyngaard and Tennekes pointed out that dependence of the skewness and kurtosis on the Reynolds number violates the original hypothesis of Kolmogorov. However, the dependence on Re is rather weak because of the smallness of the exponents, 3/32 and 1/4. To be consistent with the formulation leading to (5.2.16) and (5.2.17), it is necessary to re-interpret the dissipation in terms of a locally averaged estimate (Kolmogorov, 1962; Oboukhov, 1962).

The estimates (5.2.16) and (5.2.17) for a given value of Re were substituted in (5.2.6) to (5.2.8), and the equations solved for λ^2, Δ_2, and Δ_3 by iteration. The model must be restricted to neutral stability because there is no available information on the distribution of the u-derivative skewness and kurtosis with stability. Table 5.1 summarizes the distribution of variance, skewness, and kurtosis for various Re.

For Re $\geq 10^4$, the iterative method of solution of the non-linear algebraic equations, (5.2.6) to (5.2.8), did not converge. The skewness and kurtosis estimates according to (5.2.16) and (5.2.17) imposed by truncated of the moments to a finite number in order to represent a process with a large Reynolds number ($>10^3$) is not uniformly valid. Also, inspection of Table 5.1 indicates that the non-linear contribution to the kurtosis ($24\ \Delta_3\lambda^6$) is negative for Re $\leq 10^2$. Because only positive values of kurtosis, like variance, have physical significance, this result is indicative of an unrealistic interaction among the kernels remaining after truncation. However, for a range of Re between 10^3 and 10^4, where the model does not radically depart from a Gaussian model, the solution for λ^2 and Δ_2 and Δ_3 appears to be successful.

An empirical form

Table 5.1

Partition of variance, skewness and kurtosis of u - derivative

	Variance			Skewness			Kurtosis		
$\log_{10}$ Re	λ^2	$2\Delta_2^2\lambda^2$	$6\Delta_3^2\lambda^6$	$6\Delta_2\lambda^4$	$8\Delta_2^3\lambda^6$	$36\Delta_2\Delta_3\lambda^6$	$3\lambda^6$	$24\Delta_3\lambda^6$	$60\Delta_2^2\lambda^6$
1	.958	.012	.030	-.443	.000	.191	2.64	-1.58	.342
2	.987	.008	.004	-.377	-.002	.062	2.89	-0.64	.240
3	.966	.005	.029	-.276	.000	-.117	2.71	1.59	.131

$$D'_u(f) = \frac{A_u f^{5/3}}{1 + (B_u f)^{4/3}} L(f) \qquad (5.2.18)$$

was chosen for the spectrum of the u - derivative. L is the one dimensional similarity solution (Pao, 1965) for the viscous subrange, given by

$$L(f) = \int_0^1 (1 - \xi^2)\xi^{2/3} \exp\left[-\frac{3}{2}\alpha(\hat{f}/\xi)^{4/3}\right] \qquad (5.2.19)$$

where

$$\hat{f} = f\, Re^{-3/4} \qquad (5.2.20)$$

for neutral stability. The coefficients A_u and B_u in (5.2.18) were calculated according to the variance and dissipation compatibility conditions (Appendix A).

The linear contribution to the spectrum of the derivative is given in Figure 5.6 for several values of Re. The effect of the viscous tail does not become significant in the case of $Re = 10^3$ until $f \simeq 350$ which is considerably smaller than the scales of interest for the majority of engineering applications. However, the maximum values of Re and f of the model are underestimates of the respective atmospheric values. In Figure 5.6, there is an increase in the variance of the derivative at smaller scales with an increase in Re. The increase in the variance is itself felt in the increase in the response at smaller scales (Table 5.2).

The structure of the response function, $D_u^1(\tilde{x})$, is given in Figure 5.7 for $Re = 10^2$ and $\zeta = 0$. The response functions for a total linear representation of $\partial u/\partial x$ and the linear and non-linear representation of

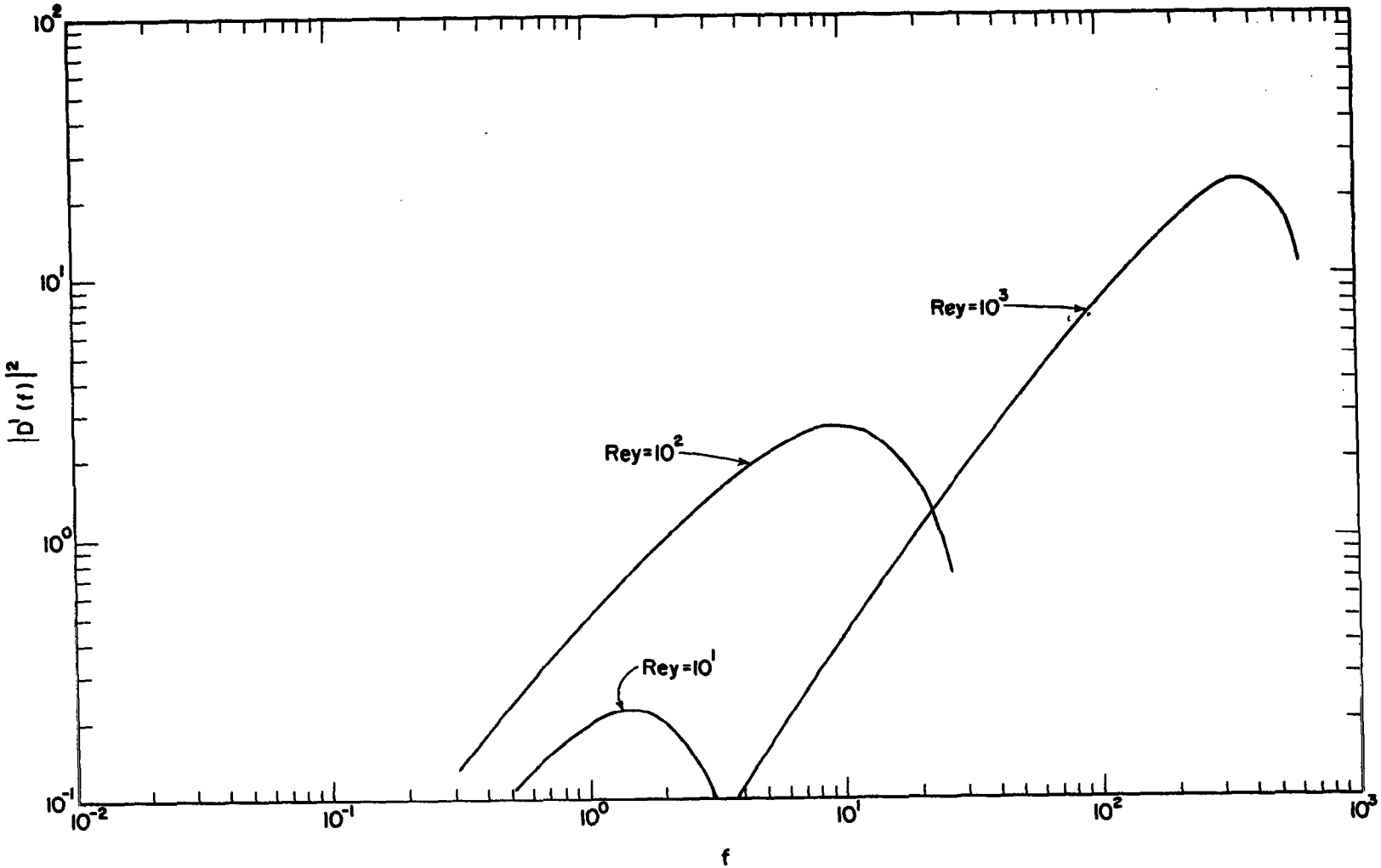

Figure 5.6. Linear part of spectrum of derivative of longitudinal velocity component for various Reynolds numbers.

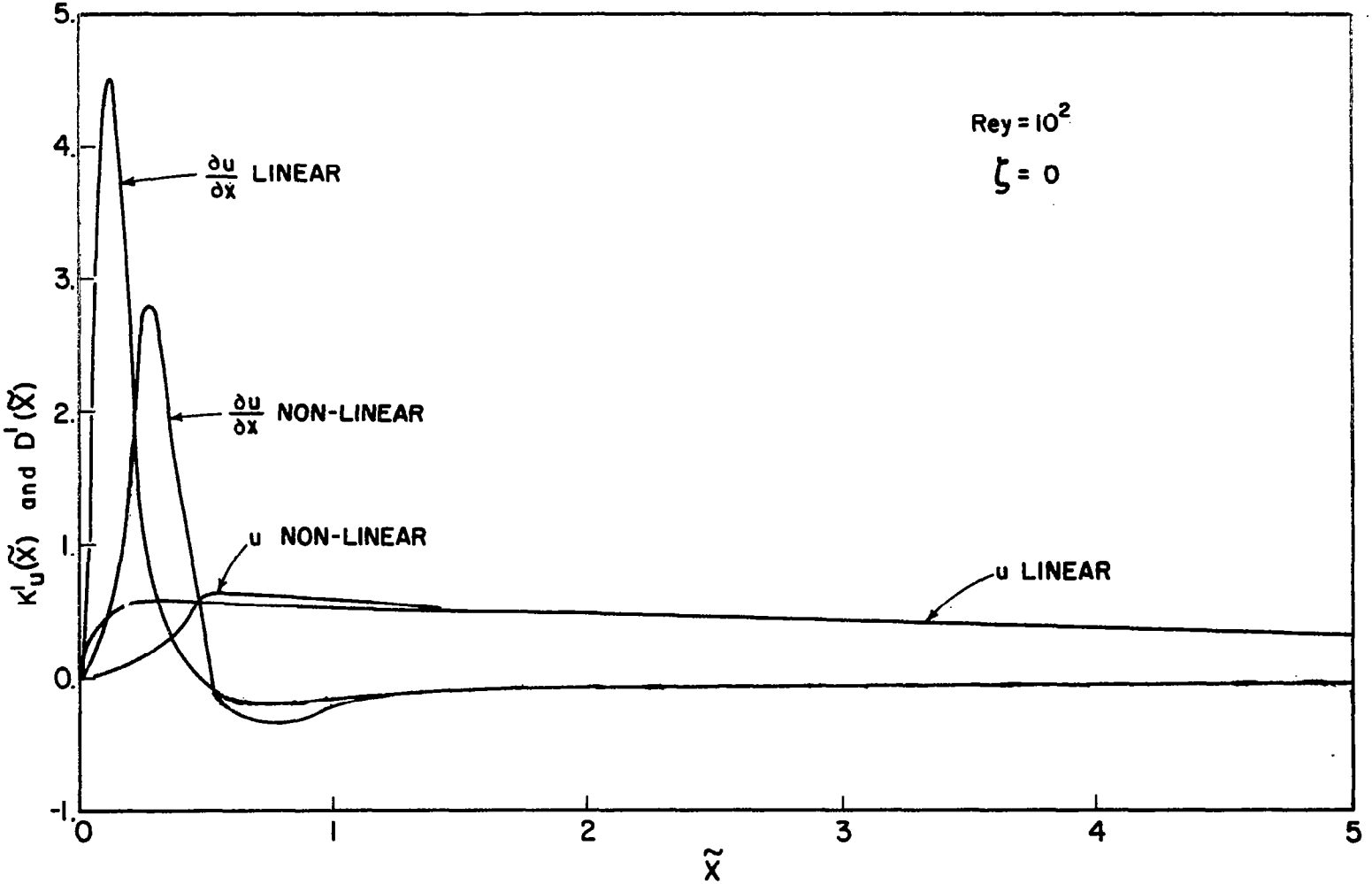

Figure 5.7. Comparison of non-linear response of derivative of longitudinal velocity component with linear response of derivative and with non-linear and linear responses of longitudinal velocity component.

Table 5.2

Magnitude and location of the maximum response and linear contribution to the memory of u - derivative model

$\log_{10}$ Re	D^1_{max}	$\tilde{x}_{max}$	Mem_1
1	0.25	0.20	0.824
2	2.8	0.027	0.0

u are also presented. The maximum response for the u - derivative process occurs at large separation and is less than the maximum response for the linear process. The reason for changes in the non-linear structure relative to the linear were discussed in Section 5.1 in relation to the non-linear velocity model. The increase of the ratio of non-linear to linear variance with decreasing scale, for a given total spectral content, is associated with the reduction in the linear response at small separations, say $\tilde{x} < 0.5$.

In the previous section, we discussed the lack of dynamical consistency for a separable model of the non-linear, non-Gaussian representation of velocity. The lack of phase interactions among the Fourier transform of the response functions, $\hat{K}^i$, resulted in a lack of energy transfer inertially. Therefore, we examine the inertial transfer properties of a separable W-H representation for the derivative for its phase and energy transfer properties. A series of equations for the

interrelationships between the kernels K^i and D^i follow from the W-H expansions for the velocity (5.1.1) and the derivative (5.2.1) when each expansion is substituted in the identity

$$u(x) = \int_{-\infty}^{x} \frac{\partial u}{\partial x'}\, dx' \tag{5.2.21}$$

Terms of the expansion are gathered in like orders of the (orthogonal) Hermite polynomials. For the separable derivative model, the interrelationships become

$$K^1(x_1) = \int_{-\infty}^{0} D^1\,(y + x_1)\, dy \tag{5.2.22}$$

$$K^2(x_1,x_2) = \Delta_2 \int_{-\infty}^{0} D^1(y + x_1)\, D^1(y + x_2)\, dy \tag{5.2.23}$$

The relationship (5.2.23) between the kernels K^i of the corresponding velocity model differs from the model of Section 5.1. In particular

$$K^2(x_1,x_2) \neq A_2\, K^1(x_1)\, K^1(x_2) \tag{5.2.24}$$

where A_2 is a constant.

A procedure similar to that used in (5.1.1) and (5.2.1), but using Fourier transformed equivalents, results in a sequence of expressions between $\hat{D}^i$ and $\hat{K}^i$ given by

$$i\, f_1\, \hat{K}^1(f_1) = \hat{D}^1\,(f_1) \tag{5.2.25}$$

$$i\,(f_1 + f_2)\, \hat{K}^2(f_1,f_2) = \hat{D}^2(f_1,f_2) \tag{5.2.26}$$

Substitution of the Fourier transform equivalent of the separability of the derivative process (5.2.5) leads to an expression for $\hat{D}^2$ in terms of $\hat{D}^1$ given by

$$\hat{D}^2 (f_1,f_2) = \Delta_2 \hat{D}^1 (f_1) \hat{D}^1 (f_2) \tag{5.2.27}$$

Finally, the combination of (5.2.25), (5.2.26) and (5.2.27) results in a succinct statement of the kernel interaction structure of the corresponding velocity model

$$\hat{K}^2 (f_1,f_2) = \Delta_2 \left(\frac{i f_1 f_2}{f_1 + f_2}\right) K^1 (f_1) K^1 (f_2) \tag{5.5.28}$$

From (5.1.21), the energy transfer for the separable derivative model becomes

$$\begin{aligned}\overline{Tr}(f) = \frac{-f}{\pi^2} \Delta_2 \, \mathrm{Im} \{ & i f |\hat{K}^1(f)|^2 \int \frac{p}{p+f} |\hat{K}^1(p)|^2 \, dp \\ & \frac{-i}{2f} \int p(f-p) |\hat{K}^1(f-p)|^2 |\hat{K}^1(f-p)|^2 \, dp\}\end{aligned} \tag{5.2.29}$$

An additional term involving a triple product of $\hat{K}^2$ (and hence Δ_2) has been neglected in (5.2.29). The expression in (5.2.29) in the brackets {} is purely imaginary in contrast to (5.1.21). Therefore, the energy cascade is non-trivial for a separable derivative model in contrast to that for a separable velocity model. For convenience, we simplify the notation by introducing a function for the common term $f|\hat{K}^1|^2$,

$$\Lambda(f) = f|\hat{K}^1(f)|^2 \tag{5.2.30}$$

Equation (5.2.29) reduces to

$$\overline{Tr}(f) = \frac{f\Delta_2}{\pi^3} \{\Lambda(f) \int \frac{\Lambda(p)}{p+f} dp - \frac{1}{2f} \int \Lambda(p)\Lambda(f-p)\, dp\} \quad (5.2.31)$$

Computationally, (5.2.31) is evaluated from estimates of Λ based on (5.2.30) and (5.2.25).

Estimates of $f\ \overline{Tr}(f)$ derived from (5.2.31) are displayed in Figure 5.8 for $Re = 10^2$. The transfer of energy is confined to the viscous region, with negligible energy transfer in the range $10^0 < f < 10^1$.

For comparison, we have indicated the theoretical prediction of the transfer function arising in the model of Pao (1965, 1968) for isotropic turbulence. Pao models the energy transfer as a convergence of spectral flux, S(f), given by

$$S(f) = \varepsilon_o \exp - 3/2\ \alpha\ (f/f_{KOL})^{4/3} \quad (5.2.32)$$

where

$$\overline{Tr}(f) = \frac{-d}{df} S(f) \quad (5.2.33)$$

The curve for $\overline{Tr}$ shown in Figure 5.8 represents a one-dimensional energy transfer estimate derived from (5.2.23) based on the assumption of isotropic energy transfer (Batchelor, 1953, p. 50). The agreement is gratifying although the Pao model contains a wider inertial subrange of nearly zero energy transfer than does the separable derivative model.

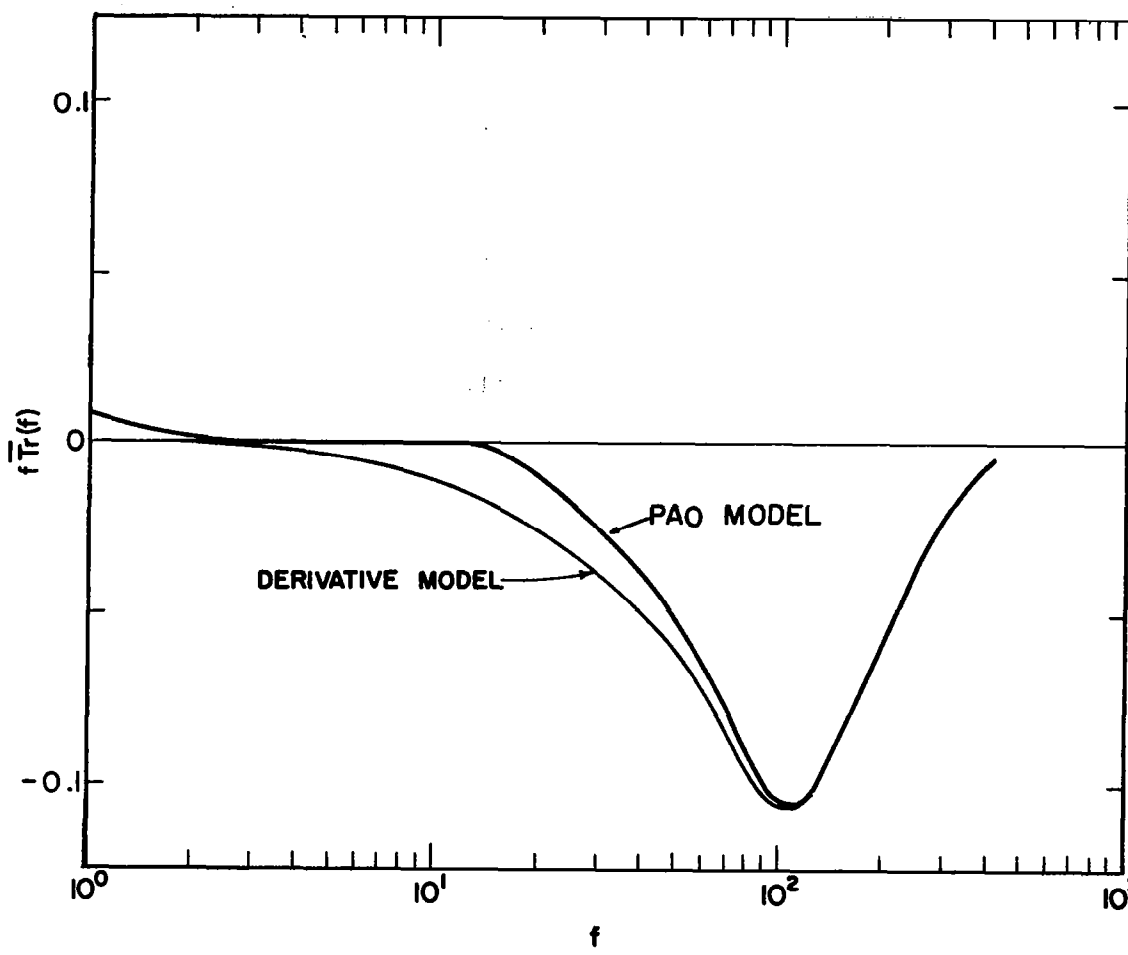

Figure 5.8. Comparison of spectral energy transfer in viscous sub-range for derivative model and similarity model of Pao.

The lack of energy transfer in the generative region (not shown) is in serious disagreement with known features of large scale turbulence (Lumley and Tennekes, 1970, p. 271). It remains an unresolved problem to develop a model based on a W-H representation which will adequately reproduce the spectral flux convergence of the generative region.

In summary, it is concluded that for a realistically large Reynolds number range ($10^3<Re<10^4$) the derivative model adequately represents the low order moment structure and the inertial properties of the u component of turbulence in the viscous subrange. For some applications such as those involved with systems response at scales comparable to the viscous subrange, the derivative model, as described above, may be sufficient. But for problems involving eddies with dimensions of the order of the energy containing eddies, neither the velocity nor the derivative models adequately represent the non-linear features of that region as manifested in a spectral transfer of energy.

We now move to an application and evaluation of the simulation of realizations of turbulence by some of the linear and non-linear models discussed in Chapters 3.0, 4.0, and 5.0.

6.0 DEMONSTRATION AND EVALUATION OF MODELS

The development of Chapters 3.0, 4.0, and 5.0 has concentrated on the calculation of the response functions from given statistical data. The linear filter is derived from a predetermined spectral form whereas the non-linear filters of Chapter 5.0 require additional empirical data in the form of third and fourth moments. It is the purpose of this chapter to briefly describe the implementation of the results derived in the previous chapters for the simulation of turbulence. The discussion is limited to linear and non-linear models of a single velocity component.

6.1 Generation of White, Gaussian Series

Standard computer sub-routines exist for the generation of randomly ordered, Gaussian series. The difficulty with using these random number generators lies in their small but significant deivations from a Gaussian distribution for moments of order greater than 2. The white spectrum condition is improved iteratively by several random order shufflings of the input series.

The problem of non-Gaussianity was overcome by generating random values from the cumulative probability density function of a Gaussian process. For a Gaussian process with mean 0 and variance 1, the probability, p, that a sampled value, s, will be less than x,

$$p = Pr(s \leq x) \tag{6.1.1}$$

is given by

$$p = \mathrm{erf}(x) \tag{6.1.2}$$

The range of p is [0,1] for a domain of x $(-\infty,\infty)$. Conversely, the Gaussian distributed variable x, which occurs with probability p is given by

$$x = \mathrm{erf}^{-1}(p) \tag{6.1.3}$$

The generation of N values of x from (6.1.3) was achieved for an equi-spaced partition of the range of probability, p, into N increments. The limit of accuracy of the routine for the inverse error function (Abramowitz and Stegun, 1964) of $5\ 10^{-5}$ for single precision computations limits the length of generated time series to about $2\ 10^{4}$ points. Conversely, because the approximation to Gaussian moments of order greater than 2 becomes increasingly dependent on several rare large deviations, it is necessary to generate a minimum number of points to achieve approximate Gaussianity in the higher moments. The minimum then depends on the degree of accuracy desired in the moments of the filtered series. The conditions on the length of the series are less stringent for linear simulations because of a lack of interaction among moments.

6.2 Linear Model Test

Several methods are available for the evaluation of the transformation

$$y(t) = \int K^{1}(\tau)\ \xi(t - \tau)\ d\tau \tag{6.2.1}$$

where K^1 is the filter and ξ and y are the white and filtered series respectively. The direct evaluation of (6.2.1) by either a discrete analog or a quadrature scheme results in an additional shaping of the input spectrum in addition to the filtering by $|\hat{K}^1|^2$. Therefore, it is advantageous to utilize the Fourier transform equivalent of (6.2.1), given by

$$\hat{y}(\omega) = \hat{K}^1(\omega)\ \hat{\xi}(\omega) \tag{6.2.2}$$

The evaluation of $\hat{K}^1$ in (6.2.2) may be made in either of several ways. The first method is the direct evaluation of $\hat{K}^1$ from K. However, this method was found to be inexact in specifying the low frequency (wave number) spectral content. This error in filtering the large scales arises from the recursion involved in estimating the Laguerre coefficients (Appendix B). A second method which is more exact involves by-passing the redunant step of computing K^1 and its Fourier transform. The method of spectral factorization (Chapter 2.0 and Appendix B) results in an exact estimate of $\hat{K}^1$ directly from the given input spectrum. However, in order to accommodate the fast Fourier transform techniques it is necessary to interpolate the estimate of $\hat{K}^1$, or more correctly, its regularized spectral equivalent to equal increments of ω (or f). As a result of the spectral factorization $\hat{K}^1$ is tabulated at equal increments of u where

$$\omega = \tan u/2 \quad . \tag{6.2.3}$$

The procedure used to estimate $\hat{K}^{1}(\omega)$ was to interpolate the regularized spectral factors for the u derived from the inverse of (6.2.3) and then to transform the ω-space using the relationship (Rino, 1970)

$$\hat{K}^{1}(\omega) = \hat{g}(\omega)\ [2^{-1/2}\ (1 + \exp(-iu))]^{n+1} \qquad (6.2.4)$$

where $\hat{g}$ and n are defined in Appendix B. The interpolation scheme used to interpolate $\hat{g}$ was a third-order spline function routine. The success of this second method is guaranteed by the fact that the regularized spectral density functions are smooth, slowly varying functions of scale.

The combined error of spectral factorization to estimate $\hat{g}$ and its interpolation to estimate $\hat{K}^{1}$ was found by computations to be less than 10^{-3} of the modulus at a given scale. Therefore in estimating a spectrum the only discernible disparity between an input spectrum of turbulence and its simulation lies in the deviation of the white noise spectrum from unity or in its statistical variability. This non-whiteness can be eliminated in spectral comparisons by normalization of the output spectrum by the input spectrum. Figure 6.1 presents a comparison of the empirical and simulated spectra of vertical velocity for a total length of simulation equivalent to about 10^{3} integral scales. The empirical form chosen for the spectrum of w is discussed in Chapter 3.0 and Appendix A. It can be seen from Figure 6.1 that the Kolmogorov spectral form for $f >> 1$ has been faithfully reproduced. It is concluded that within the extremes of statistical variability expected in a single finite length of record, the spectrum of the

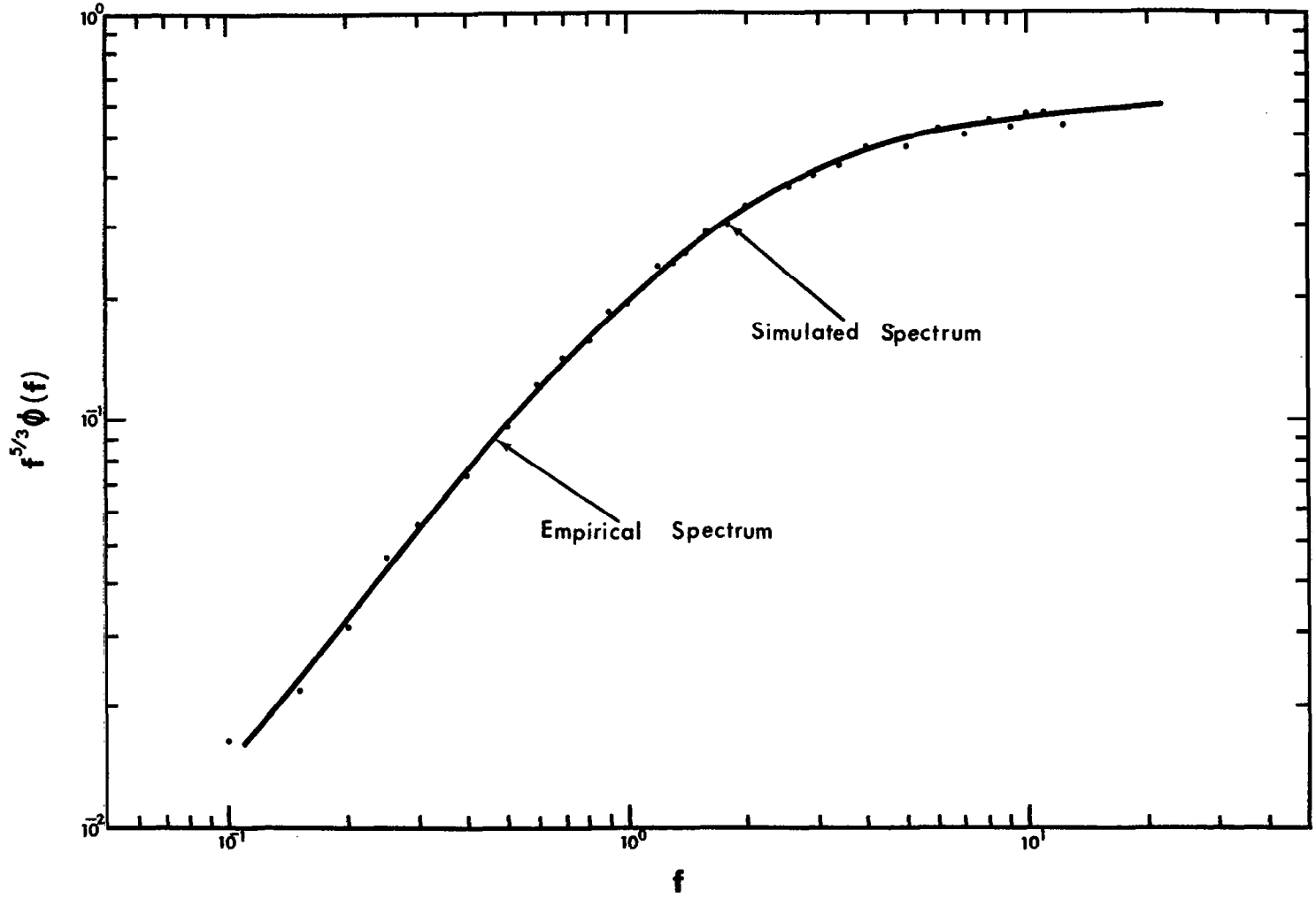

Figure 6.1. Comparison of spectra of empirically specified model and of simulated turbulence for a linear representation.

simulated turbulence normalized by the sample white spectrum is identical to the prescribed, empirical spectrum.

This completes the demonstration of the linear filtering method, and we turn to an evaluation of a non-linear model.

6.3 Non-Linear Model Test

The specification of a white Gaussian input for stimulation is more critical for a non-linear simulation. Deviations from a white, Gaussian input process result in spurious correlations between the kernels of different orders. For example, in Section 5.1, if the input was non-white or non-Gaussian, the moment expansions developed there would contain various correlation functions of the input process in place of the integer coefficients. In particular, for an input series, h(t), with correlation functions

$$R_2(\tau) = \overline{h(t)\ h(t+\tau)} \tag{6.3.1}$$

$$R_3(\tau_1\ \tau_2) = \overline{h(t)\ h(t+\tau_1)\ h(t+\tau_2)} \tag{6.3.2}$$

$$R_4\ (\tau_1,\ \tau_2,\ \tau_3) = \ldots. \tag{6.3.3}$$

the variance expansion is given symbolically

$$\begin{aligned}\overline{u^2} = &\int \cdot \int K^1K^1R_2 + \int \cdot \int K^2K^2R_4 + \int \cdot \int K^3K^3R_6 \\ &+ \int \cdot \int K^1K^2R_3 + \int \cdot \int K^1K^3R_4 + \int \cdot \int K^2K^3R_5\end{aligned} \tag{6.3.4}$$

to third order. The lack of orthogonality (relative to a Gaussian p.d.f.) results in the last three terms. The non-whiteness of the input process also results in multiple moment-kernel interactions. Consequently, deviations in output statistics for a non-ideal input are attributable to several sources of error simultaneously.

Just as in the development of techniques for implementing the linear model, it is advantageous to first compute the Fourier transform of a simulated realization of turbulence. The expansion of the realization

$$\hat{u}(k) = \hat{K}^1(k)\,\hat{H}_1(k) + \int \hat{K}^2\,(p_1\ k-p)\,\hat{H}_2(p_1\ k-p)\,dp + \ldots. \tag{6.3.5}$$

requires only a given input series $\hat{H}_1$ because the $\hat{H}_i$ are related to $\hat{H}_1$ by the Gram-Schmidt orthogonalization procedure. For example

$$\hat{H}_2(k_1,\ k_2) = \hat{H}_1(k_1)\,\hat{H}_1(k_2) - \delta(k_1 + k_2) \tag{6.3.6}$$

Further, the expansion (6.3.5) reduces to

$$\hat{u}(k) = \hat{y}(k) + A_2\int \hat{y}(p)\,\hat{y}(k - p)\,dp + \ldots + A_2\,\hat{K}^1(o)\,\hat{K}^1(k) + \ldots \tag{6.3.7}$$

where

$$\hat{y}(k) = \hat{K}^1(k)\ \hat{H}_1(k) \tag{6.3.8}$$

for separable kernels.

The form of (6.3.7) represents a functional expansion in $\hat{y}$ with corrections for non-orthogonality. The generation of $\hat{y}$ was described in Section 6.2. The actual simulation of u(x) involves an inverse Fourier transformation after the computation of (6.3.7).

Some results of a sample computation for a non-Gaussian process with a given skewness 0.23 and a given kurtosis 3.6 are displayed in Figure 6.2. The method of generation of the white, Gaussian input series was the same as described in Section 6.2. The procedure consisted of generating repeated, serial samples of 10ℓ up to an arbitrary upper limit of $10^3\ell$. The results for the skewness and kurtosis are not exactly those of the input. An examination of the higher moments of the input, $\overline{\xi^n}$, for $n \geq 5$, revealed that the number of points in each of the individually generated realizations of length 10ℓ, had a weakly non-Gaussian structure ($\overline{\xi^5} = 0.06$, and $\overline{\xi^6} = 14.5$ rather than their Gaussian values of $\overline{\xi^5} = 0$ and $\overline{\xi^6} = 15$). The error in the limiting values of skewness and kurtosis are believed to arise by spurious kernel-moment interactions as discussed earlier. Two methods are available to eliminate such errors -- either a trial and error method of varying the specified input skewness and kurtosis, or a generation of a longer, single realization, say $10^3\ell$, so that the errors in the Gaussian generator are reduced.

A second characteristic of the non-linear test simulation is displayed in Figure 6.3. The spectrum weighted by wavenumber raised to a

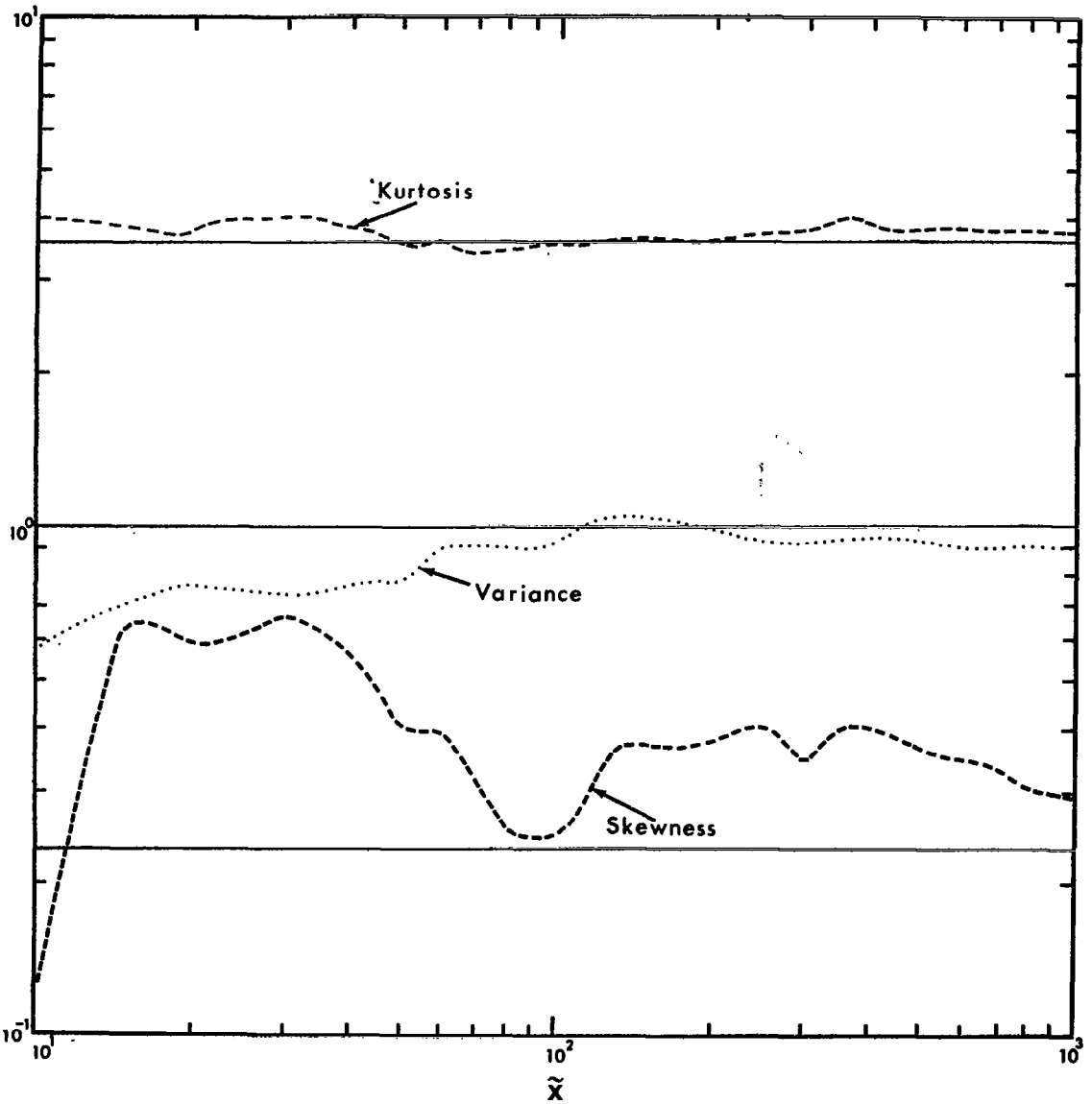

Figure 6.2. Comparison of moments of simulated process for successive increments to length of series with input values.

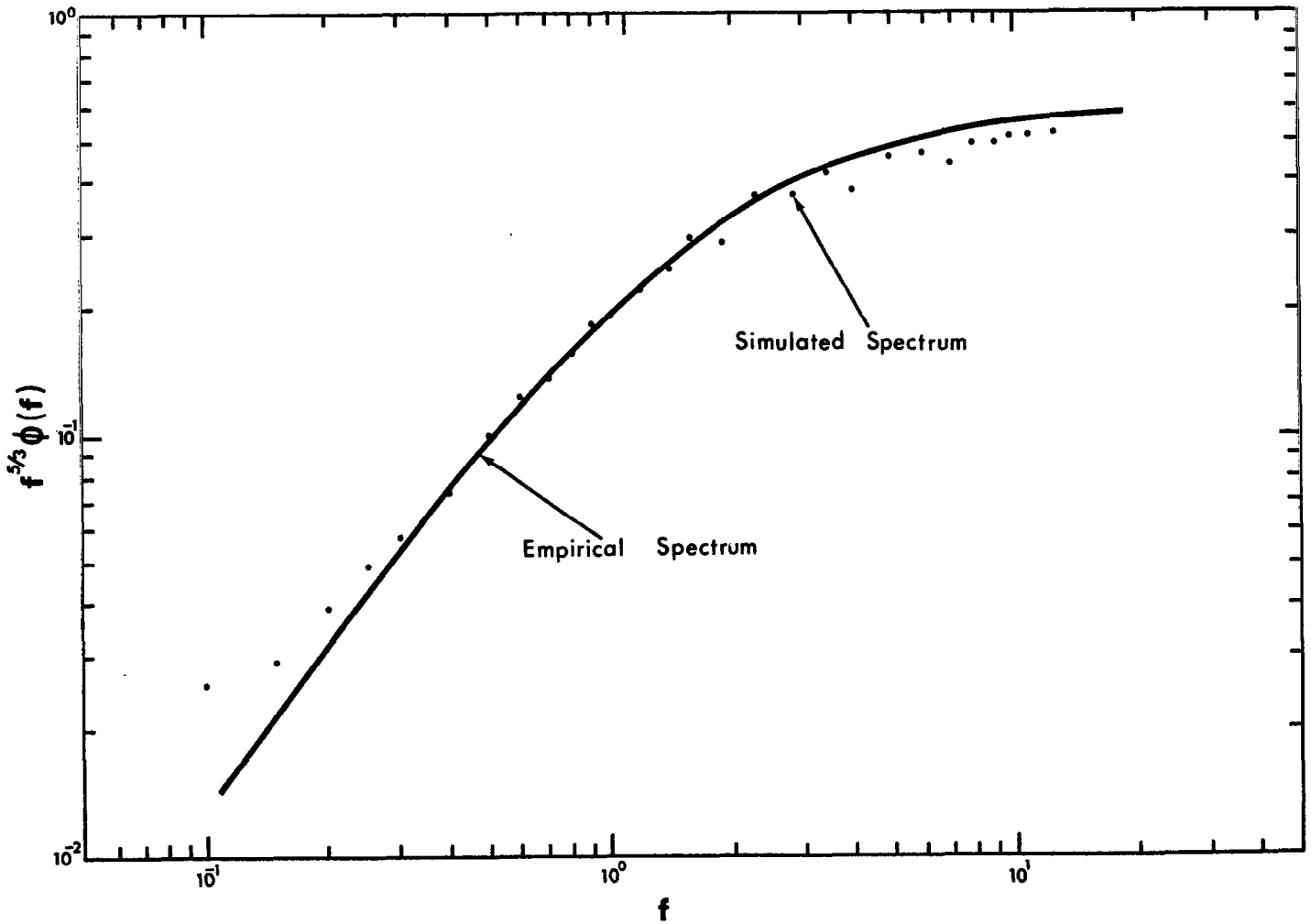

Figure 6.3. Comparison of spectra of empirically specified model and of simulated turbulence for a non-linear representation.

5/3 power displays a slight systematic underestimation of the spectral content of the inertial sub-range and an overestimate at scales $f < 1$. Apparently, the spurious moment interactions which result in an underestimate the total variance (Figure 6.2) vary in scale, as might be expected. Their accumulated effect is to reduce the effective value of the response function near $x = 0$ and increase the response at large scales. Further simulations utilizing single large arrays for individual sample realizations can be expected to overcome this implementation difficulty, in that the moment-kernel interactions will be reduced.

It is concluded that the mechanics of simulating turbulence require a close scrutiny of the Gaussian and spectral properties of the input process in order to achieve realistic results. Further, it is recommended that computations be conducted in phase space in order to utilize the accuracy of the spectral factorization procedure, with a transformation to real space after filtering.

7.0 SUMMARY AND CONCLUSIONS

We have examined the method of simulating turbulence by filtering a white noise process. The development of models has been directed towards overcoming three areas of weakness in previous filtering methods. First, the calculation of filters by digital spectral factorization of empirical spectra of surface layer turbulence eliminates the need to use spectra with known spectral factors. Second, the development of linear, multi-component models follows from the methods of uni-component models after diagonalization of the spectral matrix. Third, the non-Gaussian structure of the velocity and derivative of a turbulent component which is associated with the patchy nature of turbulence was examined in several non-linear models. The results of each of these three areas of model development are reviewed and summarized.

7.1 Linear, Uni-Component Models

Because the linear filtering technique has enjoyed considerable success in a variety of applications, similar models were developed and expanded in Chapter 3.0 to incorporate aspects of boundary layer similarity and general spectral forms. A comparison of several empirical formulations, for surface layer spectra and the kernels derived from them, showed that the response structure, particularly for large scales, was sensitive to the original empiricism. A definitive formulation for the energy containing sizes of the turbulence awaits further experimentation and theoretical consolidation.

The initial response and width of appreciable response were also examined relative to the thermal stratification. Initial response of velocity, normalized by surface stress, was shown to increase in any stratification. Also, the range of response broadened with decreased stability. The simulated turbulence has a somewhat larger memory than the more common first order linear model -- a property of interest for control problems. The initial response was shown to increase with height under all stratifications, but to increase more rapidly in unstable stratifications. The response function for the vertical velocity component was approximated empirically by the relationship

$$K^1(\tilde{x};\zeta) = \gamma_w^{1/2}(\zeta) \exp - (\tilde{x}/B_w)^{2/3} H(\tilde{x}) \qquad (7.1.1)$$

where

$$\gamma_w^{1/2} = 0.75 \ (1 + 0.75 \ |\zeta|) \qquad (7.1.2)$$

$$B_w = 0.7 \ (1 + 0.75\zeta + 3.0\zeta^2) \qquad (7.1.3)$$

$$H(\tilde{x}) = 0.5 \ (1 + \exp - 2.5 \ \tilde{x}^{2/3}) \qquad (7.1.4)$$

over the range

$$- 1.5 \leq \zeta \leq 0.5 \qquad (7.1.5)$$

and

$$0 \leq \tilde{x} \leq 10 \qquad (7.1.6)$$

Further studies of the response structure as influenced by viscosity indicated a delay in the build-up of response to an impulse. The delay decreased and the maximum response increased with increasing Reynolds number. The viscous model for large Reynolds number converged to the "inviscid" model. The response of the turbulence in the viscous models resulted from the lower energy content at scales comparable to the viscous subrange. The memory of the simulated turbulent process decreased with an increase in the Reynolds number.

The predictive function of the turbulence is essentially a single "now" value, and the mean square error of prediction grows rapidly with prediction distance. For example, the root-mean-square error of the prediction at half an integral length into the future is estimated to be 0.8 σ_w, where σ_w is the standard deviation of the vertical velocity component. However, the model based on a -5/3 spectral slope has a slightly larger memory than the usual first order linear model.

A linear model of the derivative of the vertical velocity in the viscous subrange was examined for a later application to a non-linear model applicable to the modeling of diffusion. Because the response of the derivative is negative over a large range of scales, the memory of the derivative process is significantly less than that of the corresponding velocity process. Intuitively, the reduction in memory is compatible with the concept of increased disarray in differentiated signals of turbulent velocity or temperature.

The change in derivative response with a change in the viscosity indicated that the maximum response increased and converged towards smaller delay with increasing Reynolds number. The response at the large scales also converged to the inviscid response, indicating an increasing independence of the generative and viscous regions with increasing Reynolds number. Similarly, the memory of the derivative process decreases as the Reynolds number is increased.

7.2 Linear, Multi-Component Models

The method of linear simulation was extended to the multi-component structure of turbulence in the atmospheric boundary layer. Specifically, the model was devised to simulate the important cross-correlations between u, w, and θ. A simulation of the co-variances is equivalent to reproducing the momentum and heat fluxes characteristic of the surface layer.

The problem was simplified by diagonalizing the spectral matrix at every frequency. This was possible at scales where the matrix was diagonally dominant, or where the turbulence was nearly isotropic. The resulting eigen-spectra were spectrally factored in the same manner as followed in the single component models. The response functions were then reoriented to the original component space by a special unitary transformation which preserved the minimum phase structure of the eigen-factors.

The basic u-w model in neutral stratification was examined in terms of the corresponding single component response structure. In the multi-component model, the self-response of u and w was found to be

less than the response for a single component. Although the presence of a vertical momentum flux decreased the self-response, the total response of the vertical velocity to stimuli was increased by the cross-response. At scales greater than $\ell/10$, the total response exceeded the sum of single component responses. Despite the increase in larger scale response, there is only a small change in the predictability of the w component. In addition, the prediction process remains essentially a single point, weighted "now" value scheme.

The multi-component model was next extended to include the effects of stratification. Consideration of the w and v components revealed identical initial responses for different variances, and different memories. It was concluded that the initial response was solely a function of the spectral distribution of variance for scales much smaller than the energy-containing region. The predictability of this model increases with increasing instability, because of the increased low frequency content. The coupling between u and w also decreased with increasing instability. It was concluded that the decreased coupling was a manifestation of the loss of a principal axis with the onset of convection. The total response of w for multi-component stimuli decreased with thermal instability and increased with stable stratification.

7.3 Non-Linear Models

It is well known that a linear representation of turbulence is fundamentally invalid for dynamical simulations. The difficulties in developing an alternative, non-linear model are three-fold. First, the

degree of non-linearity varies considerably as a function of scale, and second, suitable supporting experimental evidence on which to base even a weakly non-linear model is scarce. Lastly, the complex integral equations for the expansion of the moments must be truncated both for mathematical expediency and for the limited experimental information about the moments.

Computational difficulties were overcome by invoking a simple closure for the relationships between kernels of different orders. These separability conditions are analogous to other closure schemes where higher order moments are expanded in terms of lower order moments. However, the scheme is basically incorrect in its physical interpretation. The method of separability used in the non-linear velocity model assumes that the orders of response are locally interactive whereas it is more realistic to expect higher order responses to be related to integral properties of the lower order response.

The advantage of the separable kernel method is that it reduces the simultaneous integral equation representation of the moments to simultaneous algebraic equations. These equations can then be solved by simple iteration. Because the resulting expansion of the moments is in terms of the linear variance, the model is referred to as a quasi-linear model.

The results for the variance contributions of different degrees of non-linearity indicated that the linear contribution was overwhelming, because the degree of non-Gaussian behavior was not large. The spectral content of the non-linear contributions to the variance increased with decreasing scale. The non-linear contributions erroneously

form an insignificant part of the total energy even in the inertial subrange. The initial response of the non-linear model is somewhat less than the initial response of the corresponding linear model because of the adjustment of the small scale variance in terms of non-linear contributions. It was concluded that a significantly larger response is possible in a more realistic, non-linear model of the inertial subrange. The memory of the linear contribution to the quasi-linear model is somewhat reduced by the removal of variance at small scales from the linear part of the variance. Because the non-linear contribution to the variance increases with instability, the memory also decreases as ζ increases negatively.

The quasi-linear model of velocity was developed for compatibility with the low order moment structure of a simulated turbulent velocity component. However, the model was shown to be incompatible with a spectral transfer of energy because of a lack of phasing between the kernels.

A similar separable model was developed for the derivative process of the u-component of the turbulence. Estimates of the skewness and kurtosis as a function of the Reynolds number were based on the results of Wyngaard and Tennekes (1970). The model of Pao (1965) provided an estimate of the spectrum near the viscous subrange. The results for the truncated functional expansion were found to be inconsistent with measured large deviations from the Gaussian probabilistic structure. For large Reynolds number ($Re \geq 10^4$), the non-linear algebraic equations did not converge. For $Re \leq 10^2$, the solution of the model equations was physically unrealistic in that some contributions to the kurtosis were

negative. Otherwise, for Re of the order of 10^3, the separable derivative model is physically realistic, and dynamically consistent with a non-trivial spectral energy transfer. The energy transfer function closely approximates a similar estimate based on Pao's model of spectral flux convergence.

7.4 Conclusions

In this research, we have attempted to consolidate and expand the methods for simulating turbulence in the atmospheric boundary layer. The mathematical formulation of the filtering method of simulation has been based on empirical results of the accumulated research into the spectral, spatial and probabilistic structure of turbulence. The simulation technique has been extended to spectra without analytical spectral factors, to the multi-component spectral matrix, and to the non-linear, non-Gaussian structure of turbulence.

Previously, in order to produce realizations of a process similar to turbulence, it has been customary to truncate the functional expansion of turbulence at the first (linear) order, and assume a Gaussian probabilistic structure. In addition, the spectrum of the atmospheric turbulence has usually been represented as f^{-2} rather than $f^{-5/3}$ over the range of scales of engineering interest. Although the resulting misrepresentation of variance may be rather insignificant between these spectral models, it is not known *a priori* what effect the differences in variance distribution will have on, say, the predictive structure of the turbulence for purposes of control and stability. These questions have been examined in terms of some aspects of large scale response, and of predictability.

The necessary computational technique for all the model developments was the digital spectral factorization technique. It is concluded that the range of applications of simulated turbulence has been broadened by the numerical computation of the spectral factors of rather general spectral forms.

The development of simulation models was extended to multi-component representations. The methodology was simplified considerably by diagonalization of the spectral matrix to produce multiple single component spectra. Each eigenspectrum is factored as in the uni-component model development. The multi-component spectral factors and response functions are formed by rotation of the eigenstructure by the eigenvectors of the spectral matrix.

It was concluded that the total response of the multi-component models exceeded that of corresponding uni-component models at scales greater than about $\ell/2$. However, the predictability of the simulated turbulent process was not significantly increased in the multi-component models.

The need to incorporate non-linear aspects in the simulation of turbulence, particularly in synthesizing the relatively rare, large scale gusts was discussed. Methods to achieve a reasonable simulation of the observed patchiness of atmospheric turbulence have led to the introduction of the discrete gust concept. Such discrete gust models specify that turbulent realizations contain superimposed eddies of an invariant form, such as a ramp function. The strength and frequency of occurrence of such eddies is formulated for consistency with a Kolmogorov spectral structure and empirical estimates of the exceedance

statistics of turbulence. While such methods are more realistic than linear, Gaussian spectral models, their dynamical basis is controversial. Because the invariant eddy forms, for example the ramp function, are expedient mathematical idealizations, there is no direct relationship of the parameters of the particular representation with other aspects of the structure of surface layer turbulence. The implications of such models to known dynamical and statistical structures needs to be studied.

The results here are a compromise between the discrete gust methods and the well-known filtering methods. The minimum-phase response functions constitute invariant eddy forms of random strength and occurrence. The amplitude of each eddy is determined by the history of the Gaussian, white noise input realization. The kernels which are the discrete gust form, have been shown to evolve as a natural property of the spectrum of the process. The kernels also correspond to a defineable physical mechanism, that is, as a response to an impulse. Moreover, the response functions have been demonstrated to be fundamental in describing the predictive and probabilistic structure of the turbulence. It is concluded that the development of discrete gust models is not independent of the spectral or filtering method, and can be made compatible by introducing the concept of the response structure of the turbulence.

The viewpoint taken here has been that the requirement for simulating large gusts can be met by systematic recourse to theoretical and empirical formulations of the statistical structure of turbulence in the atmospheric boundary layer. This approach involves use of the

spectral similarity theories of Kolmogorov (with appropriate extensions in the generative and viscous subranges), and use of published empirical data for the multi-component spectra against a framework of the Monin-Oboukhov similarity theory. In addition the formulation of a simple non-linear model of a velocity component has incorporated low order moment data so as to be consistent with Monin-Oboukhov and Reynolds similarity.

The reduction of the non-linear simulation problem to workable proportions requires several mathematical simplifications. The (infinite) functional expansion of the moments is truncated to the highest order of available data. An arbitrary specification of the interrelationships among kernels of various orders reduces the numerical complexities from one of solving simultaneous integral equations to simultaneous algebraic equations. Although the separable model for velocity in the form chosen misrepresents the dynamics of the turbulence, it was concluded from an examination of the separable derivative model that it is possible to produce a realistic one-dimensional energy transfer locally. It remains to develop a model based on spectral separability for the generative region.

It was concluded from an examination of test realizations based on a linear and a non-linear model that, within the limitations of generating white, Gaussian noise on a digital computer and the implementation of numerical methods in forming convolution that the method is practical and forms a useful representation of the statistical structure of turbulence in the atmospheric boundary layer as it is presently understood and described.

8.0 REFERENCES

Abramowitz, M., and I. A. Stegun, 1964: Handbook of Mathematical Functions, Dover.

Arya, S. P. S., 1972: The critical-conditions for the maintenance of turbulence in stratified flows. Quart. J. Roy. Met. Soc., 98, 264-273.

Barnett, J. F., 1963: The use of functionals in the analysis of non-linear physical systems. J. Electronics and Control, 15, 567-615.

Batchelor, G. K., 1953: The Theory of Homogeneous Turbulence. Cambridge University Press, London.

Blackadar, A. K. and H. Tennekes, 1968: Asymptotic similarity in neutral barotropic atmospheric boundary layers. J. Atmos. Sci., 25, 1015-1020.

Bode, H. W. and C. E. Shannon, 1950: A simplified derivation of linear least-square smoothing and prediction theory. Proc. Inst. Radio Eng., 38, 417-425.

Busch, N. E. and H. A. Panofsky, 1968: Recent spectra of atmospheric turbulence. Quart J. Roy. Met. Soc., 94, 132-148.

Busch, N. E. and S. E. Larsen, 1972: Spectra of turbulence in the atmospheric surface layer. Danish Atomic Energy Commission, Riso, Report No. 256, 187-207.

Businger, J. A., J. C. Wyngaard, Y. Izumi and E. F. Bradley, 1971: Flux-profile relationships in the atmospheric surface layer. J. Atmos. Sci., 28, 181-189.

Case, E. R., 1968: Development of a low altitude gust model and its application to STOL aircraft response studies. DeHavilland Aircraft of Canada, Report DHC-DIR 68-15.

Crow, S. C. and G. H. Canavan, 1970: Relationship between a Wiener-Hermite expansion and an energy cascade. J. Fluid Mech., 41, 387-403.

Deardorff, J. W., 1972a: Numerical investigation of neutral and unstable planetary boundary layers. J. Atmos. Sci., 29, 91-115.

Deardorff, J. W., 1972b: Three-dimensional numerical modeling of the planetary boundary layer. Notes of the Workshop in Micrometeorology, Boston, A.M.S.

REFERENCES (continued)

Deland, R. J. and H. A. Panofsky, 1957: Structure of turbulence at O'Neill, Nebraska, and its relation to the structure at Brookhaven. Sci. Rep. No, 2, Cont. AF-19 (604) - 1027. The Pennsylvania State University.

Dolandson, C. DuP., 1972: Calculation of turbulent shear flows for atmospheric and vortex motions. A.I.A.A.J., 10, 4-12.

Doob, J. L., 1953: Stochastic Processes, Wiley, New York.

Dutton, J. A., 1970: Effects of turbulence on aeronautical systems. Progress in Aerospace Sciences, 11, 67-109. Pergamon Press, New York.

Dutton, J. A., 1971: Simulation of atmospheric turbulence with empirical orthogonal functions. NASA CR-1189, 1-16.

Elderkin, C. E., D. C. Powell, A. G. Dunbar, and T. W. Horst, 1972: Take-off and landing critical atmospheric turbulence (TOLCAT) - Experiments and analysis. Air Force Flight Dynamics Laboratory, TR-71-172.

Fichtl, G. H. and G. E. McVehil, 1970: Longitudinal and lateral spectra of turbulence in the atmospheric boundary layer at the Kennedy Space Center. J. Appl. Met., 9, 51-63.

Frenkiel, F. N. and P. S. Kelbanoff, 1967: Higher-order correlations in a turbulence field. Phys. Fluids, 10, 507-520.

George, D. A., 1959: Continuous non-linear systems. Unpublished Ph.D. thesis, Massachusetts Institute of Technology.

Gerlach, O. H., G. A. J. van der Moesdijk, J. C. van de Vaart, 1973: Progress in mathematical modelling of flight in turbulence. Delft University of Technology, Department of Aeronautical Engineering, Memo M-196.

Gibson, C. H. and P. J. Masiello, 1971: Observations of the variability of dissipation rates of turbulent velocity and temperature fields. Proc. Symposium on Statistical Models and Turbulence, San Diego, 427-453.

Gradshteyn, I. S. and I. W. Ryshik, 1965: Table of Integrals, Series and Products. Academic Press, New York.

Grant, H. L., R. W. Stewart, and A. J. Moilliet, 1962: Turbulence spectra from a tidal channel. J. Fluid Mech., 12, 241-263.

REFERENCES (continued)

Gurvich, A. S. and A. M. Yaglom, 1967: Breakdown of eddies and probability distributions for small-scale turbulence. Phys. Fluids, 10, Supplement, 59-65.

Haugen, D. A., ed., 1973: Workshop in Micrometeorology. American Meteorological Society.

Herring, J. R., 1966: Self-consistent-field approach to non-stationary turbulence. Phys. Fluids, 9, 2106-2110.

Houbolt, J. C., 1973: Survey on effect of surface winds on aircraft design and operation and recommendations for needed wind research. NASA-CR-2360, 74 pp.

Izumi, Y., 1972: Kansas 1968 Field Program Data Report. Air Force Cambridge Research Laboratories, Report 72-0041.

Jones, J. G., 1969: Similarity theory of gust loads on aircraft, development of discrete gust theory, and introduction of empirical functions. Royal Aircraft Establishment, TR-69171.

Joppa, R. G., 1965: A proposed model of low altitude atmospheric turbulence for use in V/STOL Aircraft handling qualities studies. Boeing Company, D6-10738.

Kaimal, J. C., J. C. Wyngaard, Y. Izumi and O. R. Cote, 1972: Spectral characteristics of surface-layer turbulence. Quart J. Roy. Met. Soc., 98, 563-589.

Katzenelson, J. and L. A. Gould, 1962: The design of non-linear filters and control systems. Information and Control, 5, 108-143.

Katzenelson, J. and L. A. Gould, 1965: A spectrum factorization method for the calculation of non-linear filters of the Volterra type. Information and Control, 8, 239-250.

Kazanski, A. B. and A. S. Monin, 1961: On the dynamical interaction between the atmosphere and the earth's surface. Bull. Acad. Sci., USSR, Ser. Geophys., 5, 786-788.

Kerman, B. R., 1974a: An application of boundary layer similarity theories to an aircraft accident investigation. Boundary-Layer Met., 7, 53-63.

Kerman, B. R., 1974b: On the conversion of energy and enstrophy on the meso-scale. Proceedings of the Symposium on Atmospheric Diffusion and Air Pollution, Santa Barbara, California, pp. 41-48.

REFERENCES (continued)

Kolmogorov, A. N., 1941: Local structure of turbulence in an incompressible viscous fluid for very large Reynolds numbers. Doklady ANSSSR, 30, 201-305.

Kolmogorov, A. N., 1962: A refinement of previous hypotheses concerning the local structure of turbulence in a viscous incompressible fluid at high Reynolds number. J. Fluid Mech., 13, 82-85.

Kraichnan, R. H., 1965: Lagrangian-history closure approximation for turbulence. Phys. Fluids, 8, 575-598.

Kurkowski, R. L., G. H. Fichtl and J. Gera, 1971: Development of turbulence and wind shear models for simulation application. NASA SP-270.

Lappe, U. O., 1966: Low-altitude turbulence for estimating gust loads on aircraft. J. Aircraft, 3, 41-47.

Liepmann, H. W., 1954: Extension of statistical approach to buffeting and gust response of wings of finite span. Douglas Aircraft Report SM 15172.

Lumley, J. H. and H. A. Panofsky, 1964: The Structure of Atmospheric Turbulence. Interscience Publishers. New York.

Lumley, J. H., 1970a: Toward a constitutive relation. J. Fluid Mech., 41, 413-434.

Lumley, J. H., 1970b: Stochastic Tools in Turbulence. Academic Press. New York.

McBean, G. A., R. W. Stewart and M. Miyake, 1971: The turbulent energy budget near the surface. J. Geophys. Res., 76, 6540-6549.

McBean, G. A. and M. Miyake, 1972: Turbulent transfer mechanisms in the atmospheric surface layer. Quart. J. Roy. Met. Soc., 98, 383-398.

Meecham, W. C. and A. Spiegel, 1964: Wiener-Hermite expansion in model turbulence at large Reynolds numbers. Phys. Fluids, 7, 1178-1190.

Monin, A. S. and A. M. Oboukhov, 1954: Basic laws of turbulent mixing in the ground layer of the atmosphere. Akad. Nauk. SSSR Geofis. Inst. Trudy, 151, 163-187.

Oboukhov, A. M., 1962: Some specific features of atmospheric turbulence. J. Fluid Mech., 13, 77-81.

REFERENCES (continued)

Ogura, Y., 1963: A consequence of the zero-fourth-cumulant approximation in the decay of isotropic turbulence. J. Fluid Mech., 16, 33-40.

Orszag, S. A. and L. R. Bissonnette, 1967: Dynamical properties of truncated Wiener-Hermite expansions. Phys. Fluids, 10, 2603-2613.

Panofsky, H. A. and E. Mares, 1968: Recent measurements of cospectra for heat-flux and stress. Quart. J. Roy. Met. Soc., 94, 581-585.

Panofsky, H. A., 1969: Spectra of atmospheric variables in the boundary layer. Radio Sci., 4, 1101-1109.

Pao, Y. H., 1965: Structure of turbulent velocity and scalar fields at large wavenumbers. Phys. Fluids, 8, 1063-1075.

Pao, Y. H., 1968: Transfer of turbulent energy and scalar quantities at large wavenumbers. Phys. Fluids, 11, 1371-1372.

Parente, R. B., 1970: Nonlinear differential equations and analytic system theory. SIAM J. Appl. Math., 18, 41-66.

Pasquill, F. and H. E. Butler, 1964: A note on determining the scale of turbulence. Quart. J. Roy. Met. Soc., 90, 79-84.

Pond, S., G. T. Phelps, J. E. Paquin, G. McBean and R. W. Stewart, 1971: Measurements of turbulent fluxes of momentum, moisture and sensible heat over the ocean. J. Atmos. Sci., 28, 901-917.

Reeves, P. M., 1969: A non-Gaussian turbulence simulation. Air Force Flight Dynamics Laboratory TR-69-67.

Rino, C. L., 1970: Factorization of spectra by discrete Fourier transform. IEEE Trans. Info. Sci., 16, 484-485.

Robinson, E., 1967a: Predictive decomposition of time series with application to seismic exploration. Geophysics, XXXII, 418-484.

Robinson, E., 1967b: Multi Channel Time Series Analysis with Digital Computer Programs. Holden Day. San Francisco.

Skelton, G. B., 1968: Investigation of the effects of gusts on V/STOL craft on transition and hover. Air Force Flight Dynamics Lab., TR-68-85.

Stewart, R. W., 1951: Triple velocity correlations in isotropic turbulence. Proc. Camb. Phil. Soc., 47, 146-157.

REFERENCES (continued)

Stewart, R. W., 1969: Turbulence and waves in a stratified atmosphere. Radio Sci., 4, 1269-1278.

Tennekes, H. and J. C. Wyngaard, 1972: The intermittent small-scale structure of turbulence: data processing hazards. J. Fluid Mech., 55, 93-103.

Tennekes, H. and J. L. Lumley, 1972: A First Course in Turbulence. M.I.T. Press. Cambridge.

Teunnissen, H. W., 1970: Characteristics of the mean wind and turbulence in the planetary boundary layer. UTIAS Review No. 32, Univ. Toronto, Institute of Aerospace Studies.

Townsend, A. A., 1947: The measurement of double and triple correlation derivatives in isotropic turbulence. Proc. Camb. Phil. Soc., 43, 560-570.

Volterra, V., 1930: Theory of Functionals. Blackie. London.

Wiener, N., 1958: Non-linear Problems in Random Theory. John Wiley. New York.

Wyngaard, J. C. and H. Tennekes, 1970: Measurements of small-scale turbulence at moderate Reynolds numbers. Phys. Fluids, 13, 1962-1969.

Wyngaard, J. C. and Y. H. Pao, 1971: Some measurements of the fine structure of large Reynolds number turbulence. Proc. Sympos. Statistical Models and Turbulence. San Diego, 384-401.

Wyngaard, J. C. and O. R. Cote, 1971a: The budgets of turbulent kinetic energy and temperature variance in the atmospheric surface layer. J. Atmos. Sci., 28, 190-201.

Wyngaard, J. C., O. R. Cote and Y. Izumi, 1971b: Local free convection, similarity and the budgets of shear stress and heat flux. J. Atmos. Sci., 28, 1171-1182.

Wyngaard, J. C. and O. R. Cote, 1972: Cospectral similarity in the atmospheric surface layer. Quart. J. Roy. Met. Soc., 98, 590-603.

Zilintinkevich, S. S. and D. V. Chalikov, 1968: The laws of resistance and of heat and moisture exchange in the interaction between the atmosphere and an underlying surface. Izv. Atmos. and Ocean. Phys., 4, 765-772.

APPENDIX A EMPIRICAL RESULTS OF BOUNDARY LAYER STRUCTURE

Some recently reported observational studies (Businger et al, 1971; McBean et al, 1971; Busch and Larsen, 1972) have significantly reduced the error variance within and between the estimation of similarity functions measured at different sites. For convenience, we choose the results of the Kansas experiment reported on by Businger et al, (1971), Wyngaard and Cote, (1971a), Wyngaard et al, (1971b), Kaimal et al, (1972), Wyngaard and Cote, (1972) because of their extensiveness and their internal consistency.

The similarity functions for shear, temperature gradient and dissipation of kinetic energy are given empirically

- for unstable stratification ($-1 < \zeta < 0$)

$$\phi_m(\zeta) = (1 - 15\ \zeta)^{-1/4} \tag{A.1}$$

$$\phi_h(\zeta) = 0.74\ (1 - 9\ \zeta)^{-1/2} \tag{A.2}$$

$$\phi_\varepsilon(\zeta) = (1 + 0.5|\zeta|^{2/3})^{3/2} \tag{A.3}$$

- and for stable conditions ($0 < \zeta < 0.5$) by

$$\phi_m(\zeta) = 1 + 4.7\ \zeta \tag{A.4}$$

$$\phi_h(\zeta) = 0.74\ (1 + 6.4\ \zeta) \tag{A.5}$$

$$\phi_\varepsilon(\zeta) = (1 + 2.5\ \zeta^{3/5})^{3/2} \tag{A.6}$$

Because the 'dissipation' of temperature variance was not measured during the Kansas experiment, it was necessary to assume

$$\phi_\chi(\zeta) = \phi_h(\zeta) \quad . \tag{A.7}$$

The second moments have been fitted as quadratic polynomials in ζ, to the data listed in the catalogue of the Kansas data (Izumi, 1972). The results are displayed in Figures A.1 to A.5. The empirical representations of variance and co-variance are given by the following empirical formulae

- for unstable stratification ($-1 < \zeta < 0$)

$$\overline{\tilde{u}^2} = 6.25\ (1 - 0.40\ \zeta)^2 \tag{A.8}$$

$$\overline{\tilde{v}^2} = 3.25\ (1 - 1.0\ \zeta)^2 \tag{A.9}$$

$$\overline{\tilde{w}^2} = 1.35\ (1 - 0.90\ \zeta)^2 \tag{A.10}$$

$$\overline{\tilde{\theta}^2} = 3.24\ (1 + 0.87\ \zeta + 0.40\ \zeta^2) \tag{A.11}$$

$$\overline{\tilde{u}\tilde{\theta}} = 3.70\ (1 + 2.8\ \zeta + 2.6\ \zeta^2) \tag{A.12}$$

- and for stable stratification ($0 < \zeta < 0.5$)

$$\overline{\tilde{u}^2} = 6.25\ (1 - 0.40\ \zeta)^2 \tag{A.13}$$

$$\overline{\tilde{v}^2} = 3.25\ (1 - 0.14\ \zeta)^2 \tag{A.14}$$

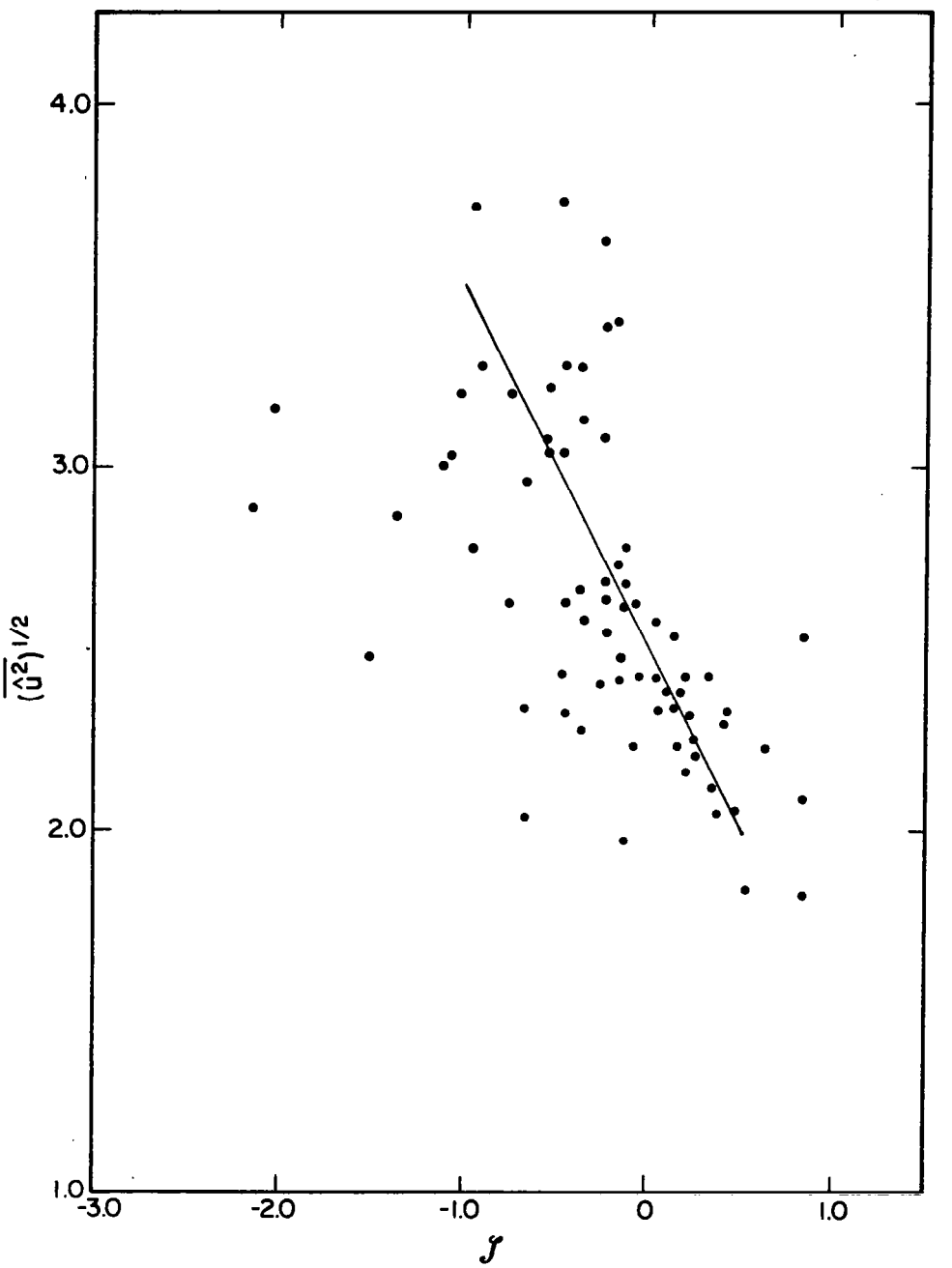

Figure A.1. Variance of longitudinal wind fluctuations with stability.

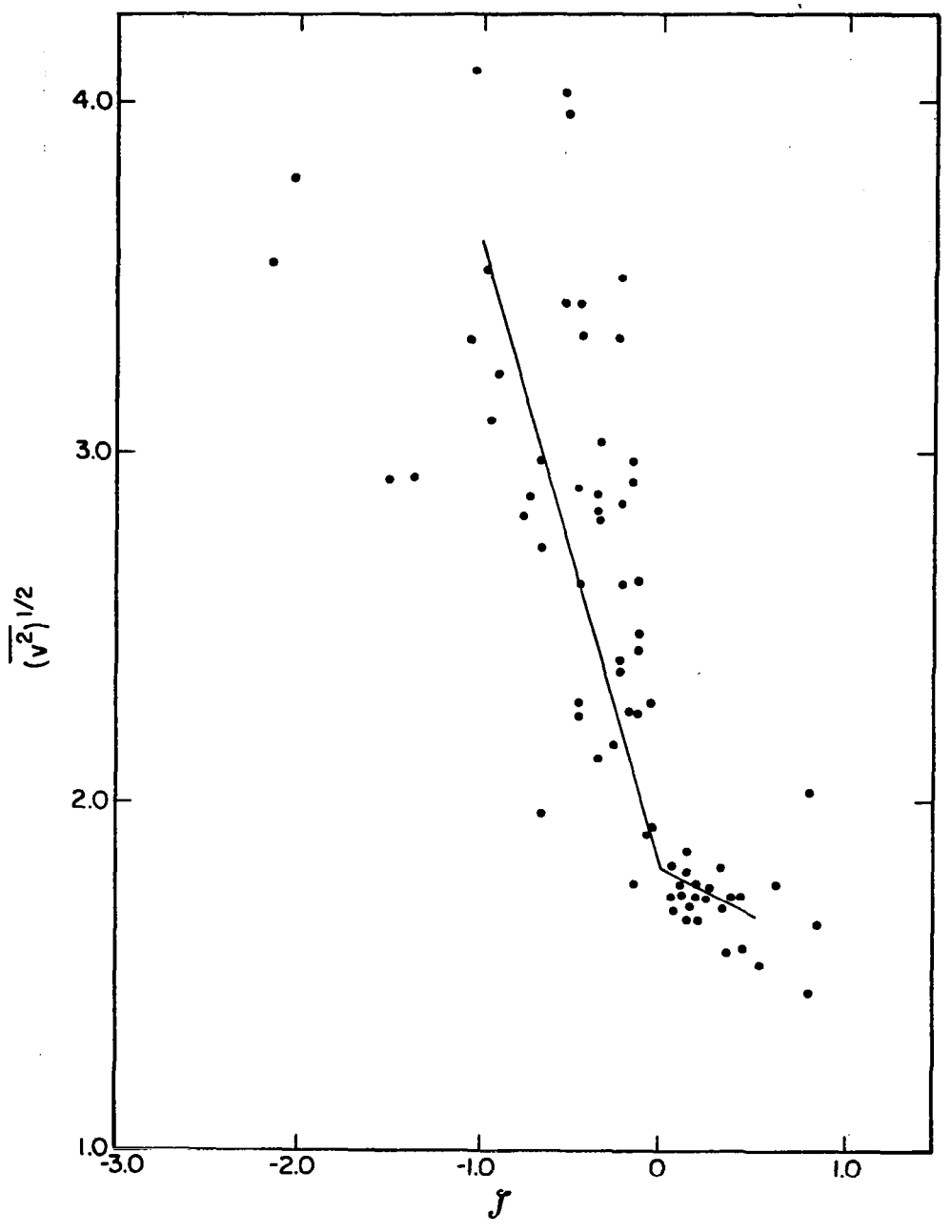

Figure A.2. Variance of lateral wind fluctuations with stability.

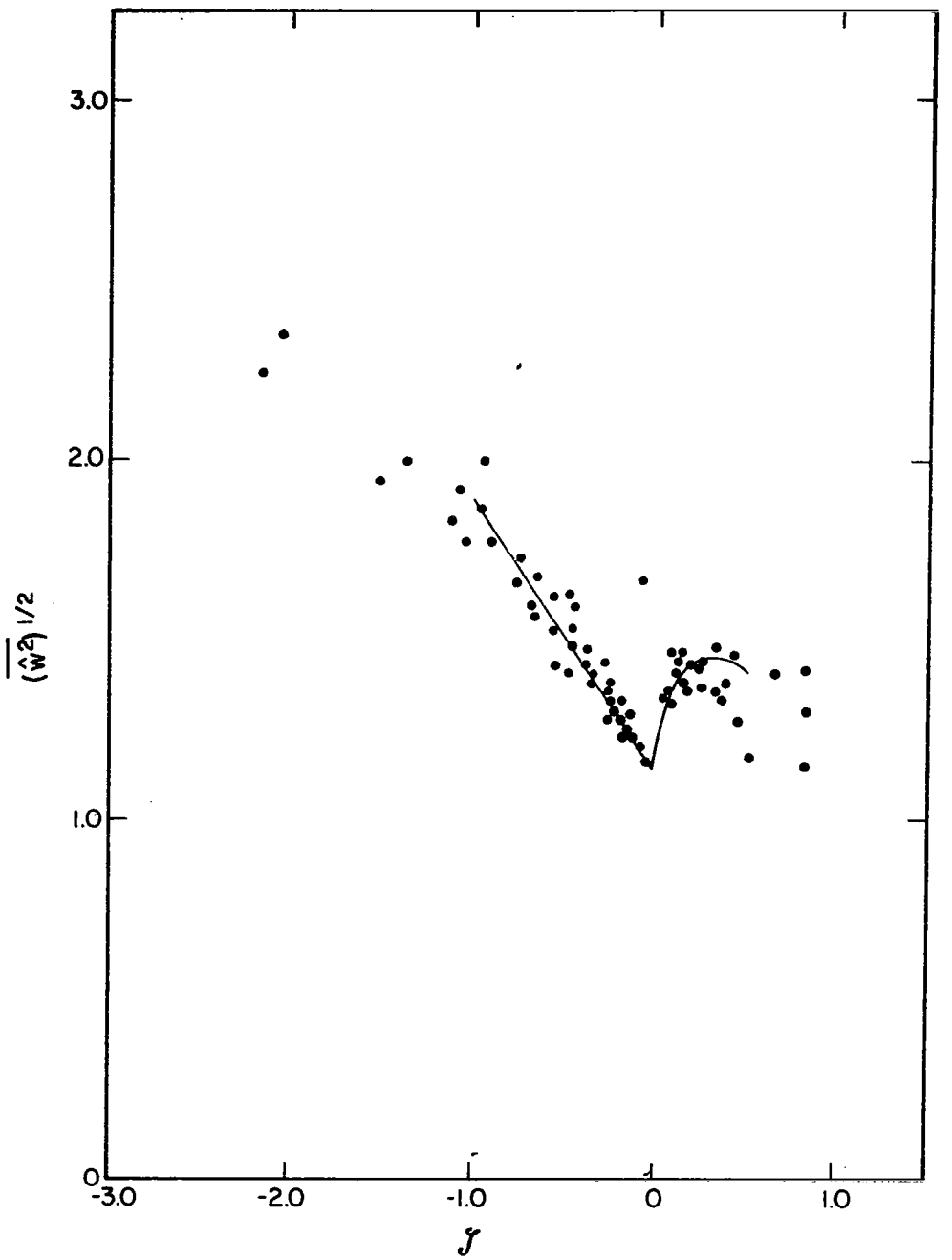

Figure A.3. Variance of vertical wind fluctuations with stability.

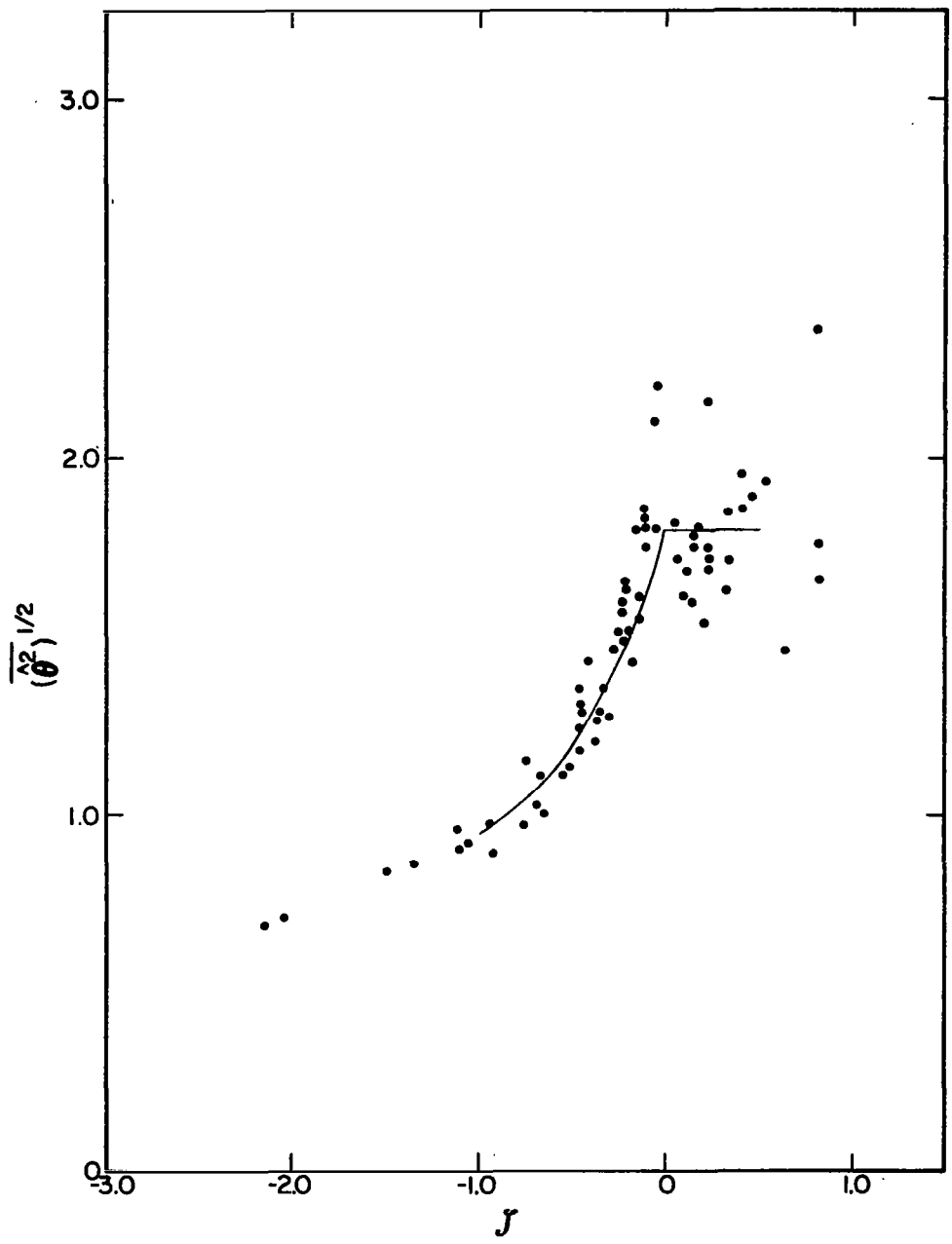

Figure A.4. Variance of temperature fluctuations with stability.

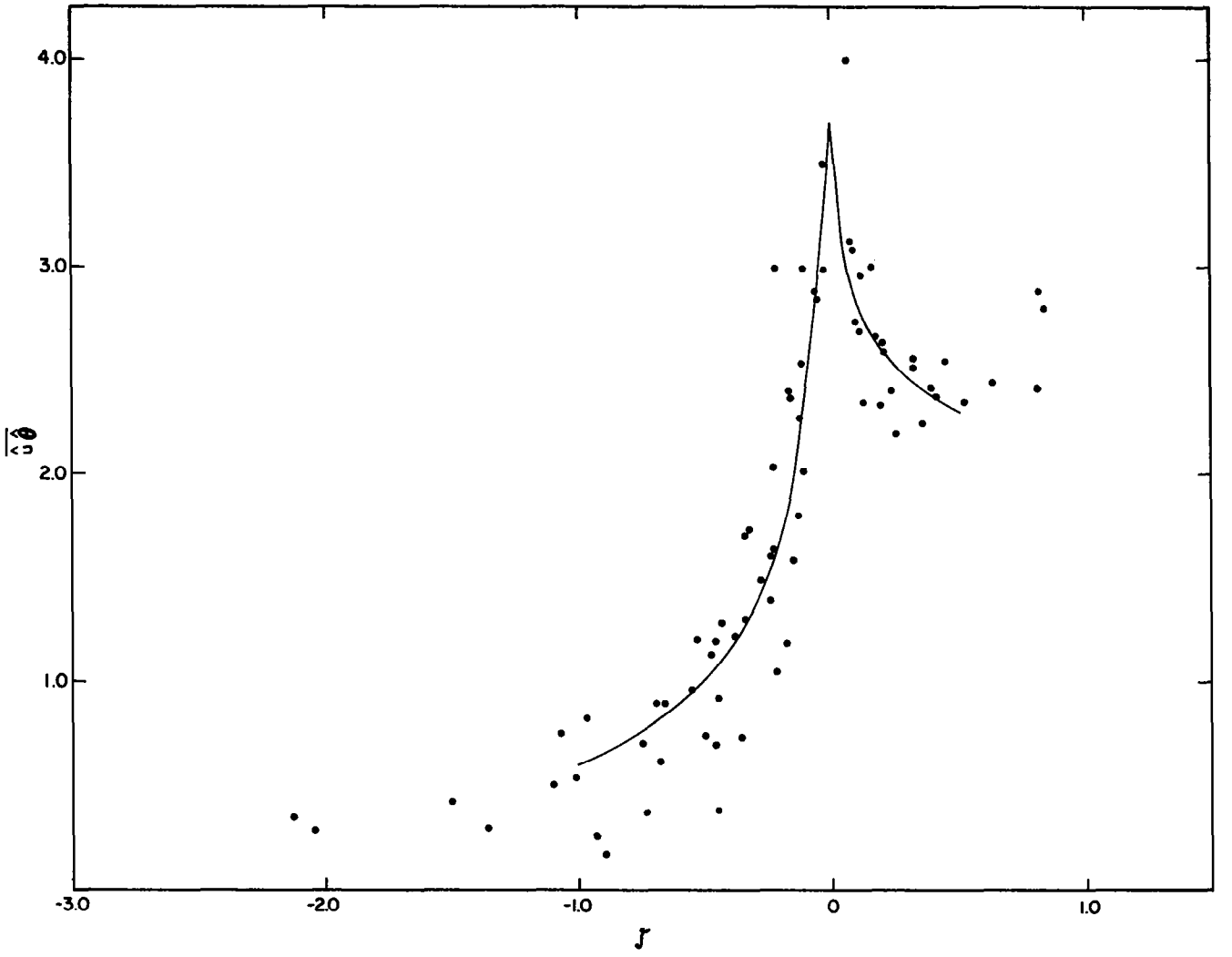

Figure A.5. Co-variance of longitudinal heat flux with stability.

$$\overline{\tilde{w}^2} = 1.35\ (1 + 3.2\ \zeta - 3.0\ \zeta^2) \qquad (A.15)$$

$$\overline{\tilde{\theta}^2} = 3.24 \qquad (A.16)$$

$$\overline{\tilde{u}\tilde{\theta}} = 3.70\ (1 - 2.0\ \zeta + 2.5\ \zeta^2) \qquad (A.17)$$

The over-bar tilda denotes a variable scaled by u_* or T_* as appropriate.

The limited range of ζ ($-1 < \zeta < 0.5$), over which the empirical functions above are valid, excludes the free convection region of extreme, negative ζ and the extremely stable region. In the later case any turbulence that exists in the stable region is considered to be associated with gravity waves, and its structure to be dissimilar to the structure in the stability range with sub-critical Richardson number ($\simeq 0.20$) (Arya, 1972). These relationships therefore define the statistical structure of the turbulence in a region where thermal effects do not overwhelm mechanical effects. Also, estimates normalized by T_* for $\zeta = 0$ necessarily represent only an average about neutral stratification.

Results for the similarity structure of spectra of velocity and temperature within the constant flux layer have been reported by many investigators (Fichtl and McVehil, 1970; McBean and Miyake, 1972; Panofsky and Mares, 1968; Pond et al, 1971) in addition to the Kansas investigators. The normalized velocity spectra $G_{ii}(f, \zeta)$ are usually represented empirically in a form

$$f\ G_{ii}(f) = \frac{A_{ii}(\zeta)\ f}{(1 + (B_{ii}(\zeta)\ f)^n)^{5/3n}} \qquad (A.18)$$

Estimates of n vary between authors, the most popular being n = 1 or n = 5/3. Because there is no clear concensus of any preferred empirical form, we have chosen a slightly different form given by

$$f\, G_{ii}(f) = \frac{A_{ii}\, \phi_\varepsilon^{2/3}\, f^{2/3}}{1 + (B_{ii}\, f)^{4/3}} \qquad (A.19)$$

The implied 2/3 slope of the energy distribution for $B_i f << 1$ disagrees with Kaimal's results but is more in agreement with Busch and Larsen's findings. However, as it is doubtful whether Monin-Oboukhov similarity holds at such large scales, the correct formulation of the spectra would require modifying more than the spectral slope for $f << 1$. The functions A_{ii} and B_{ii} are determined for compatibility of (A.19) with the known asymptotic structure of the turbulent spectra in the Kolmogorov range and the variance estimates given in (A.8) to (A.17). The condition for the variance is

$$\overline{\tilde{u}_i^{\,2}} = \int_0^\infty f\, G_{ii}(f)\, df = \phi_\varepsilon^{2/3}\, A_{ii}\, B_{ii}^{-2/3}\, (3\pi/4) \qquad (A.20)$$

and, the condition for the spectra for $1 << f << f_{KOL}$, where f_{KOL} is the normalized Komogorov scale given by

$$f_{KOL} = \kappa z(\varepsilon \nu^{-3})^{1/4} = Re^{3/4}\, \phi_\varepsilon^{1/4} \qquad (A.21)$$

becomes

$$f^{5/3} G_{ii}(f) = A_{ii} \phi_\varepsilon^{2/3} B_{ii}^{-4/3}$$
$$= \alpha_i \phi_\varepsilon^{2/3} \qquad (A.22)$$

where α_i is the Kolmogorov constant appropriate to the i^{th} variable for a non-dimensional spectral representation. From Equation (A.20), (A.23) and (A.24)

$$A_{ii} = \alpha_1 \left(\frac{4}{3} \frac{\overline{\tilde{u}_i^2}}{\alpha_i}\right)^2 \phi_\varepsilon^{-4/3} \qquad (A.23)$$

$$B_{ii} = \left(\frac{4}{3} \frac{\overline{\tilde{u}_i^2}}{\alpha_i}\right)^{3/2} \phi_\varepsilon^{-1} \qquad (A.24)$$

For a value of Kolmogorov's constant, $\alpha \simeq 1.5$, for a three dimensional kinetic energy spectrum

$$\alpha_i = (1, 4/3, 4/3)\ (18\ \alpha/55) \quad \text{for } i = 1, 2, 3 \qquad (A.25)$$

Similarly, the empirical functions for the temperature spectrum are given by Equations (A.25) and (A.26), except ϕ_ε is replaced by $\phi_\varepsilon^{1/3}\phi_\chi$ and the coefficient, α_i, replaced by the corresponding coefficient, β_1, for temperature. β_1 is not as well defined empirically as α_i, with estimates ranging from 0.4 to 0.9 (Panofsky, 1969). For consistency, we have selected the empirical estimate based on the Kansas date, $\beta_1 = 0.8 \pm 0.1$.

The cospectra of stress and vertical heat flux have been shown (Kaimal et al, 1972; McBean and Miyake, 1972) to have a -7/3 slope in the inertial subrange. These findings are in agreement with anisotropy

arguments (Tennekes and Lumley, 1972). However the horizontal heat flux co-spectrum has a spectral slope which varies both with height and stability. Kaimal, et al, report that the slope of the uθ co-spectrum decreases in unstable conditions from -3 near the ground to -7/3 at the top of the surface layer, and that in stable conditions the slope is -5/3. The difference between -7/3 and -5/3 is considered insignificant here, and the exponent of the cospectra is estimated everywhere to be -7/3. The empirical form chosen for the cospectra is

$$f\,G_{ij} = \frac{A_{ij}\,K_{ij}\,f^{5/3}}{1 + (B_{ij}\,f)^2} \qquad (A.26)$$

The scaling factors K_{ij}, which correspond to $\phi_\varepsilon^{2/3}$ and $\phi_\chi\phi_\varepsilon^{-1/3}$ in the autospectra, have been determined empirically by Kaimal to be

- for unstable conditions

$$K_{13}(\zeta) = K_{3\theta}(\zeta) = K_{1\theta}(\zeta) = 1 \qquad (A.27)$$

- and for stable conditions

$$K_{13}(\zeta) = 1 + 7.9\,\zeta \qquad (A.28)$$

$$K_{3\theta}(\zeta) = 1 + 6.4\,\zeta \qquad (A.29)$$

$$K_{1\theta}(\zeta) = 1 + 17\,\zeta \qquad (A.30)$$

The empirical coefficients, A_{ij} and B_{ij}, are determined from simultaneous algebraic conditions involving the variance and asymptotic structure

of the cospectrum, in a manner identical to the empirical representation of the spectra. The asympototic constants, c_{ij}, (corresponding to α_i and β_i in the autospectra) were estimated on the basis of the Kansas data (and the particular definition of f used in this study) to be

$$c_{13} = -0.14 \tag{A.31}$$

$$c_{3\theta} = -0.41 \tag{A.32}$$

$$c_{1\theta} = 0.14 \tag{A.33}$$

Finally, the coefficients A_{ij} and B_{ij} follow from the equivalent of Equations (A.25) and (A.26) and are given by

$$A_{ij} = c_{ij} \left(\frac{I_{ij}}{c_{ij}} \frac{\sqrt{3}}{\pi} \frac{1}{K_{ij}}\right)^{3/2} \tag{A.34}$$

$$B_{ij} = \left(\frac{I_{ij}}{c_{ij}} \frac{\sqrt{3}}{\pi} \frac{1}{K_{ij}}\right)^{3/4} \tag{A.35}$$

where the normalized variances, I_{ij}, are given as

$$I_{13} = I_{3\theta} = 1 \tag{A.36}$$

$$I_{1\theta} = \overline{\underset{\sim}{u\theta}} \tag{A.37}$$

This completes the empirical representation of the spectra and cospectra -- for a given scale height and stability. It is assumed

in what follows that the cospectra involving v are identically zero at all stabilities because of the passive role played by v in the surface layer (Lumley and Panofsky, Chapter 3.0). However, in order to complete the (complex) spectral matrix representation of the surface turbulence, it remains to establish the phase between the velocity and buoyant fluctuations. According to J. C. Wyngaard (private communication) the phase, determined on the basis of the quadrature and cospectra of the Kansas data, is indistinguishable from zero. This result which differs from the observation of Deland and Panofsky (1957) is adopted for simplicity.

We now move to a discussion of the observations of the non-Gaussian probabilistic structure of surface layer turbulence. If we consider a measured turbulent velocity conceptually as the result of a summation of multiple random influences exerted on the flow prior to the observation, it is reasonable to expect its probability distribution to at least approximate a Gaussian distribution according to the Central Limit Theorem. Early measurements (for example, Townsend, 1947) of the skewness and kurtosis tended to confirm this hypothesis. Some estimates for the skewnesses and kurtoses of single-point measurements made at Kansas (Izumi, 1972) are given in Figures A.6 to A.11 as functions of ζ. The scatter is disappointngly large for most moments. Apparently, the averaging time, which must increase with the order of the moment in order to adequately sample the rare events (Lumley, 1970b, p. 73; Tennekes and Wyngaard, 1972) is not long enough. Visually, there appears to be a general increase in all the various skewnesses with decreasing stability. Also the kurtosis of the longitudinal component, $\tilde{u}$, and the temperature are indistinguishable from a

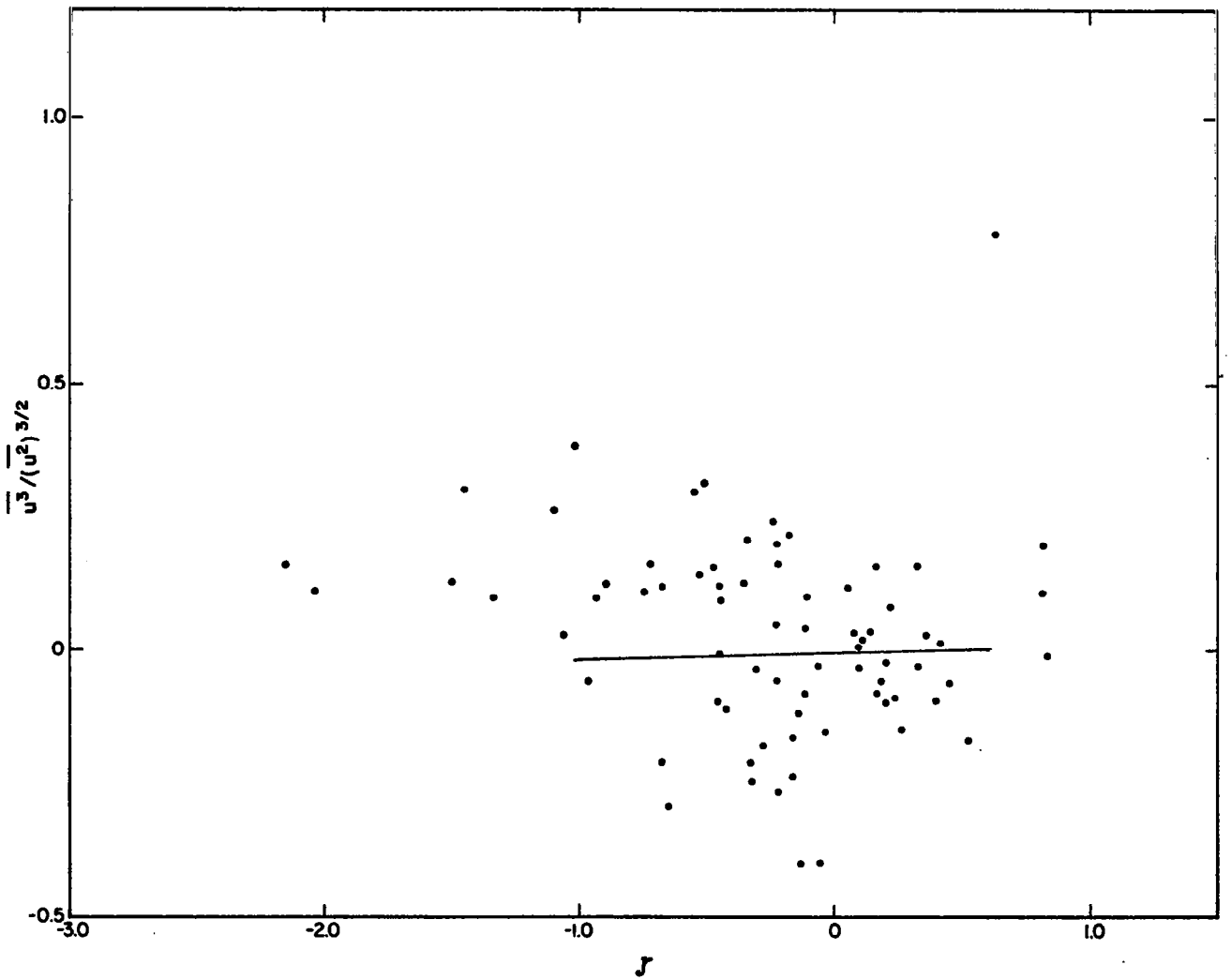

Figure A.6. Skewness of longitudinal wind fluctuations with stability.

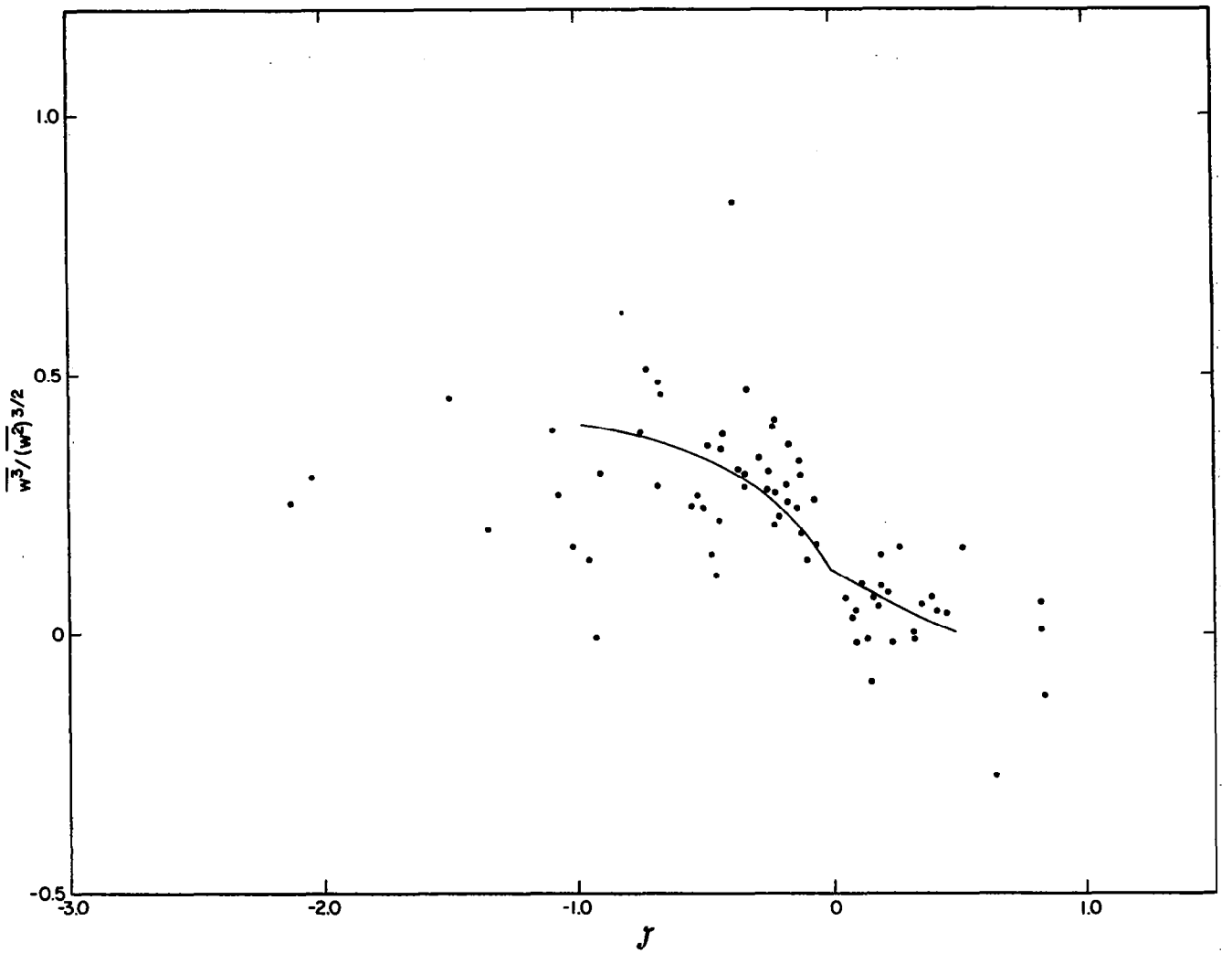

Figure A.7. Skewness of vertical wind fluctuations with stability.

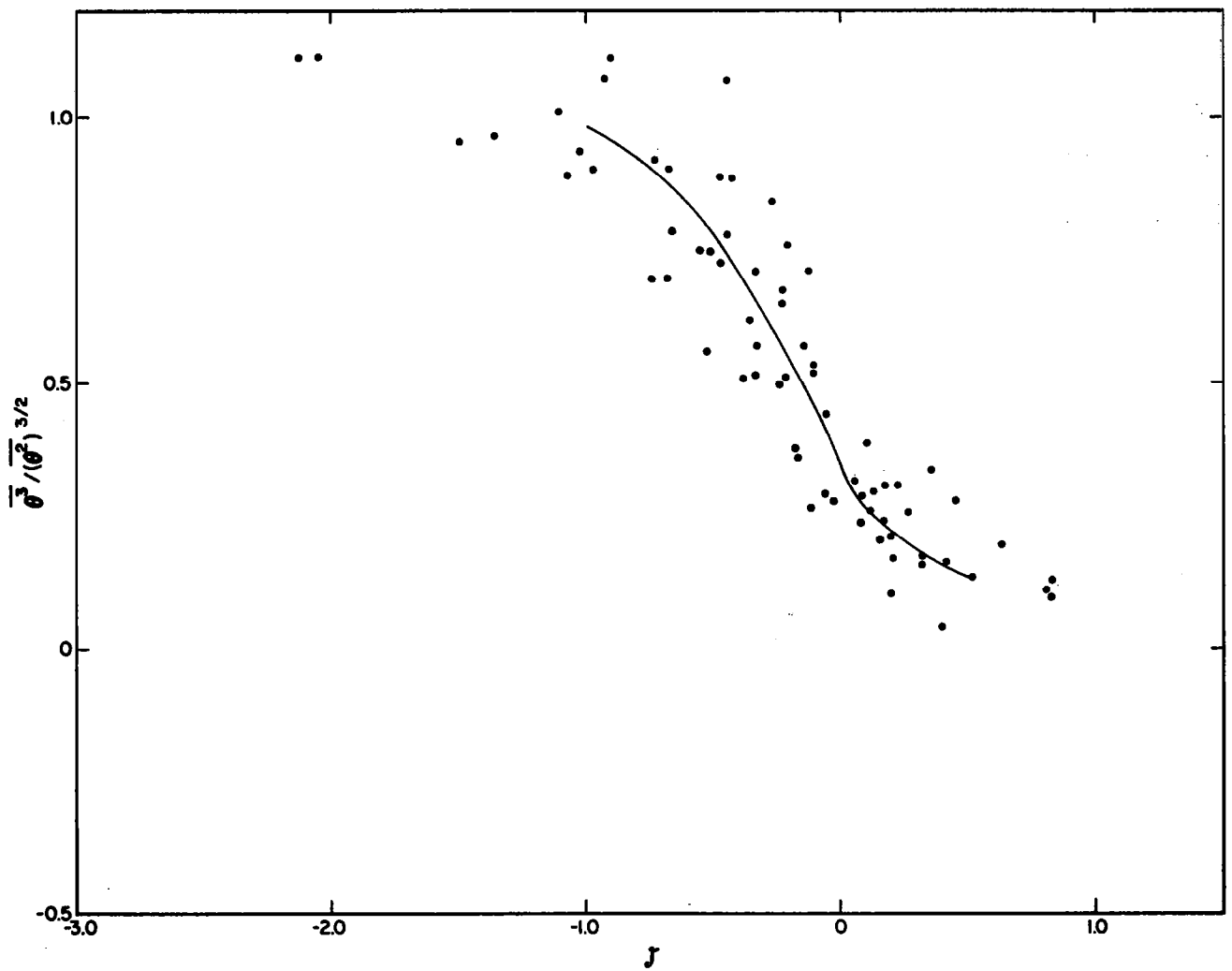

Figure A.8. Skewness of temperature fluctuations with stability.

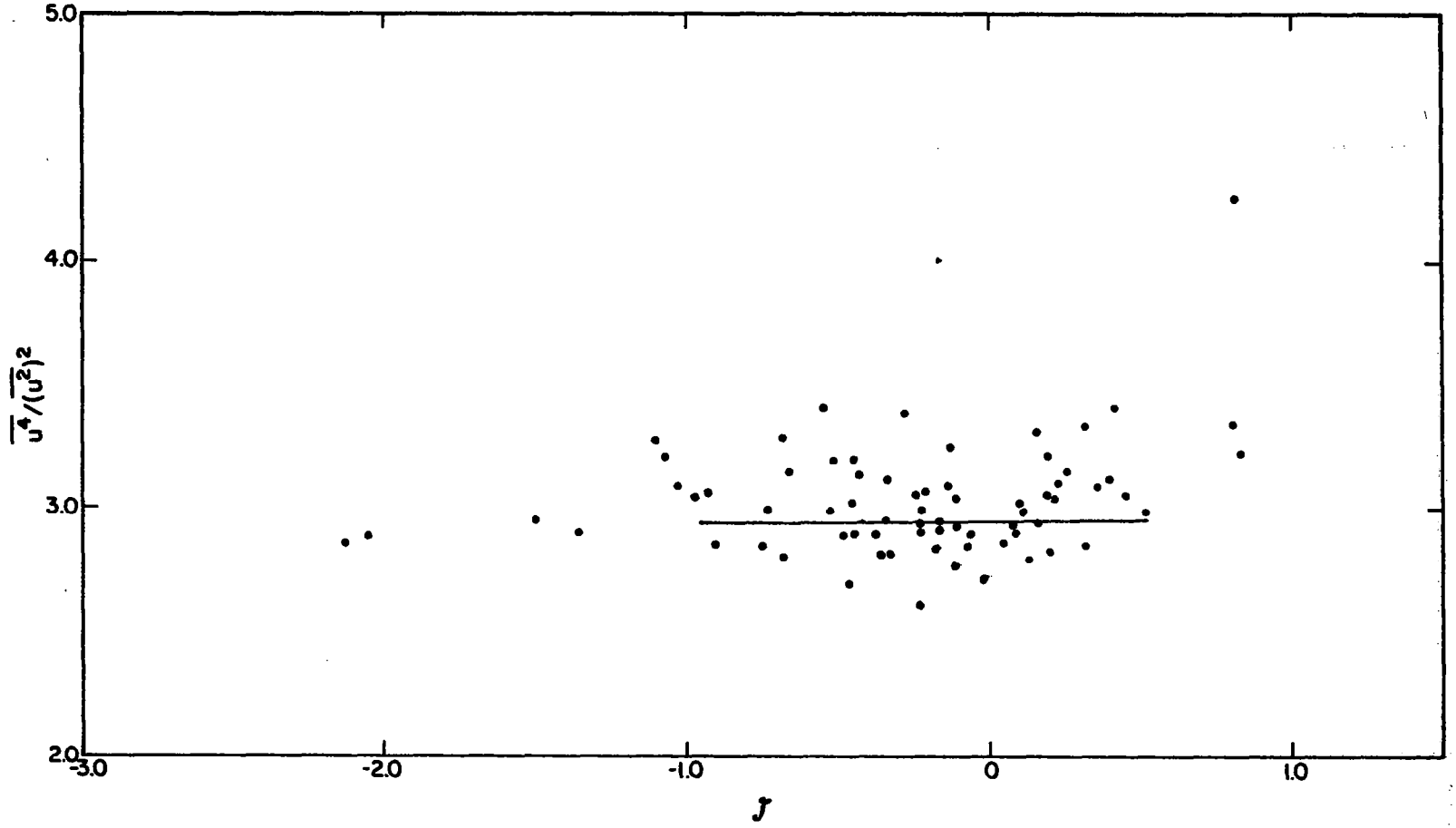

Figure A.9. Kurtosis of longitudinal wind fluctuations with stability.

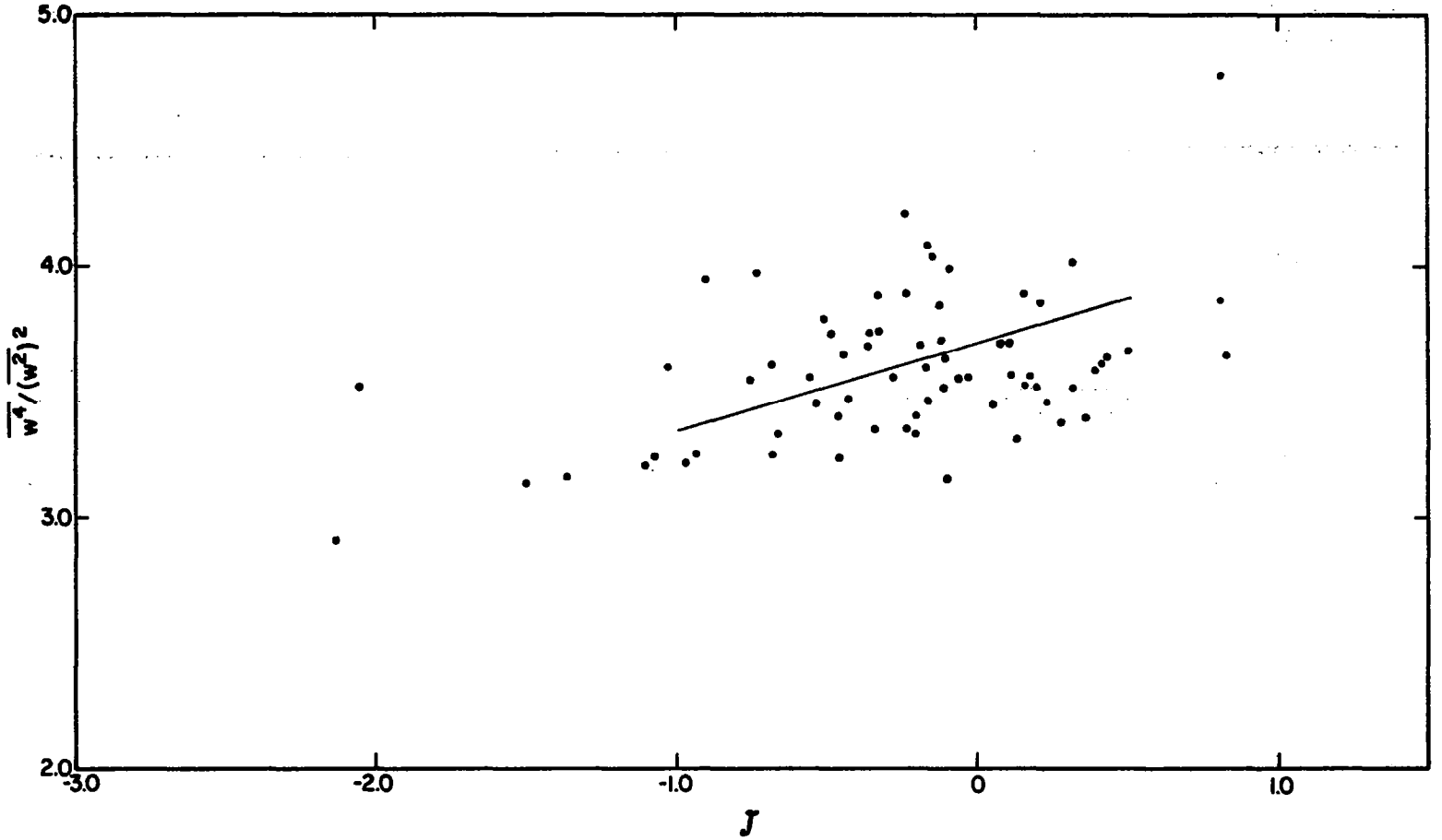

Figure A.10. Kurtosis of vertical wind fluctuations with stability.

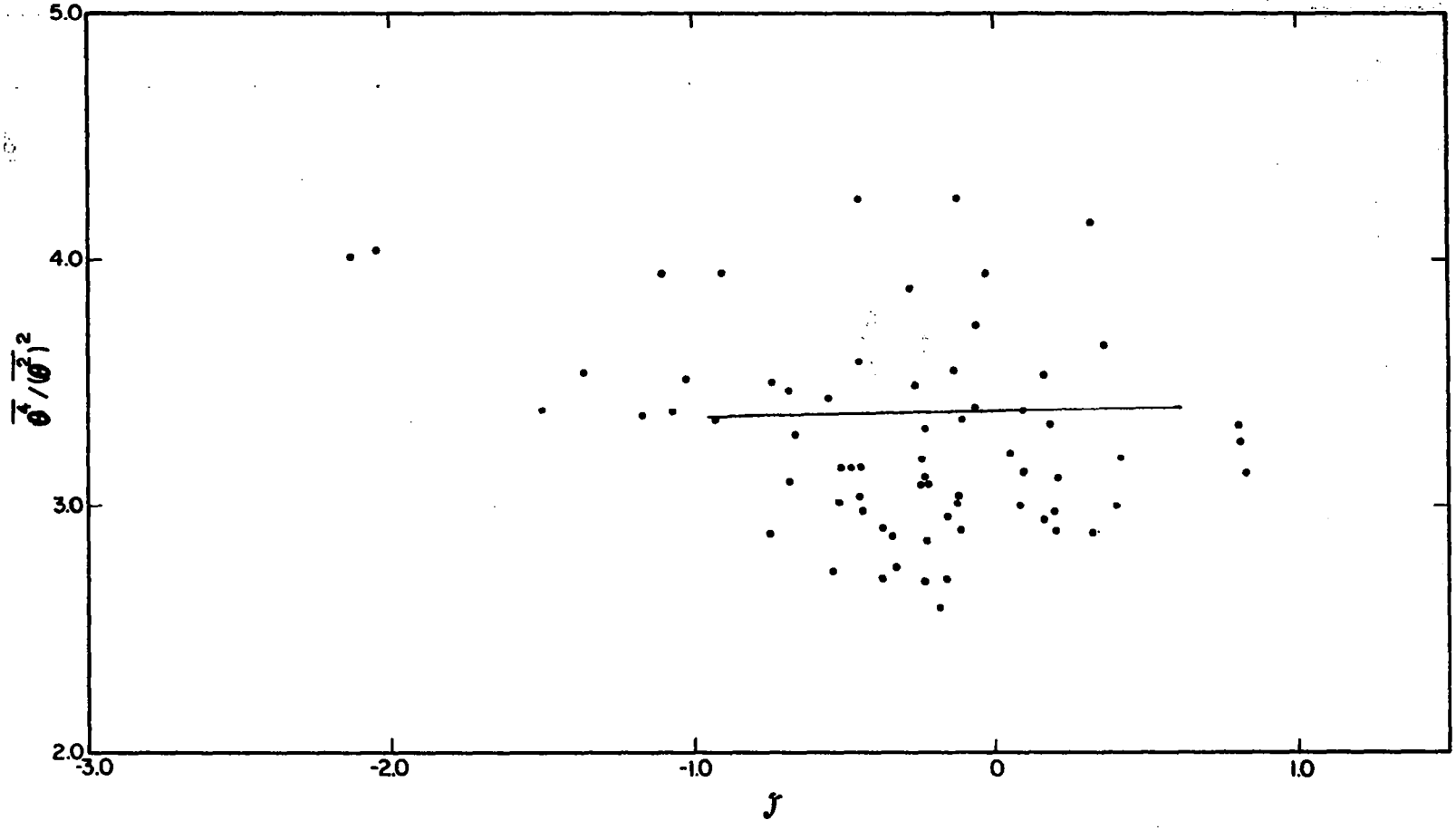

Figure A.11. Kurtosis of temperature fluctuations with stability.

constant, whereas the kurtosis of the vertical component decreases with decreasing stability. Monin-Oboukhov similarity is apparently only satisfied for the skewnesses of $\tilde{w}$ and $\tilde{\theta}$.

A positive skewness indicates a greater probability of negative fluctuations whose absolute value does not exceed a standard deviation and a greater probability density of positive fluctuations larger than a standard deviation. Therefore, the $\tilde{w}$ component, in near-neutral conditions, has more small negative and large positive excursions than a strictly Gaussian distribution. This arrangement increases in unstable conditions and decreases in stable conditions, possibly reversing itself near $\zeta = 0.5$. The temperature process is likewise skewed. Presumably, in unstable condition the more probable large positive θ excursions are associated with the increased probability of large positive w excursions. Finally, the longitudinal velocity distribution is symmetric in the range, $-1 < \zeta < 0.5$.

The kurtosis is a measure of the integrated probability density in the extremes of the distribution irrespective of the sign of the fluctuation. For a kurtosis exceeding 3, the process would have a greater concentration of large, absolute occurrences of either sign, greater than one standard deviation, than would a Gaussian process. From the data displayed in Figures A.10 and A.11 the vertical velocity and buoyancy fluctuations contain more large excursions than would occur in a Gaussian process. Also the u component (Figure A.9) is associated with a more regular process than a Gaussian process. With increasing instability, u and θ indicate no pronounced change in their content of large fluctuations, while the w process tends to become more regular.

The non-Gaussian structure in terms of the skewness and kurtosis as a function of stability has been approximated by the following relationships

- for unstable conditions ($-1 < \zeta < 0$)

$$M_3^3 = 0.12\ (1 - 4.7\ \zeta - 2.3\ \zeta^2) \tag{A.38}$$

$$M_\theta^3 = 0.34\ (1 - 3.2\ \zeta - 1.3\ \zeta^2) \tag{A.39}$$

- and for stable conditions ($0 < \zeta < 0.5$)

$$M_3^3 = 0.12\ (1 - 2.0\ \zeta) \tag{A.40}$$

$$M_\theta^3 = 0.34\ (1 - 2.1\ \zeta + 1.9\ \zeta^2) \tag{A.41}$$

while for the entire range ($-1 < \zeta < 0.5$)

$$M_1^3 = 0 \tag{A.42}$$

$$M_1^4 = 2.7 \tag{A.43}$$

$$M_3^4 = 3.7\ (1 + 0.09\ \zeta) \tag{A.44}$$

$$M_\theta^4 = 3.4 \tag{A.45}$$

APPENDIX B DIGITAL SPECTRAL FACTORIZATION

The spectral factorization method, discussed in Section 2.4, provides a technique for determining a phase characteristic to associate with the known modulus (or spectrum) of a complex function, so that its Fourier transform will be a one-sided physically realizable filter. This appendix describes the implementation of this approach computationally. Its use is not limited to rational spectra. The use of the fast Fourier transform (FFT) algorithm provides a very efficient method of solution. Other methods such as Wiener's predictive decomposition and Fejer's solution for the roots of a polynomial (Robinson, 1967b) are slow and inaccurate by comparison.

The turbulent process represented by the empirical spectra of the model is referred to as a continuous-parameter process. The necessary and sufficient condition for the spectrum of a continuous-parameter process to be factorable is that the spectrum be absolutely continuous and satisfy the Paley-Wiener condition that

$$\int_{-\infty}^{\infty} \frac{\ln \phi(f)}{1 + f^2} \, df > -\infty \qquad \text{(B.1)}$$

In other words, the spectral representation does not converge for $f \to \infty$ as rapidly as an exponential, $\exp - f^n$, where $n \geq 1$. However, $\phi(f)$ must nevertheless approach zero in the limit of large f.

The application of the FFT algorithm to spectral factorization requires that the continuous-parameter process defined over $-\infty < f < \infty$, be converted to a discrete-parameter process over a finite range $-\pi \leq u \leq \pi$, where

$$u = 2 \tan^{-1} f \tag{B.2}$$

For a discrete-parameter, process with spectrum ψ, to be factorable its spectrum must be regular, or alternatively,

$$\int_{-\pi}^{\pi} \ln \psi \, du > - \infty \tag{B.3}$$

Rino (1970) has shown that the discrete parameter spectrum will be regular only if the continuous parameter spectrum approaches zero in the limit of large f no faster than a power of $(1 + f^2)^{p+1}$ or in the limit

$$0 < \lim_{f \to \infty} \phi(f) \; (1 + f^2)^{p+1} < \infty \tag{B.4}$$

where p is some positive integer approximating the behavior of the spectrum in the limit. The coordinate transformation (B.2) guarantees that ψ defined by

$$\psi(u) = (1 + \cos u)^{-(p+1)} \; \phi(\tan u/2) \tag{B.5}$$

will be regular on $[-\pi, \pi]$.

We will follow the development of Section 2.4 in implementing spectral factorization, but with Fourier transformations in terms of the FFT algorithm. The expansion of $\ln \psi^{1/2}$ becomes

$$\ln \left[\psi\left(\frac{2\pi n}{N}\right)\right]^{1/2} = \sum_{t=0}^{N-1} \alpha_t \exp\left(-i \frac{2\pi n t}{N}\right) \tag{B.6}$$

Equivalently, the α coefficients for the regularized process are

$$\alpha_t = \frac{1}{N} \sum_{n=0}^{N-1} \ln \left[\psi\left(\frac{2\pi n}{N}\right)\right]^{1/2} \cos\left(\frac{2\pi nt}{N}\right) \tag{B.7}$$

From (2.4.20) the minimum-phase kernel transform, $\hat{g}$, whose modulus is ψ, is given by

$$\hat{g}\left(\frac{2\pi n}{N}\right) = \exp h\left(\frac{2\pi n}{N}\right) \tag{B.8}$$

where

$$h\left(\frac{2\pi n}{N}\right) = \frac{\alpha_o}{2} + \sum_{t=1}^{N/2-1} \alpha_t \left(-i\,\frac{2\pi nt}{N}\right) + (-1)^n \frac{\alpha_{n/2}}{2} \tag{B.9}$$

The final step is the recovery of K, where

$$\hat{K}\,\hat{K}^* = \phi \tag{B.10}$$

from $\hat{g}$ where

$$\hat{g}\,\hat{g}^* = \psi \tag{B.11}$$

The solution is given as an approximation (Rino, 1970)

$$K(\tau) \simeq \sqrt{2}\, e^{-\tau} \sum_{n=0}^{N} \gamma_n^j\, L_n(2\tau) \tag{B.12}$$

where L_n is the Laguerre polynomial of order n. The coefficient γ_n is derived from $\hat{g}$ by a Fourier transformation

$$\hat{g}\left(\frac{\pi}{N}\right) = \sum_{t=0}^{N} \gamma_t \exp\left[-i\,\frac{2\pi nt}{N}\right] \tag{B.13}$$

Also, γ_n^j is derived from γ_n, by iteration

$$\gamma_0^M = \frac{1}{\sqrt{2}}\,\gamma_o^{M-1} \tag{B.14}$$

$$\gamma_j^M = \frac{1}{\sqrt{2}}\,(\gamma_{j-1}^{M-1} + \gamma_j^{M-1}) \qquad j \geq 1 \tag{B.15}$$

$$\gamma_0^0 = \frac{1}{\sqrt{2}}\,\gamma_o \tag{B.16}$$

$$\gamma_j^0 = \frac{1}{\sqrt{2}}\,(\gamma_{j-1} + \gamma_j) \qquad j \geq 1 \tag{B.17}$$

The computer program written to factor a given spectrum was calibrated for a spectral form

$$\phi(f) = (1 + f^2/N)^{-N} \tag{B.18}$$

which has a known response function (for a given N) of

$$K(\tilde{x}) = \frac{N^{N/2}\,\tilde{x}^{N-1}}{N-1!}\exp - N^{1/2}\tilde{x} \qquad \tilde{x} \geq 0 \tag{B.19}$$

$$= 0 \qquad \tilde{x} < 0 \tag{B.20}$$

The difference between the analytical and numerical solution, for various values of N, are displayed in Figure B.1. The error is insignificant up to about $\tilde{x} = 7$ and $N = 4$ and is insignificant to large $\tilde{x}$ as N decreases. For $N = 1$, the error is of the order of the single precision

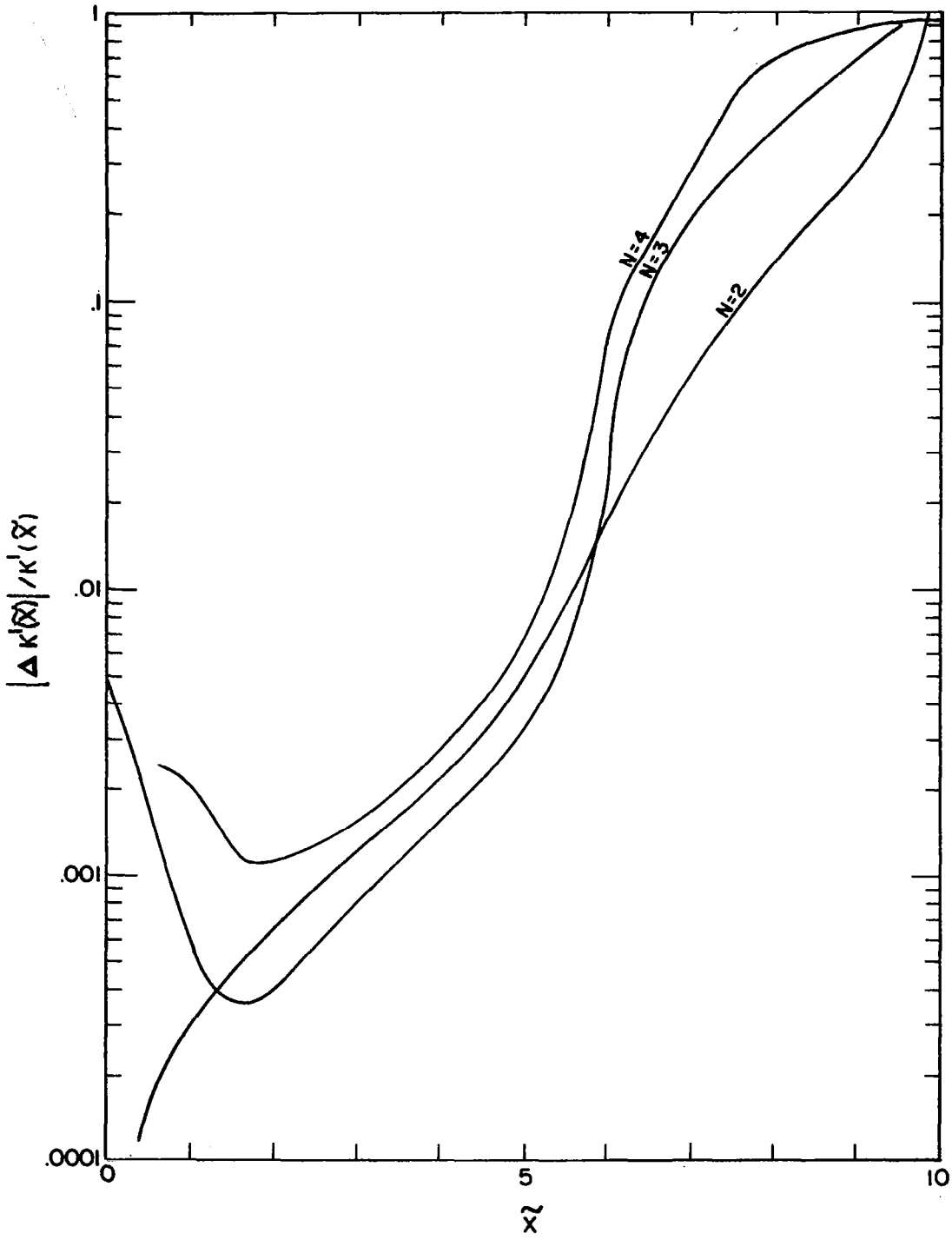

Figure B.1. Numerical error in estimating response functions of several spectra.

accuracy. Although the response function itself is relatively small ($\sim 10^{-3}$), for large $\tilde{x}$, say $\tilde{x} > 5$, for all N, it is of the order of the error in the method. As a result any simulation of turbulence at scales about 10 times the energy-containing scales using the kernels can be expected to be in error. However, as such scales are not of immediate practical concern, the algorithm for spectral factorization is considered accurate for most purposes.

To be factorable, a given spectrum must satisfy (B.4). The question arises as to the compatibility of spectra which vary as f^{p+1} in the limit of large f, where p is not an integer. The approach used in this study has been to ensure that the largest frequency, say, f_{MAX}, represented by the FFT is at a scale much smaller than the resolution desired in constructing the filter. The nearest integer approximation to the parameter p in (B.4) is then computed on the basis of the spectral energy densities at f_{max} and $f_{max}/2$. Succeeding computations are then inaccurate only in their representation of the spectrum near f_{max}, or in the computation of K very near $\tilde{x} = 0$. Suitable convergence for a $f^{-5/3}$ spectral form was found by choosing $f_{max} > 40$, or well into the inertial subrange.

Simulation of Atmospheric Turbulence by Proper Orthogonal Decomposition

John A. Dutton and Erik L. Petersen

ABSTRACT

A method that produces realistic simulations of atmospheric turbulence is developed and analyzed. The procedure makes use of a generalized spectral analysis, often called a proper orthogonal decomposition or the Karhunen-Loeve expansion.

A set of criteria, emphasizing a realistic appearance, a correct spectral shape and non-Gaussian statistics, is selected in order to evaluate the model turbulence.

An actual turbulence record is analyzed in detail providing both a background for comparison and input statistics for the generalized spectral analysis, which in turn produces a set of orthonormal eigenfunctions and estimates of the distributions of the corresponding expansion coefficients.

The simulation method utilizes the eigenfunction expansion procedure to produce preliminary time histories of the three velocity components simultaneously, and then, as a final step, a spectral shaping procedure is applied.

Two experiments are performed, providing two time histories of the velocity components of 30 minutes duration. This experimental turbulence is analyzed and judged to be a realistic simulation of actual turbulence.

The method is unique in modeling the three velocity components simultaneously, and it is found that important cross-statistical features are reasonably well-behaved. It is concluded that the model provides a practical operational atmospheric turbulence simulator.

Simulation of Atmospheric Turbulence by Proper Orthogonal Decomposition

John A. Dutton and Erik L. Petersen

1.0 INTRODUCTION

The demands for a realistic simulation of atmospheric turbulence have increased over the years because of its obvious importance in diffusion, aeronautics, wind-loading of structures, and all boundary layer processes.

Requirements to be imposed on turbulence simulation schemes must produce a compromise between the accuracy with which the empirical statistical structure is represented and the feasibility of the computational scheme. A set of criteria were suggested in a previous NASA report by Dutton and Deaven (1971). They are, slightly modified:

(1) The model, through variation of internal parameters, should be able to simulate the various intensities of turbulence in the atmosphere and to provide an estimate of the likelihood of occurrence of each time history. This flexibility makes it possible to generate time sequences that approach threshold (or catastrophic) intensities for the systems whose response is being studied and to estimate the probability of failure.

(2) The model should produce time histories that exhibit the sequential behavior of actual turbulence.

(3) The model should produce signals that possess the most notable observed statistical characteristics of actual turbulence: the non-Gaussian behavior of the density function and the exceedance statistics and the dependence of the energy spectrum on the -5/3 power of the wave number or frequency over a wide range.

Standard methods that filter a white noise process so that the resulting spectra resemble those of turbulence fail to satisfy most of

these criteria. Usually a linear filter is used with Gaussian white noise as input, and so the resulting simulated turbulence is also a Gaussian process, clearly contradictory to observed evidence.

The direct use of observed turbulence, which obviously satisfies the last two requirements, has only limited value because the first requirement is not satisfied.

The fluid motions to be modeled are described completely by the Navier-Stokes differential equations together with appropriate boundary and initial conditions. Despite the simplicity these equations possess compared to the complexity of the motions they describe, it is by no means feasible at the present, nor in the foreseeable future, to use these equations directly in operational simulation models.

The model to be presented in this report is based on an approach suggested by Dutton (1968) and further elaborated by Dutton (1969) and Dutton and Deaven (1971).

Information is extracted from measured turbulence by means of Loeve-Karhunen expansions and is carried in the model by the orthogonal functions and the statistics of the expansion coefficients. The method is based on the Proper Orthogonal Decomposition Theorem.

In contrast to most models, this model generates all three velocity components simultaneously, and it is found that the simulated time histories can meet most of the requirements stated above. Moreover, cross-statistics between components seem to be modeled satisfactorily to at least second order.

2.0 REVIEW OF SOME PREVIOUS SIMULATION METHODS BASED ON THE PROPER ORTHOGONAL DECOMPOSITION THEOREM

The first attempt to apply the Proper Orthogonal Decomposition Theorem in the study of turbulence apparently was made by Lumley (1965). Before that, the basic theorem, given by Loeve (1955), had proven useful in the study of large-scale meteorological features (for example, Lorenz, 1965; Kutzbach, 1967).

The outline for the application of the method in the simulation of atmospheric turbulence was given by Dutton (1968) and Dutton and Deaven (1969). The theory was discussed in some detail and an attempt was made to use the method to determine if the large gusts as measured at Cape Kennedy had a characteristic structure. Sixty large gusts for each of the components u and v were extracted from a turbulence record. It was found that eight eigenfunctions explained at least 97 percent of the variance for each component, leading to the conclusion that the large gusts had a characteristic structure.

This result pointed to the possibility of simulating large gusts by using the eigenfunctions and by sampling the expansion coefficients from estimates of their respective distributions.

Before this approach can be applied in practice, it is obviously necessary to determine:

(1) how to model the turbulence between the gusts,

(2) how large a fraction of the record shall be occupied by the large gusts,

(3) how much of the total variance shall be due to the large gusts.

An answer to these questions was attempted by Smith (1971) in the research done under NASA contract NASA-21140 for his Master of Science degree. Smith tested and evaluated several simulation methods using the three criteria described in section 1. These three criteria were compressed to the following tests:

(1) Does the simulated turbulence look like turbulence records?

(2) Does the energy spectrum fall off as the -5/3 power of wavenumber?

(3) Does the probability of getting small and large values exceed the Gaussian probability even though the density function is nearly Gaussian?

(4) Does the exceedance statistics, as represented by the probability of crossing a certain level per unit time, look like those obtained from real turbulence?

The following description (2.1-2.6) of methods and their evaluation is largely extracted from Smith (1971). Results of tests against the four criteria above are given in Table 1.

2.1 Random White Noise

Random noise as a discrete random signal that contains equal energy at all frequencies can be generated using the random generator available in almost all computer systems. It is constructed as an ordered set of random variables such that for each point in time, the random variable is selected independently from a normally distributed population.

TABLE 1 - AN EVALUATION OF SOME PREVIOUS SIMULATION METHODS

Generation Scheme	Criteria: Realistic Sequential Appearance of the Time-History	Criteria: A - 5/3 Slope in the Energy-Spectrum	Criteria: Non-Gaussian Density Functions	Criteria: Realistic Exceedance Statistics
Random white noise	no	no	no	no
Shaped random white noise	improved	yes	no	no
Random noise with gusts	no (It is too easy to distinguish the gust.)	yes	yes but exaggerated	no
Shaped random noise with gusts	no (as above)	yes	yes	yes but exaggerated
Random noise with variable gusts	no (as above)	no	yes	yes
Shaped random noise with variable gusts	improved	yes	yes	yes

2.2 Shaped Random Noise with Preserved Phase Angles

Because random noise clearly failed criterion 2 because of the flat energy spectrum, an obvious step was to take random noise and then shape the energy spectrum to give it the correct -5/3 slope. This was accomplished by taking the Fourier transform of the generated series and changing the Fourier amplitudes according to a predescribed scheme. The scheme also included an algorithm for preserving the Fourier phase, because these are believed to be of some importance for the intermittency of the turbulence (see section 2.8).

2.3 Random Noise with Gusts

The most pronounced failure of the method above was its inability to produce the non-Gaussian nature of the probabilistic structure. The method proposed by Dutton using the basic structure of large gusts as revealed by empirical eigenfunctions was then attempted. From the first eight eigenfunctions, a number of gusts were constructed and inserted at random into a white noise series. By trial and error it was found that the best result was obtained when the gusts occupied 40 percent of the total series, and when the ratio of variance of gusts to variance of white noise was 19.

2.4 Shaped Random Noise with Gusts

The series generated in Section 2.3 was then subjected to a spectral shaping as described in Section 2.2.

2.5 Random Noise with Variable Gusts

The same procedure as described in Section 2.3 was followed except that before the gusts were inserted into the series, the length of the gusts was made variable by randomly expanding the gusts by factors of one, two, or three.

2.6 Shaped Random Noise with Variable Gusts

The series generated above was subjected to the spectral shaping process. Although this model apparently turned out as acceptable, it does not satisfy the requirement that it should be possible to generate a wide range of turbulence simulations by adjusting a few parameters and so the tests for sensitivity to changes in the various parameters would be very cumbersome. Actually the parameters in the model are those describing the orthogonal functions representing the gusts, the distribution functions of expansion coefficients, the ratio of gusts to total record, the ratio of variance of gusts to variance of total record, variations in the length of gusts, the points where the gusts are to be inserted, and the spectrum to be produced by the shaping process.

2.7 Simulation Using Empirical Orthogonal Functions

The possibility of simulating turbulence by using empirical orthogonal functions to represent the entire time series was investigated by Dutton and Deaven (1971) and Smith (1971). An alternative approach suggested by Hirose and Kutzbach (1969) was applied to a sample of nine turbulence runs each of 1024 points.

The approach makes it possible to obtain the eigenvalues and the eigenfunctions by diagonalization a 9 × 9 matrix instead of a 1024 × 1024 matrix as required by the conventional method. Eight eigenfunctions and corresponding expansion coefficients distributions were extracted and then used to simulate turbulence runs. The method apparently fails because of dependence between expansion coefficients and dependence between and within the eigenfunctions.

2.8 Simulation by Manipulating Fourier Phases

An attempt was made by Spark and Dutton (1972) to assess the importance of phase angle (Fourier-phases) considerations in the modeling of intermittent turbulence. The conclusion of the study was that intermittency appears to be dependent on some higher order association in Fourier space and that any mathematical model in Fourier space for intermittency would extremely involved. Nevertheless, based on qualitative arguments it was suggested the Fourier angles might be used to simulate turbulence by the following procedure:

(1) generate a random Gaussian series,

(2) obtain its Fourier transform and the Fourier coefficients,

(3) form the phase angles from the coefficients,

(4) replace the original spectrum with a smoothed -5/3 spectrum

(5) adjust a suitable number of phase angles according to a preassigned schedule devised by Spark and Dutton,

(6) use (5) to find the new Fourier coefficients and back-transform these to obtain the simulated turbulence.

Because the manipulation of the angles under step 5 essentially creates gustlike events in the series, this model bears strong resemblence to the model described in section 2.6. Unfortunately, it also shares with it some of the disadvantages, including the difficulty in assessing the sensitivity to changes in the various parameters.

3.0 THE GENERALITY OF TURBULENCE PRODUCED BY MODELS

Empirical turbulence models of the type discussed in this report evidently will depend on information extracted from one or more actual turbulence records. Consider the case where a turbulence record measurement at 6 meters height at mean wind speed of 6m/sec has been used in the creation of the model, and the model turns out to work satisfactorily in the sense of simulating turbulence resembling actual turbulence occurring under the above conditions. Will it then also be possible to use the model to simulate turbulence as found in clear air turbulence with, say, a length scale of 600 meters and a mean windspeed $\bar{u}$ = 30m/sec? If the answer is no, the usefulness of the model will certainly be severely restricted.

Fortunately, measurements in the troposphere and the stratosphere show that turbulence possesses in the inertial subrange a high degree of self-similarity[1]. Because amplitudes are related to the 1/3 power of the wavelength, if the wavelength in a turbulence record obtained in the inertial subrange is expanded by a factor β, then an amplification of the velocity amplitudes by $\beta^{1/3}$ would yield a record similar to turbulence (Dutton and Deaven, 1969).

---

1) In the sense of B. Mandelbrodt's (1965) concept of self-similarity: A process with random variable X is self-similar if the variable X_h obtained by the magnification of the wavelength by h can be represented as a suitable magnification of the amplitude of X so that both X and X_h have the same probabilistic structure.

From above, for the first example, we have: a length scale of $L = 6m$ and a velocity scale of $\bar{u} = 6m/sec$, yielding a time scale $T = L/\bar{u} = 1$ sec.

For the second example: $\bar{u} = 30m/sec$ and $L = 600m$, $T = 20$ sec. Thus we have to expand the temporal scale by a factor of 20, hence the velocity amplitudes have to be magnified by a factor $20^{1/3}$.

The "1/3 power law" is only valid in the inertial subrange where the spectra fall off as -5/3 in a log-log plot. In general, the concept of self-similarity is only useful for processes in which the spectra exhibit power law behavior. Unfortunately, most turbulence spectra in the form $\kappa S(\kappa)$ have a rather flat maximum from which the spectra fall off towards both higher and lower numbers.

However, for many engineering applications, it is usually the energy content in the inertial subrange that is of most importance, and so if turbulence can be simulated in this range by an appropriate model, then time and velocity scales can be changed as required by particular applications.

Another strategy would be to assume the spectra exhibit different power laws, on opposite sides of a particular wave number, κ_{MAX}, an assumption which finds some support from observed turbulence. Then we would have

$$\kappa S(\kappa) = A\kappa^{\gamma} \qquad S(\kappa) = A\kappa^{\nu-1} \qquad \kappa \leq \kappa_{MAX}$$

for

$$\kappa S(\kappa) = B\kappa^{-\gamma} \qquad S(\kappa) = B\kappa^{-\gamma-1} \qquad \kappa \geq \kappa_{MAX}$$

Denoting the temporal multiplication factor by β and the velocity factor by h, we have from Dutton and Deaven

$$h = \beta^{-\nu/2} \qquad \kappa \leq \kappa_{MAX}$$

for

$$h = \beta^{\gamma/2} \qquad \kappa \geq \kappa_{MAX}$$

where it follows that $\gamma + 1 = 5/3$ gives $h = \beta^{1/3}$.

In this approach, we would obtain the Fourier transform of the simulated sequence and then all amplitudes on the side $\kappa < \kappa_{MAX}$ would be adjusted by the factor appropriate for those wavenumbers while all amplitudes on the other side would be adjusted by the other factor. These adjusted amplitudes would be used in a back-transform to produce a series appropriate for the expanded time scale.

4.0 THE THEORY AND THE MODEL

The experience gained through the various studies mentioned in the previous sections emphasizes the difficulties in generating the correct time sequence of the empirical turbulence, even if reasonably chosen statistics seem to be modeled rather well. But the experience also showed that one way to success could be to emphasize the creation of gust-like events in the generated series, thus simulating the so-called "surprise" of real turbulence. The current model is based on such an approach, and the philosphy behind it is given a fuller treatment in the last section. For the present, it is sufficient to note that in order to find the structure of the gusts it is necessary to select a certain type of analysis and perform it on records of actual turbulence.

Imagine the turbulence records to be composed of intervals of "passive turbulence" and of intervals of "active turbulence", where by active turbulence intervals we understand sequences of the records in which it is observed that a gust prevails for some specific length of time, T. Hypothesize further that the active turbulence is composed of a quasi-deterministic gust structure to which is added passive turbulence. We can then confine our attention to the active intervals because, if we can find the gust structure, and if we can find a way to represent the passive turbulence, we know from an analysis of the turbulence records how the passive and the active intervals are distributed in the records, and a model proposes itself: generate series of passive turbulence and add to it the gust structure in such

a way that the passive and the active intervals become distributed as in the actual record.

It is shown in Section 8 that imposing certain principles in order to find the gust structure and an economical representation of the passive turbulence lead to the Fredholm integral equation

$$\int_0^T R(s,t)\ \phi_k(t)\ dt = \lambda_k \phi_k(s)$$

where

$$R(s,t) = E\{f(s)\,f(t)\}$$

and $f_n(t)$ is the nth interval ($t_n \leq t \leq t_n + T$) of active turbulence taken out of the records and then redefined over the interval (0,T). The expectation operation $E\{\ \}$ is performed on the ensemble of $f_n(t)$, $n = 1,2, \ldots$

The ϕ's are orthonormal eigenfunctions of the correlation matrix R(s,t) and under the assumptions stated above, ϕ_1 reveals the gust structure and ϕ_2, ϕ_3, ... provide us with an optimal expansion of the passive turbulence over intervals of length T.

We have for an interval of active turbulence

$$(4.1) \qquad g_A(t) = \sum_{k=1}^{\infty} \alpha_k \phi_k(t)$$

and for an interval of passive turbulence

$$(4.2) \qquad g_B(t) = \sum_{k=2}^{\infty} \alpha_k \phi_k(t)$$

The probability density functions of the expansion coefficients α_k are estimated from the f_n's

$$\alpha_k^n = \int f_n(t)\ \phi_k(t)\ dt$$

hence the α_k's in (4.1) and (4.2) are sampled from their respective distributions.

Representing the gust structure by a function that is orthogonal to all the functions used in the expansion of the passive turbulence obviously requires that the two processes, the gust and the passive turbulence, be orthogonal, a requirement we only can expect to be met approximately. Then, because of a possible non-orthogonality between gust and passive turbulence, we would expect ϕ_1 to give most of the gust structure plus a little of the passive turbulence, ϕ_2 some of the gust and more of the passive turbulence, and so on. To account for this in a generating scheme, one approach would be to use all the ϕ's to construct all sequences of the turbulence, but to diminish the amplitudes of the first eigenfunctions approximately in the intervals with passive turbulence, for example by transforming the probability density functions for the expansion coefficients.

4.1 The Model

The discussion above proposes that the model be established in two parts: an analysis scheme and a generating scheme. Thus, the first scheme describes how to obtain the eigenfunctions and the second scheme how to use them.

The analysis scheme

The steps in carrying out the computation are:

A1 Select one or more observed turbulence records.

A2 Select a characteristic feature in the records believed to be of importance for the intermittency of the turbulence and select the corresponding time interval, T. (Such a feature may be a large gust.)

A3 Extract as many as possible time intervals containing the feature in order to construct a representative ensemble $f_n(t)$. Estimate the probability density function for the time interval between the occurence of the feature.

A4 Subject the ensemble to a Proper Orthogonal Decomposition to obtain eigenfunctions and expansion coefficients and estimate the appropriate probability density functions of the coefficients.

The generating scheme

Because the eigenfunctions are defined on a fixed interval, it is necessary to generate the turbulence in multiples of this interval. From A3 we know the distribution of the time intervals between the events, and we can then pick values from such a distribution to determine where in the generated series the special events shall occur. From the appearance of the eigenfunctions, one can estimate how much active turbulence and how much passive turbulence the first few eigenfunctions explain. According to this estimate the weight of these eigenfunctions is diminished in the passive intervals.

The generating scheme then becomes:

G1 Generate a set of random numbers, using the probability density functions from A3, to establish the sequence of intervals of active and passive turbulence.

G2 Generate the active intervals by sampling the expansion coefficients from their probability density functions (from A4) and multiply the respective expansion coefficients and eigenfunctions and add the functions together.

G3 Generate the passive intervals as above, but make appropriate transformations of the first few probability density functions, and if necessary,

G4 Obtain the Fourier-Transform, let the phases be unchanged, but

1. Change the amplitudes such that the energy spectrum is proportional to the -5/3 power of the frequency over a certain range (see Section 7).

2. Obtain the appropriate time and length scales by multiplying the amplitudes by a constant which has been determined in accordance with Section 3.

Then back transform to the time domain.

5.0 CONSTRUCTION OF THE MODEL

The ensemble $f_n(t)$ was selected from a turbulence record that will be described in the next section. It is composed of 0.10 second block-averaged values of the u,v, and w components; the total length of the record is 50 minutes.

The selection of the ensemble $f_n(t)$ was then done heuristically in the following way:

1. T was chosen to be 5 sec (=50 data points)

2. The record was divided into 100 segments, each of the length 30 sec (=300 data points)

3. Inside each segment, the maximum value of w was found and a 5 second interval of data centered around this value was picked for all the components

4. The mth ensenble function f_m, was then obtained from the mth segment for $1 \leq m \leq 100$, and the function was constructed by patching together the u,v, and w components (150 data points) sequentially. The occurence statistics were then very simple, and a gust interval of 5 seconds duration was placed at random inside each sequence of 30 seconds length.

The numerical approximation of (4.3) becomes

$$\Sigma R(s,t)\phi_n(t) = \lambda_n \phi_n(s) \tag{5.1}$$

which is the usual eigenvector equation used in principal component analysis.

We have

$$R(s,t) = \frac{1}{m} \Sigma_m F_m^T(s) F_m(t)$$

where T denotes transpose and F_m is a $1 \times M$ and F_m^T a $M \times 1$ matrix. The matrix F_m has the following structure

$$F_m(t) = [U_m(1), U_m(2), \ldots, U_m(50), V_m(1), V_m(2), \ldots, V_m(50), W_m(1), W_m(2), \ldots, W_m(50)]$$

which gives R(s,t) the structure

$$\begin{bmatrix} UU & UV & UW \\ VU & VV & VW \\ WU & WV & WW \end{bmatrix}$$

where, for example, UV is the 50 x 50 uv correlation matrix.

A more straightforward way to perform the analysis would be to create three ensembles, one for each of the components, u, v, and w, and then get three sets of eigenfunctions by solving (5.1) for R(s,t) = UW, VV, and WW respectively. But then we would have disregarded all cross statistical information, and it would be difficult to introduce it into the analysis later.

The way the eigenfunctions are constructed in this analysis by patching together u, w, and w enables us to use all the second order cross statistical information available to construct the eigenfunctions. The function $\phi_1(t)$ would then give the most likely simultaneous occurence of u, v, and w during a gust in w.

The patching of ensemble functions has been used by Jaspersen (1971) to analysis vertical profiles of meteorological variables.

5.1 The Eigenvalue Spectrum and the Eigenfunctions

A diagonalization was performed on the 150 × 150 matrix, R(s,t), giving the eigenvalue spectrum shown in Table 2 and the 150 eigenfunctions of which the first 14 are shown in Figure (5.1) and the first 20 are listed in Table 3.

The first two eigenfunctions seem to explain the average values of u, w, and w during the "gust", and it is not surprising that this is the most highly cross-correlated feature. We could have prepared the ensemble from which the eigenfunctions were calculated in such a way that the mean of u, v, and w was zero in each ensemble function, or we could have removed the ensemble mean from each ensemble function. In both cases we would then have to carry some additional statistical information in the model which can be carried by the eigenfunctions and the expansion coefficient distributions themselves.

The third eigenfunction is mostly devoted to the peak in w, and to a lesser degree so are the fourth and fifth eigenfunctions. Fig. (5.1) reveals how the eigenfunctions, as the number increases, tend to explain features on a smaller scale.

Table 2 shows that 72% of the total variance in the ensemble is explained by the first 5 eigenfunctions, 82% by the first 10, and 91% by the first 20. In the final generation scheme, the first 20 eigenfunctions were applied.

Because only 100 ensemble functions were used to create the 150 × 150 matrix R(s,t), the actual order is 99, and only 99 non-zero eigenvalues can be calculated. This creates some interdependency between the eigenfunctions. However, the appearance of some degree of dependence does not seriously compromise the method.

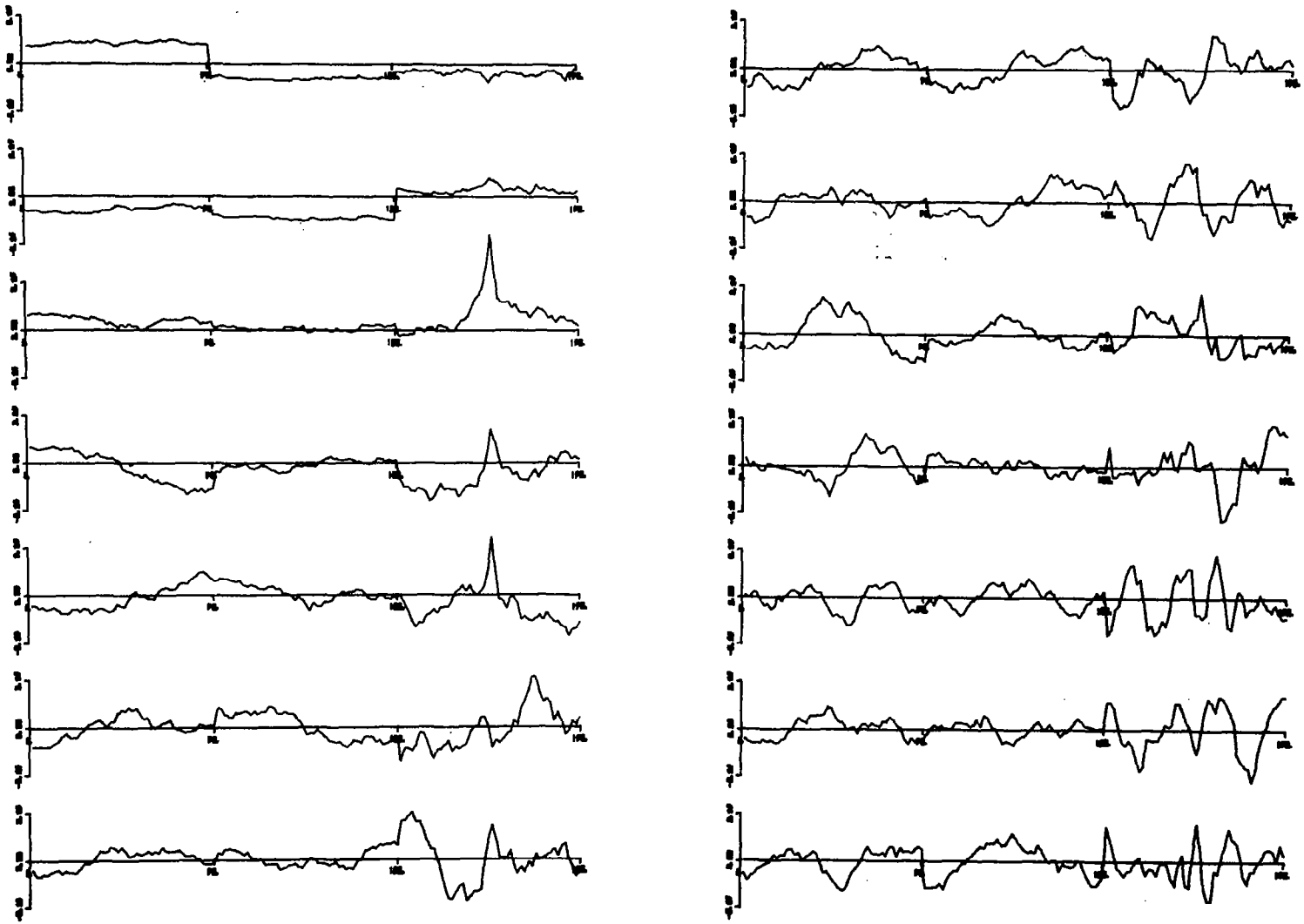

Figure 5.1 First 14 eigenfunctions. Points 1-50 are the u-component, points 51-100 the v-component, and points 101-151 the w-component.

TABLE 2

EXPANSION STATISTICS FOR THE FIRST 20 EIGENFUNCTIONS

Eigenfct.	Expansion coeff.		Eigenvalues		
Nr.	Mean	Stand. dev.		%	Accum. %
1	-1.72	6.63	47.0	27.0	27.0
2	1.39	6.28	41.4	23.8	50.7
3	3.39	2.92	20.0	11.5	62.2
4	0.96	3.15	10.8	6.2	68.4
5	0.83	2.29	5.95	3.4	71.8
6	-0.22	2.21	4.92	2.8	74.7
7	0.17	2.00	3.98	2.3	76.9
8	-0.06	1.91	3.67	2.1	79.0
9	-0.09	1.70	2.89	1.7	80.7
10	0.21	1.63	2.69	1.5	82.2
11	0		2.26	1.3	83.5
12			2.20	1.3	84.8
13			2.03	1.2	86.0
14			1.68	1.0	86.9
15			1.56	0.9	87.8
16			1.46	0.8	88.7
17			1.26	0.7	89.4
18			1.19	0.7	90.1
19			1.08	0.6	90.7
20			1.04	0.6	91.3

TABLE 3 - LISTING OF THE FIRST 20 EIGENFUNCTIONS

EIGENFUNCTIONS 1 - 10, POINTS 101 - 150 : THE W COMPONENT

EIGENFUNCTION

1	2	3	4	5	6	7	8	9	10
-0.04206	0.04389	-0.02797	-0.08581	-0.00463	-0.18030	0.19475	-0.15006	0.04910	0.00224
-0.04081	0.04160	-0.02414	-0.12440	-0.04763	-0.11376	0.20585	-0.17187	0.11482	-0.08762
-0.04783	0.03728	-0.02649	-0.12406	-0.08169	-0.11044	0.22616	-0.20451	0.07148	-0.07456
-0.03543	0.03181	-0.01783	-0.14562	-0.13505	-0.12440	0.24878	-0.18648	0.04803	-0.04762
-0.03569	0.02959	-0.02074	-0.14946	-0.16944	-0.09793	0.20090	-0.18632	-0.01538	-0.04336
-0.03065	0.02801	0.00547	-0.13323	-0.14963	-0.03332	0.19717	-0.15749	0.00247	-0.01444
-0.03531	0.02330	0.00501	-0.14107	-0.14873	-0.03103	0.15961	-0.08936	-0.01681	0.00850
-0.03729	0.01678	-0.00723	-0.15541	-0.11165	-0.06508	0.10041	-0.00897	-0.09484	0.13964
-0.03315	0.01598	0.00937	-0.20086	-0.10016	-0.12310	0.05649	-0.03765	-0.08899	0.15014
-0.03898	0.01299	0.01624	-0.18986	-0.08036	-0.16348	0.05509	0.06043	-0.10717	0.13249
-0.03226	0.02259	-0.00139	-0.14884	-0.09328	-0.12046	-0.00780	0.04969	-0.18441	0.09698
-0.04470	0.02147	0.02805	-0.11219	-0.06660	-0.11473	-0.05921	0.03403	-0.19178	0.12276
-0.04119	0.02036	0.01994	-0.13702	-0.06330	-0.09598	-0.14827	0.00654	-0.14193	0.12207
-0.05724	0.02577	0.01675	-0.13657	-0.06202	-0.07455	-0.20963	0.02609	-0.08035	0.09553
-0.04820	0.02001	0.00250	-0.14097	-0.03094	-0.12678	-0.20989	-0.01728	-0.02754	0.07973
-0.04767	0.01477	-0.00540	-0.13932	0.01100	-0.10488	-0.17647	-0.02024	0.03502	0.07443
-0.04190	0.02738	0.01973	-0.18026	0.02416	-0.11262	-0.14657	-0.03500	0.10122	0.06765
-0.03003	0.03051	0.04513	-0.15510	0.04619	-0.10466	-0.13660	-0.06051	0.08827	0.10674
-0.03914	0.03976	0.05669	-0.12474	0.01881	-0.08477	-0.22298	-0.04703	0.13343	0.04903
-0.02324	0.03649	0.06973	-0.11510	0.04623	-0.02557	-0.20088	-0.06677	0.14174	0.00397
-0.02599	0.04075	0.11781	-0.12141	0.01166	-0.00022	-0.17554	-0.12818	0.20154	0.00783
-0.03628	0.04732	0.16444	-0.12159	-0.00252	0.00066	-0.16886	-0.17291	0.20463	0.00760
-0.04038	0.05686	0.18183	-0.06258	0.01485	0.04940	-0.16356	-0.14064	0.15665	0.05365
-0.04488	0.05902	0.24642	-0.03696	0.04607	0.05312	0.00568	-0.11573	0.18844	0.07625
-0.06744	0.07061	0.33675	0.06246	0.13729	-0.01027	0.10859	-0.08119	0.03728	0.09279
-0.09402	0.09857	0.50081	0.17845	0.30385	-0.10615	0.17679	-0.03966	-0.05826	0.21527
-0.07177	0.08984	0.31521	0.12002	0.12825	-0.06839	0.11482	0.08750	-0.06038	0.09310
-0.05552	0.07758	0.16737	0.03343	-0.02116	-0.08492	0.00764	0.18096	-0.12368	-0.03007
-0.06373	0.06169	0.14509	-0.02709	-0.03690	-0.06446	0.00823	0.17638	-0.16599	-0.08999
-0.04609	0.03394	0.14624	-0.02670	-0.07162	-0.03872	0.00516	0.14867	-0.13519	-0.00975
-0.03868	0.04018	0.14897	-0.02868	-0.01957	-0.02856	0.04137	0.13508	-0.07319	-0.11692
-0.04100	0.04274	0.11854	-0.06016	-0.01204	0.03643	-0.03757	0.05377	-0.07016	-0.12204
-0.04654	0.03722	0.13155	-0.05263	-0.04680	0.01168	-0.07781	0.03032	-0.09439	-0.11369
-0.05133	0.05453	0.09698	-0.08474	-0.12999	0.10268	-0.04540	0.03782	-0.09816	-0.09389
-0.05076	0.04241	0.08998	-0.08854	-0.11661	0.14014	-0.07145	0.03059	0.00367	-0.04726
-0.06192	0.03346	0.09272	-0.09174	-0.13449	0.19044	-0.02181	-0.01298	0.04520	-0.00838
-0.06132	0.02018	0.06683	-0.06410	-0.13872	0.25737	-0.04249	0.00599	0.06692	0.00732
-0.05577	0.03073	0.08516	-0.03320	-0.12680	0.26244	0.02164	0.07116	0.08718	-0.11679
-0.06628	0.06401	0.11209	-0.07511	-0.10986	0.18101	-0.00313	0.06551	0.12372	-0.09897
-0.06197	0.04246	0.10604	-0.04339	-0.13220	0.13255	0.00482	0.10830	0.11302	-0.09997
-0.04793	0.04778	0.09115	-0.02115	-0.09404	0.14719	0.02228	0.07108	0.03773	-0.10614
-0.03735	0.03851	0.06541	0.03253	-0.11768	0.12808	0.03409	0.02566	0.09192	-0.05138
-0.03416	0.04054	0.06947	0.02845	-0.13926	0.03479	0.05272	0.01010	0.07256	-0.04703
-0.03273	0.03850	0.04315	0.00512	-0.13930	0.07750	0.02081	0.02411	0.10115	-0.06141
-0.04333	0.02138	0.06380	0.04869	-0.16254	0.03805	0.06536	0.00303	0.02126	-0.03373
-0.05688	0.02753	0.07046	0.05918	-0.17244	-0.03749	0.08191	0.01892	-0.03258	-0.08743
-0.08358	0.02323	0.05452	0.05223	-0.21742	-0.02139	-0.00500	0.01750	-0.09941	-0.05372
-0.04834	0.02620	0.05092	0.02323	-0.18563	0.03201	-0.04456	0.04827	-0.12165	-0.03964
-0.03762	0.01868	0.04071	0.03386	-0.17822	0.01389	-0.09210	0.05976	-0.08513	-0.00726
-0.02114	0.02995	0.02220	0.01798	-0.14597	0.05043	-0.06935	0.03040	-0.09305	-0.01299
-0.07741	0.07562	0.08443	-0.05637	-0.09798	-0.05196	-0.10021	-0.08565	-0.08500	0.03746

TABLE 3 - LISTING OF THE FIRST 20 EIGENFUNCTIONS (continued)

EIGENFUNCTIONS 11 - 20, POINTS 1 - 50 : THE U COMPONENT

EIGENFUNCTION									
11	12	13	14	15	16	17	18	19	20
0.03746	0.01031	-0.05298	-0.06590	-0.04472	0.05953	-0.10501	-0.03323	-0.14053	0.02210
-0.00435	-0.00463	-0.06376	-0.10204	-0.04699	0.02974	-0.08112	-0.05525	-0.11389	0.01297
0.01608	0.01883	-0.07415	-0.08231	-0.08090	0.03044	-0.08794	-0.06041	-0.06453	0.02259
-0.00439	0.02611	-0.07064	-0.06663	-0.08710	0.04397	-0.09231	-0.06306	-0.04795	0.05092
-0.02420	-0.01051	-0.07468	-0.04378	-0.04279	0.04248	-0.01053	-0.08716	-0.04302	0.08855
-0.02562	-0.04473	-0.05892	-0.02928	0.00446	0.02815	0.00858	-0.05748	-0.04433	0.05305
0.01000	-0.03701	-0.06614	-0.01594	0.01993	0.02153	0.00102	-0.05226	-0.02257	0.05220
0.00589	-0.06322	-0.06208	-0.00767	0.02940	0.00537	0.02417	-0.04158	0.01296	0.05817
0.00273	-0.05462	-0.06944	0.02714	0.09904	0.02258	0.02434	0.05206	-0.01333	0.02258
-0.01036	-0.00059	-0.07385	0.01670	0.09098	-0.01417	-0.02239	0.05112	0.04225	-0.00176
-0.01453	-0.02389	-0.06264	0.02775	0.05915	-0.02352	0.00657	-0.00718	0.04518	0.00344
-0.01516	-0.00408	-0.05142	0.02605	0.02845	-0.02854	0.03126	-0.01733	0.02830	0.00775
-0.02275	0.01852	-0.01772	0.05782	0.04657	-0.04481	0.05566	0.00653	0.03840	-0.04218
-0.02563	0.03387	-0.00428	0.06575	0.05445	-0.05625	0.04018	0.03877	0.03704	-0.00143
-0.03542	0.02865	0.03225	0.03546	0.05278	-0.04426	0.01563	0.04369	0.07604	0.01103
-0.03143	0.01495	0.05736	0.04013	0.01975	-0.08385	-0.03397	0.06571	0.07343	0.02603
-0.05006	0.02136	0.04647	0.01023	-0.01525	-0.11852	-0.02082	0.05979	0.01572	-0.00714
-0.02438	0.05134	0.03299	0.01788	-0.02197	-0.06826	0.00868	0.04149	0.03096	-0.02038
-0.03267	0.06409	0.07072	0.03422	-0.04964	-0.06621	-0.02444	0.06094	0.03775	-0.05185
-0.07707	0.03484	0.07472	0.05084	-0.08811	-0.07000	-0.02089	0.08591	0.07516	-0.07695
-0.07113	0.01988	0.07540	0.03792	-0.11230	-0.05088	-0.03620	0.13771	0.04036	-0.09011
-0.08689	0.01724	0.07527	-0.01427	-0.12246	0.00213	-0.04078	0.18394	0.02835	-0.09256
-0.11777	-0.03238	0.08256	-0.06252	-0.09488	0.03204	0.00772	0.14568	-0.00612	-0.07492
-0.16274	-0.06476	0.11526	-0.05782	-0.03959	0.06154	0.02929	0.05599	-0.00223	-0.06568
-0.10425	-0.10085	0.11144	-0.08713	-0.03549	0.06415	0.01589	0.04667	-0.04937	-0.03968
-0.05350	-0.09233	0.06832	-0.11699	0.00683	0.07781	0.00619	0.00985	-0.08540	-0.08089
-0.04512	-0.10315	0.03959	-0.14175	0.06164	0.06680	0.00786	-0.02983	-0.07228	-0.02846
-0.03411	-0.10868	0.03713	-0.15798	0.11695	0.10293	0.02720	-0.02593	-0.04906	0.01795
-0.00402	-0.14973	-0.00228	-0.15032	0.12611	0.09845	0.00939	-0.03671	-0.03628	0.08902
0.06266	-0.14878	0.00442	-0.10668	0.11333	0.03958	0.00867	-0.08179	-0.00841	0.08952
0.07288	-0.12864	0.01179	-0.05907	0.08901	-0.05997	0.03436	-0.11034	-0.05436	0.14692
0.09763	-0.05765	-0.01844	-0.04033	0.10318	-0.10504	0.06935	-0.13886	-0.03774	0.15548
0.13060	-0.01504	0.01720	-0.00795	0.07171	-0.11520	0.06801	-0.13878	-0.05661	0.08077
0.16980	0.01161	0.02876	0.03894	0.02729	-0.10533	0.00688	-0.11636	-0.07000	0.06944
0.14875	0.05640	0.01377	0.07752	-0.01376	-0.08851	-0.01630	-0.02632	-0.06169	0.09837
0.14220	0.05965	0.03454	0.04767	-0.03867	-0.09548	-0.04348	-0.02924	0.01656	0.06503
0.09532	0.06332	0.02222	0.03873	-0.04165	-0.07756	-0.00274	0.01668	0.02212	0.02997
0.07034	0.04892	0.01301	0.03648	-0.00951	-0.02080	-0.02424	-0.00526	0.05537	0.00202
0.07551	0.05506	0.03979	0.04316	-0.04084	0.02151	-0.02555	0.01999	0.07665	0.01552
0.09736	0.06978	0.03935	0.03462	-0.06004	0.06292	-0.08500	-0.03688	0.08875	0.00722
0.10863	0.08189	0.06507	0.07469	-0.06656	0.06292	-0.07352	-0.01057	0.07748	-0.01015
0.10106	0.08123	0.05449	0.07736	-0.04892	0.10642	-0.00587	0.04680	0.07918	0.00873
0.05957	0.05774	0.01795	0.02896	-0.03011	0.06025	0.02194	0.06576	0.05341	0.00546
0.02741	0.01250	0.00500	0.07176	-0.02286	0.02603	0.03036	0.03165	-0.02326	0.01971
-0.00341	-0.03828	-0.05288	0.05211	-0.00265	0.02052	0.00711	0.06858	-0.10485	-0.00928
-0.03587	-0.07757	-0.07695	0.05815	0.01550	0.02936	0.03385	0.05177	-0.07633	-0.01550
-0.04495	-0.06603	-0.04863	0.04420	0.03069	0.06145	0.06429	-0.00750	-0.04485	-0.03215
-0.09049	-0.07368	-0.06369	0.06174	0.03204	0.02548	0.03661	-0.00175	0.00047	-0.15806
-0.08301	-0.04907	-0.05933	0.07893	0.03448	-0.01214	0.05033	-0.01416	-0.00070	-0.21790
-0.07638	-0.05314	-0.05424	0.06402	0.00924	-0.01971	0.05578	0.02764	-0.02089	-0.23445

TABLE 3 - LISTING OF THE FIRST 20 EIGENFUNCTIONS (continued)

EIGENFUNCTIONS 1 - 10, POINTS 51 - 100 ; THE V COMPONENT

EIGENFUNCTION

1	2	3	4	5	6	7	8	9	10
-0.07608	-0.09949	0.01143	-0.04806	0.07408	0.09537	0.03633	-0.08310	-0.08512	-0.03010
-0.07004	-0.10300	0.01505	-0.04789	0.08545	0.10088	0.03138	-0.06731	-0.07121	-0.01960
-0.06655	-0.10857	0.02303	-0.02438	0.08692	0.06914	0.05441	-0.08045	-0.07597	-0.03118
-0.06880	-0.11121	0.01634	-0.01500	0.08428	0.06098	0.05933	-0.09214	-0.07871	-0.03996
-0.07641	-0.11062	0.01856	-0.01633	0.07520	0.05405	0.05592	-0.09427	-0.06701	-0.05194
-0.07682	-0.10859	0.02065	-0.02025	0.06798	0.07786	0.04830	-0.11796	-0.06664	-0.05631
-0.07795	-0.10934	0.01203	-0.01492	0.07480	0.08080	0.03958	-0.12597	-0.04867	-0.03387
-0.07716	-0.10691	0.01070	-0.01120	0.05668	0.08584	0.02893	-0.09492	-0.05020	-0.04709
-0.07765	-0.10757	0.00913	0.00023	0.04493	0.08869	0.04096	-0.07853	-0.03351	-0.04157
-0.08298	-0.10564	0.00325	-0.01953	0.05085	0.07084	0.01389	-0.10210	-0.04235	-0.03442
-0.08425	-0.10554	0.00308	-0.02990	0.04939	0.08708	0.00690	-0.09406	-0.06432	-0.02599
-0.08345	-0.10796	-0.00216	-0.02784	0.03585	0.07332	-0.00367	-0.10047	-0.08084	-0.02637
-0.08550	-0.10946	0.00686	-0.01874	0.02710	0.08247	-0.00552	-0.10223	-0.07750	-0.02221
-0.08579	-0.11007	0.00405	-0.01544	0.02909	0.08375	-0.02953	-0.09850	-0.07845	0.00520
-0.08673	-0.11034	-0.00239	-0.02428	0.03986	0.10822	-0.02545	-0.05576	-0.08011	0.01504
-0.08571	-0.11008	0.00013	-0.03564	0.04328	0.10933	-0.02603	-0.04640	-0.10906	0.02331
-0.08485	-0.11837	-0.00088	-0.04288	0.03207	0.08307	-0.02714	-0.04345	-0.12389	0.04189
-0.08940	-0.11477	-0.00303	-0.05216	0.03030	0.07268	-0.05329	-0.06697	-0.12292	0.06604
-0.09235	-0.11652	-0.00256	-0.05067	0.00784	0.08121	-0.04815	-0.04319	-0.10829	0.05742
-0.08804	-0.11904	0.01367	-0.04745	0.00266	0.07923	-0.03812	-0.05175	-0.09016	0.08977
-0.08938	-0.12079	0.01648	-0.04167	-0.00248	0.07653	-0.02952	-0.03939	-0.06727	0.10382
-0.09111	-0.12858	0.01513	-0.01969	-0.02460	0.06653	-0.02578	-0.00529	-0.03242	0.09199
-0.08351	-0.12629	0.00720	-0.01335	-0.01254	0.03379	-0.03870	0.03123	-0.00922	0.09121
-0.08137	-0.12155	0.00848	-0.01850	-0.02608	0.00856	-0.04879	0.06195	-0.00363	0.07682
-0.08795	-0.12949	0.01765	-0.01548	-0.05473	-0.03800	-0.02293	0.08345	0.01606	0.07566
-0.08657	-0.12819	-0.01019	-0.01407	-0.08232	-0.03499	0.00461	0.09586	0.03369	0.06826
-0.08534	-0.11727	-0.01260	-0.01577	-0.04513	-0.03387	0.00523	0.06766	-0.01061	0.04006
-0.08384	-0.11470	0.00359	-0.01735	-0.05715	-0.01573	-0.01878	0.06919	-0.01382	0.03782
-0.07834	-0.11919	0.00064	-0.00070	-0.06458	-0.03037	-0.02086	0.06908	0.00347	0.03729
-0.07788	-0.12765	-0.00005	0.01170	-0.04244	-0.04850	-0.02317	0.04850	0.02323	0.02160
-0.07638	-0.12276	0.00139	0.02177	-0.03590	-0.06398	-0.03100	0.03560	0.04521	-0.01563
-0.08098	-0.11837	-0.00139	0.03336	-0.03173	-0.07835	-0.03050	0.02270	0.07204	-0.00845
-0.08001	-0.11720	-0.00187	0.02368	-0.00806	-0.08195	-0.01188	0.02576	0.10139	-0.01027
-0.07265	-0.11829	0.00897	0.01701	-0.00410	-0.08011	-0.04027	0.03429	0.14344	-0.02347
-0.07269	-0.11136	-0.00115	0.01335	0.01248	-0.09176	-0.03820	0.05412	0.13304	-0.02496
-0.07089	-0.11348	-0.00292	0.01564	0.01077	-0.10606	-0.05156	0.05074	0.13812	-0.01434
-0.07207	-0.11604	-0.00656	0.01989	0.01153	-0.09475	-0.04884	0.07472	0.12276	-0.01142
-0.07166	-0.12392	-0.00835	0.01598	0.01367	-0.06786	-0.05189	0.09184	0.09102	-0.06114
-0.07301	-0.12412	-0.00248	0.00857	0.02457	-0.06931	-0.01236	0.10649	0.10293	-0.06703
-0.07354	-0.11470	0.00687	0.00806	0.02366	-0.08551	-0.00506	0.10177	0.11557	-0.06501
-0.06314	-0.10596	0.02623	0.00026	0.01113	-0.04904	0.04181	0.11006	0.07919	-0.05739
-0.07210	-0.10553	0.02955	-0.00337	-0.01222	-0.04798	0.05229	0.12020	0.07513	-0.07473
-0.07878	-0.10069	0.02362	-0.00328	-0.02487	-0.04701	0.06427	0.10036	0.09149	-0.07256
-0.07930	-0.10506	0.02620	0.00620	-0.02501	-0.07140	0.05738	0.08451	0.09268	-0.07081
-0.07610	-0.10945	0.02785	0.02072	-0.00838	-0.07088	0.07583	0.07386	0.09197	-0.04858
-0.08155	-0.11651	0.02600	0.02052	-0.00498	-0.08988	0.07529	0.06117	0.08183	-0.02275
-0.07485	-0.11848	0.01690	0.00604	-0.01747	-0.08721	0.08160	0.06837	0.07664	-0.02968
-0.07340	-0.12313	0.01874	0.01322	-0.02307	-0.07675	0.08265	0.05817	0.06345	0.00963
-0.07689	-0.12856	0.02366	0.00754	-0.01447	-0.06889	0.08956	0.06113	0.02729	0.00840
-0.07313	-0.12680	0.03202	0.01455	-0.01277	-0.05483	0.07677	0.05149	0.04233	0.01602

TABLE 3 - LISTING OF THE FIRST 20 EIGENFUNCTIONS (continued)

EIGENFUNCTIONS 11 - 20, POINTS 51 - 100 : THE V COMPONENT

EIGENFUNCTION									
11	12	13	14	15	16	17	18	19	20
0.05688	-0.03221	-0.02521	-0.13979	0.04338	0.02371	-0.03005	0.00472	0.04154	0.01141
0.06320	-0.00738	-0.00567	-0.14288	0.01617	0.06357	-0.02942	0.02092	0.01358	-0.04162
0.06152	-0.03905	0.02219	-0.13783	0.01515	0.08155	0.02421	0.09733	0.02345	-0.03354
0.06971	0.00172	0.01144	-0.13824	0.00622	0.07683	0.03872	0.09458	-0.01912	-0.00746
0.05061	0.00593	0.02020	-0.11874	0.02933	0.06801	0.02446	0.09594	-0.03452	-0.05353
0.02484	-0.01005	0.00421	-0.14603	0.00290	0.04231	-0.04136	0.07557	-0.03602	-0.05983
0.02664	-0.02759	0.00093	-0.10400	-0.03389	0.02707	-0.04200	0.05622	0.00041	-0.03722
0.02494	-0.05509	0.00283	-0.07151	-0.05447	0.02513	-0.01748	0.01847	-0.01940	-0.00382
0.02307	-0.06746	0.03434	-0.05409	0.00085	0.00809	0.00843	0.03727	0.01396	0.03761
0.01233	-0.09240	0.03857	-0.05253	0.01107	-0.00447	-0.04376	0.04586	0.02862	0.01339
-0.00062	-0.08848	0.03400	-0.01779	0.03291	-0.01391	-0.02906	-0.01011	0.03750	0.02224
0.00742	-0.05497	0.03472	-0.01126	-0.00556	-0.05653	-0.02642	-0.04293	0.00559	0.01611
0.03813	-0.02845	0.01679	0.01721	-0.03466	-0.08904	-0.01520	-0.03304	0.01011	0.00913
0.04297	-0.01415	0.02313	0.03619	-0.03461	-0.08016	0.00141	-0.03179	0.00603	0.03891
0.02492	0.00531	0.05008	0.05542	0.02223	-0.05483	0.02456	-0.03136	-0.00895	0.04002
0.01223	0.01285	0.01867	0.08276	0.02502	-0.08287	0.04990	-0.05767	-0.01083	0.02385
0.02578	0.02994	0.07382	0.07250	-0.03389	-0.13487	0.00869	-0.04250	-0.04375	0.02719
0.00131	0.06487	0.06515	0.09419	-0.06405	-0.15082	-0.02412	-0.06223	-0.03486	0.00529
-0.02767	0.07947	0.01470	0.09660	-0.05841	-0.13311	-0.02742	-0.05348	-0.01326	0.00046
-0.03654	0.07203	0.00455	0.10054	-0.06107	-0.15579	-0.01386	-0.04761	-0.02691	-0.04227
-0.01423	0.06461	-0.03287	0.11874	-0.04952	-0.13729	0.01248	-0.01705	0.00263	-0.05782
0.00819	0.08047	-0.06907	0.08726	-0.01762	-0.06570	-0.00829	0.00856	-0.02451	0.00009
0.03514	0.03821	-0.06153	0.09052	0.07749	-0.03601	-0.01458	0.02158	-0.07442	0.03151
-0.00557	0.00948	-0.06731	0.11590	0.12059	0.02018	-0.01465	0.08216	-0.07348	0.07647
-0.01126	0.03352	-0.08087	0.14759	0.13856	0.06844	0.04730	0.12635	-0.09522	0.09524
0.03626	0.04596	-0.05248	0.12490	0.16224	0.11036	0.00689	0.13853	-0.05606	0.04841
0.02295	0.06941	-0.03801	0.09585	0.12634	0.10917	-0.03659	0.15398	0.00616	-0.07603
0.02250	0.06393	-0.03341	0.06535	0.20796	0.11941	-0.03310	0.08314	0.05253	-0.08249
0.03368	0.10115	-0.01362	0.04915	0.20636	0.11039	-0.00470	0.06067	0.01199	-0.04502
0.01827	0.08332	0.00864	0.05700	0.17941	0.05303	0.04247	0.02191	-0.04229	-0.04861
0.01151	0.05982	0.03047	0.04620	0.15614	0.07655	-0.00597	0.02900	-0.07679	-0.06550
0.00208	0.03039	0.04355	0.08993	0.09279	0.11746	0.01908	-0.01867	-0.06888	-0.04058
-0.00676	0.00212	0.01003	0.06441	0.02961	0.12764	0.05297	-0.05556	-0.12476	-0.03539
-0.04351	0.01885	0.00444	0.01854	-0.02331	0.11815	0.05881	-0.09414	-0.09070	-0.04572
-0.05922	0.03724	0.02829	-0.00562	-0.03874	0.07379	0.06945	-0.09609	-0.06560	-0.03121
-0.03563	0.01906	0.00221	0.00340	-0.04412	0.00393	0.06567	-0.06779	-0.07556	-0.01722
-0.04570	-0.01747	-0.00501	0.00345	-0.03601	-0.05847	0.07190	-0.07033	-0.04132	0.01649
-0.02603	-0.04824	-0.03122	-0.04710	-0.07342	-0.07869	0.00072	-0.04678	-0.04050	0.08741
-0.02404	-0.06813	-0.01836	-0.01530	-0.10108	-0.01999	0.01623	-0.03461	0.00138	0.09193
-0.05756	-0.08897	-0.00717	-0.02754	-0.12764	-0.05176	-0.00355	-0.06598	0.04759	0.06622
-0.06259	-0.08693	0.01689	-0.03260	-0.11100	-0.05443	-0.00139	-0.06284	0.08744	0.02757
-0.02755	-0.08202	0.03972	-0.02837	-0.08640	-0.02204	0.03483	-0.01107	0.08075	0.06258
-0.01428	-0.09811	0.06217	0.00263	-0.05643	0.01263	0.01147	-0.00101	0.08463	0.06158
0.01043	-0.07735	0.04140	-0.00866	-0.06825	-0.02326	-0.03579	-0.01382	0.06599	0.03471
-0.01809	-0.03219	0.01681	-0.05234	-0.07384	-0.01734	-0.07132	-0.04797	0.08792	-0.00387
-0.01641	-0.02240	0.01690	-0.08993	-0.08051	0.00853	-0.05015	-0.06537	0.09109	-0.02385
-0.00931	-0.00046	0.00946	-0.12622	-0.10361	-0.00596	0.00091	-0.05120	0.10069	-0.02461
-0.02175	0.02653	0.00329	-0.13094	-0.06941	-0.00143	-0.01920	-0.04695	0.10969	-0.03524
-0.02385	0.00497	0.00936	-0.11317	-0.07227	-0.01829	-0.05571	-0.05407	0.06703	-0.04011
-0.02248	0.03229	0.00198	-0.08873	-0.06243	-0.02042	-0.05487	-0.02816	0.06852	-0.06932

TABLE 3 - LISTING OF THE FIRST 20 EIGENFUNCTIONS (continued)

EIGENFUNCTIONS 1 - 10, POINTS 1 - 50 : THE U COMPONENT

EIGENFUNCTION

1	2	3	4	5	6	7	8	9	10
0.08600	-0.07741	0.07562	0.08443	-0.05637	-0.09798	-0.05196	-0.10021	-0.08565	-0.08500
0.08946	-0.07105	0.08128	0.07696	-0.05877	-0.09849	-0.08333	-0.09487	-0.08679	-0.07833
0.08826	-0.07269	0.08379	0.06700	-0.07093	-0.09637	-0.08531	-0.04756	-0.11991	-0.06447
0.08902	-0.08000	0.08512	0.07255	-0.06657	-0.09813	-0.07565	-0.03345	-0.11229	-0.06650
0.09047	-0.08799	0.07999	0.07736	-0.07871	-0.10165	-0.07576	-0.03736	-0.10356	-0.08198
0.09276	-0.08312	0.07994	0.08178	-0.07279	-0.09125	-0.06434	-0.06110	-0.08850	-0.07537
0.09660	-0.08054	0.08384	0.08721	-0.06469	-0.07929	-0.05539	-0.08143	-0.08668	-0.04603
0.10089	-0.08408	0.08001	0.08088	-0.07941	-0.06886	-0.05295	-0.10841	-0.04376	-0.05933
0.10308	-0.08465	0.07719	0.07065	-0.09543	-0.04663	-0.07084	-0.09563	0.00252	-0.08265
0.10679	-0.08812	0.06979	0.07173	-0.09797	-0.02975	-0.05719	-0.11337	0.02540	-0.06612
0.10651	-0.09369	0.07081	0.07404	-0.09570	-0.04779	-0.06157	-0.11630	0.03681	-0.06224
0.10934	-0.09459	0.06154	0.07977	-0.07743	-0.05249	-0.06316	-0.09220	0.02424	-0.07262
0.11324	-0.08652	0.07078	0.06421	-0.07402	-0.04565	-0.06416	-0.10036	0.02484	-0.05458
0.10907	-0.08964	0.07060	0.06163	-0.08554	-0.02565	-0.04665	-0.10742	0.02933	-0.03600
0.10764	-0.08918	0.06693	0.04358	-0.07158	-0.00854	-0.01785	-0.11010	0.02685	0.00167
0.10999	-0.09124	0.06020	0.02572	-0.07183	0.01697	-0.01553	-0.08331	0.03912	0.03343
0.10875	-0.08731	0.05683	0.03574	-0.09661	0.02472	-0.00702	-0.05105	0.03856	0.05160
0.11215	-0.08868	0.06516	0.03873	-0.08496	0.03394	0.01819	-0.06197	0.02636	0.10008
0.10855	-0.08656	0.06043	0.04758	-0.07370	0.04299	0.04519	-0.02786	0.02300	0.12699
0.11732	-0.08745	0.05127	0.03416	-0.07072	0.02443	0.04313	0.00529	0.01686	0.13764
0.11330	-0.07701	0.04539	0.02757	-0.08185	0.00410	0.04667	0.03075	0.01889	0.15187
0.10745	-0.07519	0.03119	0.02256	-0.08776	0.02672	0.06727	0.01022	0.03455	0.19174
0.10546	-0.07225	0.03647	0.02665	-0.08153	0.03543	0.06796	0.01576	0.03416	0.16943
0.09849	-0.06316	0.02665	0.01585	-0.04939	0.07511	0.05051	0.01519	0.06945	0.15511
0.08851	-0.05040	0.01134	0.00862	-0.05730	0.08921	0.06897	0.02853	0.05313	0.12156
0.09134	-0.04964	0.02568	-0.03228	-0.06250	0.09066	0.05052	0.02550	0.01480	0.09192
0.10443	-0.05464	0.01553	-0.04167	-0.02866	0.10413	0.01914	0.01427	-0.01807	0.08504
0.10760	-0.05985	0.03069	-0.04648	-0.00043	0.09601	0.02718	0.01798	0.02455	0.13879
0.11196	-0.06945	0.02059	-0.06003	0.01568	0.10173	0.04007	0.02505	0.03977	0.16896
0.11382	-0.06366	0.01787	-0.06072	-0.00836	0.07841	0.03108	0.03368	0.06086	0.12386
0.11688	-0.06333	0.00234	-0.07567	-0.00878	0.04588	0.03471	0.05550	0.03848	0.10503
0.10934	-0.06217	0.00283	-0.06241	-0.01611	0.05179	0.04522	0.09601	0.05634	0.10989
0.10858	-0.06273	0.01188	-0.07934	-0.01815	0.01251	0.03692	0.09472	0.04859	0.08735
0.10710	-0.06323	0.02403	-0.09309	-0.02229	-0.00043	0.04322	0.09733	0.03296	0.06369
0.11014	-0.06106	0.03699	-0.08913	0.00832	0.00775	0.03985	0.10242	0.03948	0.01201
0.11510	-0.05830	0.04363	-0.10843	0.02739	0.01933	0.06785	0.11506	-0.00341	0.00042
0.12037	-0.05531	0.05674	-0.10481	0.03664	0.02868	0.04759	0.11417	-0.01051	0.00596
0.11868	-0.04659	0.05354	-0.10408	0.03295	0.03704	0.04548	0.09121	-0.02262	0.00044
0.11854	-0.04407	0.05399	-0.11105	0.02865	0.00235	0.04747	0.07894	-0.04862	-0.04187
0.12790	-0.03840	0.05439	-0.12490	0.03538	-0.01061	0.05389	0.05477	-0.08418	-0.06058
0.12178	-0.04116	0.04969	-0.13649	0.06071	-0.01653	0.04122	0.05691	-0.06874	-0.10723
0.11682	-0.04272	0.05244	-0.14385	0.06101	-0.02349	0.02634	0.06036	-0.01418	-0.08814
0.10921	-0.04435	0.05976	-0.16532	0.06047	-0.01990	0.02594	0.05867	-0.01742	-0.11622
0.10826	-0.05186	0.06349	-0.15429	0.08420	-0.01829	0.02744	0.05787	-0.02812	-0.13093
0.09999	-0.05373	0.06415	-0.14023	0.09616	-0.01250	0.01218	0.02777	-0.01988	-0.12888
0.09878	-0.06171	0.05467	-0.14844	0.11655	0.01812	0.00051	0.02991	-0.00796	-0.14333
0.10490	-0.05489	0.03309	-0.13795	0.12401	0.01224	-0.01774	0.05802	0.00073	-0.15082
0.10188	-0.05766	0.03882	-0.15488	0.11683	0.00752	-0.02258	-0.00517	-0.00251	-0.12184
0.10263	-0.05826	0.03828	-0.14094	0.09593	0.01183	-0.02699	0.00433	0.00676	-0.12253
0.09859	-0.05745	0.04362	-0.13367	0.07950	0.01327	-0.01306	0.01193	0.01513	-0.14284

TABLE 3 - LISTING OF THE FIRST 20 EIGENFUNCTIONS (concluded)

EIGENFUNCTIONS 11 - 20, POINTS 101 - 150 : THE w COMPONENT

EIGENFUNCTION									
11	12	13	14	15	16	17	18	19	20
0.10667	-0.19881	0.14119	0.18613	-0.08963	-0.09413	0.01297	0.02248	-0.10424	-0.07118
-0.04926	-0.16964	0.14633	0.12483	0.08197	-0.07028	0.16882	0.11868	-0.18638	0.01249
-0.04917	-0.05849	0.12257	0.03769	0.06482	0.01106	0.11969	0.06269	-0.12641	0.09687
-0.02942	-0.03542	0.01446	-0.03029	0.03893	-0.06073	0.00575	0.00725	-0.11335	0.18617
-0.02980	0.03074	-0.06140	-0.04942	0.08115	-0.06235	-0.03922	-0.14716	0.02531	-0.00123
-0.02379	0.12501	-0.08023	-0.07718	0.06085	0.03133	-0.08046	-0.04837	0.09259	0.00997
-0.03133	0.17024	-0.05585	-0.05120	0.03160	0.07408	-0.13642	0.03901	0.07830	0.11485
-0.01752	0.18222	-0.08415	-0.04322	-0.03559	0.12860	-0.15715	-0.06188	0.01581	0.16564
-0.08537	0.08066	-0.13553	0.00130	-0.10752	0.08541	-0.05750	-0.07720	-0.00260	-0.01270
-0.04823	0.09770	-0.21427	0.02445	-0.19086	0.02794	0.06086	-0.03515	-0.12467	-0.15774
-0.02950	-0.02743	-0.19884	-0.01677	-0.10962	-0.01456	0.11363	0.00432	-0.08807	-0.12646
-0.01618	-0.16612	-0.04862	-0.07068	-0.02464	0.03496	0.22602	-0.04655	0.01090	-0.12945
-0.03529	-0.14378	-0.05334	-0.04039	-0.04180	-0.04526	0.26636	0.01912	0.08620	-0.07486
-0.02803	-0.19572	-0.05580	-0.04024	0.02386	-0.01190	0.14719	0.19345	0.13511	0.08201
0.01049	-0.17580	-0.05387	-0.07295	0.07985	-0.03065	-0.03388	0.10232	0.14555	0.18128
0.08268	-0.11797	-0.02150	-0.01271	0.16152	-0.02554	-0.11088	-0.01720	0.25246	0.12797
0.03163	-0.14798	0.03028	-0.00727	0.08499	0.01721	-0.21758	-0.02976	0.23240	-0.05584
0.08644	-0.07232	0.01766	-0.01842	-0.02401	-0.02383	-0.27231	0.06290	0.06287	-0.11522
-0.00171	0.06301	0.03378	-0.08789	-0.10070	-0.04168	-0.22832	0.14493	-0.27349	-0.10915
-0.01381	0.13070	0.14226	-0.12695	-0.08356	-0.02672	-0.10762	0.16261	-0.17154	0.08709
0.07304	0.08889	0.14571	-0.01968	0.00675	-0.12117	-0.06906	0.10525	-0.11578	0.11476
0.07570	0.12262	0.09999	0.03873	-0.02516	-0.07551	0.13063	-0.11046	0.04790	-0.02055
0.13536	0.15553	0.04180	-0.12669	-0.03958	0.18346	0.27644	-0.14985	0.06026	-0.01013
0.11576	0.15821	0.00046	-0.14055	-0.00271	0.10364	0.19544	-0.15590	0.04249	-0.15444
-0.00598	-0.08171	-0.07982	0.06572	-0.00695	-0.01889	-0.01852	-0.04789	0.08797	-0.04621
-0.01026	-0.08393	-0.11978	0.20267	-0.03400	0.03023	-0.00099	0.05151	0.06137	0.09699
0.01222	-0.10130	-0.00064	0.06218	0.06845	0.07381	-0.11014	0.01952	-0.19862	0.10997
0.01869	-0.08366	0.10484	-0.14038	0.15882	-0.16934	-0.21684	-0.07846	-0.21904	-0.07494
0.03224	0.09013	0.16631	-0.20828	0.23190	-0.18464	-0.05281	-0.01514	-0.12775	-0.19740
-0.02359	0.15600	0.14896	-0.20443	0.12139	-0.05782	0.16874	-0.03652	-0.05243	-0.01226
-0.16921	0.23103	0.10503	-0.04664	0.12175	-0.00107	0.19001	0.11122	0.12898	0.18935
-0.28446	0.13273	0.17800	-0.06099	0.06307	-0.05709	0.09103	0.08584	0.13503	0.08918
-0.28119	0.02249	0.16905	0.04728	-0.09589	0.00838	-0.04164	0.02130	0.05325	0.06587
-0.23209	-0.14945	0.13909	0.10222	0.05469	0.07905	-0.17952	-0.13968	0.10796	0.08088
-0.19207	-0.16660	0.10041	0.17593	0.07153	0.11445	-0.12198	-0.14807	-0.05114	-0.09252
-0.19272	-0.04224	0.04859	0.11923	-0.02541	0.06301	-0.00395	-0.22937	-0.04219	-0.06196
-0.04584	0.03539	-0.12566	0.10559	-0.07590	0.13538	-0.01949	-0.12290	-0.15681	0.14224
0.05734	0.02209	-0.15821	0.03299	-0.10953	0.18551	-0.07916	0.03511	0.00278	0.13388
0.02390	-0.08731	-0.19068	-0.07414	-0.10344	0.05543	0.00678	0.18611	-0.05560	0.00677
0.01105	-0.05687	-0.19780	-0.11700	-0.10231	-0.14165	-0.02905	0.29623	-0.12250	0.03751
0.03695	-0.05063	-0.27091	-0.05206	0.02192	-0.20601	0.08363	0.06454	0.05082	-0.03863
-0.01756	-0.03135	-0.21497	-0.04779	0.07466	-0.30438	0.06994	-0.01712	0.03726	-0.02406
0.02313	0.01880	-0.08095	-0.00028	0.11840	-0.19666	-0.06356	-0.11390	0.05212	-0.12499
0.11653	-0.02387	-0.01951	0.02666	0.09252	-0.03567	-0.13468	-0.08756	0.06021	-0.26212
0.20281	-0.05299	0.02618	0.06666	0.05107	0.12888	-0.05872	0.00407	0.11633	-0.17709
0.22151	-0.06731	0.09186	0.06734	0.00890	0.02738	0.00664	0.15550	0.12561	-0.13030
0.22464	-0.03583	0.12392	0.05893	-0.09449	0.00082	0.11362	0.14139	0.08255	0.01947
0.18157	-0.07757	0.14140	0.00105	-0.19731	0.01480	0.10296	0.00281	-0.09223	0.10125
0.19336	-0.10422	0.17120	0.08997	-0.17411	0.10315	0.04366	-0.00560	-0.02390	0.02443
0.17056	-0.10204	0.18126	0.03662	-0.05179	0.10977	0.01454	-0.09821	-0.06997	-0.04999
0.01031	-0.05298	-0.06590	-0.04472	0.05955	-0.10501	-0.03323	-0.14053	0.02210	0.00000

5.2 The Sampling Properties of the Expansion Coefficients

Forming a 100 × 150 matrix F of the 100 ensemble functions and a 150 × 20 matrix E of the 20 first eigenfunctions and performing the matrix multiplication

$$F \times E = B$$

gives us the 100 × 20 matrix, B, consisting of the expansion coefficients, α_n. A histogram is then calculated for each of the 20 columns and the corresponding probability density function estimated. The goodness of the fit can be tested by various tests.

In this analysis, a subjective study of the histograms revealed Gaussian probability density functions for the expansion coefficients, so that the only statistics necessary are the means and the variance of the 20 columns. If we had prepared the ensemble in such a way that $E\{f_n\} = 0$, we would have had

$$E\{\alpha_n\} = 0$$

(5.2)

$$E\{\alpha_n \alpha_k\} = \lambda_n \delta_{nk}$$

and due to the Gaussian assumption all the probability density functions would be known, in a statistical sense, because λ_n, which equals the variance of the n^{th} expansion coefficients, is known. In this analysis, the relation (5.2) provides an internal check on the calculations because for one expansion coefficient, the variance plus the squared mean must

equal the corresponding eigenvalue. Table 2 gives the mean and the variance for the 20 expansion coefficients. As would be expected, only the few first have a mean significantly different from zero.

The mean and the variance for a particular expansion coefficient are only estimates of the true values, and by standard statistical methods we can obtain 95% confidence limits for both quantities; in the application of the model we can investigate the effects of choosing values inside as well as outside these limits.

The apparent Gaussian distribution of the expansion coefficients needs further discussion, especially since Smith (1971) reports he found them to be uniformly distributed.

When the domain of definition is extended to $(-\infty,\infty)$ and $R(s,t) = R(s-t)$, then (4.3) becomes

$$\int_{-\infty}^{\infty} R(s-t)\ \phi_n(s)\ ds = \lambda_n \phi_n(t)$$

but in this limit the eigenvalue spectrum becomes continuous, and we can write

$$\int_{-\infty}^{\infty} R(s-t)\ \phi(\omega,t)\ dt = \lambda(\omega)\ \phi(\omega,\ s)$$

with the solution $\phi(\omega,\ t) = e^{-i\omega t}$. Hence, $\lambda(\omega)$ is the Fourier transform of the correlation function, the usual power spectrum. And so the expansion coefficients become in the limit equal to the usual Fourier coefficients, which for all practical purposes can be assumed to have a Gaussian distribution.

5.3 The Probability of Occurrence

A direct assessment of the probability of occurence of generated time sequences which are critical to the system being studied is not a straightforward procedure with the model developed here.

However, in order to analyze the problems let us consider the theoretically simpler model in which an ensemble of k records each of N points, $k \geq N$, with the correlation function R(s,t) has led to N eigenfunctions each specified at N points and to N probability density functions, one for each of the N expansion coefficients $\alpha_1, \alpha_2, \ldots, \alpha_N$. Artificial time histories are generated using the eigenfunctions and by sampling in the probability density functions. The generated series will also have the correlation function R(s,t), and the first probability to be determined is the probability that the systems we are concerned with will encounter turbulence with the given R(s,t). This probability can presumably be estimated by considering the measured ensemble in relation to the total collection of empirical data about turbulence.

The next probability we must determine is the probability of obtaining a critical time sequence by sampling in an ensemble of functions with the correlation function R(s,t).

Let us assume that all the critical functions with this correlation function are in the subspace Ω_A of the total phase space Ω, where

$$\Omega_A: \quad (a_1 \leq \alpha_1 \leq a_1 + \Delta a_1, \ \ldots, \ a_N \leq \alpha_N \leq a_N + \Delta a_N)$$

$$\Omega: \quad (-\infty < \alpha_1 < \infty, \ \ldots, \ -\infty < \alpha_N < \infty)$$

Here Prob$(\alpha_1,\alpha_2, \ \ldots \ \alpha_N \in \Omega) = 1$, and the probability we want to determine is Prob $(\alpha_1, \alpha_2, \ldots \alpha_N \in \Omega_A)$. In order to limit the search for Ω_A, we realize that we are only interested in probabilities that exceed a certain limit, P_E say. The part of Ω in which the higher order expansion coefficients differ significantly from zero is very likely to be associated with very small probabilities (see Table 2), hence it is justifiable to search for Ω_A only in the space

$$\Omega_B \sim (\alpha_1, \alpha_2, \ldots \alpha_m, \alpha_{m+1} = 0, \ldots, \alpha_N = 0)$$

where the limits for $\alpha_1, \ldots, \alpha_m$ are connected with P_E.

Suppose that in addition to the lack of correlation expressed by (5.2), the coefficients are also Gaussian distributed, an assumption justified in Section 5.2. Then the coefficients are independent and after having established by trial and error the boundaries of Ω_A the probability we are searching can then be estimated from the Gaussian probability density functions $p_1, p_2, \ldots p_m$,

$$\text{Prob}(\alpha_1, \alpha_2, \ldots, \alpha_m \in \Omega_A) = \int_{a_1}^{a_1+\Delta a_1} p_1 \, d\alpha_1 \int_{a_2}^{a_2+\Delta a_2} p_2 \, d\alpha_2 \ldots \int_{a_m}^{a_m+\Delta a_m} p_m \, d\alpha_m$$

Mainly because of computer limitations, we are forced to generate the time-sequences in small pieces which are patched together and then to perform transformations in Fourier space in order to move energy to low frequencies. Hence it is obvious that the above described procedure for obtaining the probability of occurence of critical time sequences cannot

be applied to the model formed in the preceding sections. We will have to rely on physical arguments, not as much to calculate probabilities, but merely to establish whether the generated critical time series appears to be physically realizable.

6.0 DESCRIPTION OF THE TURBULENCE RECORD

The turbulence record was obtained by analog instrumentation during the 1969 Kansas Experiment by N. E. Busch and S. E. Larsen (Larsen (1971), Busch and Larsen (1972)). It was measured at 5.66 meters height (between 15:31 - 16:31 on 30 July, 1968). The stratification was slightly unstable, the Richardson number being -0.101. The mean wind speed was 6.56 m/sec and the variances for the fluctuations u, v, w, and T (temperature) were 2.414 $m^2 sec^{-2}$; 1.904 $m^2\ sec^{-2}$; 0.359 $m^2\ sec^{-2}$; 0.761° C^2.

The analogue signal was later digitized at 1000 Hz and transferred to digital tape. For the purpose of this analysis, the signal was further block averaged over 100 points to give a 10 Hz signal. A sequence of 50 minutes was selected giving 30,000 data points for each of the components u, v, and w (the temperature data was not used in this study). Figure 6.7 shows the whole record with 1 second block averaged values, and Figure 6.8 shows 100 seconds of the record with 10 Hz values. In the last figure, all the data has been normalized to mean zero and variance 1. The analogue signal was reversed in time during the handling and so we will expect our model to generate time reversed turbulence. A simulated record should then be time reversed before applied in practice.

In order to assess whether the generated turbulence behaves like real turbulence or not, a set of criteria were proposed in section 1. One of the criteria requires the model to produce signals that possess the notable observed statistical characteristics of observed turbulence.

In the rest of this section some of these characteristics will be estimated from the turbulence record and the results will be compared with those obtained from a similar analysis by Dutton and Deaven (1971) (hereafter referred to as DD).

6.1 Probability Densities and Distributions

The use of the probability functions is extended to powers of the velocity variables, here to the fourth order. Figures 6.1 and 6.2 show the probability density and distribution functions for the standardized velocity components. In each graph, the solid line illustrates the Gaussian behavior with the curves for higher orders derived from the transformation

$$p_y(y) \left|\frac{dy}{dx}\right| = p_x(x)$$

DD reached the conclusion that the frequency functions departed from those of a Gaussian process from a set of figures which showed a behavior quite similar to Figures 6.1 and 6.2.

6.2 Increments

Using one of the component series, for example u, we can construct a new series

$$u(x,L) = u(x) - u(x + L) \tag{6.1}$$

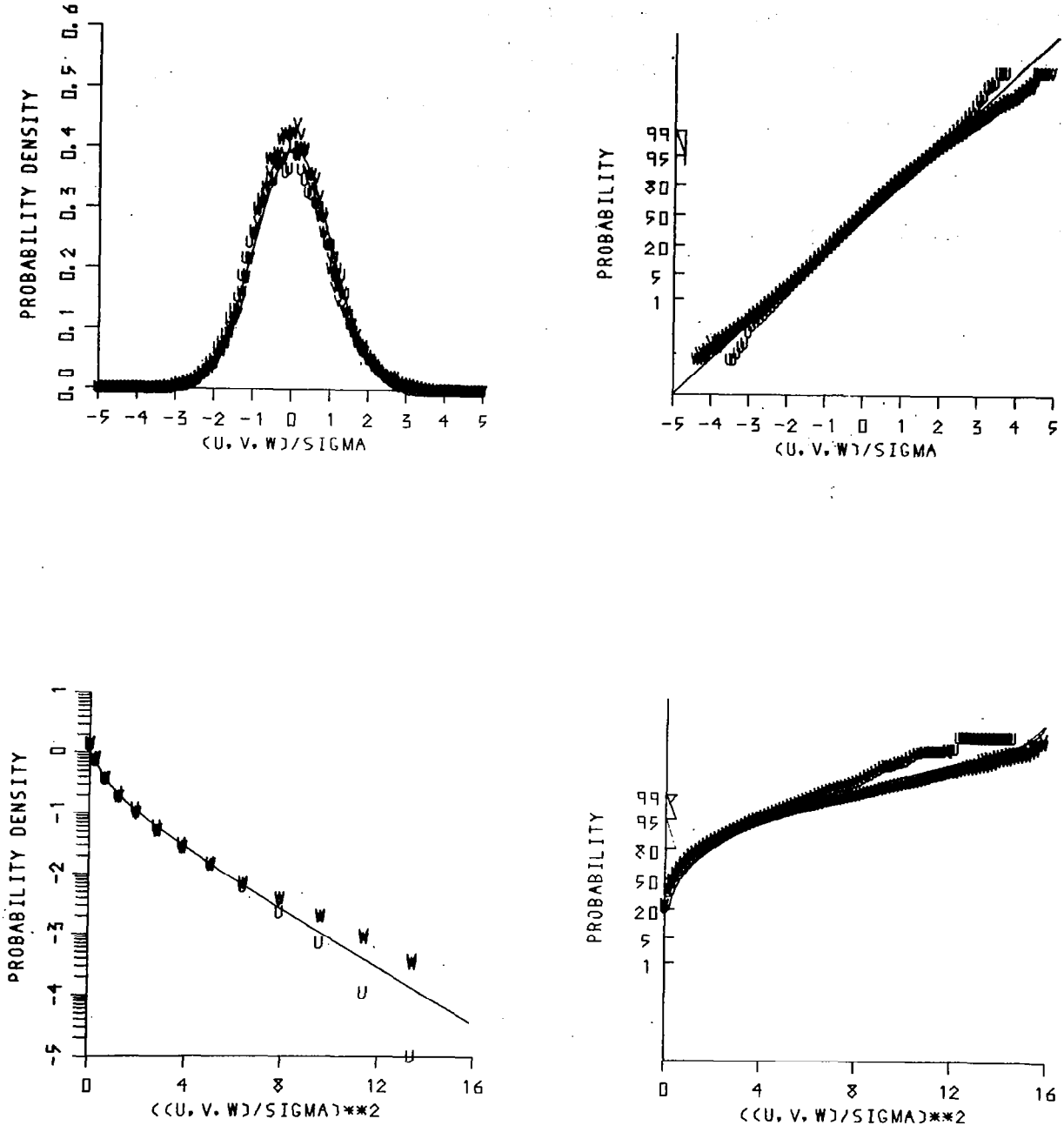

Figure 6.1 Kansas turbulence. Probability density and distribution functions for the first and second power of the standardized data. The Gaussian case is illustrated by a solid line. Integers on logarithmic vertical axis denote power of 10

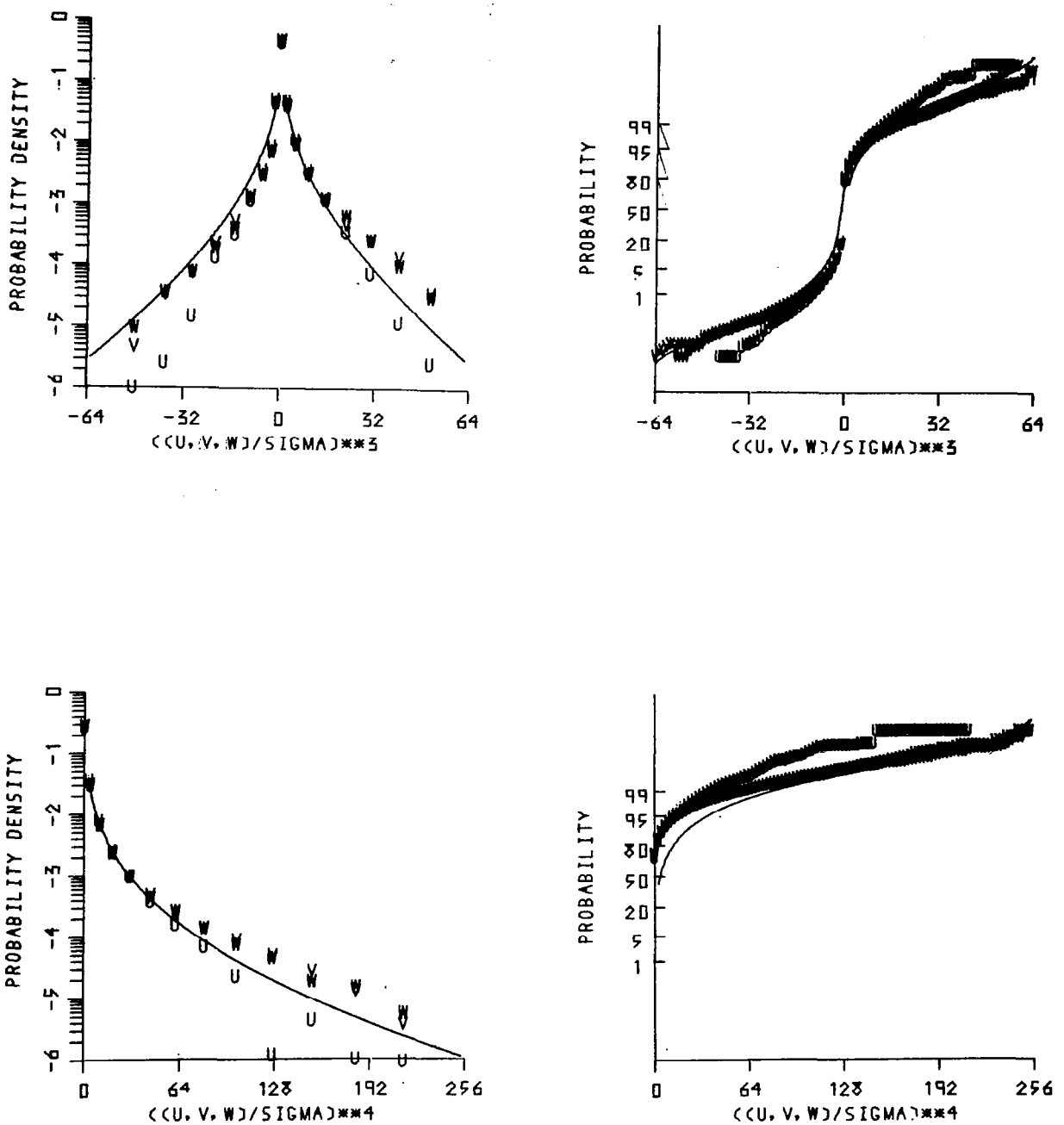

Figure 6.2 Kansas turbulence. Probability density and distribution functions for the third and fourth power of the standardized data. The Gaussian case is illustrated by a solid line. The integers on the vertical axis denote power of 10

by means of which we can analyze spatial variations in the turbulence. The timestep $\Delta t = 0.1$ sec is transformed into a length step Δx using Taylor's hypothesis: $\Delta x = \bar{u}\Delta t = 6.56$ m sec^{-1} 0.1 sec = 0.656 meters.

The structure function, Figure 6.6, is defined with these increments as

$$D(L) = E\{u^2(x,L)\} \tag{6.2}$$

and it should be dependent only on internal conditions of the flow.

The statistical properties of the increments are important in several ways. First they characterize the spatial variations in the turbulence--hence the distribution of increments provides insight into the uniformity of spatial structure of the velocity fields; second, if the series u(x) are Gaussian, the distribution of increments would also be Gaussian; and third, they are useful in the study of whether the data is self-similar in the sense of Mandelbrot as described in Section 3.

The probability functions for the increments are shown in Figure 6.3 and Figure 6.4 for lags 0.66, 6.6, 66, and 666 meters. Again, the curves are very similar to those given by DD, demonstrating that the increments with small lags deviate more sharply from Gaussian behavior than the increments at large lags.

6.3 Measures of Intermittency

As argued by DD, the non-Gaussian behavior appears to be intimately related with the intermittency of the turbulence and they provided further measures of the intermittency. Dutton, Lane, et al. (1969) define

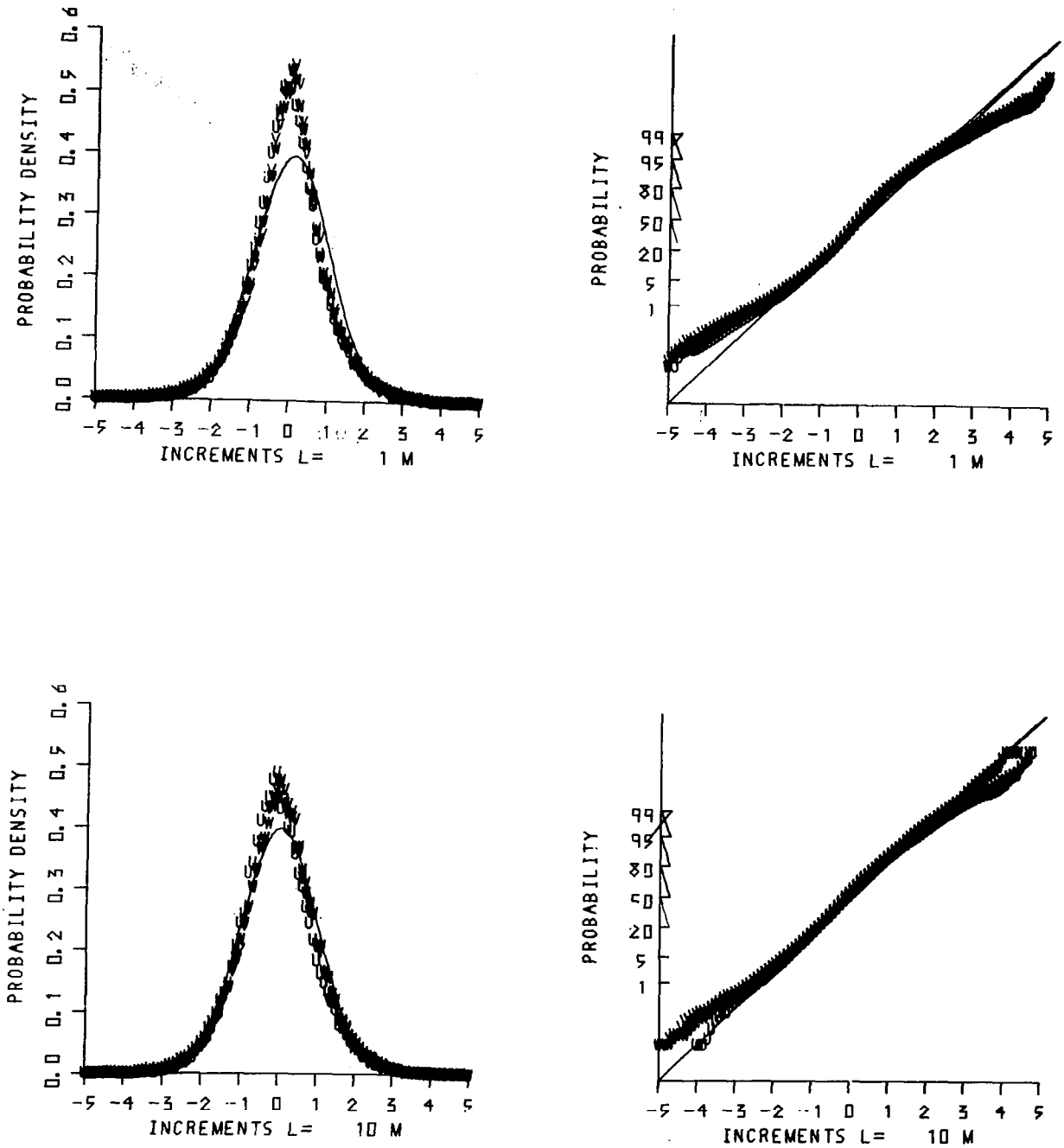

Figure 6.3 Kansas turbulence. Probability density and distribution functions for the standardized data. The intervals 1 and 10 m indicated on the graphs signify actual lags of 0.66 and 6.6 m. The Gaussian case is illustrated by a solid line

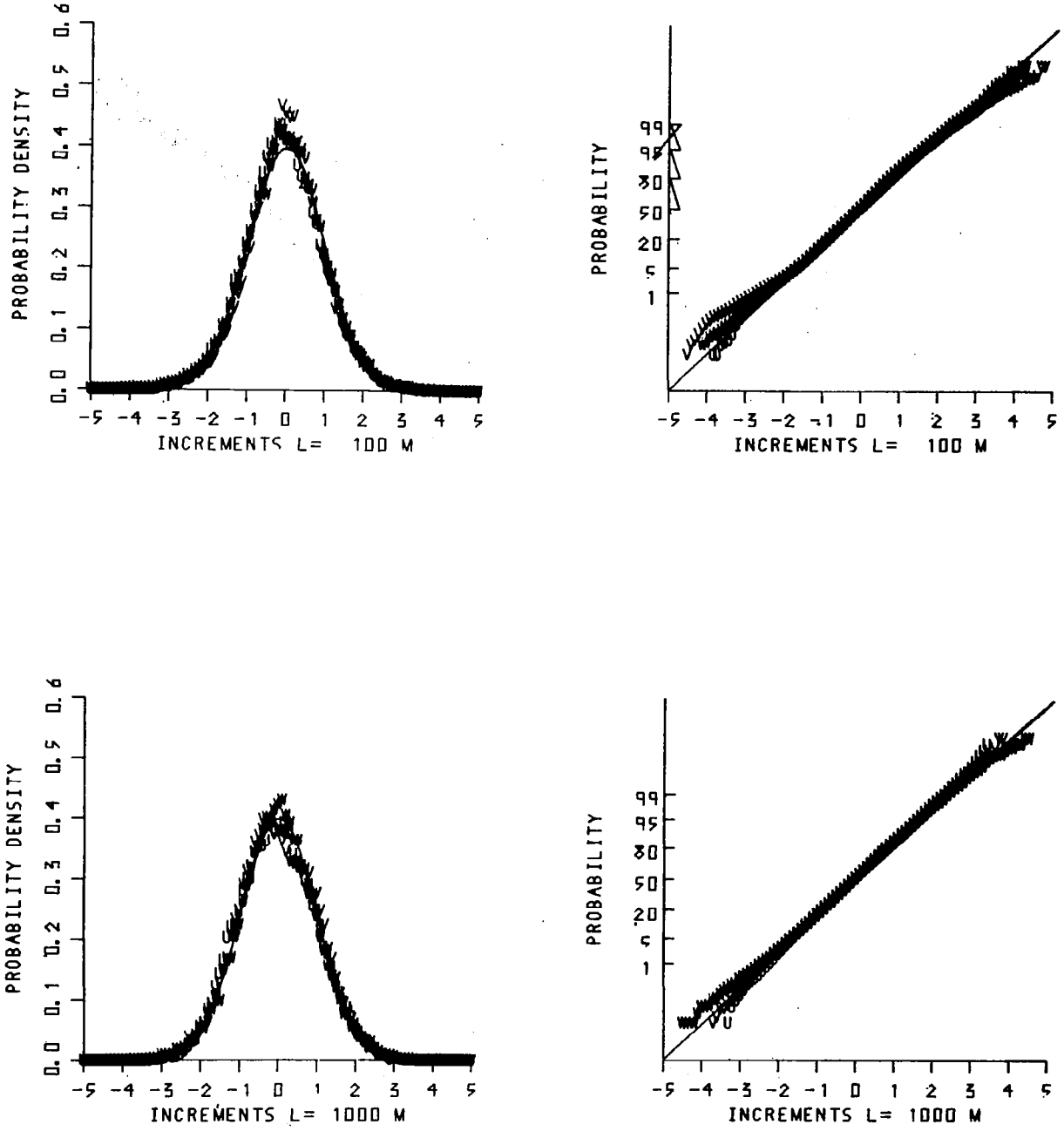

Figure 6.4 Kansas turbulence. Probability density and distribution functions for the standardized data. The intervals 100 and 1000 m indicated on the graphs signify actual lags of 66 and 666 m. The Gaussian case is illustrated by a solid line

an intermittent process as a process where a relatively large fraction of the variance is contributed by a relatively small fraction of the total record. DD then considered how moments such as the variance, skewness, and kurtosis accumulate as a function of the fraction of the total record length. These statistics are shown in Figure 6.5. The numerical algorithm can be thought of as a process in which the record is rearranged so that the observations are ordered by size; the curves are then obtained by summing the appropriate power of these observations and plotting the result against the fraction of the observations used in the sum. DD showed that the same curves can be obtained from the probability density function as follows:

The fraction of the $2m^{th}$ moment ($m = 1,2,\ldots n$) contributed by observations with absolute value greater than $|y|$ is

$$F_{2m}(y) = \left[\int_{-\infty}^{-|y|} x^{2m}\, p_y(x)dx + \int_{|y|}^{+\infty} x^{2m}\, p_y(x)dx\right]$$

$$F_{2m}(y) = \frac{\left[\int_{-\infty}^{-|y|} x^{2m}\, p_y(x)dx + \int_{|y|}^{+\infty} x^{2m}\, p_y(x)dx\right]}{\left[\int_{-\infty}^{\infty} x^{2m}\, p_y(x)dx\right]^{-1}}$$

and the fraction of record occupied by observations with absolute value greater than $|y|$ is

$$R_{2m}(y) = \int_{-\infty}^{-|y|} p_y(x)dx + \int_{|y|}^{+\infty} p_y(x)dx$$

For odd moments we have the contribution by observations with values less than y

$$F_{2m+1}(y) = \int_{-\infty}^{y} x^{2m+1}\, p_y(x)dx \left[\int_{-\infty}^{\infty} x^{2m+1}\, p_y(x)dx\right]^{-1}$$

$$R_{2m+1}(y) = \int_{-\infty}^{y} p_y(x)\, dx$$

Thus, if the density functions $p_y(x)$ are known, then both F and R can be determined as function of y and so F is known as function of R.

Also, these figures are very similar to those given by DD with only a slight departure from the Gaussian case for the variance and a distinct deviation for the skewness and the kurtosis. The difference found between the components can also be found in some of DD's figures.

6.4 Exceedance Statistics

Among the various exceedance statistics that can be used for studying statistical structures, DD choose N(y)/N(0) which is the ratio of the number of crossings of value y with positive slope per unit time to the number of crossings of zero with positive slope. Figure 6.5 shows N(y)/N(0), and again we find the same behavior as found by DD.

6.5 Spectra and Covariance Functions

The analysis of turbulence relies heavily on the theory of second order processes, the covariance function being one of the most important characteristics of such processes. From the covariance function, a generalized spectral representation can be obtained, as shown in

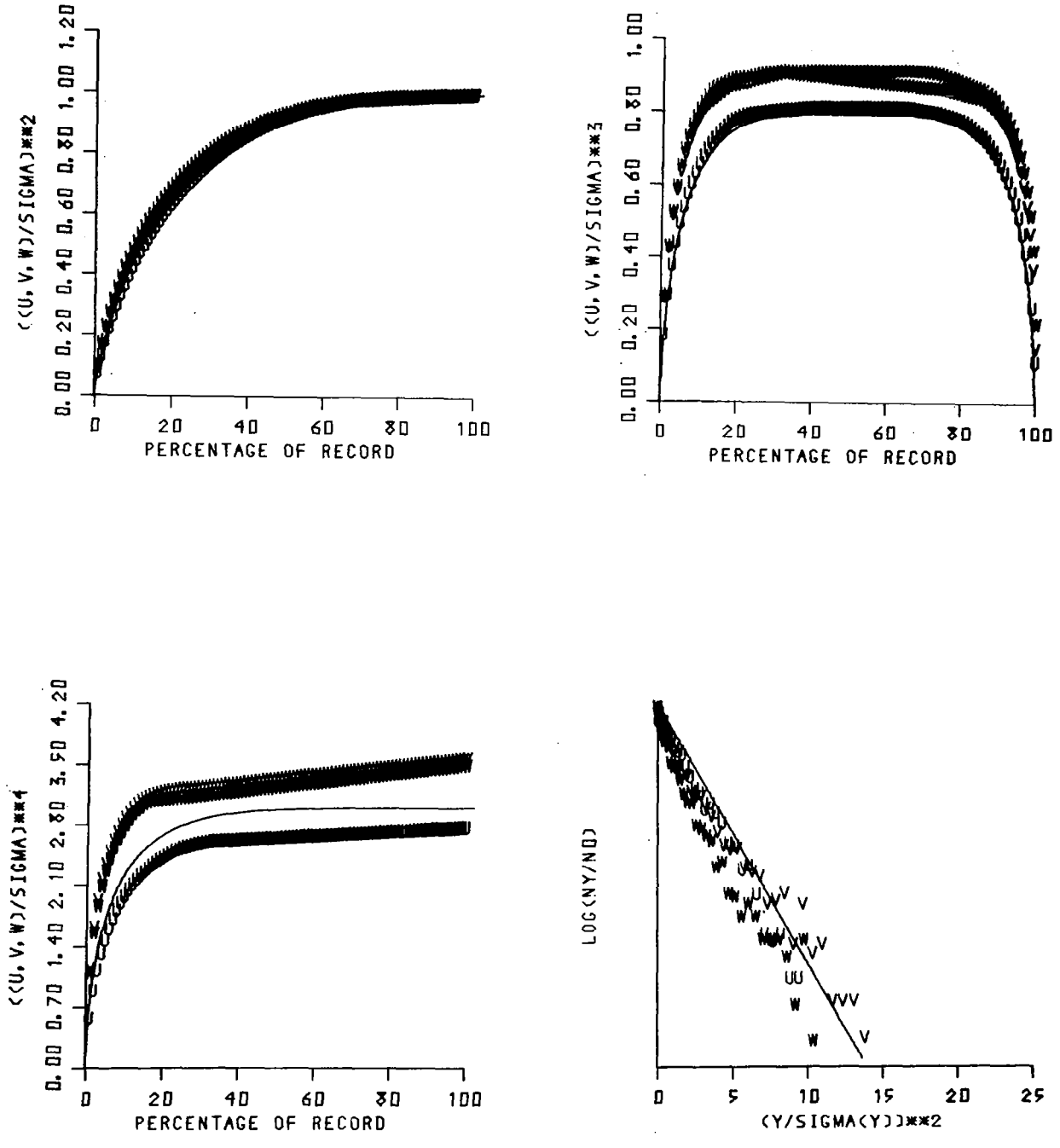

Figure 6.5 Kansas turbulence. Accumulation of variance, skewness, and kurtosis (on the vertical axis) as a function of the percentage of the record. Note that the final symbol on the right gives the average variance, skewness, and kurtosis respectively. Lower right graph: the ratio for the standardized data of the number, $N(\dot{y})$, of crossing of level y with positive slope to the number, $N(0)$, of crossing of zero with positive slope as a function of y/σ_y

Section 4, where the shape of the eigenfunctions can be argued to be of some significance. Further, the eigenfunctions gave a unique representation of the correlation function, and in the limit where we could assume stationarity and infinite integration limits, this representation produced the well-known fact that the correlation function and the spectrum constitute a Fourier transform pair.

By means of correlation functions and spectra, the analyst is able to investigate the sequence of events throughout an enormous amount of data by looking at smooth curves. Although the correlation functions and the spectra contain the same amount of information, the spectra are normally best suited for a subjective analysis because they reveal how the variance (or the covariance) is distributed over wave numbers and hence how the energy is distributed on scales.

The autocorrelation functions R_{uu}, R_{vv}, R_{ww} and the cross-correlation functions R_{uv}, R_{uw}, R_{vw} are shown in Figure 6.6 on a logaritmic lag scale. As found in DD, the correlation of the horizontal components u and v is higher in the midrange than that of the vertical component w. The R_{uw} function shows the expected behavior to tend to a negative value significantly different from zero at small lags indicating a downward transport of horizontal momentum (the Reynolds stress). Also shown on the figure is the structure function D(r), where for a spatially homogeneous process, the relation between R(r) and D(r) is easily found to be

$$D(r) = 2\sigma^2 (1 - R(r)) \tag{6.3}$$

a relationship that can be seen to hold well for the curves in Figure 6.6.

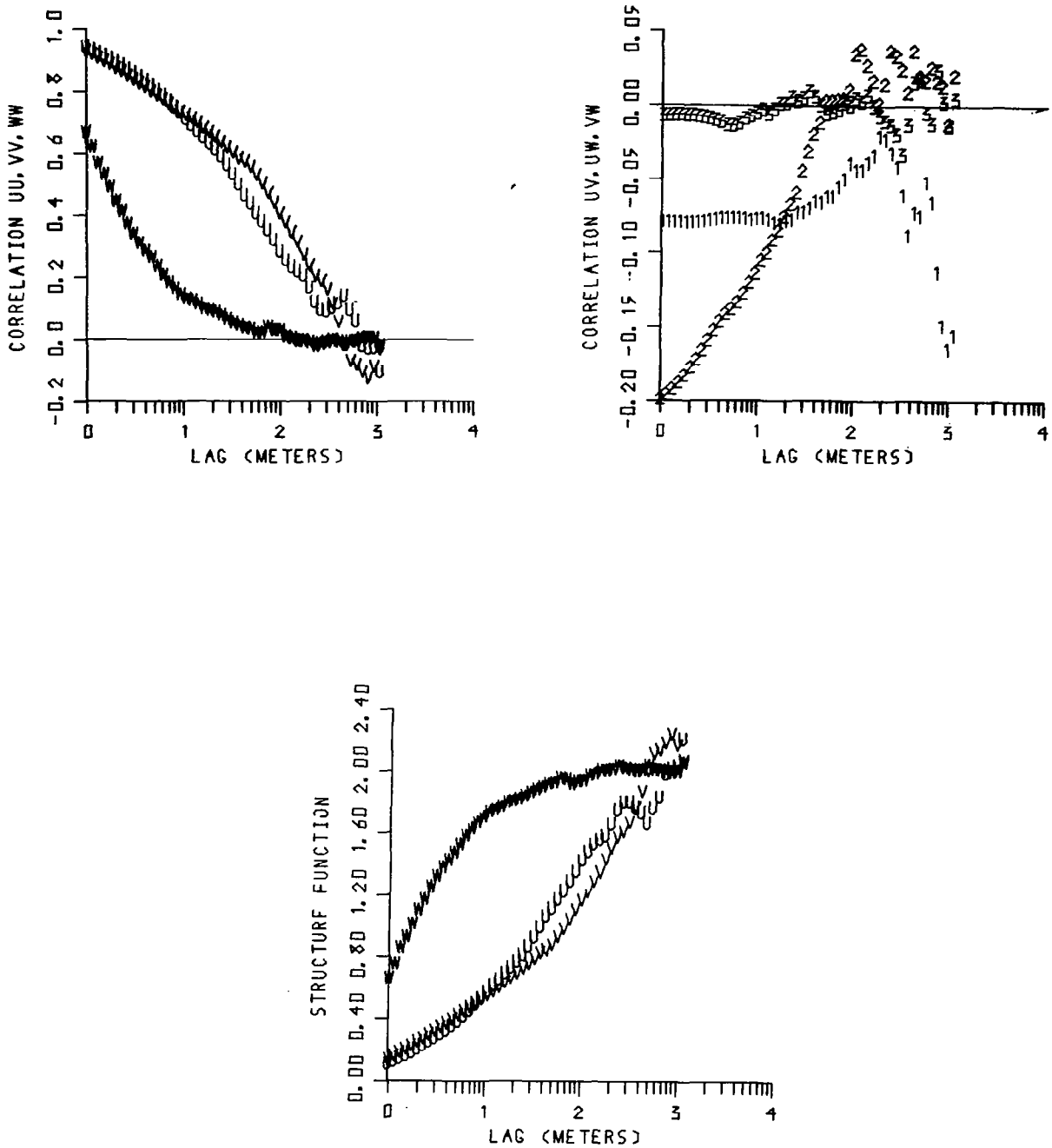

Figure 6.6 Kansas turbulence. Autocorrelation, cross-correlation and structure functions for the standardized data plotted as a function of the lag on a logarithmic scale. The plotted 1 refers to the u-v correlation functions, the 2 to u-w, the 3 to v-w. The integers on the horizontal axis denote powers of 10

The spectra S_u, S_v, S_w and the cospectra S_{uw} are shown in Figure 6.7. The most pronounced characteristic of the spectra is the -5/3 slope exhibited by the u and v components over one decade of frequencies. The w component is seen to flatten out at low frequencies. The cospectrum C_{uw} gives the wavenumber decomposition of the Reynolds stress responsible for the transformation of mechanical energy and hence is an important statistic to model correctly. The cospectrum C_{uw} is seen to be significantly different from zero at frequencies 0.01 - 1, indicating the active scales in the downward transport of momentum to be of the order 600 m to 6 m.

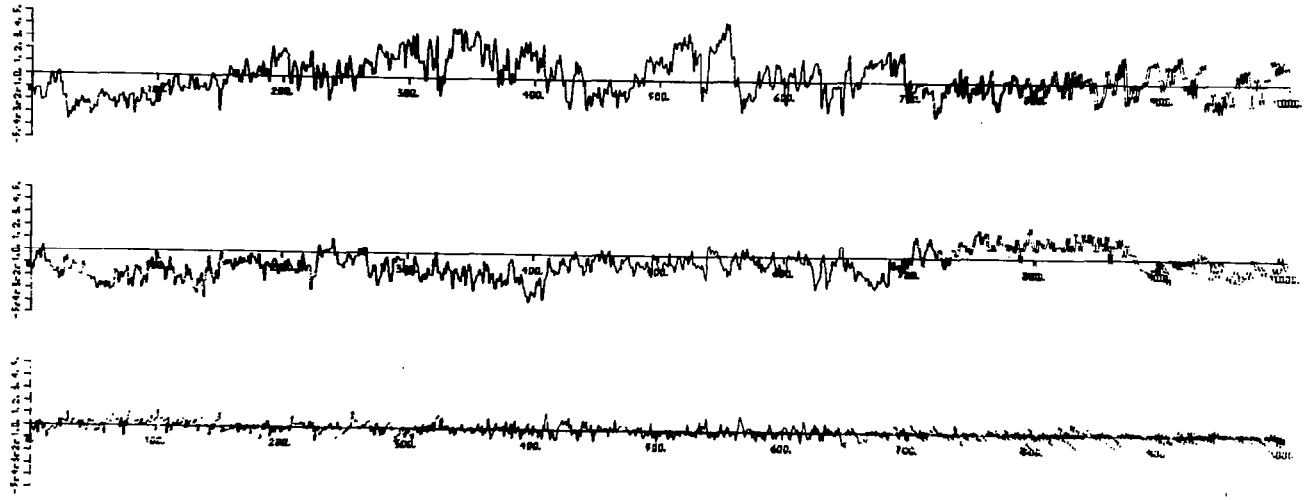

Figure 6.7a Kansas turbulence. First third of record; not normalized. One second averages plotted versus time; the numbers on the horizontal and vertical axis denote seconds and meters per second respectively

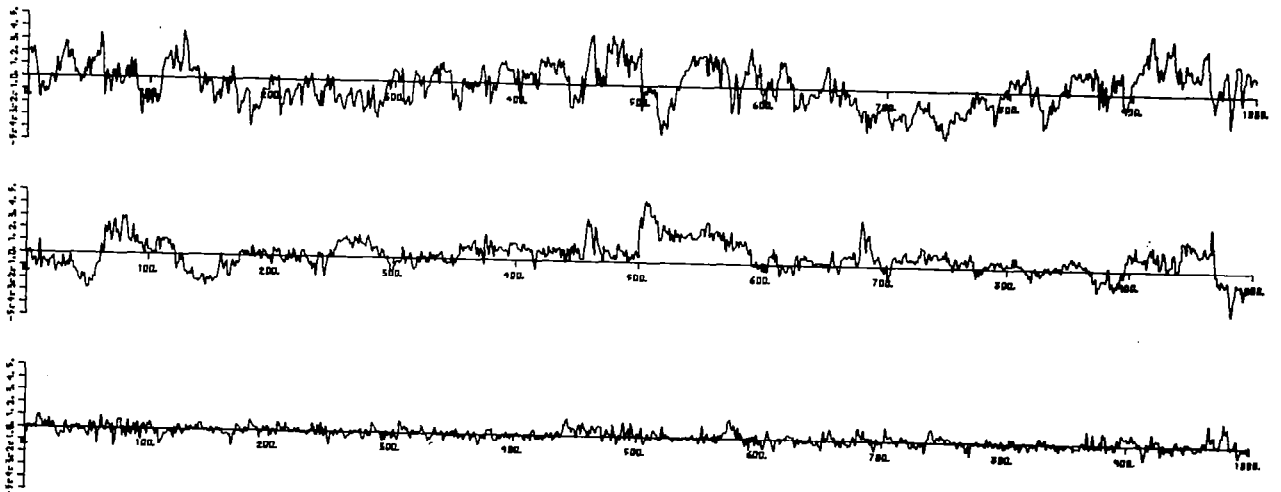

Figure 6.7b Kansas turbulence. Second third of record; not normalized. One second averages plotted versus time; the numbers on the horizontal and vertical axis denote seconds and meters per second respectively

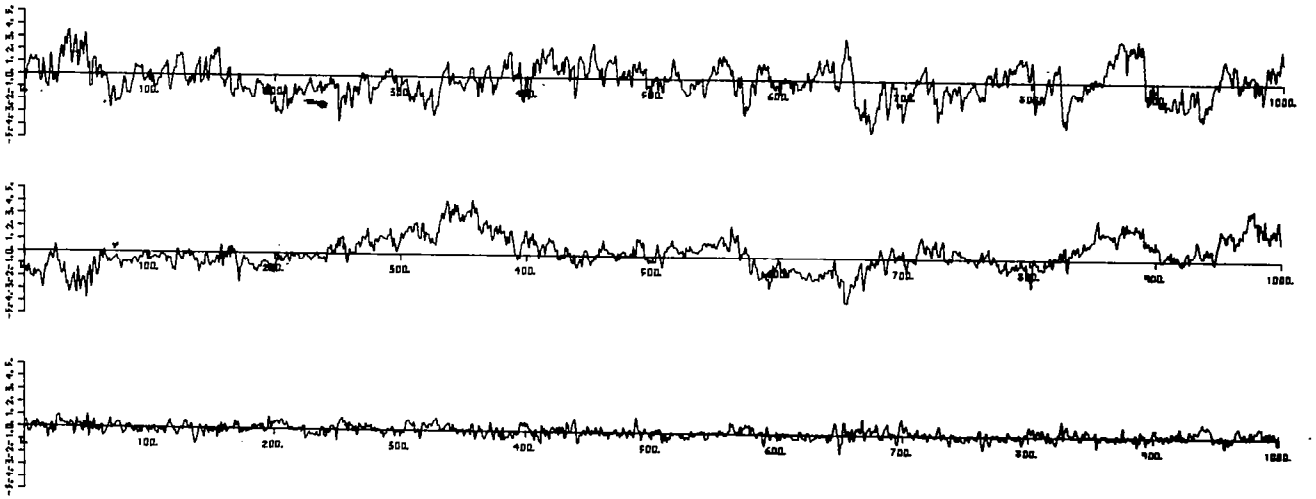

Figure 6.7c Kansas turbulence. Last third of record; not normalized. One second averages plotted versus time; the numbers of the horizontal and vertical axis denote seconds and meters per second respectively

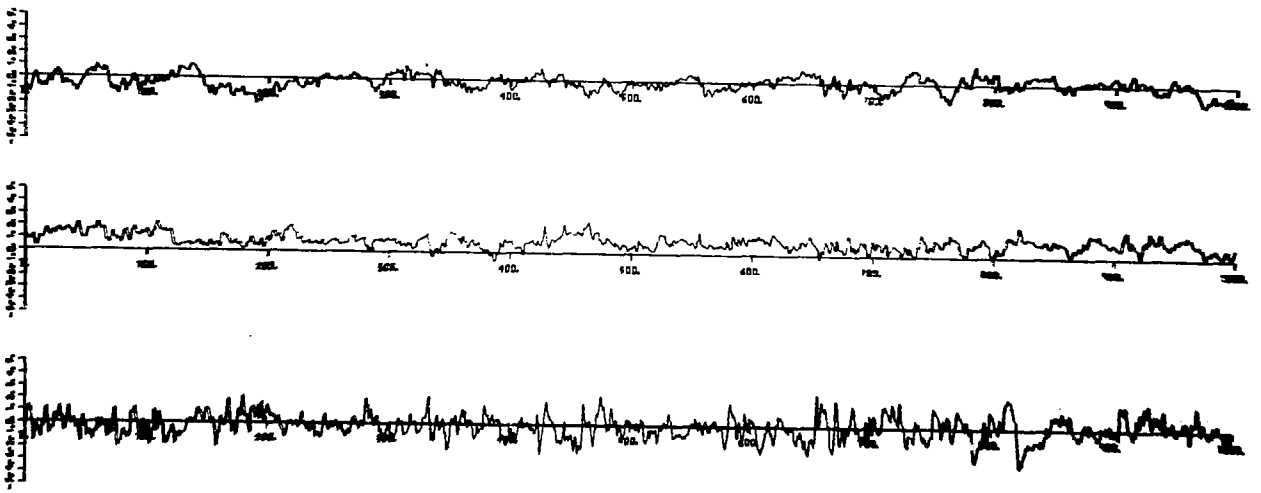

Figure 6.8 Kansas turbulence. Time history consisting of 1000 one tenth of a second averages plotted as normalized magnitude versus time. The numbers on the horizontal axis denote seconds

7.0 TESTING AND FURTHER DEVELOPMENT OF THE MODEL

Two experiments with the model are discussed in this section. The generation of the turbulence follows the generation scheme given in Section 5.3.

As a first step we choose to generate the series in sequences of length 30 sec (= 300 datapoints). This is six times the length of one of the component parts of the eigenfunctions and our choice is obviously motivated by the way the ensemble $f_n(t)$ was constructed. Inside every 30 second interval we construct the turbulence in pieces of 5 seconds. One of the pieces, selected at random, is created as active turbulence and the five other pieces as passive turbulence.

The differences between the two experiments are as follows:

1. The uniformly distributed random series consisting of integers between 1 and 6 which give the position of the 5 sec active turbulence piece inside the 30 sec sequence is sampled for each experiment.

2. A Gaussian distributed random series is sampled to obtain the expansion coefficients for each experiment.

3. In experiment 1, the mean and the standard deviation for the expansion coefficient distributions are the same as given in Table 1. In experiment 2, the standard deviations were changed to $(\sigma_1, \sigma_2, \sigma_3) = (8.0, 8.0, 4.0)$.

4. The alteration of the expansion coefficients in the five passive intervals was done by multiplying each of the three first expansion coefficients by a uniformly distributed random number between 0 and 1 for experiment 1 and 0.5 and 1 for experiment 2.

In both experiments, the third expansion coefficient was, for every 5 sec generated interval, multiplied by +1 or -1 picked at random. The justification for this procedure lies in the shape of the eigenfunctions and the distributions of the expansion coefficients. It follows from Table 2 that in contrast to all the other expansion coefficients α_3 has a much larger mean than standard deviation, implying much greater probabilities for obtaining positive rather than negative values. Figure 5.1 shows that most of the contribution of the third eigenfunction is the peak in the w-component, which in creating of the ensemble $f_n(t)$ was chosen positive. But we want to generate negative gusts as well as positive, and therefore the $\pm$ 1 multiplication of α_3 was introduced.

7.1 Statistical and Sequential Characteristics of the Two Experiments

Some 8200 datapoints were generated for each component for each experiment and then subjected to the analysis applied to the turbulent record in Section 6. The result is displayed in the Figures 7.1 - 7.18.

The probability densities and distributions in Figures 7.1 - 7.14 show no large deviations from experiment 1 to experiment 2 and a comparison with the Figures 6.1 and 6.2 reveals the generated turbulence to exhibit the expected non-Gaussian behavior.

The distribution of increments at lags 0.6, 6, 66, and 666 meters given in the Figures 7.5 - 7.8 all show the turbulence behavior from the Figures 6.3 and 6.4 with small lags deviating more sharply from Gaussian behavior than large lags.

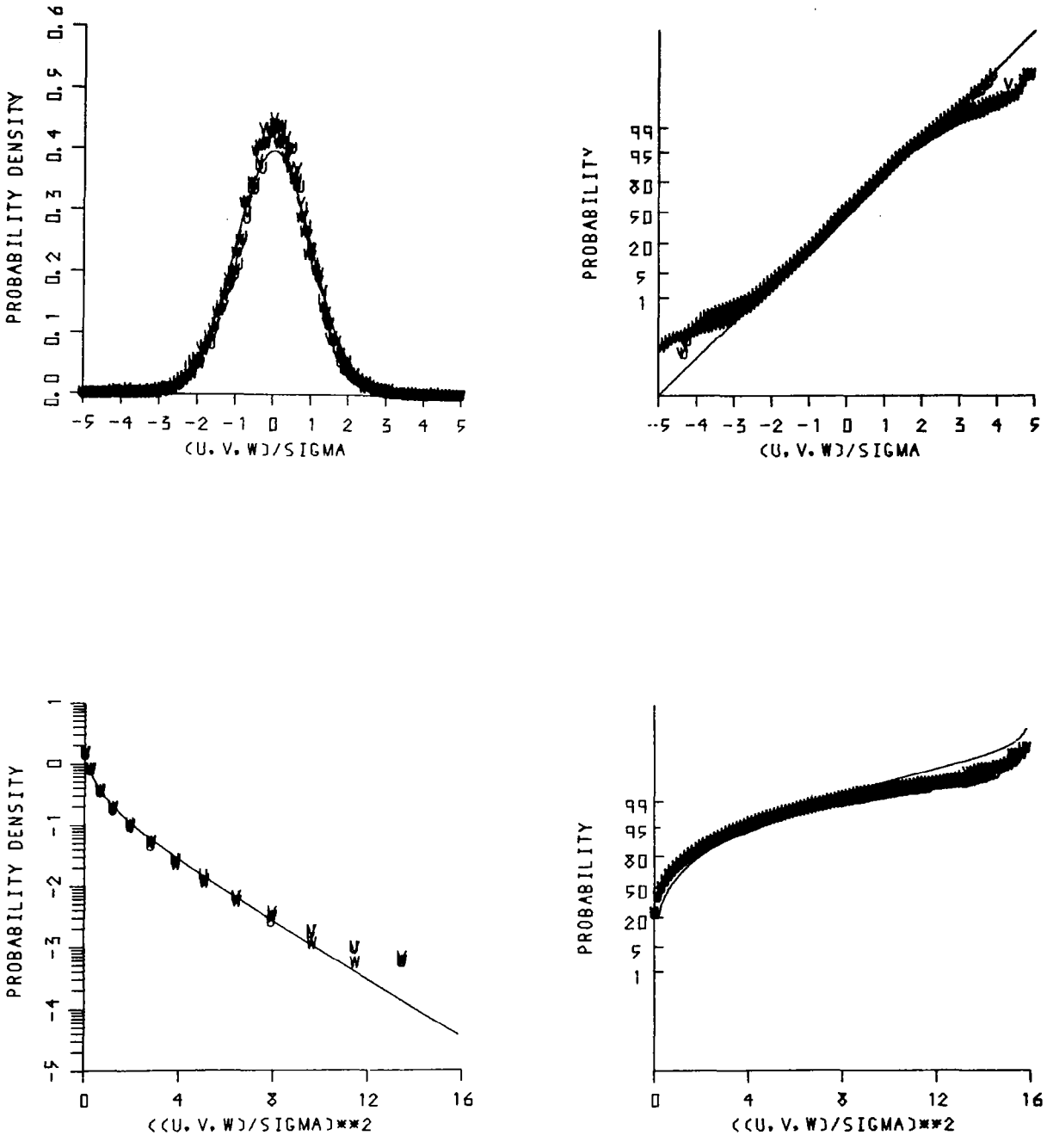

Figure 7.1 Experiment 1. For further details see the legend for figure 6.1

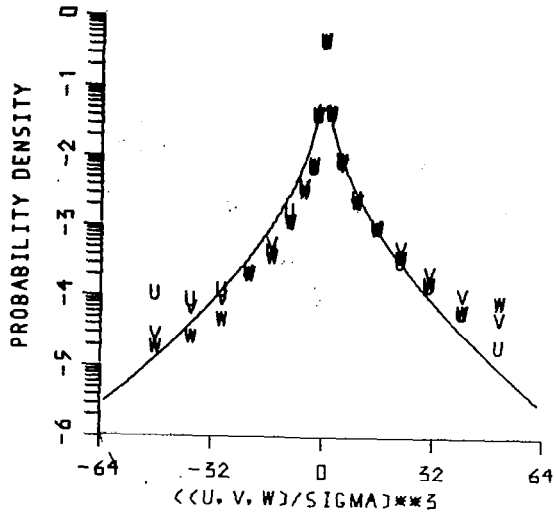

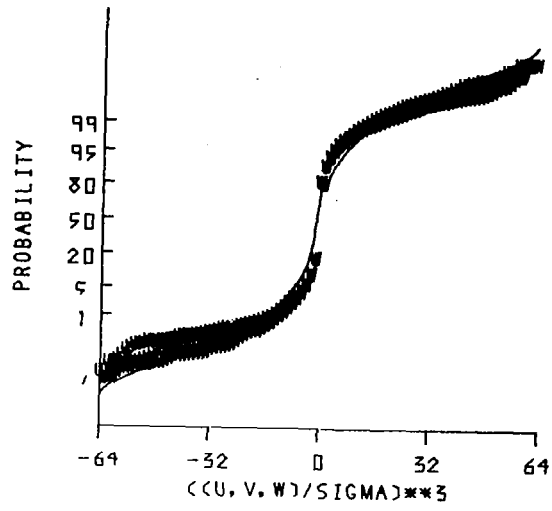

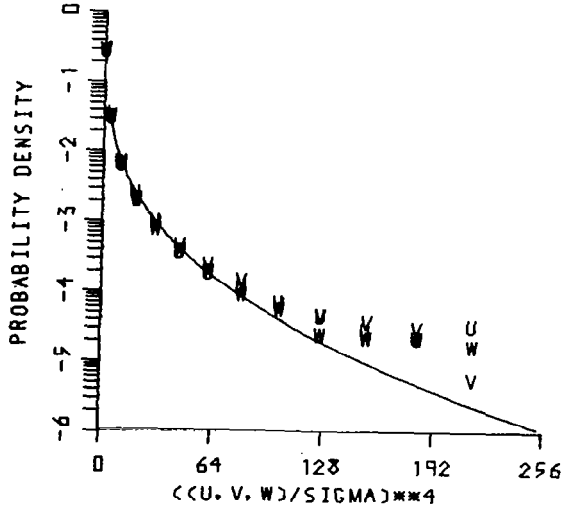

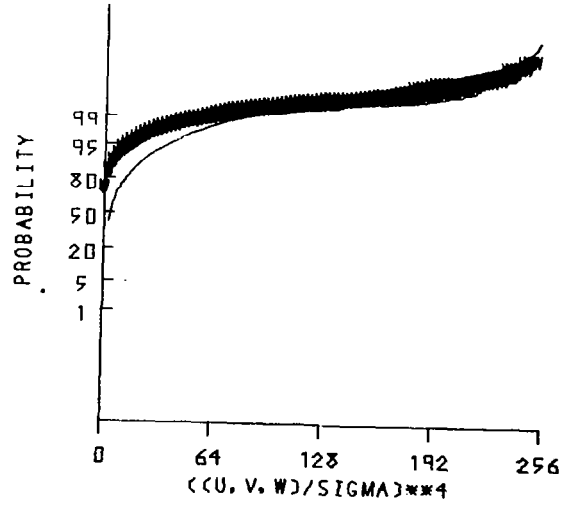

Figure 7.2 Experiment 1. For further details see the legend for figure 6.2

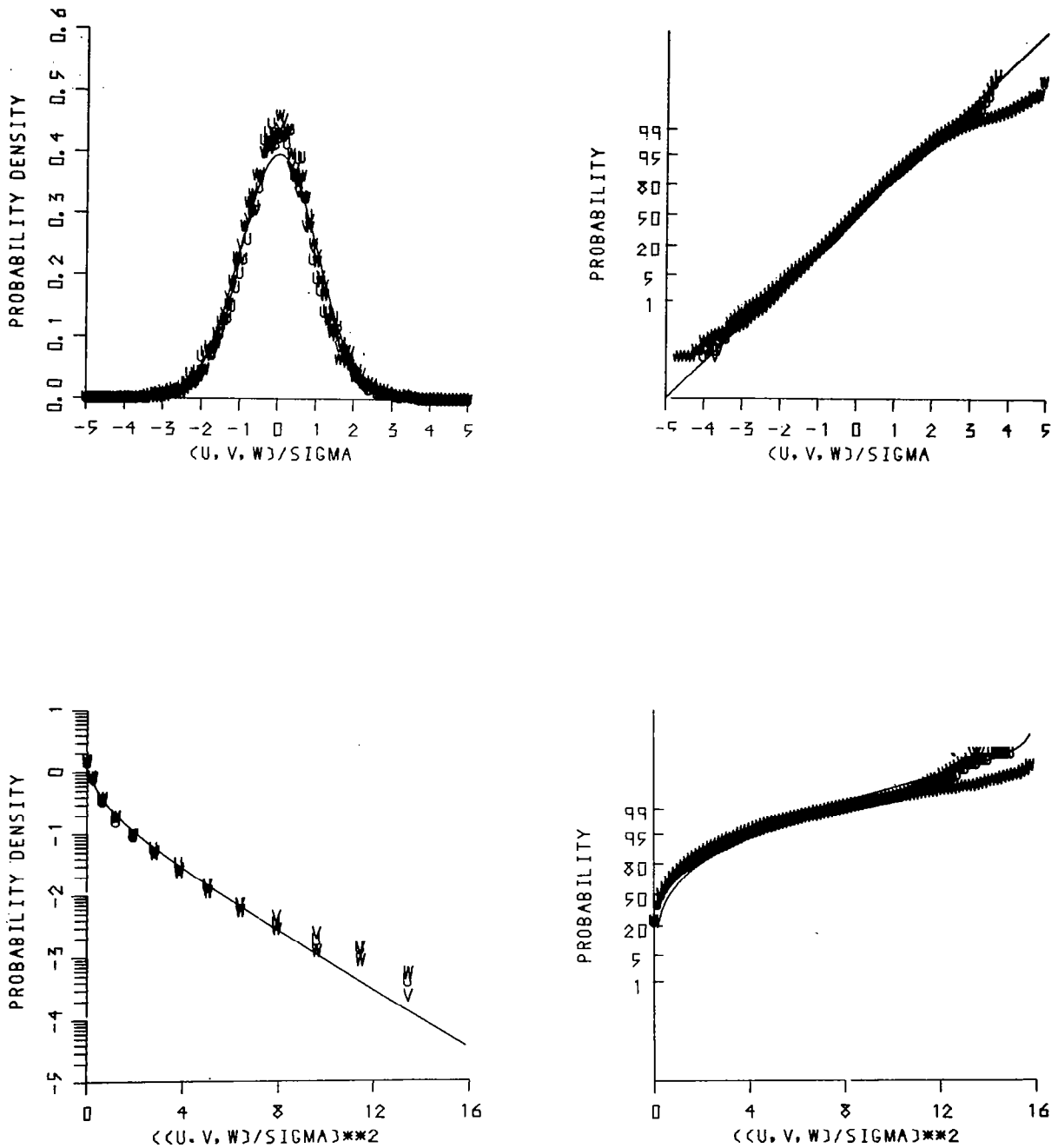

Figure 7.3 Experiment 2. For further details see the legend for figure 6.1

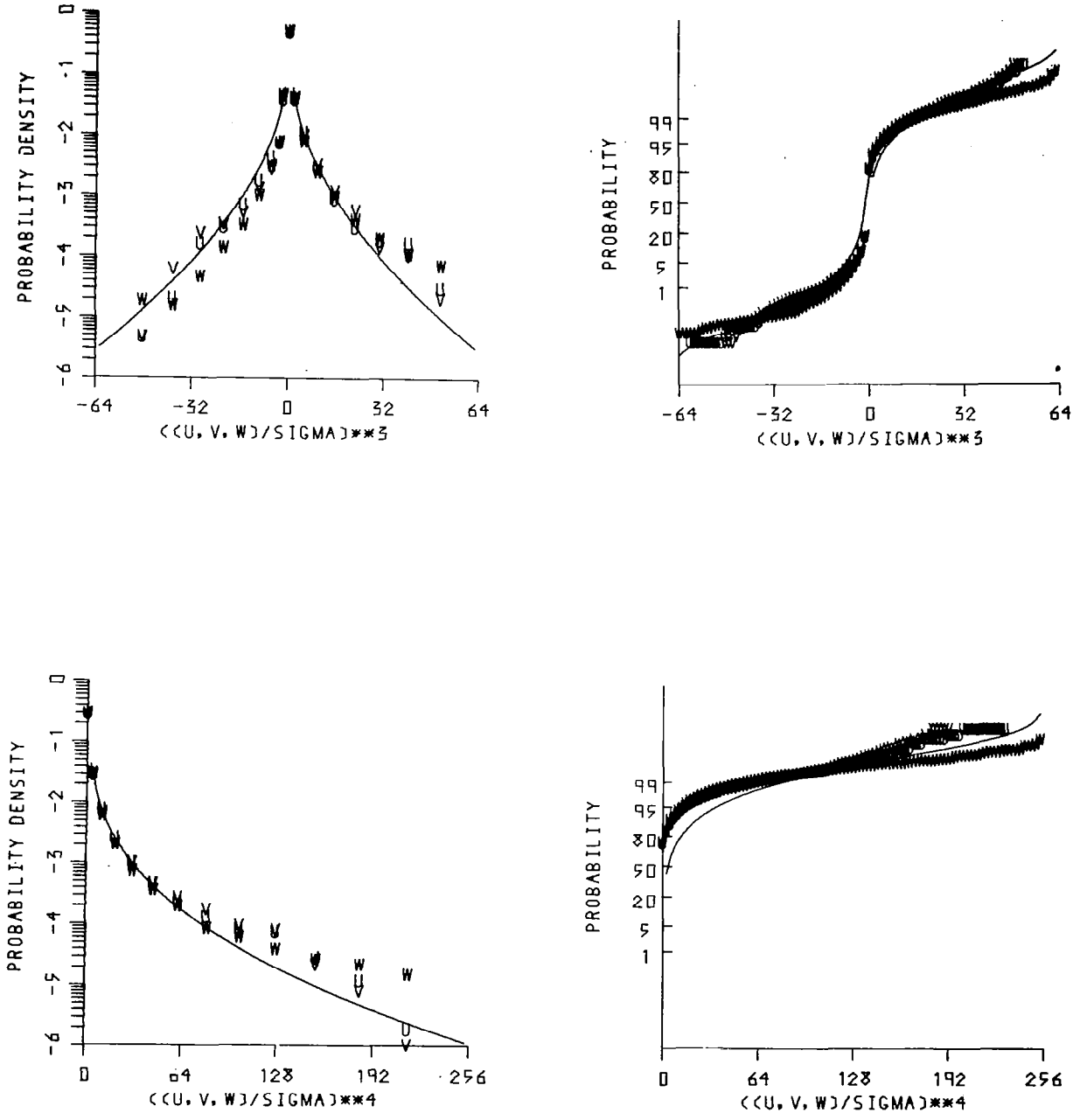

Figure 7.4 Experiment 2. For further details see the legend for figure 6.2

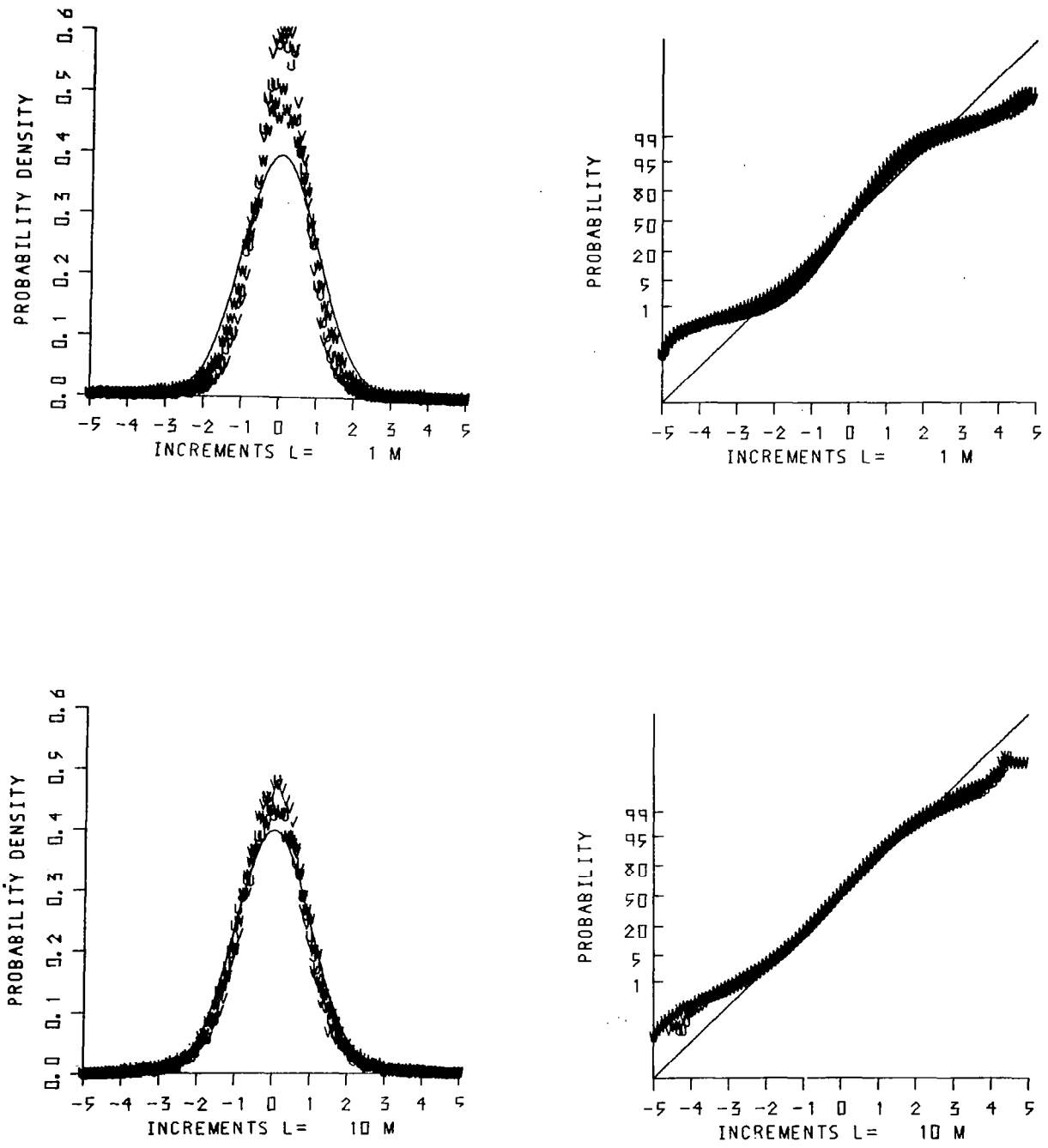

Figure 7.5 Experiment 1. For further details see the legend for figure 6.3

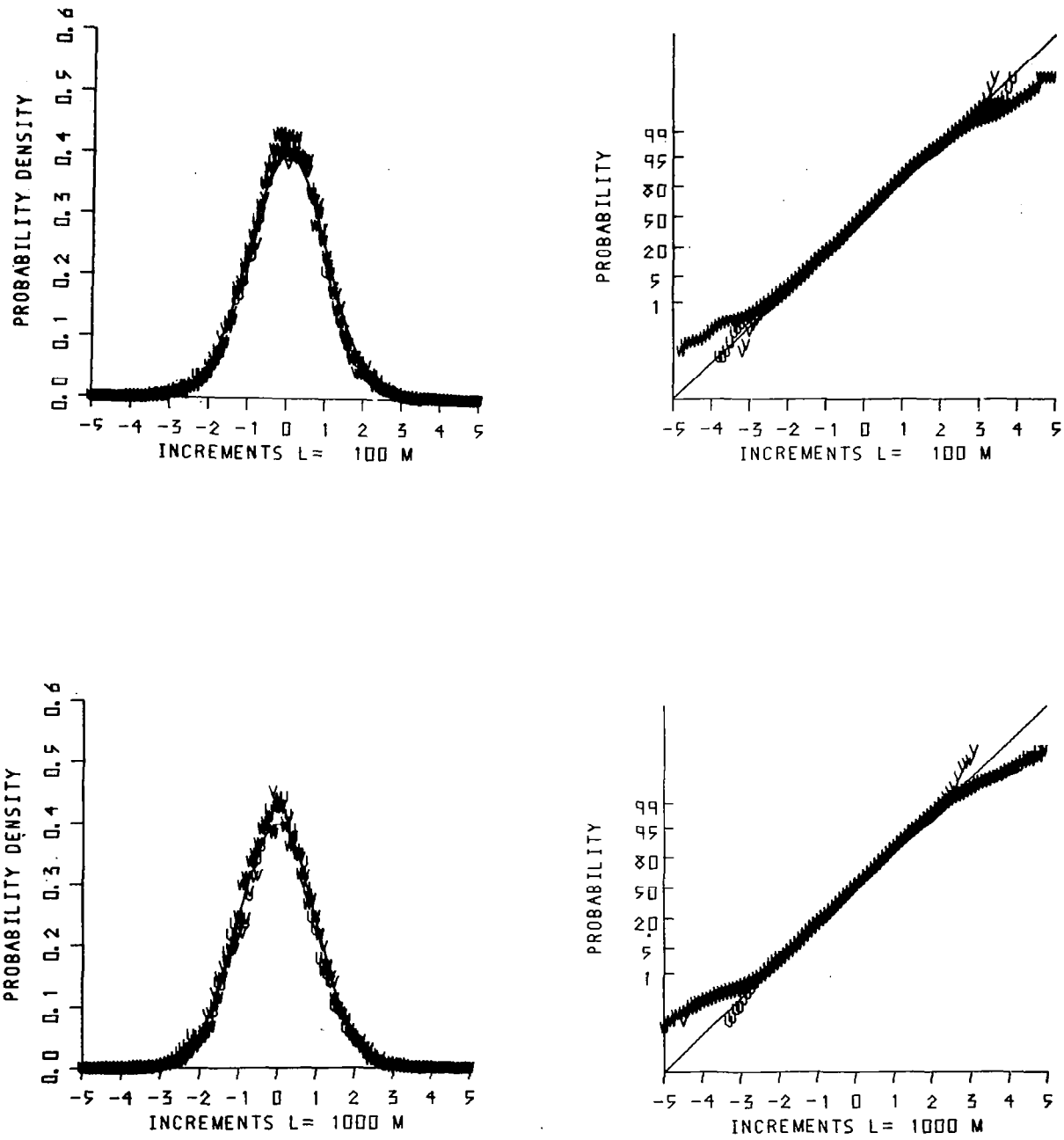

Figure 7.6 Experiment 1. For further details see the legend for figure 6.4

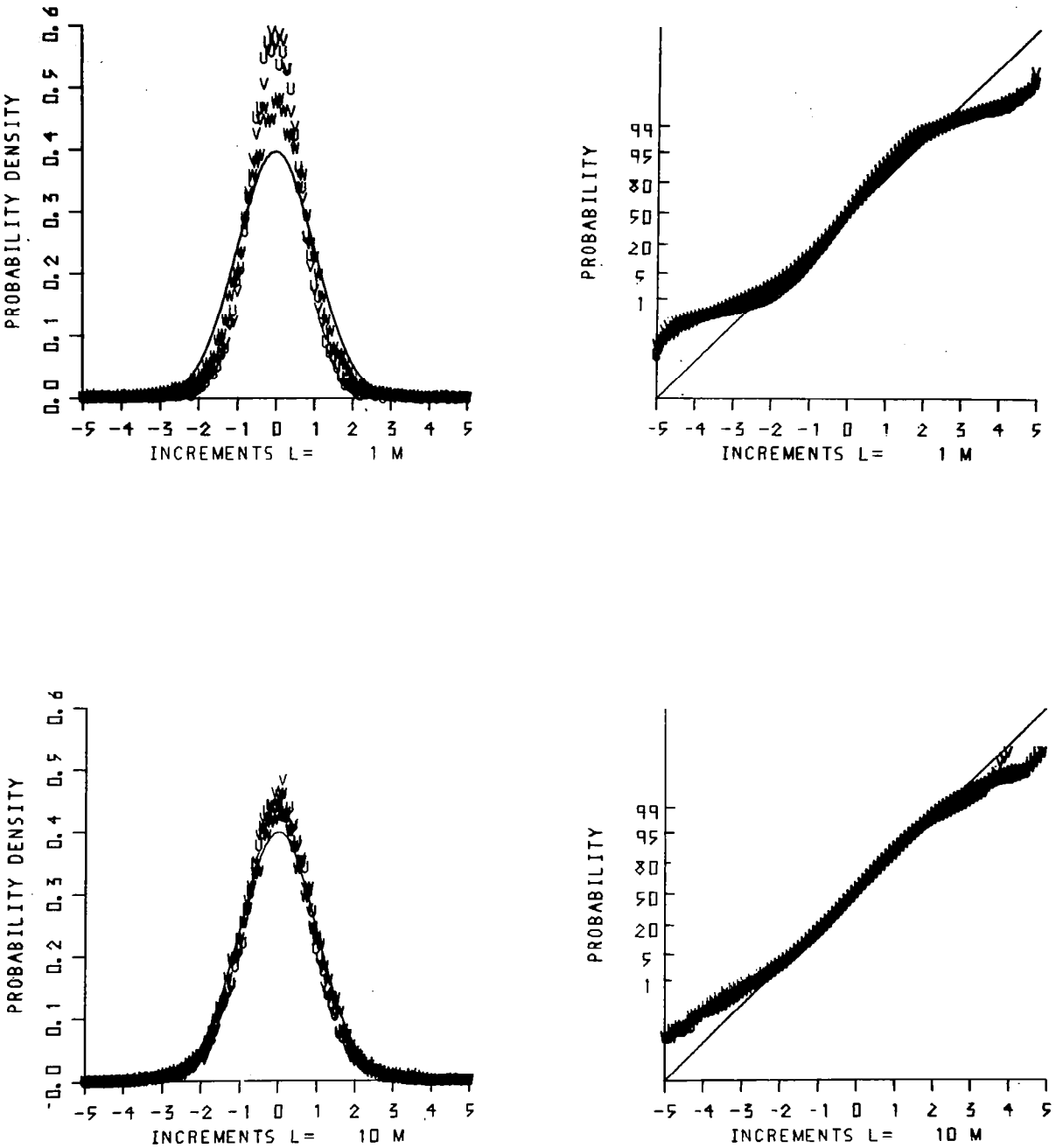

Figure 7.7 Experiment 2. For further details see the legend for figure 6.3

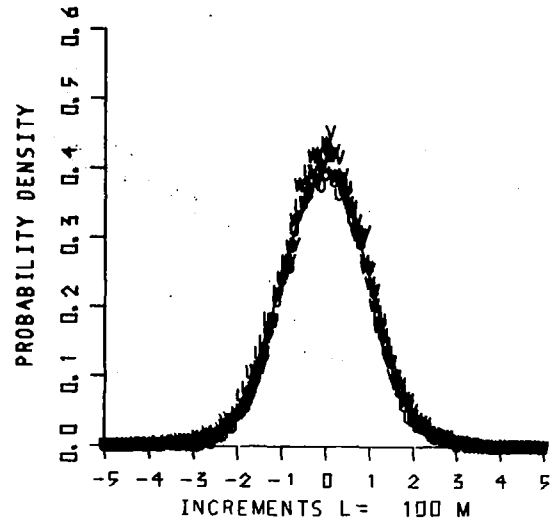

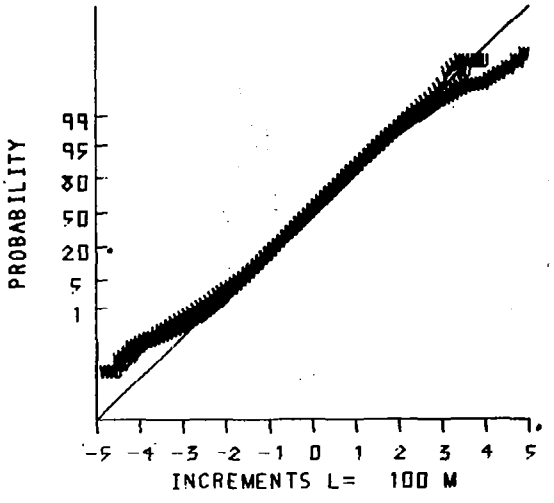

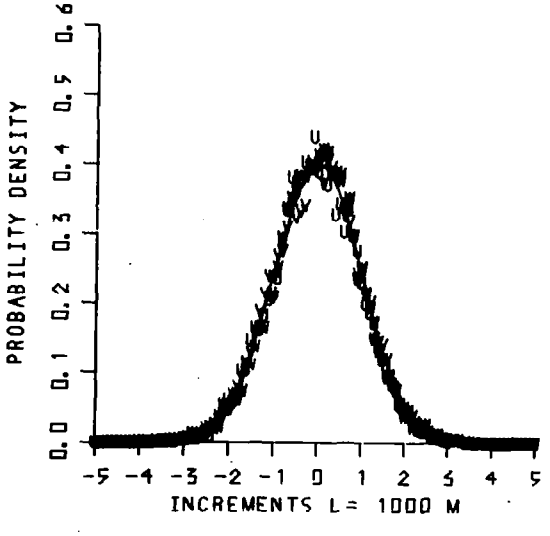

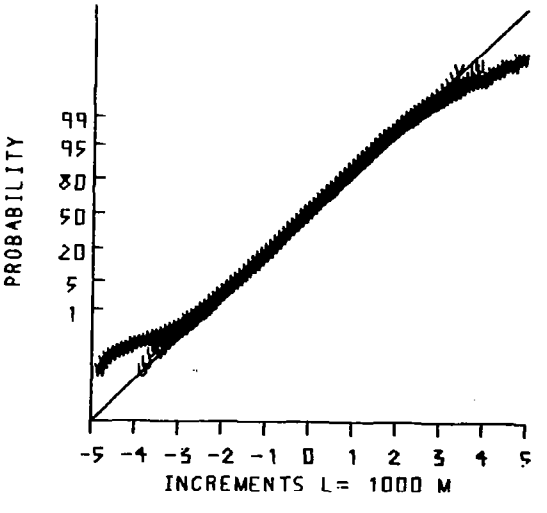

Figure 7.8 Experiment 2. For further details see the legend for figure 6.4

The accumulated moments as given by the Figures 7.9 and 7.10 show some differences from experiment to experiment to the actual turbulence, Figure 6.5, but no serious discrepancies. This is also the case for the exceedance plot.

The auto- and cross-correlations and the structure function, Figures 7.11 and 7.12, do not differ much between the experiments. From experiment to the actual turbulence, Figure 6.6, there is, however, one discrepancy; the experimental u and v fall off much too rapidly.

The relation between the correlation function $R(\tau)$ for a stationary time-series and the correlation function $R_T(\tau)$ calculated over the length T is given by

$$(7.1) \qquad R_T(\tau) = R(\tau)\ (1 - \frac{|\tau|}{T})$$

The generated 5 sec pieces will on average have the same correlation function as the ensemble from which the eigenfunctions were obtained. This ensemble was obtained from the turbulence record, and although it is not justifiable to call this ensemble stationary, it seems that the transformation above can explain the main differences between Figure 6.6 and Figures 7.11 and 7.12, especially when it is remembered that the triangular window plots like an exponential function on log-linear axes.

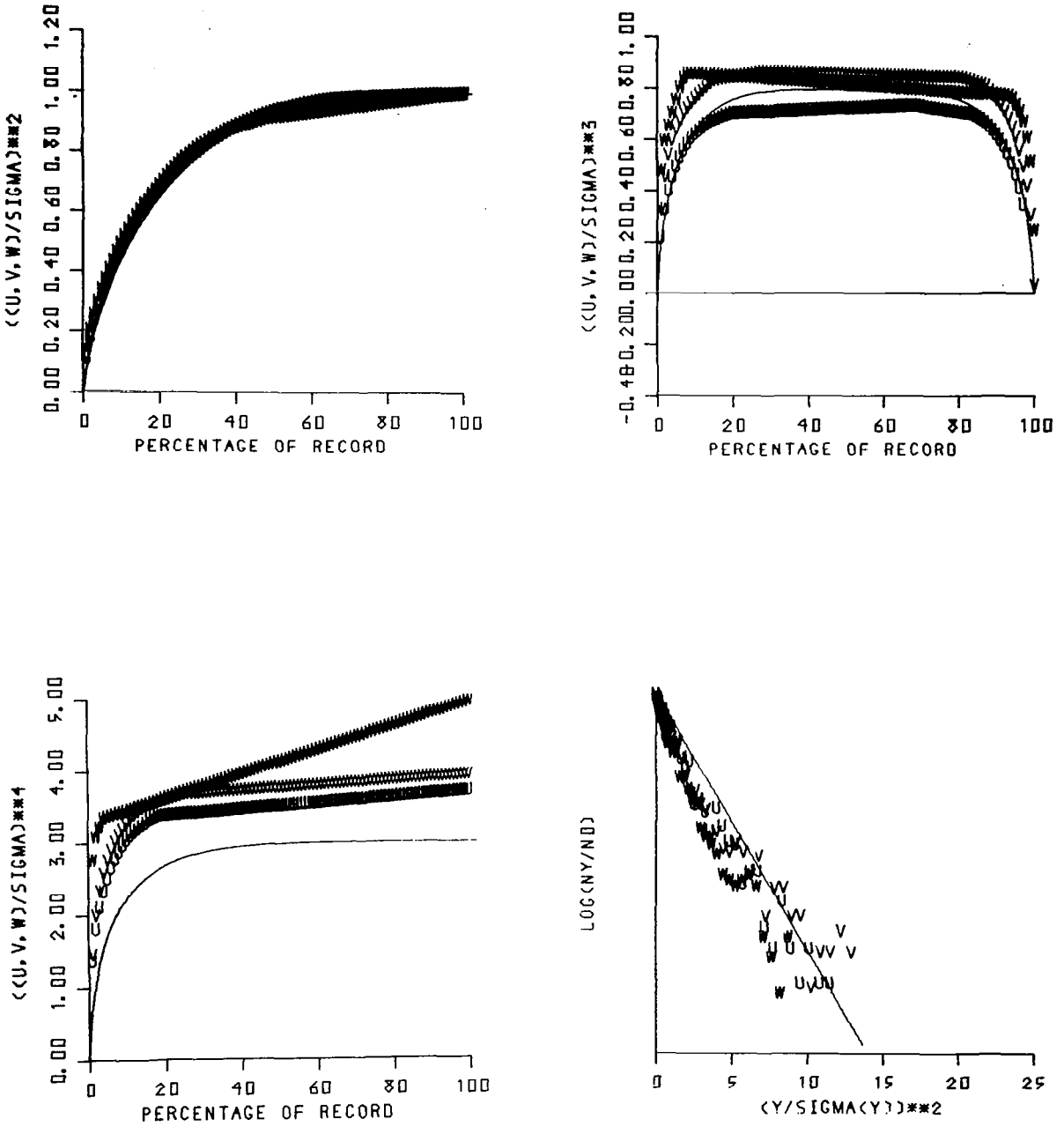

Figure 7.9 Experiment 1. For further details see the legend for figure 6.5

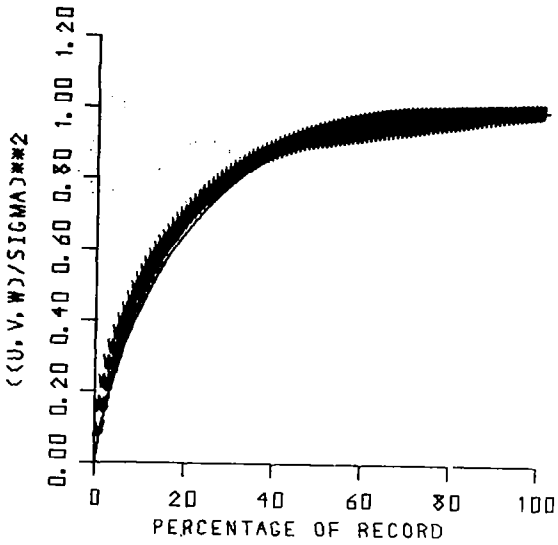

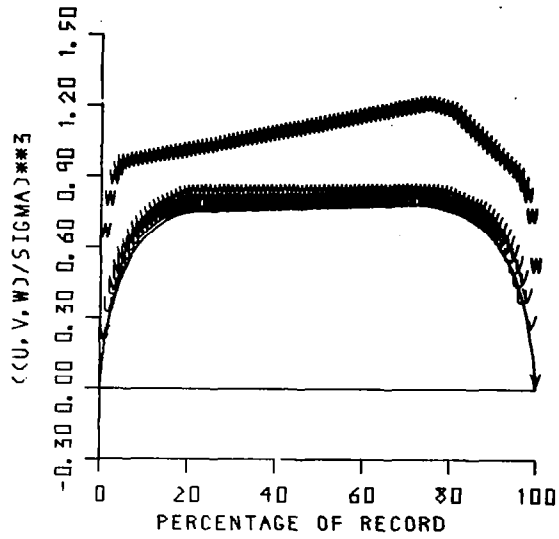

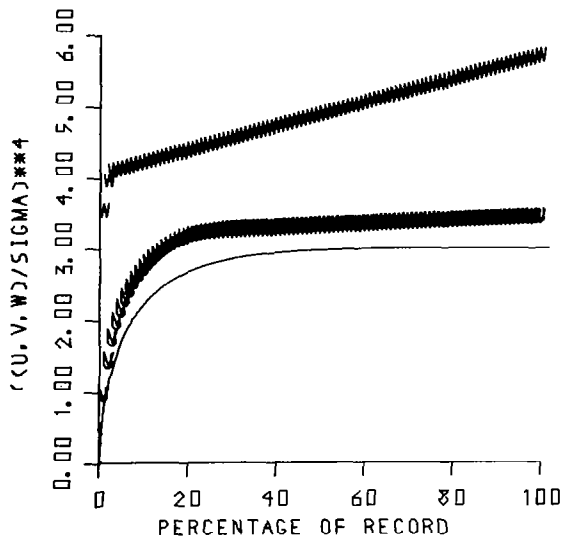

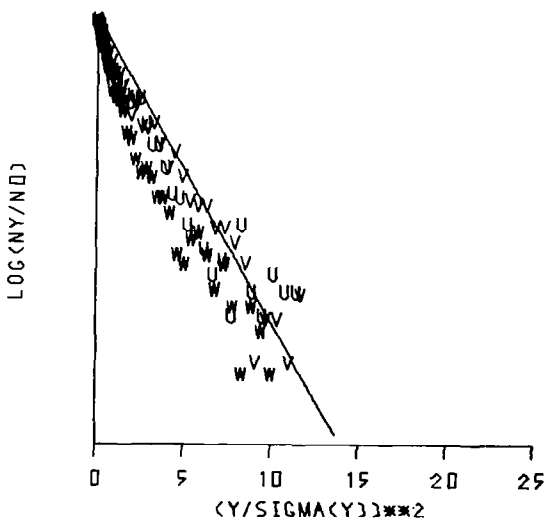

Figure 7.10 Experiment 2. For further details see the legend for figure 6.5

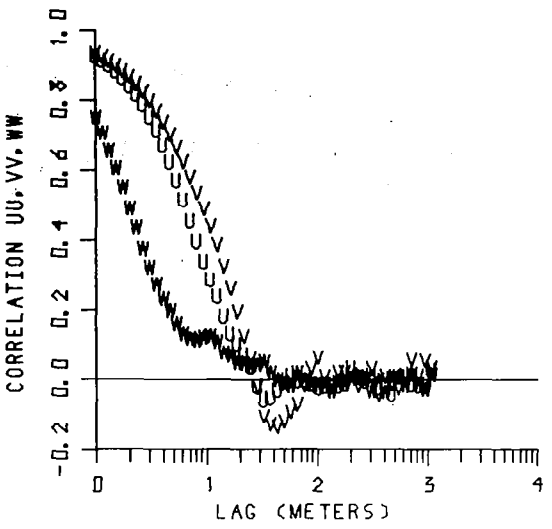

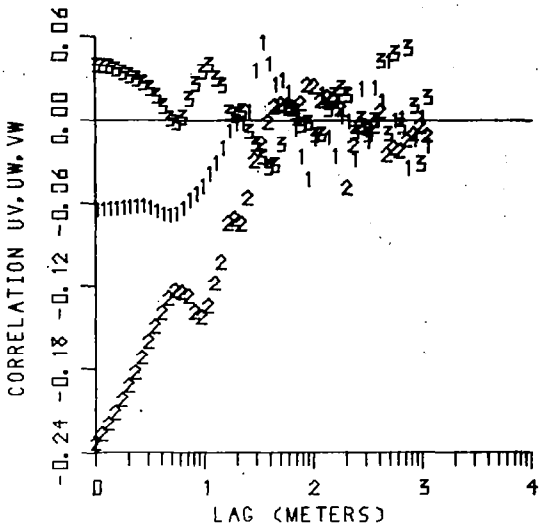

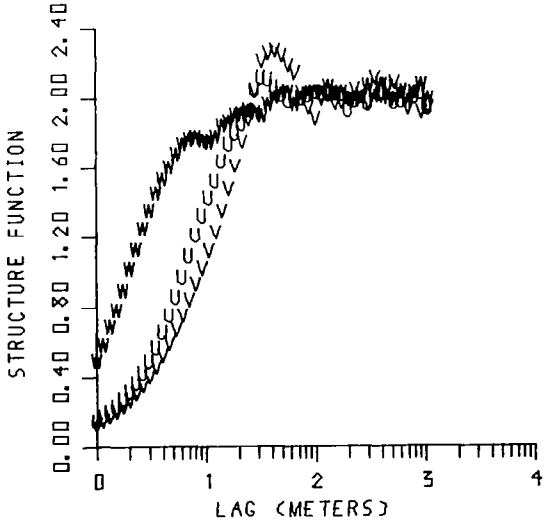

Figure 7.11 Experiment 1. For further details see the legend for figure 6.6

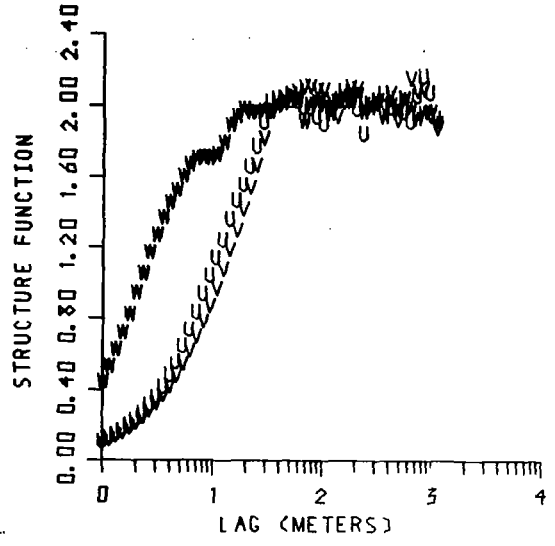

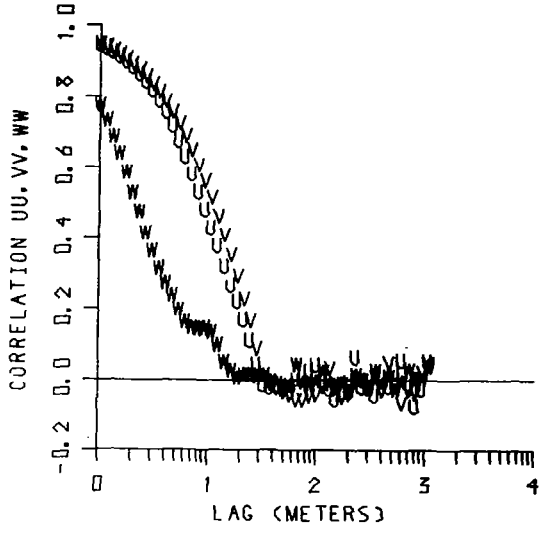

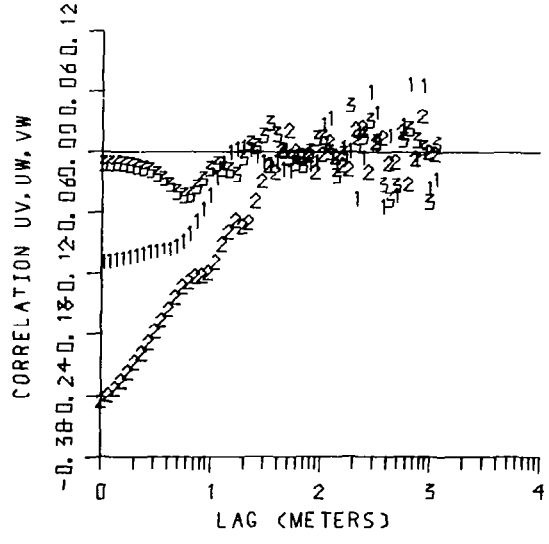

Figure 7.12 Experiment 2. For further details see the legend for figure 6.6

The generating interval was 5 sec, and with a mean wind speed of 6.6 m sec^{-1} this corresponds to a length of 33 m, and so after a lag of 33 m the autocorrelation should drop to zero, which actually is the case. For the real turbulence, the zero value is reached around 600 m. With this knowledge, we would expect the generated turbulence to look different from the turbulence recorded for the u and v components.

The cross-correlations agree well for lags less than 30 m, and it is worth emphasizing the behavior of the important uw correlation. The remarks on the autocorrelation can also be applied to the structure function.

The u, v, and w spectra are plotted on the Figures 7.13 - 7.15 together with the turbulence spectra. The u and the v spectra fall off like the turbulence spectra with a -5/3 slope for frequencies larger than 1 Hz. Between 1 Hz and 0.03 Hz (scales 6.6 m to 330 m), the epxerimental spectra exceed the turbulence spectra, and from 0.03 Hz and less the opposite is true. We could have expected a pronounced peak in the experimental spectra at 0.2 Hz due to the generation of the turbulence in 5 sec pieces, but this is not the case: the effect, if any, has been spread over more than one decade of frequencies.

The w-spectra follow the same pattern, although they seem to coincide much better except for high freqencies where the experimental spectra fall off too fast. This probably means that the eigenfunctions from 21 and up still have some significant high frequency features to add to w, but not to u and v.

The implication of the transformation 7.1 would be a folding of the spectra with a $(\sin \omega/\omega)^2$ function, which except for some end effects will tend to preserve power law behavior.

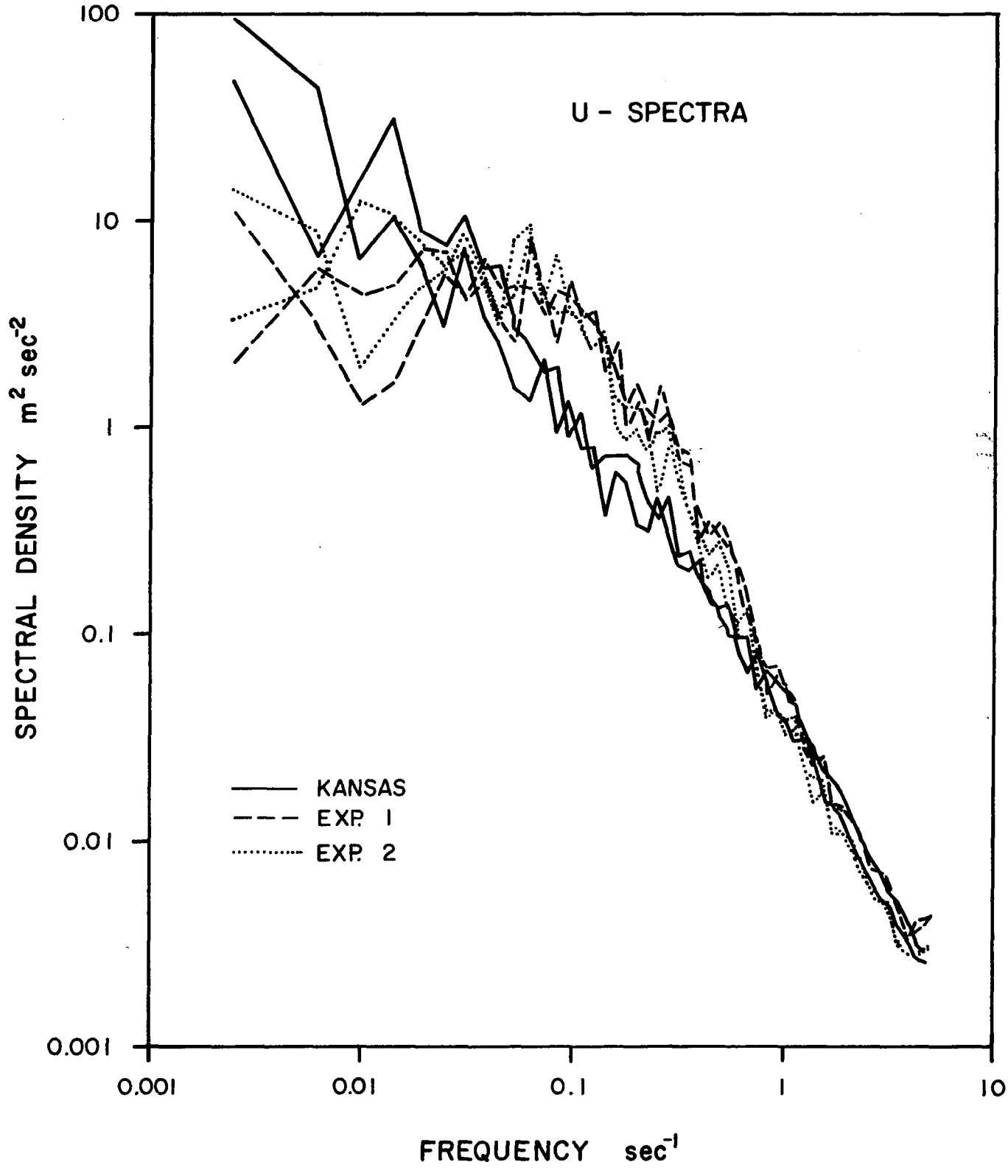
U - SPECTRA
SPECTRAL DENSITY m² sec⁻²
100
10
1
0.1
0.01
0.001
0.001
0.01
0.1
1
10
FREQUENCY sec⁻¹
KANSAS
EXP. 1
EXP. 2

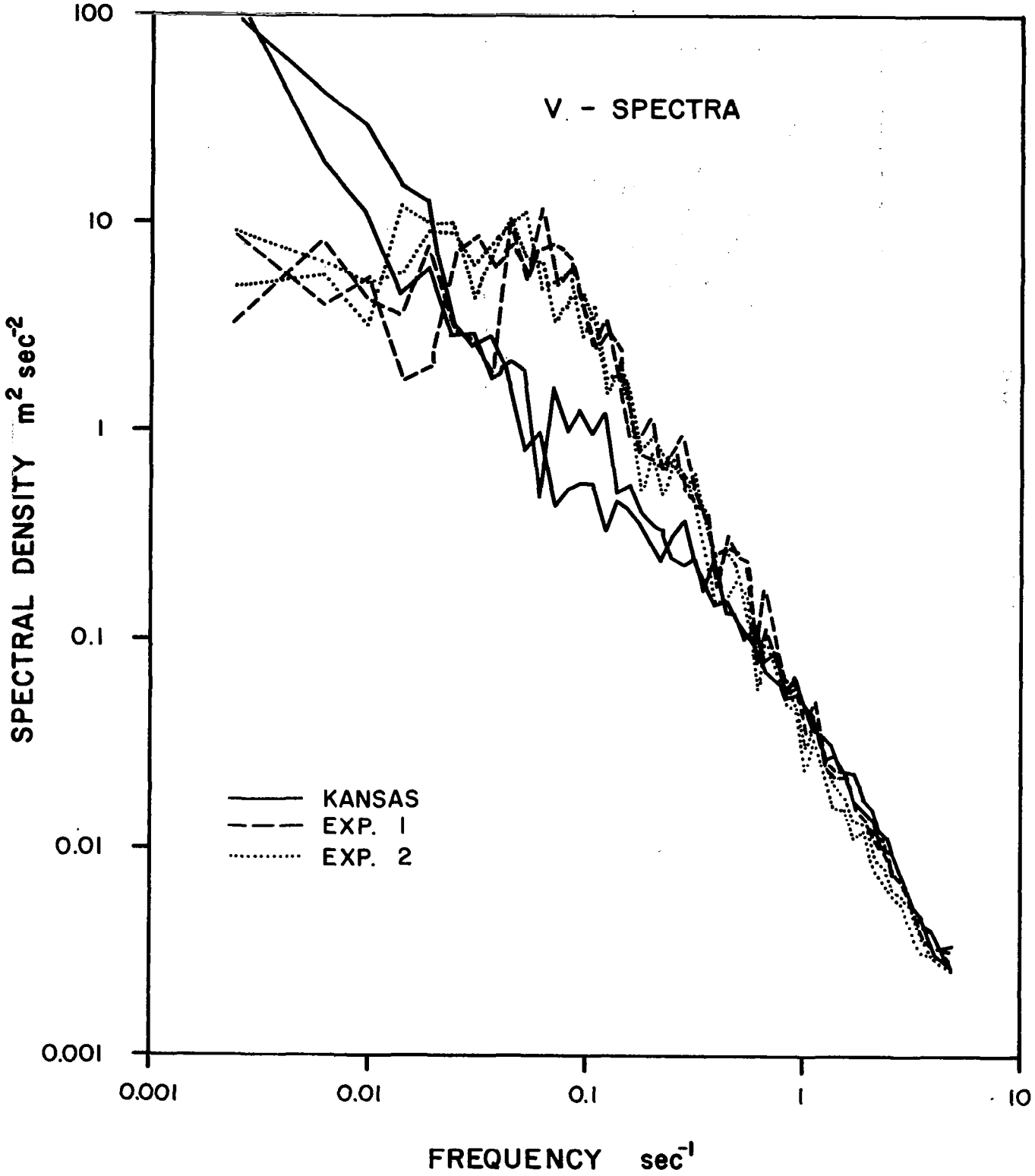
V - SPECTRA
100
10
1
0.1
0.01
0.001
SPECTRAL DENSITY m² sec⁻²
KANSAS
EXP. 1
EXP. 2
0.001
0.01
0.1
1
10
FREQUENCY sec⁻¹

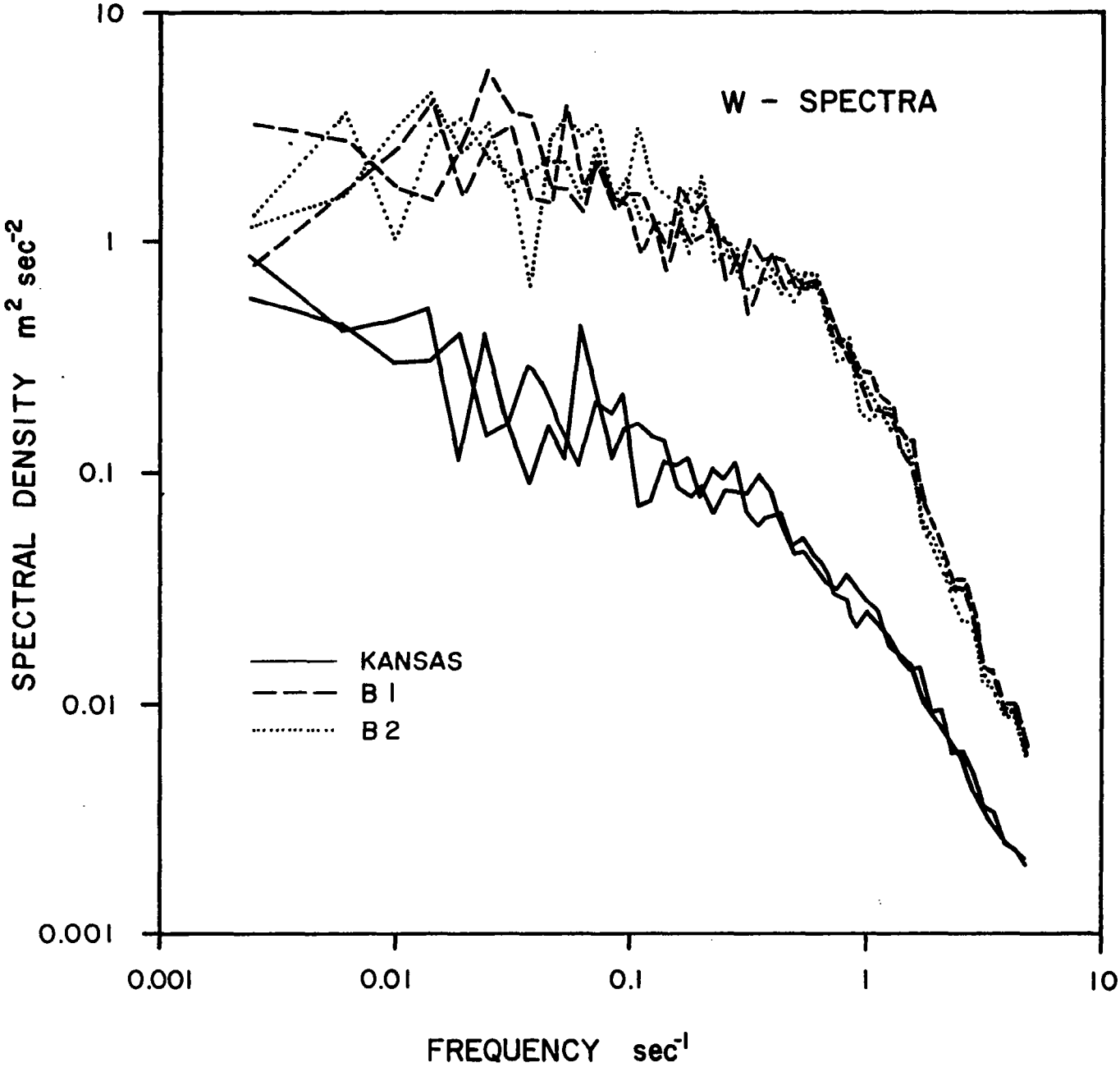
W - SPECTRA
SPECTRAL DENSITY m² sec⁻²
FREQUENCY sec⁻¹
10
1
0.1
0.01
0.001
0.001
0.01
0.1
1
10
KANSAS
B 1
B 2

The agreement between the uw-cospectra in Figure 7.16 and those in Figure 6.7 are very good.

The whole turbulence time history, block averaged from 10 Hz to 1 Hz, is displayed in Figure 6.8. The two experimental turbulence records were normalized to have the same means, zero, and variances as the turbulence record at 10 Hz and then block averaged to 1 Hz. As is evident from the former discussion, the differences between the two experiments are small, and we will therefore further on confine our attention to experiment 1. Figure 7.17 shows 1000 sec of the experimental turbulence and as could be expected from the discussion of the correlation functions and the spectra, the u and v components have too much variation in the mid-frequency range, but apparently none at low frequencies.

Figures 6.9 and 7.18 display 100 sec of the turbulence and the experiment respectively, all data at 10 Hz and normalized with mean zero and variance 1. As before, the w-components agree very well and so do the u and v components at intervals less than 10 seconds. The effect of patching the 5 sec intervals together is seen to cause some excessive large jumps, a deficiency which has to be corrected, possibly by establishing a patching procedure.

7.2 Spectral Shaping

In the final development of the model, some spectral shaping seems unavoidable, first because of the problems of generating energy at low wavenumbers, and secondly, because in practical applications care must be exercised so that the energy is maximized at the appropriate wavenumbers.

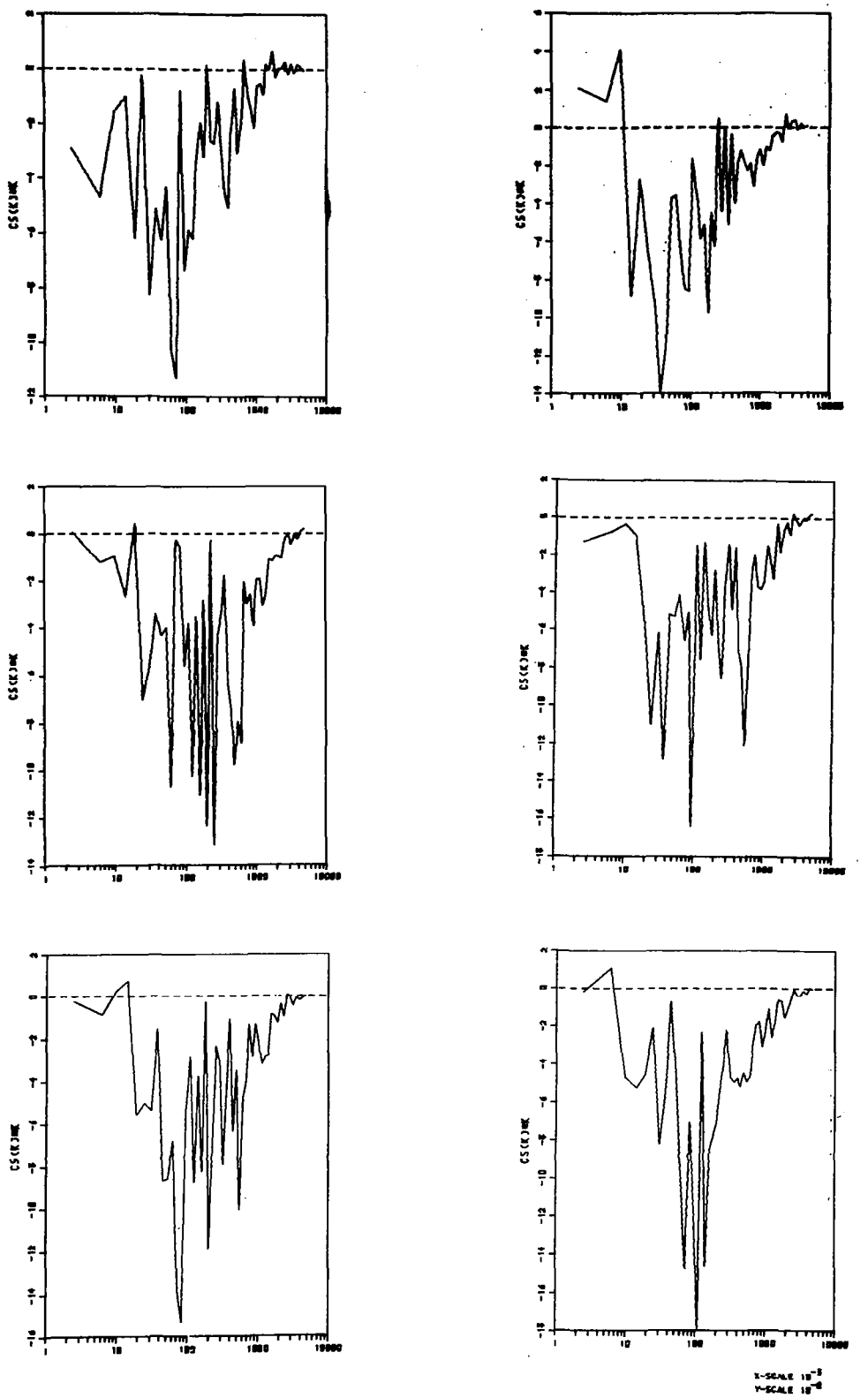

Figure 7.16 Co-spectra of the standardized u- and w-components of two samples of Kansas turbulence (top), experiment 1 (middle), and experiment 2 (bottom). Each sample consists of 8192 points (819.2 sec)

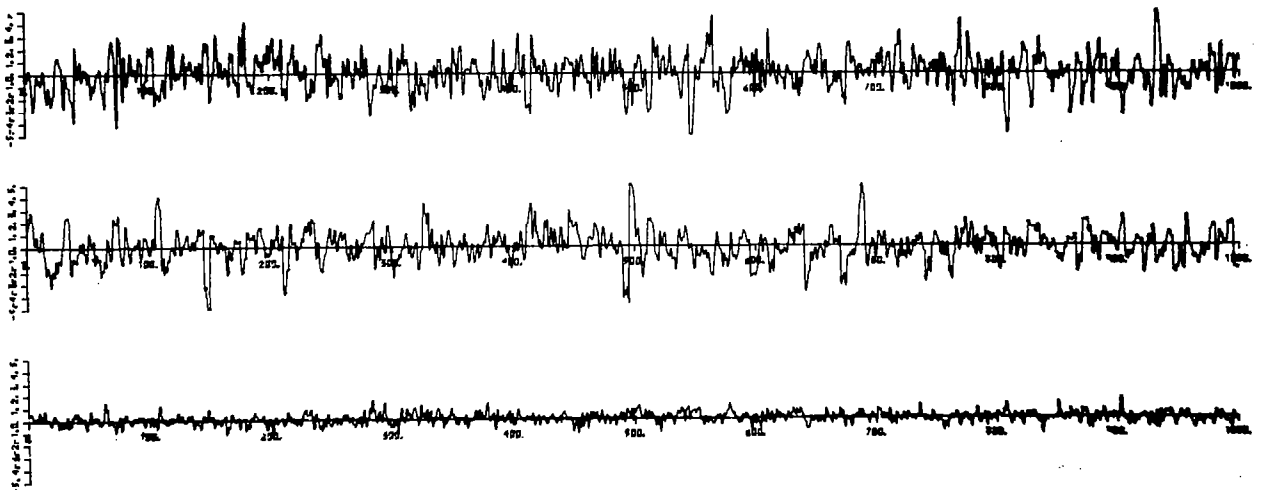

Figure 7.17 Experiment 1. Time history consisting of 1000 second averages, normalized to the same variance as the turbulence record. The numbers on the horizontal and vertical axis denote seconds and meters per second respectively.

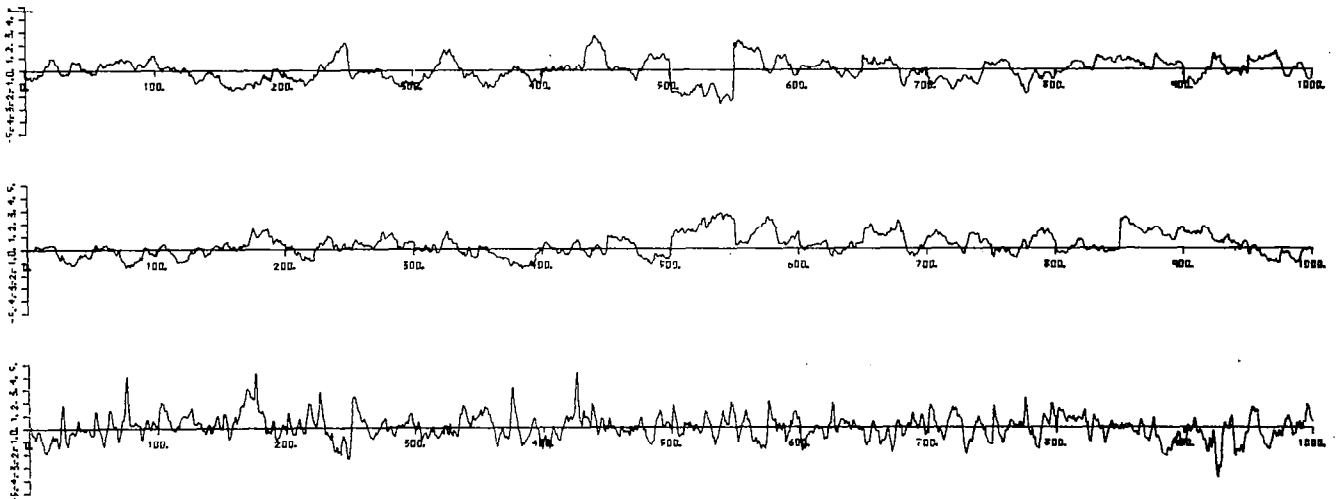

Figure 7.18 Experiment 1. For further details see the legend for figure 6.8

Several methods exist, probably the most well-known being to let the spectra match the behavior of the von Karman or the Dryden spectrum (Smith, 1971, Fichtl, 1973). Another approach is to use the semi-empirical spectral formulaes obtained by the micrmeteorological researchers (Busch, 1973).

The fair degree of coincidence of the measured spectra and the experimental spectra leads us to the conclusion that in order to shape the low wavenumber end of the experimental spectral we could as well shape them over the whole wavenumber range using the measured spectra. This was accomplished in the following way:

Calculate the discrete Fourier transform for one component at a time and let the series of Fourier coefficients be given by

$a_o, b_o, a_1, b_1, \ldots . a_N, b_N$: the measured turbulence

$c_o, d_o, c_1, d_1, \ldots . c_N, d_N$ the generated turbulence

$e_o, f_o, e_1, f_1, \ldots . e_N, f_N$: the generated and shaped turbulence

where

$$(7.2) \qquad (e_i, f_i) = \left[c_i \frac{(a_i^2 + b_i^2)^{1/2}}{(c_i^2 + d_i^2)^{1/2}} \; , \; d_i \frac{(a_i^2 + b_i^2)^{1/2}}{(c_i^2 + d_i^2)^{1/2}} \right]$$

which gives

$$e_i^2 + f_i^2 = a_i^2 + b_i^2 \tag{7.3}$$

and

$$\frac{f_i}{e_i} = \frac{d_i}{c_i}$$

so that we have changed the spectral shape of the generated turbulence to that of the measured turbulence, but we have preserved the phase angles from the generated series. The series (e_i, f_i) is then back transformed to obtain the series in the time domain.

The effects of the shaping are shown for experiment 1 in Figures 7.19 - 7.26. The autospectra and the autocorrelation are not shown as they obviously have to be the same for the measured record (the autocorrelation function approximately). The agreement between the various statistical and sequential characteristics for the real turbulence and the simulated turbulence are evident.

One desirable effect of the shaping is that it seemingly smooths out the effect of patching the generated 5 seconds together, and thereby relaxing the requirement for a patching procedure.

7.3 Summary Conclusions and Recommendations

In this study several tasks were undertaken all with the primary goal of producing an operational turbulence simulation model.

In Section 2, earlier attempts to use the Proper Orthogonal Decomposition in turbulence modeling were reviewed and the conclusions summarized in Table 1. The experience gained through these studies suggested the development of the present model.

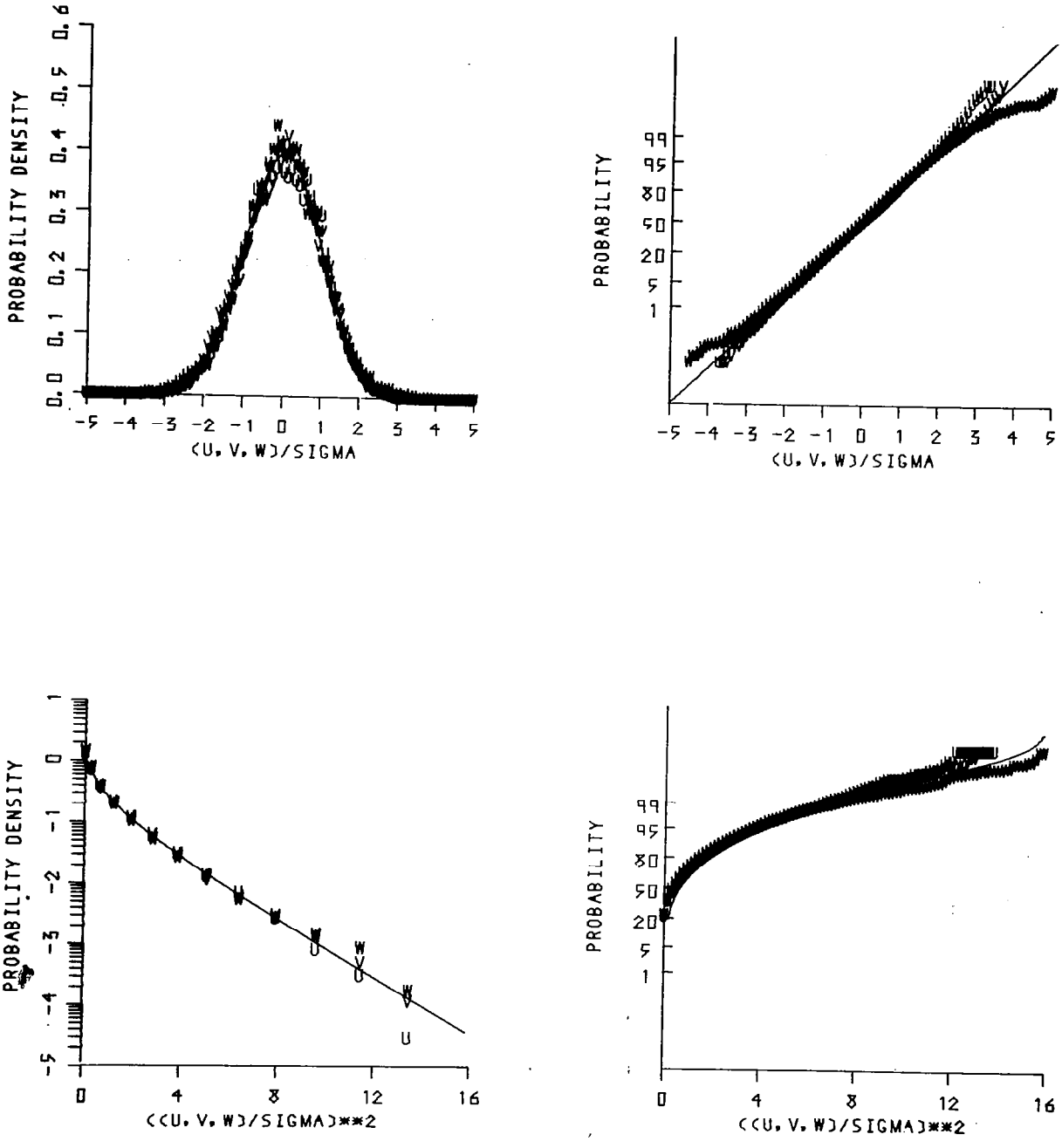

Figure 7.19 Experiment 1 after spectral shaping. For further details see the legend for figure 6.1

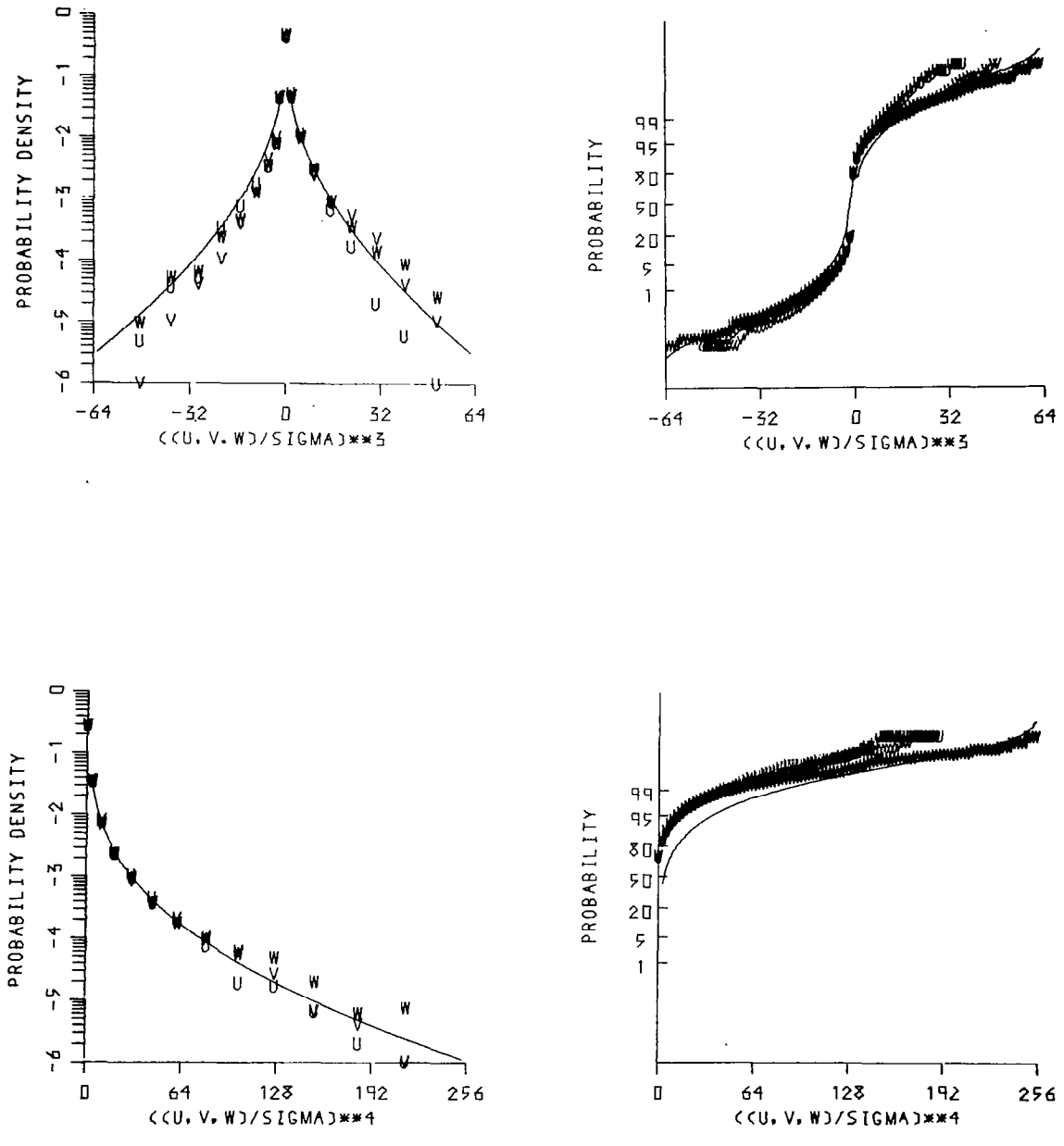

Figure 7.20 Experiment 1 after spectral shaping. For further details see the legend for figure 6.2

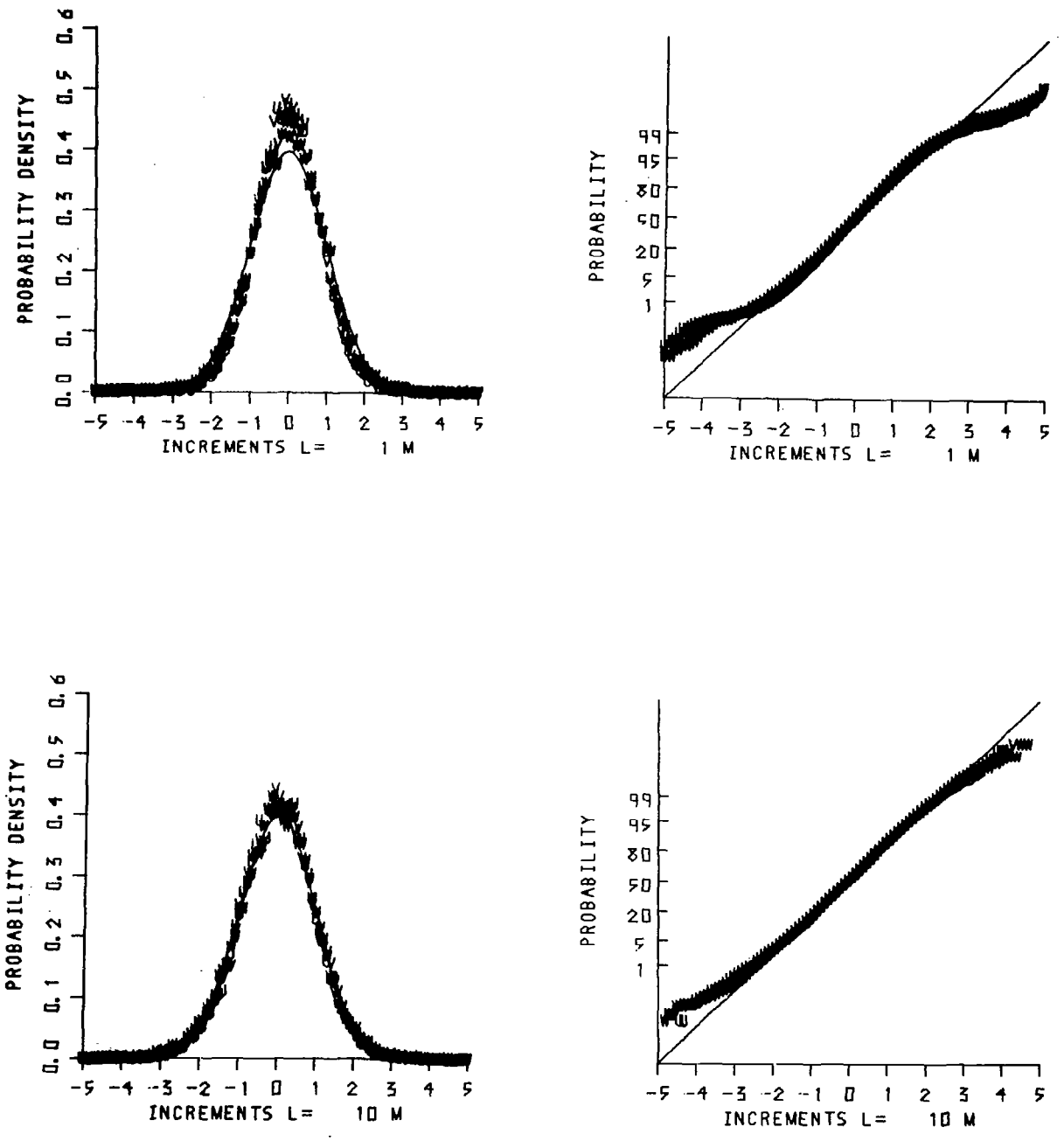

Figure 7.21 Experiment 1 after spectral shaping. For further details see the legend for figure 6.3

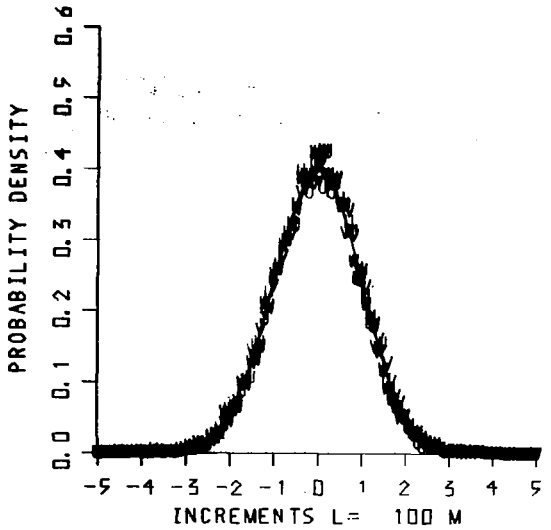

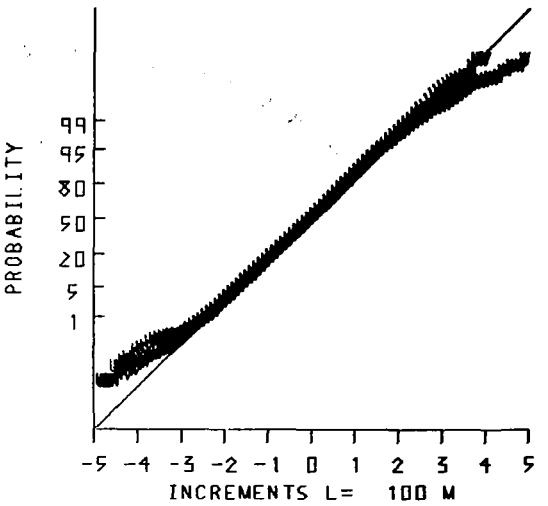

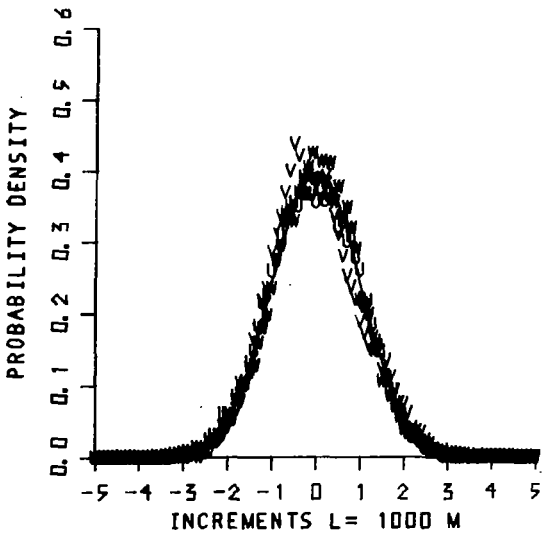

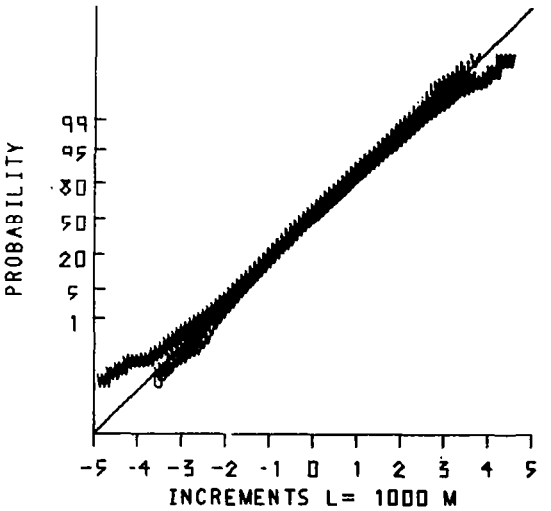

Figure 7.22 Experiment 1 after spectral shaping. For further details see the legend for figure 6.4

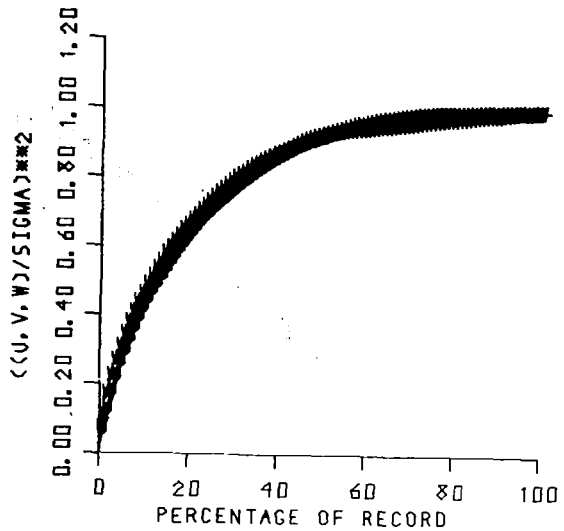

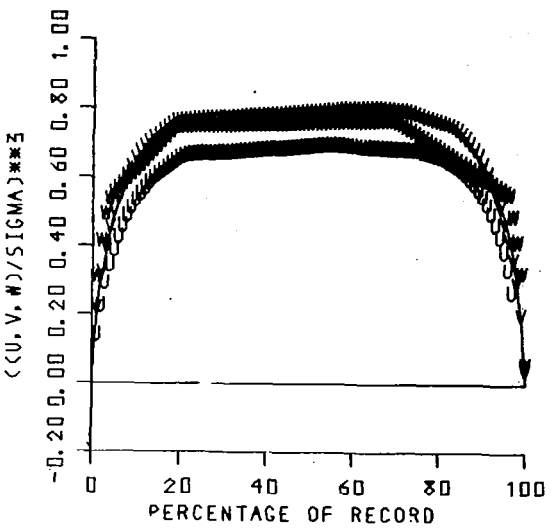

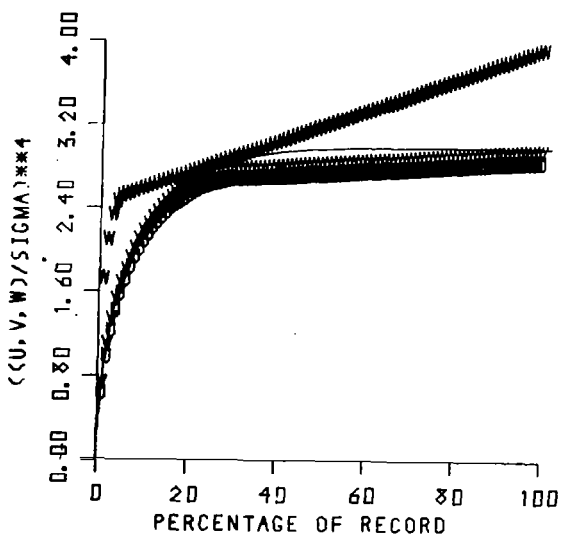

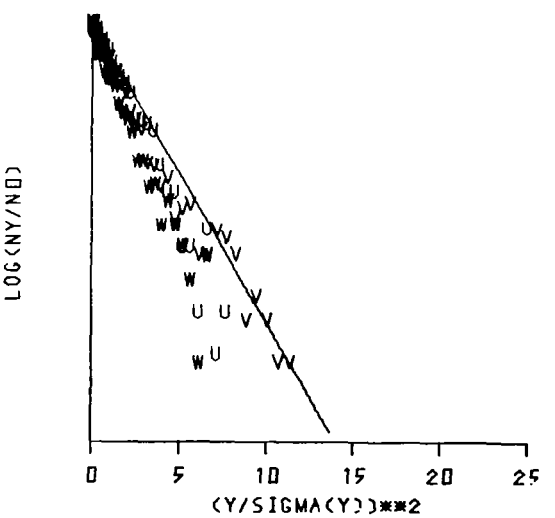

Figure 7.23 Experiment 1 after spectral shaping. For further details s-e the legend for figure 6.5

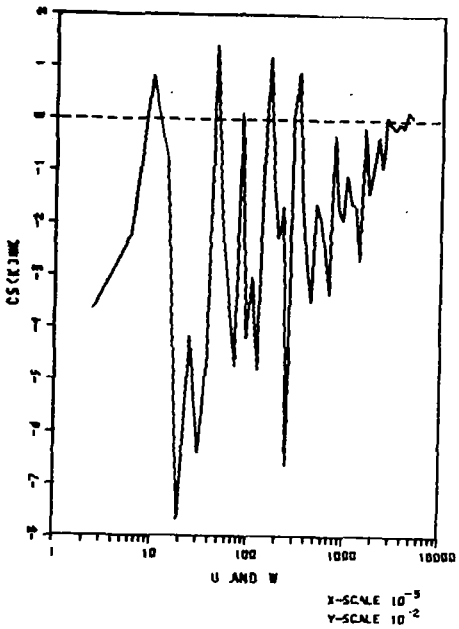

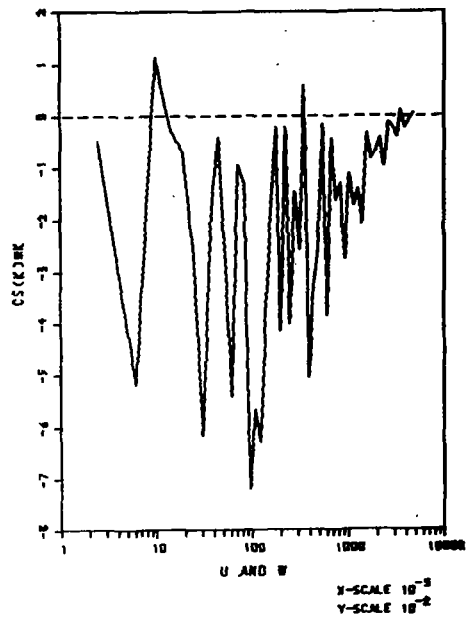

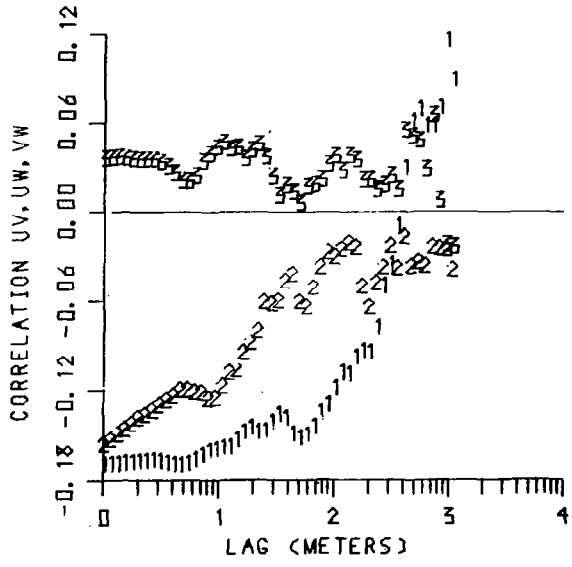

Figure 7.24 Experiment 1 after spectral shaping. Top: Co-spectra of two samples of the standardized u-and w-components. Each sample consists of 8192 points (819.2 sec). Bottom: cross correlation for the standardized data plotted as functions of the lag on a logarithmic scale. The plotted 1 refers to the u- and v-correlation, the 2 to u-w, the 3 to v-w. The integers on the horizontal axis denote power of 10

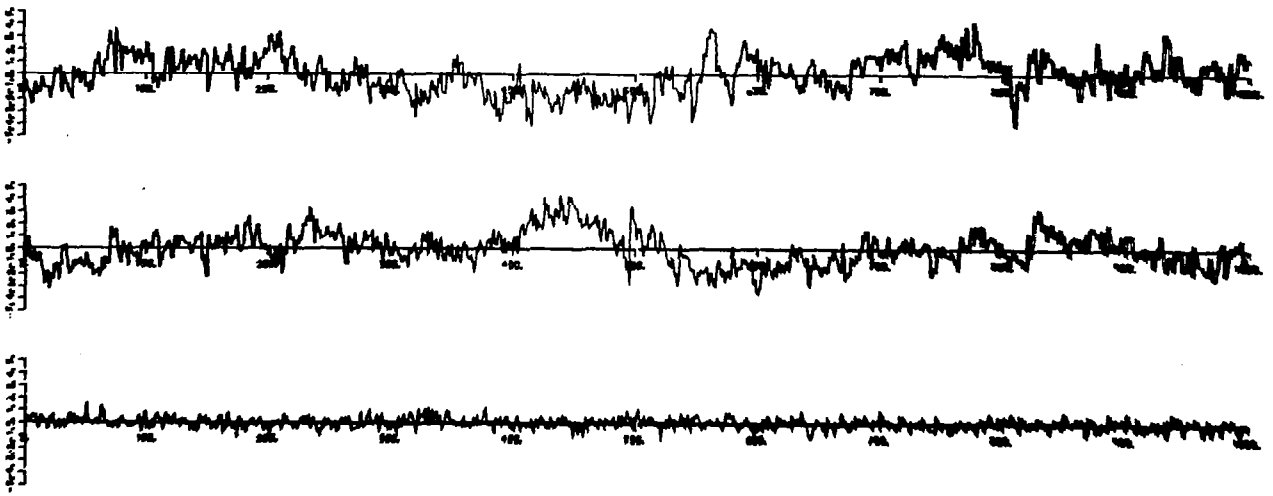

Figure 7.25 Experiment 1 after spectral shaping. For further details see the legend for figure 7.17

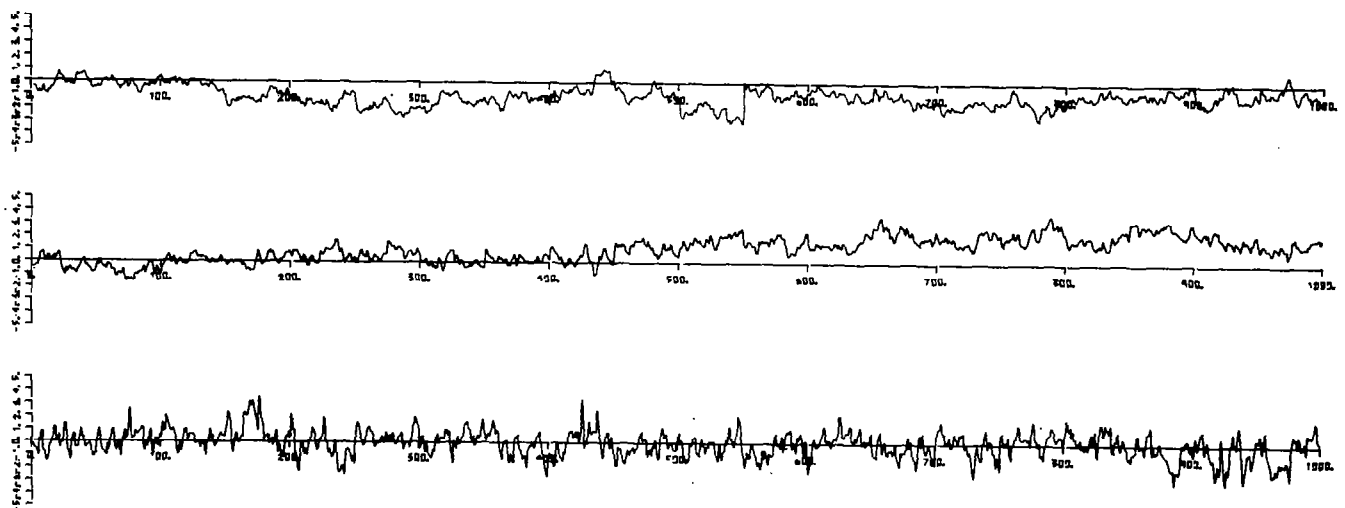

Figure 7.26 Experiment 1 after spectral shaping. For further details see the legend for figure 6.8

Because the Proper Orthogonal Decomposition method eventually has to extract information from one or more actual records, it was argued in Section 3 that under some justifiable assumptions of selfsimilarity and spectral power-laws, this does not limit the generated turbulence to fixed length and time-scales.

The theory behind the Proper Orthogonal Decomposition and its application in practice was briefly outlined in Section 4. The argument for applying this theory in the model went as follows. From earlier studies we know that it is essential to model the "surprise" in turbulence. The proper Orthogonal Decomposition provides us with a method to represent this phenomenon by a set of orthogonal functions in which the first function has the closest resemblence in a least-square sense to large gusts. The motion between these large gusts can also be represented by a set of orthogonal functions, which if provided by the Proper Orthogonal Decomposition, give a unique optimal expansion of a stochastic process. Making the simplifying assumption that the motion in the gust intervals consists of a gust structure plus an orthogonal stochastic process allowed us to concentrate the analysis to certain selected gust intervals.

The construction of the model was described as a two part process, first the analysis scheme to obtain the orthogonal functions, and second, the generating scheme which uses these functions. The two schemes were summarized at the end of Section 4.

The results of the analysis scheme were discussed in Section 5 and an investigation of the eigenfunctions revealed the first few to be a mixture of gust structure and non-gust-motion with a decreasing emphasis on the gust as the order of the eigenfunctions increases. The distribution of the expansion-coefficients were estimated to be Gaussian.

The actual turbulence record was subjected to a fairly detailed analysis, reported in Section 6, in order to provide a set of statistics for comparison with those of the generated turbulence. The calculated statistics were compared with those obtained in other studies to ensure the representativeness of the record. The statistics were chosen with emphasis on the importance of the non-Gaussian behavior of turbulence processes as well as the importance of the second order sequential statistics.

Section 7 describes two experiments that were performed with the model and compared the generated turbulence with the actual turbulence. The analysis was performed twice before and after spectral shaping. The main conclusions before the shaping were:

1. The two experiments differed no more than actual turbulence records.

2. The non-Gaussian behavior was well-modeled.

3. The sequentially dependent statistics and characteristics were modeled well on time scales less than the length of the eigenfunctions.

4. The time history showed some excessive jumps due to patching generated intervals together.

The spectral shaping was accomplished by transforming the generated turbulence into series with spectra equal to those of the actual turbulence, and preserving the phase angles during the process. After the spectral shaping, the experimental turbulence appeared to be as close to real turbulence as any practical model might produce.

However, the model is not perfect and for future work we would recommend that:

1. More turbulence records be used in the analysis.

2. The length of the ensemble functions selected to determine the eigenfunctions to be chosen with more considerations to the integral scales of the process,

3. Several choices of the feature to be tested, for example certain events in the uw and uvw correlations,

4. The probability density function and the time interval between the events should be estimated properly from the turbulence records,

5. The effects of preparing the selected ensemble in different ways should be investigated,

6. The difficult choice of the transformation of the density-functions for the first eigenfunctions could be eased by extending the analysis so that two sets of eigenfunctions are calculated, one set for the integrals with special features and one set for all other intervals. Both sets could then be used in the generating scheme, or they could be mixed, depending on an investigation of the similarities between the two sets. This procedure would provide a test of whether a characteristic feature exists in the chosen ensemble, because if the two sets of eigenfunctions show close resemblance, this is clearly not the case.

7. Alternative spectral shapings should be investigated.

The actual computer programs that generate the turbulence are rather simple and not very time consuming, and so a lot of experiments can easily be performed, in order to establish how the properties of the generated turbulence vary with changes in the model. However, it is a laborious task to make a thorough study of each experiment as can be

judged from the number of figures in this report. A solution might be to investigate just a few experiments with extreme variations in the parameters, and then to test other experiments by applying the generated turbulence in practice and judging the outcome.

8.0 SOME CONSIDERATIONS ON USE OF THE KARHUNEN-LOEVE EXPANSION IN DATA ANALYSIS

Erik L. Petersen

The Proper Orthogonal Decomposition Theorem has been used by an increasing number of researchers in a variety of fields to investigate time or space series for quasi-deterministic structures. Among them are Lorenz (1956), Lumley (1965), Dutton, et al. (1968), (1969), (1971), Holstrøm (1970), Jasperson (1971), Busch and Petersen (1971), just to mention a few.

Let us here be concerned with whether quasi-deterministic behavior appears in the functions in $\{f(t)\}$ where $\{f(t)\}$ is an ensemble of second order real valued random functions of the parameter $-\infty < t < \infty$ and where

$$\begin{aligned} E\{f(t)\} &= 0 \\ E\{f^2(t)\} &= 1 \\ E\{f(s)f(t)\} &= R(s,t) \end{aligned} \tag{8.1}$$

Let $\{f_T\}$ be subensembles formed from $\{f\}$ by assembling the sequential values over intervals of length T of some functions $f \in \{f\}$. For example, if

$$H(x) = \begin{cases} 1 & |x| < \frac{T}{2} \\ 0 & |x| \geq \frac{T}{2} \end{cases} \tag{8.2}$$

then $H(x+a)f(x)$ would be in one of the ensembles $\{f_T\}$ for every a. For ease of computation, each function in $\{f_T\}$ is redefined over the domain $[0, T]$.

If we suppose a quasi-deterministic component appears in $\{f\}$, then the question is how to select a criterion that will give a function $\phi(t)$, $0 \leq t \leq T$, that resembles the deterministic part of the functions in an optimum manner.

Several measures of resemblance are possible; the one we will choose is quadratic and has been discussed previously (Lumley, 1965, Dutton, 1969).

Let $\{f_T\}$ be one of the subensembles of $\{f\}$. Then we define

$$\lambda = E_{\{f_T\}} \frac{\left[\int_o^T f(t)\ \phi(t)\ dt\right]^2}{\int_o^T f^2(t)dt \int_o^T \phi^2(t)dt} \tag{8.3}$$

The function ϕ we are seeking maximizes λ over the collection of all subensembles $\{f_T\}$ for various values of T. Adopting other criteria in order to determine the quasi-deterministic behavior given by ϕ would in general lead to other approaches, but it is the criterion above that brings the Karhunen-Loeve expansion into the analysis. This expansion known to have some very general properties, and this in turn justifies the criterion.

The question whether there exists a unique solution to (8.4) such that it is possible to find a subensemble $\{f_T\}$ determining a function $\phi(t)$ which gives an absolute maximum of λ will be considered in the last part of this section.

If a maximum is found, let $\{f_T\}^*$ be the associated ensemble and let $\{f_T\}^-$ be constructed as

$$\{f_T\}^- = \{f_T\} - \{f_T\}^*$$

which is to say that $\{f_T\}^-$ are subensembles formed from $\{f\}$ by assembling sequential values over intervals of length T which have not been used in the construction of $\{f_T\}^*$.

We will now make the assumption that almost all the information contained in $\{f\}$ can be estimated from $\phi(t)$ and $\{f_T\}^-$. A necessary but not a sufficient condition for this assumption to be true is that $R(s,t)$ does not differ significantly from zero outside $|s-t| > T$. Let us further assume that we need a representation of the sequential characteristics of $\{f_T\}^-$ which is as economical as possible. Such a representation may be found by expanding $\{f_T\}^-$ in complete orthogonal systems, if it is possible to find an expansion that gives a good approximation to the ensemble functions by an economically small number of terms.

The optimal expansion of a random function, the Karhunen-Loeve expansion, is suitable for this purpose. The expansion is optimal in the sense that the series truncated at any point minimizes the integrated mean square deviation between the actual and the approximated random functions. Any other expansion using the same number of terms cannot have an integrated mean square deviation which is less. This is to say that minimizing the error e(N)

$$E\{e(N)\} = E\{\int \left| f(t) - \sum_{n=1}^{N} \alpha_n \psi_n(t) \right|^2 dt\}$$

leads to an expansion (see e.g. Dutton, 1969)

$$f(t) = \sum_{k=1}^{\infty} \alpha_k \psi_k(t) \qquad (8.4)$$

where the functions used in this expansion $\psi_k(t)$, are the eigenfunctions of the Fredholm integral equation

$$(8.5) \qquad \int_0^T R(s,t)\ \psi_k(t)\ dt = \lambda_k\ \psi_k(s)$$

and

$$(8.6) \qquad \int \psi_k(t)\ \psi_\ell(t)dt = \delta_{k\ell}$$

$$(8.7) \qquad E\ \{\alpha_n\ \alpha_m\} = \lambda_n\ \delta_{nm}$$

$$(8.8) \qquad \alpha_n = \int f(t)\ \psi_n(t)\ dt$$

where the λ_n's have been arranged in a non-increasing sequence.

This follows from the Proper Orthogonal Decomposition Theorem, Loeve (1955), which states that a mean-square continuous random function f(t) defined on a closed interval $0 \leq t \leq T$, has the decomposition (8.4) with the properties given by (8.6), (8.7), and (8.8) if and only if λ_n are the eigenvalues and $\psi_n(t)$ the orthonormal eigenfunctions belonging to the correlation function R(s,t), and thus are solutions to (8.5). The theory is based on Mercer's Theorem, which states that a non-negative definite function, R(s,t) continuous over the closed interval $0 \leq s,t \leq T$ has the expansion

$$(8.9) \qquad R(s,t) = \sum_n \lambda_n\ \psi_n(s)\ \psi_n^*(t)$$

where λ_n and $\psi_n(t)$ are the solutions of (8.5) and the asterisk denotes a complex conjugate.

Solving the equations (8.5) - (8.8) gives us the Karhunen-Loeve expansion, sometimes referred to as a generalized spectral representation because of the lack of correlation between the coefficients of expansion.

From the equations (8.7) and (8.8) we get

$$E\{\frac{1}{T}\int_0^T f^2(t)dt\} = \frac{1}{T}\sum_n \lambda_n$$

which shows that the eigenvalues reveal the fraction of the total variance which is explained by the associated eigenfunction.

Our problem now is to find $\{f_T\}^*$, and thereby $\{f_T\}^-$ and ϕ, by solving the variational problem as given by (8.3). Unfortunately, we are not able to do this in full generality. We cannot analytically find the subensemble $\{f_T\}^*$ that maximizes λ over all subensembles $\{f_T\}$; however, if by some other methods we can establish $\{f_T\}^*$ we can solve (8.3) for the function ϕ which maximizes λ over the ensemble $\{f_T\}^*$. An approximate solution could be obtained by calculating λ and plotting it for various choices of $\{f_T\}$, but the work involved is staggering.

Let us then assume that we are able to select a subensemble $\{f_T\}$ subjectively which is not far from the optimizing subensemble if one exists.

Applying the techniques of the calculus of varitions to (8.3) to find the maximizing function, $\phi(t)$, leads to the integral equation:

$$\int R(s,t)\ \phi_k(t)\ dt = \lambda_k\ \phi_k(s)$$

and we observe that the function most like each of the functions in the ensemble $\{f_T\}$ is determined by the Karhunen-Loeve expansion of $\{f_T\}$, and we have $\phi(t) = \phi_1(t)$. The expansion can be interpreted in the following way: ϕ_1 is the single function that explains the most variance in the ensemble, but it does not explain all of the variance, so we form a new ensemble of functions $\{f_T - a_1 \phi_1\}$ and find the one function most like the residual function; the answer will be ϕ_2 and so we consider a new ensemble $\{f_T - a_1 \phi_1 - a_2 \phi_2\}$ and so on.

With the assumptions made through this section we are now able to represent the sequential characteristics of $\{f\}$ by the two orthonormal systems, ψ_k and ϕ_k, together with the sampling properties of the corresponding expansion coefficients.

The two systems can be reduced to one system if further assumptions are made: if the quasideterministic structure we are seeking occurs over the length T, and if this structure is orthogonal to the rest of the process taking place over the length T, and if this structure is given entirely by the first eigenfunction ϕ_1, then the ensemble $\{f_T - a_1 \phi_1\}$ will have the same properties as $\{f_T\}$ hence ψ_1 will be the same as ϕ_2, ψ_2 as ϕ_3 and so on. Such an assumption was made in the construction of the model discussed in the preceding part of this report.

But does there exist a unique solution to (8.3) such that it is possible to find a subensemble $\{f_T\}^*$ determining a function $\phi(t)$ which gives an absolute maximum of λ? An example will show that such an ensemble does not exist in general.

8.1 The Karhunen-Loeve Expansion of a First Order Autoregressive Series

For the example we will use a stationary time series f(t) with the correlation function $R(s-t) = e^{-\alpha|t-s|}$, $\alpha > 0$. This is the correlation function for a first order autoregressive series.

$$f(t) = R(\tau=1)\ f(t-1) + \varepsilon(t),\ t = 0,\ 1,\ 2,\ \ldots$$

where $\varepsilon(t)$ is normally distributed with $E\{\varepsilon(t)\} = 0$ and $E\{\varepsilon(t)\ \varepsilon(s)\} = \delta_{s,t}\ \sigma_\varepsilon^2$. This form of a correlation function is quite often a good approximation for geophysical time series despite its lack of microscale, i.e., $R(\tau)$ is not differentiable for $\tau = 0$. A very obvious reason for choosing $R(\tau)$ is that it is then possible to find an analytic solution to the Fredholm integral equation (8.5).

Let us first prove a theorem that often can be useful.

Theorem: The Karhunen-Loeve expansion of a stationary second-order process yields eigenfunctions that are either odd or even.

Proof: From Mercer's Theorem, (8.9) we have

$$(8.10) \qquad R(s-t) = \sum_n \lambda_n\ \phi_n(s)\ \phi_n(t),\ 0 \leq s,t \leq T$$

which upon replacing s with T-s and t with T-t gives

$$(8.11) \qquad R(-s+t) = \sum_n \lambda_n\ \phi_n\ (T-s)\ \phi_n\ (T-t)$$

But R is an even function so that $R(-s+t) = R(s-t)$, and thus combining (8.10) and (8.11) gives

$$R(s-t) = \sum_n \lambda_n \phi_n(s) \phi_n(t) = \sum_n \lambda_n \phi_n(T-s) \phi_n(T-t)$$

From the uniqueness of the Karhunen-Loeve expansion it then follows immediately that for every $0 \leq t \leq T$

$$\phi_n(t) = \pm \phi_n(T-t)$$

so that the eigenfunctions are either odd or even with respect to the point T/2. This concludes the proof.

Although the converse is not true because a set of odd or even eigenfunctions only ensure that we have a correlation matrix symmetric with respect to the two main diagonals, one could use the theorem with care to estimate the non-stationarity of a certain ensemble. If, for example, the eigenfunctions appear to be even or odd from the m^{th} eigenfunction on, and if the first m-1 eigenfunctions explain P% of the variance, then a reasonable hypothesis would be that approximately P% of the variance in the ensemble could be due to instationarities.

Proceeding with the example, let us consider an ensemble over the closed interval $0 \leq t \leq T$ with the following properties

$$E\left\{\frac{1}{T}\int_0^T f(t)\, dt\right\} = 0$$

$$E\left\{\frac{1}{T}\int_0^T f^2(t)\, dt\right\} = 1$$

$$E\left\{\frac{1}{T}\int_0^T f(t)\, f(t-\tau)\, dt\right\} = e^{-\alpha|\tau|}$$

The eigenfunctions of the correlation function are determined by

$$\int_0^T e^{-\alpha|t-s|}\,\phi_n(s)ds = \lambda_n\,\phi_n(t)$$

or, dropping the subscript n

$$\lambda\phi(t) = \int_0^t e^{-\alpha(t-s)}\,\phi(s)ds + \int_t^T e^{-\alpha(s-t)}\,\phi(s)ds \tag{8.12}$$

Differentiating twice, using the rule for differentiating under the integral sign, we have first

$$\lambda\phi'(t) = -\alpha\int_0^t e^{-\alpha(t-s)}\,\phi(s)ds + \alpha\int_t^T e^{-\alpha(s-t)}\,\phi(s)ds$$

and then

$$\lambda\phi''(t) = \alpha^2\left[\int_0^t e^{-\alpha(t-s)}\phi(s)ds + \int_t^T e^{-\alpha(s-t)}\phi(s)ds\right] - 2\alpha\phi(t)$$

so that

$$\phi''(t) + \frac{2\alpha - \alpha^2\lambda}{\lambda}\,\phi(t) = 0$$

As a first case, we consider

$$\frac{2\alpha - \alpha^2\lambda}{\lambda} < 0 \Rightarrow \lambda > \frac{2}{\alpha}$$

The general solution to the differential equation is

$$\phi(t) = C_1 e^{at} + C_2 e^{-at}$$

but it is easily seen that no coice of C_1, C_2 can make $\phi(t)$ either odd or even over the interval (0, T) hence, no solutions exist for $\lambda > 2/\alpha$.

As a second case, we have $\lambda < 2/\alpha$. The general solution is now

$$\phi(t) = C_1 \cos(\omega t) + C_2 \sin(\omega t), \quad \omega = \sqrt{\frac{2\alpha - \alpha^2\lambda}{\lambda}}$$

or

$$\phi(t) = A \sin(\omega t + \theta_1)$$

which we can write as

$$\phi(t) = A \sin\left(\omega\left(t - \frac{T}{2}\right) + \theta\right)$$

To determine A, ω, θ and λ we have the integral equation, (8.12), and the condition of orthogonality (8.6). After some algebra we find

$$(8.13) \qquad \phi_n(t) = \sqrt{\frac{2}{\lambda_n + T}} \sin\left(\omega_n\left(t - \frac{T}{2}\right) + \frac{n\pi}{2}\right)$$

and the eigenvalue spectrum is given by

$$(8.14) \qquad \lambda_n = \frac{2\alpha}{\alpha^2 + \omega_n^2}$$

where the ω_n's are solutions to the equation

$$(8.15) \qquad \tan(\omega_n T) = -\frac{2\alpha\,\omega_n}{\alpha^2 - \omega_n^2}$$

where

$$(8.16) \qquad \frac{(n-1)\pi}{T} < \omega_n < \frac{n\pi}{T}, \quad n = 1,2,\ldots$$

The normalization of the ensemble gives

$$(8.17) \qquad \frac{1}{T}\sum_n \lambda_n = 1$$

The integral scale for the process f(t) is defined as

$$I = \int_0^\infty e^{-\alpha|\tau|}\, d\tau = \frac{1}{\alpha}$$

A variable C is introduced by

$$(8.18) \qquad C = \alpha T \ (= \frac{T}{I})$$

which is seen to be the ratio between the chosen length of the eigenfunctions and the integral scale.

Introducing C into (8.14) and (8.15) yields:

$$(8.19) \qquad \frac{\lambda_n}{T} = \frac{2C}{C^2 + (\omega_n T)^2}$$

$$(8.20) \qquad \tan(\omega_n T) = -\frac{2C(\omega_n T)}{C^2 - (\omega_n T)^2}$$

We can now numerically solve (8.17) - (8.20) to give λ_n/T, n = 1, 2, ..., as a function of C. The result is shown on Figure 8.1 on a logarithmic scale.

As expected, it is not possible to find, in a statistical sense, an ensemble $\{f_T\}^*$ that gives an absolute maximum for λ_1 because $\lambda_1/T \to 1$ for T, C $\to$ 0.

It is thus seen that applying the Karhunen-Loeve expansion to a certain selected ensemble and finding that the first eigenfunction accounts for a tremendous amount of the variance does not automatically ensure that a characteristic structure is revealed by the first eigenfunction.

Before we conclude this example, we will show an interesting relationship, in this case, between the Fourier spectrum and the eigenvalue spectrum.

The normalized Fourier spectrum of f(t) is given by

$$(8.21) \qquad S(\omega) = \frac{2}{\pi}\int_0^\infty e^{-\alpha\tau}e^{-i\omega\tau}\,d\tau = \frac{2}{\pi}\frac{\alpha}{\alpha^2 + \omega^2}$$

and the normalized eigenvalue spectrum by

$$\lambda_n = \lambda_n(\omega_n) = \frac{2}{T}\frac{\alpha}{\alpha^2 + \omega_n^2}, \quad \frac{(n-1)\pi}{T} < \omega_n < \frac{n\pi}{T}$$

and then all the eigenvalues are, except for a constant factor, lying on the curve given by the Fourier spectrum.

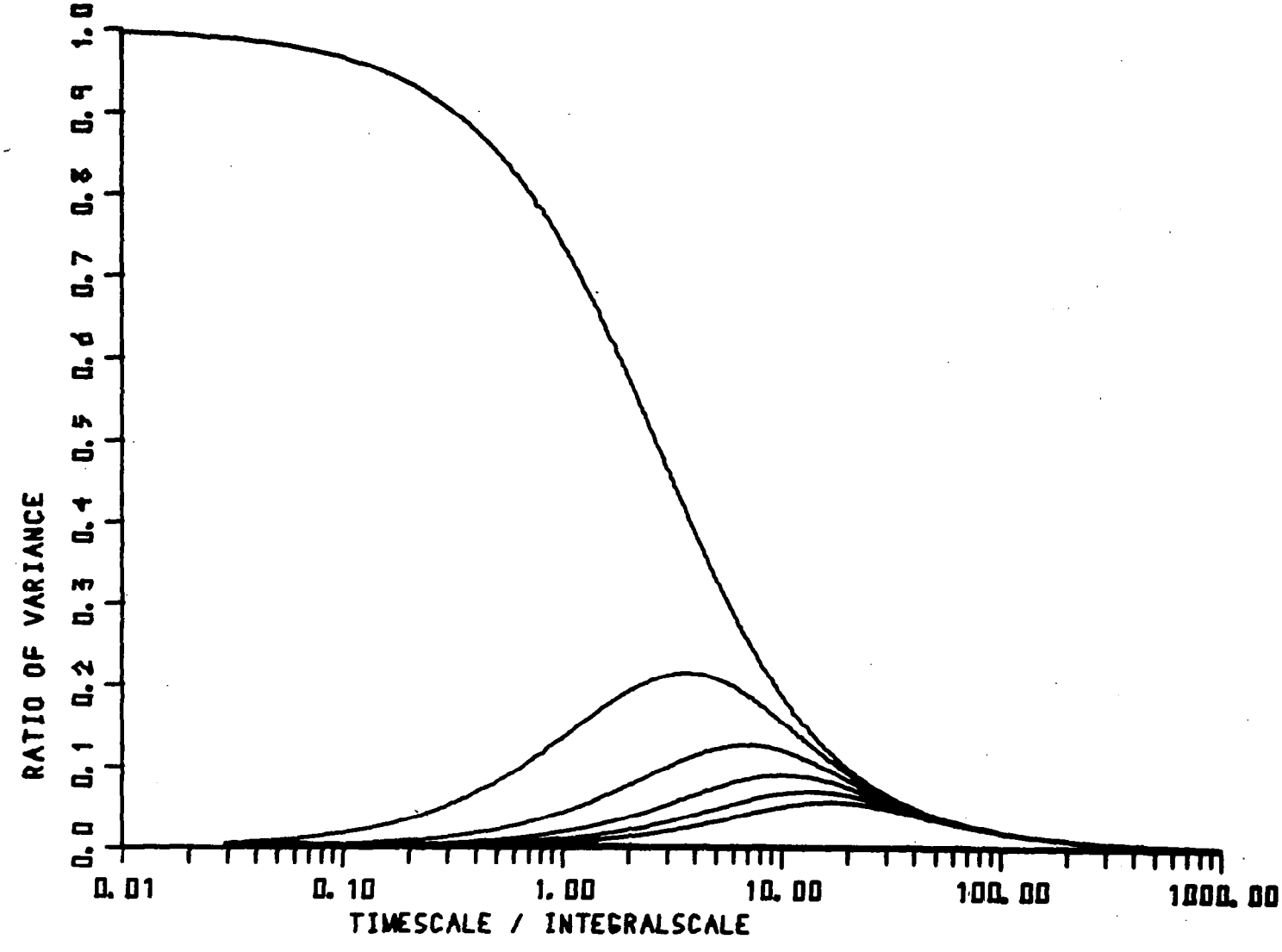

Figure 8.1 Curves showing for each of the first six eigenfunctions of a first order auto-regressive series the amount of normalized variance explained as function of the ratio of the length of the eigenfunctions and the integral scale of the series. The curve for eigenfunction n+1 is always below the curve for eigenfunction n

The mean value theorem gives

$$\int_{(n-1)\frac{\pi}{T}}^{n\frac{\pi}{T}} S(\omega)\, d\omega = \frac{\pi}{T}\frac{2}{\pi}\frac{\alpha}{\alpha^2 + \omega_\ell^2} = \frac{2}{T}\frac{\alpha}{\alpha^2 + \omega_\ell^2}, \quad \frac{(n-1)\pi}{T} < \omega_\ell < \frac{n\pi}{T}$$

where $\omega_\ell \to \omega_n$ for $T \to \infty$.

Two approximate formulas:

$$\frac{\lambda_n}{T} \to \frac{2}{\pi} \text{ arc tan } \frac{C\pi}{C^2 + n\,(n-1)\,\pi^2}$$

for $\omega_\ell \to \omega_n$

$$\sum_{n=1}^{m} \frac{\lambda_n}{T} \to \frac{2}{\pi} \text{ arc tan } \frac{m\pi}{C}$$

8.2 The Karhunen-Loeve Expansion of a Bandlimited White Noise Process

A slightly different approach for solving the integral equation (8.5) with an exponential kernel can be found in Davenport and Ross (1958) and Pugachev (1965) and (1959). In Slepian, Pollak, and Landau (1961) a specially interesting case is analyzed where the timeseries is band-limited white noise:

$$S(\omega) = \begin{cases} 1/2\ \Omega, & |\omega| < \Omega \\ 0\ , & |\omega| > \Omega \end{cases}$$

$$R(\tau) = \int_{-\Omega}^{\Omega} \frac{1}{2\Omega} e^{i\omega\tau}\, d\omega = \frac{\sin \Omega\tau}{\Omega\tau}$$

The solutions to

$$\int_{-T/2}^{T/2} \frac{\sin \Omega(t-s)}{\Omega(t-s)} \phi_n(s)\, ds = \lambda_n \phi_n(t)$$

are known as prolate spheroidal wave functions ψ_n

$$\phi_n(t) = \psi_n(t;c), \quad c = \Omega T$$

The eigenfunctions and the eigenvalues depend only on c or say

$$I = \int_0^\infty R(\tau)\, d\tau = \int_0^\infty \frac{\sin \Omega\tau}{\Omega\tau} d\tau = \frac{1}{\Omega} \frac{\pi}{2}$$

$$c = \Omega T = \frac{\pi}{2} \frac{T}{I}$$

They depend as in the previous example only on the ratio between the length of the ensemble function and the integral scale of the process.

8.3 Conclusion

The Karhunen-Loeve expansion (or the Proper Orthogonal Decomposition or the Generalized Spectral Representation) has often proved to be a powerful tool in mathematical-statistical analysis of random processes especially where advantages can be taken of the lack of correlation between the expansion coefficients. However, the method is not without disadvantages when compared with the usual Fourier analysis. One is that the eigenfunctions have to be tabulated or plotted while sines and cosines are well-known functions. Another is that a physical interpretation of the eigenvalue spectrum is often difficult, if possible, at all, in contrast to Fourier spectra where the amount of explained variance

is plotted versus frequency or wavenumber and hence makes direct reference to time or length scales in the process being studied.

Fourier analysis usually requires the process to be stationary and ergodic whereas the Proper Orthogonal Decomposition can be applied to non-stationary ensembles. But in order to use the latter method, it is necessary to establish an ensemble, and in the process of doing so it is of the utmost importance to be sure that all the ensemble functions included are equal members of the ensemble. It is obvious that in order for the method to reveal a characteristic structure in the ensemble, the ensemble functions have to be properly aligned. If for example the structure is a sinusoid, there must be no phaseshift from one ensemble function to another.

In this section we have outlined the theoretical basis for the model which was developed in the preceding sections. We believe that this basis can support further investigations of the potential of the Proper Orthogonal Decomposition in studying and modeling physical processes. We have also pointed to the necessity of investigating the statistical structure of the series being studied before it is decided how to create the ensemble functions the method actually required as input.

REFERENCES

Busch, N. E. and E. L. Peterson, 1971: Analysis of nonstationary ensembles. Statistical Methods and Instrumentation in Geophysics. Proceedings of the NATO Advanced Study Institute in Norway, April 1971. Ed. A. G. Kjelaas. Teknologisk Forlag, Oslo, 1971. 71-92.

Busch, N. E. and S. E. Larsen, 1972: Spectra of turbulence in the atmospheric surface lyaer. Risø Rept. No. 256, 187-207.

Busch, N. E., 1973: On the mechanics of atmospheric turbulence. Workshop on Micrometeorology. Ed. D. A. Haugen. The American Meteorological Society, Boston.

Davenport, W. B., Jr. and W. L. Root, 1958: An Introduction to the Theory of Random Signals and Noise. McGraw-Hill, New York.

Dutton, J. A., 1970: Effects of Turbulence on Aeronautical Systems. Progress in Aerospace Sciences, Vol. II, Dr. D. Kuchemann, Editor, Pergamon Press - Oxford & New York, pp. 67-109.

Dutton, J. A., 1969: A preliminary study of the probabilistic structure of turbulent forcing of launch vehicles. Investigation of the Turbulent Wind Field Below 150 M Altitude at the Eastern Test Range, NASA Contractor Report CR-1410.

Dutton, J. A. and D. G. Deaven, 1969: A selfsimilar view of atmospheric turbulence. Radio Science, Vol. 4, 12, 1341-1349.

Dutton, J. A. and J. A. Lane, 1969: Intermittency of small scale structure. Radio Science, Vol. 4, 12, 1357-1359.

Dutton, J. A. and D. G. Deaven, 1971: Simulation of atmospheric turbulence with empirical orthogonal functions. Statistical Properties of Turbulence at the Kennedy Space Center for Aerospace Vehicle Design, NASA Contractor Report CR-1189.

Dutton, J. A. and D. G. Deaven, 1971: Some observed properties of atmospheric turbulence. Lecture Notes in Physics, 12. Statistical Models and Turbulence. Proceedings of a Symposium held at the University of California, San Diego (la Jolla) July 15-21, 1971. Ed. M. Rosenblatt and C. Van Atta. Springer Verlag, New York.

Fichtl, G. H., 1973: Problems in the simulation of atmospheric boundary layer flows. Flight in Turbulence AGARD Flight Mechanics Panel Symposium.

Holmstrom, J., 1970: Analysis of Time Series by Means of Empirical Orthogonal Functions. Tellus XXII, 6, 638-647.

Jasperson, W., 1971: Representation of meteorological variables by empirical orthogonal functions. Statistical Methods and Instrumentations in Geophysics. Proceedings of the NATO Advanced Study Institute in Norway, April, 1971. Ed. A. G.Kjelaas. Teknologisk Forlag, Oslo, 1971. 109-119.

Kutzbach, J. E., 1967: Empirical eigenvectors of sea level pressure, surface temperature, and precipitation complexes over North America. J. Appl. Meteor., 6, 791-802.

Larsen, S. E., 1971: Hot-wire measurements of atmospheric turbulence near the ground. Risø Rept. No. 233.

Loeve, M., 1955: Probability Theory. Van Nostrand, New York.

Lorenz, E. N., 1956: Empirical orthogonal functions and statistical weather prediction. Scientific Report No. 1 under Contract AF19 (604) 1566, AFCRC-TN-57-256, AD 110268.

Lumley, J. L., 1965: The structure of inhomogeneous turbulent flows. Atmospheric Turbulence and Radio Propagation. Eds. A. M. Yaglom and V. T. Tatarsky, Publishing House Nanka, Moscow.

Mandelbrot, B., 1965: Self-semilar error clusters in communication systems and the concept of conditional stationarily. IEEE Trans. Commun. Technol., 13, 71-90.

Pugachev, V. S., 1959: A method for the determination of the eigenvalues and eigenfunctions of a certain class of linear integral equations. Applied Mathematics and Mechanics. Pergamon Press. Vol. 23 745-753.

Slepian, D., H. O. Pollack and H. J. Landau, 1961: Prolate Spheroidal Wave Functions, Fourier Analysis and Uncertainty, I + II. The Bell System Technical Journal, January, 1961.

Smith, G. W., 1971: A study in the simulation of atmospheric turbulence. M.S. thesis, Department of Meteorology, The Pennsylvania State University, 65 pp.

Sparks, E. H. and J. A. Dutton, 1972: Phase angle considerations in the modeling of intermittent turbulence. Journal of Atmospheric Sciences, Vol. 29, 2, 300-303.

*U.S. GOVERNMENT PRINTING OFFICE: 1976 - 735-004/12